The Mediator kinase module: structural and functional studies in transcription regulation

Dissertation

for the award of the degree

“Doctor rerum naturalium”

of the Georg-August-Universität Göttingen

within the doctoral program IMPRS Molecular Biology

of the Georg-August University School of Science (GAUSS)

submitted by

Sara Osman

from Cairo, Egypt

Göttingen 2019

Members of Thesis Committee

Prof. Dr. Patrick Cramer
Department of Molecular Biology
Max Planck Institute for Biophysical Chemistry, Göttingen

Prof. Dr. Blanche Schwappach
Dept. of Molecular Biology
University Medical Center Göttingen

Prof. Dr. Holger Stark
Department of Structural Dynamics
Max Planck Institute for Biophysical Chemistry, Göttingen

Members of the Examination Board

Prof. Dr. Patrick Cramer (1st Referee)
Department of Molecular Biology
Max Planck Institute for Biophysical Chemistry, Göttingen

Prof. Dr. Holger Stark (2nd referee)
Department of Structural Dynamics
Max Planck Institute for Biophysical Chemistry, Göttingen

Further members of the Examination Board

Prof. Dr. Henning Urlaub
Research Group Bioanalytical Mass Spectrometry
Max Planck Institute for Biophysical Chemistry, Göttingen

Dr. Vladimir Pena
Research Group Macromolecular Crystallography
Max Planck Institute for Biophysical Chemistry, Göttingen

Prof. Dr. Markus Zweckstetter
Protein structure determination using NMR
Max Planck Institute for Biophysical Chemistry

Date of oral examination: 16th of July 2019

Acknowledgements

I would like to thank Patrick Cramer for creating an environment that fosters creativity and freedom, for the great opportunity to do my PhD in his lab, for his supervision, the trust he put in my work, and insightful scientific discussions.

I would like to thank my thesis committee members: Blanche Schwappach for her kind mentorship along the way, and Holger Stark for profound support, both moral and technical, at times of overwhelming confusion and self-doubt in the face of repeated failures, which gave me the push I needed to continue.

I would like to thank Fanni Bazsó, Alexandra Stützer, and Henning Urlaub for smooth and fruitful mass spectrometry collaborations, Carina Burzinsky, for enthusiastic and reliable technical support, and Marc Böhning, for introducing me to fluorescence microscopy and the concepts of phase separation. I would like to thank Katharina Hofmann for proofreading parts of this thesis.

I would like to thank members of the Pol-II initiation lab, past, present, and affiliated, particularly Sarah Sainsbury, Christian Dienemann, Paulina Seweryn, Haibo Wang, Felix Wagner, Goran Kokic, Isaac Fianu, Julio Abril-Garrido and Sandra Schilbach for exciting scientific exchange, and an environment which is free of judgment, and where ridiculousness is encouraged, because that's where the best (and worst) ideas are born!

To my wonderful friends, Paulina Seweryn, Anna Sawicka and Felix Wagner, who have opened me up to a world of exhilarating new experiences, exploring Europe, from my first alpine mountaintop, to bike touring around beautiful Polish lakes, to my first rock music festival, and philosophical discussions under the stars, it's been a pleasure. Thanks also to Saskia Gressel for her friendship and support, and Marco Dombrowski, for sharing my passion for the written word.

Finally, to Felix, thank you for your endless love and unrelenting support.

1 ABSTRACT 5

2 INTRODUCTION 6

2.1 EPIGENETIC REGULATION 6
2.2 TRANSCRIPTION 6
2.2.1 The transcription cycle 8
2.2.2 The RNAPII CTD and transcriptional kinases 9
2.2.3 Transcription initiation 11
TBP 11
TFIIA 11
TFIIB 11
TFIIF 12
TFIIE 12
TFIIH 12
Structure of the transcription Pre-initiation complex (PIC) 13
Architecture of promoters 17
2.2.4 Transcription activation 18
Architecture of upstream activation sequences (UASs) 18
Transcription activators 18
Mechanism of activator function 19
Transcription coactivators 19
The Mediator complex 20
Mediator structural biology 22
The Mediator kinase module 24
Phase separation 25
2.3 AIMS OF THIS STUDY 26

3 MATERIALS 27

3.1 VECTORS 27
3.2 RECOMBINED PLASMIDS 27
3.3 DNA SCAFFOLDS 28
3.4 CHEMICALS 29
3.5 CELL CULTURE 30
3.5.1 E.coli strains 30
3.5.2 S.cerevisiae strains 30
3.5.3 Insect cell lines 30
3.5.4 Cell culture media 31
3.5.5 Antibiotics and additives 31
3.6 ANTIBODIES 32
3.6.1 Primary antibodies 32
3.6.2 Secondary antibodies 32
3.7 STANDARD BUFFERS AND DYES 32

4 METHODS 33

4.1 DNA METHODS 33
Cloning strategies 33
Vector digestion 33
Insert generation by PCR 33
Primer design 33
Template DNA 34
PCR reactions 35
Site-directed mutagenesis 35

Agarose gel electrophoresis for product size verification 36
Gel extraction of product 36
DNA quantification 36
Combining vector and insert 36
Preparation of chemically competent XL1-blue *E.coli* cells 37
Bacterial transformation by heat shock 37
Isolation and verification of recombined plasmids 38
Generation of polypromoter plasmids with multiple genes 38
A compilation of recombined plasmids with the cloning methods and primer sequences used to generate them 39
Strand annealing of DNA scaffolds 41
4.2 INSECT CELL METHODS 41
Modifying baculoviral bacmids using insect cell transfer vectors 41
Preparation of electrocompetent DH10αEMBacY *E.coli* cells 42
Transformation by electroporation 42
Isolation and storage of bacmid DNA 42
Insect cell culture 43
Sf9 cell transfection (V0 production) 44
Virus propagation in Sf9 or Sf21 cell culture (V1) 44
Monitoring virus progression 45
V1 expression test pull-downs 45
Protein expression in Hi5 insect cells (V2) 46
4.3 PROTEIN METHODS 46
Preparation of chemically competent BL21 (DE3 RIL), Rosetta, or LOBSTR cells for protein expression 46
Large-scale yeast fermentation culture for isolation of endogenous complexes 47
Cell lysis methods 47
Protein buffers and handling 47
SDS-PAGE 48
Native-PAGE 48
Chromatographic methods 48
Sucrose gradient ultracentrifugation 48
Bioinformatic tools 49
Phos-Tag™ Gels 49
Western Blot Analysis 49
Fluorescent-labeling of proteins 51
4.3.1 Mass spectrometry 51
Protein identification and phosphosite mapping 51
Cross-linking/mass spectrometry 51
4.3.2 Light microscopy methods 52
mPEGylation of glass slides 52
Fluorescence microscopy 53
4.3.3 Electron microscopy methods 53
Sample fixation 53
Quenching 54
EM Grids 54
Glow discharging 54
Negative staining 54
Cryo-EM 55
Buffer exchange 55
Plunge freezing 55

Imaging (Neg stain and Cryo) 56
Image Processing 56
4.3.4 Purified proteins 57
Mediator Cdk8 Kinase module (CKM A or KD) 57
Core Mediator (cMed) 58
Endogenous Mediator (eMed) 59
Gcn4 61
GFP-Gcn4 61
mCherry-Med15 62
Med15_KIX123 62
CTD of RNAPII 64
RNAPII and transcription initiation factors 64
Kinase assays 64
Immobilized-Template Assay 64
CKM Phosphoproteomics of the PIC 65
CKM-cMed-PolII competition assay 66
Droplet assays 67
Fluorescence anisotropy of Gcn4-DNA 68
Electromobility shift assay of Med15_KIX123 and GFP-Gcn4 70

5 RESULTS 71

5.1 PART I: SAMPLE PREPARATION 71
5.1.1 A strategy for recombinant expression and purification of CKM 71
5.1.2 Cloning of the complete S.cerevisiae CKM on a single vector 71
5.1.3 A baculovirus expression vector system for CKM 72
5.1.4 A purification strategy yielding pure, stoichiometric CKM 73
5.1.5 Design of a catalytically inactive CKM 75
5.1.6 Verification of the integrity of recombinant CKM 75
Recombinant CKM is catalytically active on known substrate 75
Negative stain electron microscopy of recombinant CKM is consistent with endogenous CKM 77
5.1.7 Purified proteins toolbox 78
5.1.8 Complex formation of CKM with cMed 79
5.2 PART II: CHARACTERIZATION OF CKM-CMED BINDING IN THE CONTEXT OF TRANSCRIPTION INITIATION 81
5.2.1 CKM is not a part of the transcription pre-initiation complex 81
5.2.2 CKM directly competes with RNAPII for Mediator binding 82
5.2.3 A shared binding interface of CKM and RNAPII on Mediator accounts for their mutually exclusive binding behavior 83
5.3 PART III: CKM IN VITRO PHOSPHOPROTEOMICS 86
5.3.1 CKM undergoes extensive autophosphorylation 86
5.3.2 CKM phosphoproteomics of the PIC 87
CKM phosphorylates Mediator and impairs its binding to the PIC 88
CKM phosphorylates PIC components TBP and TFIIF and does not affect their PIC binding 90
5.3.3 PIC components form liquid-like droplets that dissolve upon CKM phosphorylation 90
5.4 PART IV: CHARACTERIZATION OF THE FUNCTION OF THE CKM IN ACTIVATOR-DEPENDENT TRANSCRIPTION 92
5.4.1 CKM targets the activator Gcn4 for phosphorylation 92
CKM phosphorylation of Gcn4 impairs its genomic binding 93

CKM phosphorylation impairs the interaction of Mediator with activators and dissolves activator/mediator liquid droplets 95
5.5 PART V: CRYO-EM OF CKM AND CKM-CMED 98
5.5.1 Cryo-EM of CKM 98
Heavy aggregation of CKM on cryo-EM grids compared to negative stain grids 99
Systematic solution condition testing 99
Effect of pH 105
Effect of crosslinker concentration 105
Effect of buffer exchange method and detergents 105
A cryo-EM grid condition with homogeneous single particles of CKM 106
5.5.2 Cryo-EM of CKM-cMed 106
6 DISCUSSION 112
The structural effect of CKM 113
The kinase activity of CKM 114
Phase separation 115
Experimental drawbacks 116
An integrative model of CKM function 117
Experiments needed to test this model 124
Structural and unstructural biology of CKM and CKM-cMed 126
The aggregation problem 127
CKM from yeast to human 128
Clinical implications 129
Future perspectives 129
7 BIBLIOGRAPHY 131
8 LIST OF FIGURES 141
9 LIST OF TABLES 142
10 LIST OF ABBREVIATIONS 143
11 CURRICULUM VITAE 145
12 SUPPLEMENTARY INFORMATION 146

1 Abstract

Transcription of protein-coding genes occurs when RNA polymerase II (RNAPII) and general transcription factors (GTFs) assemble at genomic promoter regions, forming a transcription pre-initiation complex (PIC), which initiates DNA opening and DNA-directed RNA synthesis. Upstream of promoters, gene-specific transcription activators bind upstream activation sequences (UASs), and they relay their activation signal to the RNAPII transcription initiation machinery through an intermediary complex of proteins known as the Mediator complex, which is found universally on all protein-coding genes in eukaryotes. The Mediator complex is a large multisubunit complex of 25 subunits in yeast, and 30 in human, amounting to a total of near 1.5 MDa, and 2 MDa in molecular mass, respectively. Mediator is divided into four structural and functional modules: the head, the middle, the tail, and the Cdk8 kinase modules. The head and middle modules, together known as the core Mediator (cMed), are essential for viability in yeast, and act as a GTF, engaging directly with the PIC and supporting its assembly and function. The tail module is responsible for the majority of interactions with activators, thereby connecting the bridge that allows communication between UASs and promoters. Disorder in the tail accommodates the versatility of Mediator-activator interactions. The Cdk8 kinase module (CKM) is dissociable, and occupies only a subpopulation of Mediator complexes in the cell. It contains the Cdk/cyclin pair Cdk8/cyclin C, which is the only catalytic activity within the Mediator complex. Generally thought to regulate Mediator function by repressing transcription, the exact role of the CKM and its mode of action remain enigmatic. Here, we aimed to investigate the role of the CKM in transcription initiation by a combination of biochemical and structural analyses. We established a new method for recombinant expression and purification of the complete *S.cerevisiae* CKM. We investigated CKM binding to the PIC and cMed in an *in vitro* reconstituted system with purified transcription initiation components, and found that CKM is excluded from the PIC, but binds cMed. Using crosslinking-mass spectrometry, we determined that the reason for that was an overlapping binding interface on cMed between the CKM and RNAPII. Furthermore, we explored CKM phosphorylation targets, and found novel targets within the PIC. We modeled the UAS-activator-Mediator interaction *in vitro*, and found that CKM phosphorylation of activators disrupts both UAS-activator and activator-Mediator interactions and attenuates their phase separated droplets. Taking our findings together with knowledge from published *in vivo* studies, we propose a hypothetical model for CKM function, which we believe can guide future experiments. Finally, to illuminate the CKM-Mediator interaction, we tried to solve the structures of recombinant CKM and CKM-cMed complexes by cryo-electron microscopy, but were unsuccessful despite extensive trials.

2 Introduction

Cells in a multicellular organism all carry the same genetic information. Yet, morphological and functional heterogeneity are an indispensable preliminary to the evolution of complex life. How such divergence arises from the same genetic information is the subject of the cardinal question of molecular biology. The answer to this question lies in the way genetic information is processed.

The central dogma of molecular biology states that genetic information is stored stably in the form of genomic DNA, copied transiently in the form of RNA (transcription), and read and translated into proteins (translation), which make up the cell's repertoire of molecular effectors [1]. Differential regulation of processes along the flux of information from genes to proteins in response to environmental changes makes diversity possible.

2.1 Epigenetic regulation

To fit into the limited spatial confines of the eukaryotic nucleus, genomic DNA is wrapped around an octameric core of histone proteins, forming units called nucleosomes, which are further arranged into compact higher order structures [2]. DNA sequences buried within these structures are inaccessible to processing, and are thus silenced. This gives the cell the first means of regulatory control over the processing of genetic information. Various enzymes and structural proteins are involved in gene silencing. On the other hand, histone acetyl transferases (HATs) acetylate histone tails, neutralizing their charge, and weakening their interaction with DNA [3]. This primes nucleosomes for remodeling by specialized chromatin remodeling complexes, such as SWI/SNF, ISWI, CHD and INO80 family remodelers, that slide, eject or substitute nucleosomes in an ATP-dependent manner to create and maintain exposed genomic regions [4].

2.2 Transcription

Exposure of promoter regions allows transcription, the first step in the processing of genetic information, to take place. In this process, RNA is synthesized using genomic DNA as a template, catalyzed by DNA-dependent RNA polymerases [5]. These enzymes catalyze the formation of phosphodiester bonds between incoming ribonucleotides that have base-paired with an unwound DNA coding strand by a classical two-metal ion mechanism [6]. One magnesium ion present in the active center, and a second provided by the incoming nucleotide, are held in place during the catalysis reaction by conserved aspartate residues in the polymerase active site [6]. The first magnesium ion enhances the nucleophilicity of the 3' hydroxyl group of the last nucleotide of the growing RNA chain, thereby activating it for nucleophilic

attack on the α-phosphate of the incoming ribonucleotide triphosphate. The second magnesium ion stabilizes the pyrophosphate that results from the nucleophilic substitution reaction. As such, each new ribonucleotide is added to the 3' end of the pre-existing one, and the RNA chain is extended by repetition of the nucleotide addition cycle, as the polymerase translocates on the DNA template in a 5' to 3' direction.

Eukaryotes possess three DNA-dependent RNA polymerases that are highly conserved across species; RNA polymerase I transcribes the ribosomal RNA precursor (rRNA), RNA polymerase II transcribes messenger RNA (mRNA) from protein-coding genes, and RNA polymerase III transcribes transfer RNA (tRNA), and other small non-coding RNAs [7].

In this work, we focus on transcription of protein-coding genes by RNA polymerase II (RNAPII) and its associated processes. Yeast RNAPII is composed of 12 subunits designated Rpb1 to Rpb12. Structural characterization of RNAPII revealed four mobile elements; the core, shelf, clamp and jaw lobe elements; as well as a less tightly associated stalk (figure 2.1). Together, these elements form a deep cleft with the active site buried at its base. DNA enters from one side of the cleft, which can open or close by virtue of a large swinging motion of the clamp domain in the absence of the dissociable stalk, to accommodate the passage of DNA through it [8]. When the stalk is present, however, the clamp is wedged in place, and only single-stranded DNA can insert into the deeply buried active site [9]. Newly synthesized RNA exits the cleft through an opening between the wall and the clamp, and along the stalk protruding from the base of the clamp. Rpb1 and Rpb2 make up the catalytic cleft, Rpb4 together with Rpb7 make up the polymerase stalk, and Rpb9 is involved in RNA cleavage, whereas the remaining subunits serve scaffolding and stabilization roles [7].

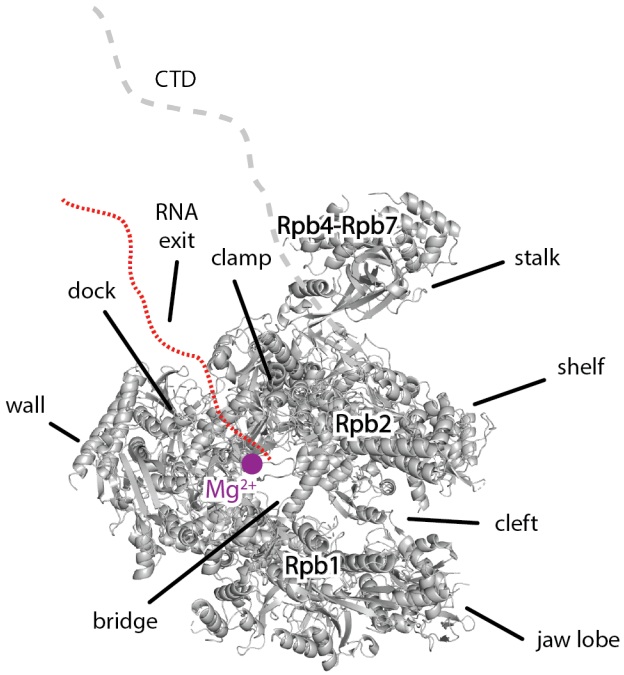

Figure 2.1 | Key aspects of the RNAPII structure.
Key structural elements of the RNA polymerase II (RNAPII) structure, which will be referred to in the course of this work are highlighted. The RNAPII structure shown here is from PDB ID: 5OQJ, with the other factors hidden.

2.2.1 The transcription cycle

RNAPII transcription commences at promoter regions and institutes a transcription cycle, which can be viewed in three distinct stages; initiation, in which RNAPII and its associated factors are positioned at the right place, DNA is opened, and transcription begins; elongation, in which the RNAPII extends its pre-mRNA product while migrating along the gene body, and coordinates the co-transcriptional processes of 5' capping and splicing into mature mRNA; and termination, in which the RNAPII encounters sequences that trigger cleavage and 3' polyadenylation of mRNA, and exonuclease digestion of the remaining RNAPII-associated RNA (figure 2.2). Post-translational modifications and an exchange of factors elicit the transitions from one stage to the next, and will be detailed in the following sections.

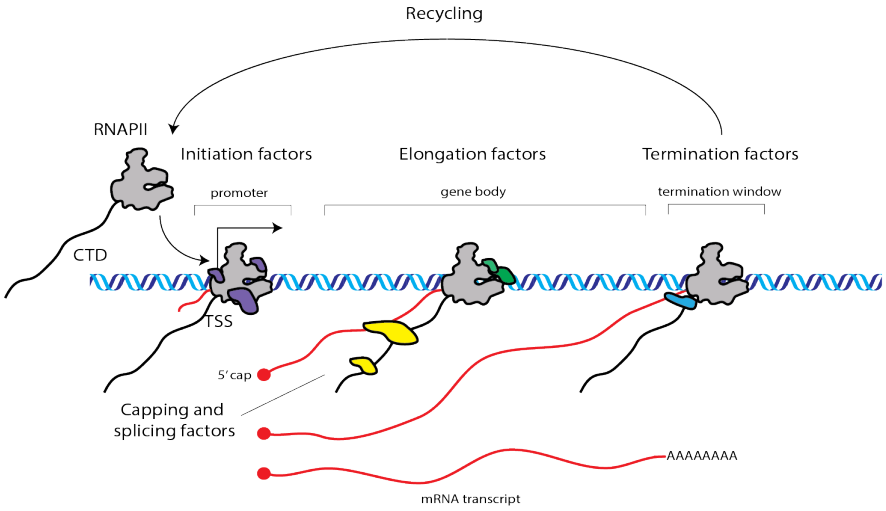

Figure 2.2 | The RNAPII transcription cycle.
The RNAPII transcription cycle beginning with the assembly of an initiation complex at promoters, elongation of the pre-mRNA transcript with concomitant capping and splicing, followed by polyadenylation and cleavage of the mature mRNA transcript.

2.2.2 The RNAPII CTD and transcriptional kinases

The largest subunit of RNAPII, Rpb1, has a long unstructured C-terminal domain (CTD), comprising a repetition of the seven amino acid consensus sequence Tyr1-Ser2-Pro3-Tyr4-Ser5-Pro6-Ser7 ($Y_1S_2P_3T_4S_5P_6S_7$). The number of tandem heptad repeats correlates to the complexity of the organism, with 26 repeats present in yeast, 44 in drosophila, and 52 in human [10]. The RNAPII CTD serves as a landing platform for transcription-associated factors.

Throughout the transcription cycle, the RNAPII CTD is subject to phosphorylation by transcriptional kinases, which orchestrate the binding and dissociation of factors with the elongating and terminating polymerase. Three cyclin-dependent kinases have been linked to transcription; Cdk7, Cdk8 and Cdk9. Their roles, targets, homologs, and the complexes they belong to are shown in table 2.1, and detailed in the following description.

Table 2.1 | **Transcriptional kinases.** An overview of the kinases involved in transcription, their homologs, targets and characterized functions.

Human kinase	Yeast homolog	CTD phosphorylation	Additional targets in transcription	Complex	Function
Cdk7(CycH)	Kin28 (Ccl1)	Ser5	Mediator subunits	Transcription Factor IIH (TFIIH)	Promoter escape – recruitment of capping factors and histone modifiers
Cdk8(CycC)	Srb10 or Ssn3 (Srb11 or Ssn8)	Ser5	Activators	Mediator Cdk8 kinase module (CKM)	Repression or activation of transcription at the initation step – not clear
Cdk9(CycT1)	Ctk1/Bur1 (Ctk2/Bur2)	Ser2	DSIF and NELF(mammals) Spt4/5 (yeast)	P-TEFb (mammals)	Phosphorylation of elongation factors – entry into late elongation. Pause-release in mammals.

After initiation, phosphorylation of the RNAPII CTD by Cdk7 at Ser5 instigates dissociation of the initiation complex and promoter escape [11]. Ser5-phosphorylated RNAPII CTD recruits the mRNA capping complex, which caps the 5' end of mRNA as it emerges from the RNAPII exit channel [12]. Additionally, this modification helps recruit the histone H3K4 methyl transferase Set1, which marks transcriptionally active genes [13]. As RNAPII elongates further downstream, Ser5 phosphorylation tapers, and is replaced by Ser2 phosphorylation [14]. On the one hand, a Ser5 phosphatase, Rtr1, removes phosphorylation from Ser5 [15]. On the other hand, Cdk9 in mammals [16], or Ctk1 and Bur1 in yeast [17], are recruited to Ser5-phosphorylated CTD and the capping complex, respectively, and deposit phosphorylation on Ser2. Additionally, the mammalian and yeast kinases phosphorylate the elongation factors DRB-sensitivity factor (DSIF) and Spt4/5, respectively, prompting the transition into late elongation. In metazoans, after transcribing 20 to 100 nucleotides, elongating RNAPII pauses due to the binding of the Negative Elongation Factor (NELF). Coordinated release from this pause into productive elongation provides an additional level of regulatory control, not present in lower eukaryotes. Cdk9 additionally phosphorylates NELF and alleviates this pause in response to the appropriate signal [16].

Cdk8 phosphorylates the RNAPII CTD at the initiation stage at Ser5, but its role remains unclear. Conflicting reports have indicated repressive [18], and activating [19] effects of the Cdk8 kinase phosphorylation of the RNAPII CTD redundant with Cdk7. *In vitro,* Cdk8 can substitute for Cdk7, and inhibition of both Cdk7 and Cdk8 *in vivo* is required for maximal transcription inhibition [19].

RNAPII has been observed in granules that distribute throughout the nucleus. Recent studies have shown that the RNAPII CTD is responsible for the formation of these condensates, and that the size and stability of these condensates correspond

to the number of CTD heptad repeats [20]. Moreover, Cdk7 phosphorylation of the RNAPII CTD releases it from these condensates, suggesting a possible mechanism by which Cdk7 phosphorylation of the RNAPII CTD results in promoter escape.

2.2.3 Transcription initiation

On its own, RNAPII is not able to complete a transcription reaction from a DNA template. Rather, it requires assistance from associated factors that help it find the position to initiate transcription, unwind DNA, translocate, and maintain an open transcription bubble. Seminal studies in the early 1990s identified the minimal set of factors needed to reconstitute transcription *in vitro* as the five factors now known as TBP, TFIIB, TFIIF, TFIIE and TFIIH [21]. These factors, together with TFIIA, and the Mediator complex, which were identified later, are called general transcription factors (GTFs). The roles that these factors play are described in the following sections, introduced in the order of their recruitment. Structural characterization (figure 2.3) of all the intermediates of initiation complex assembly has made it possible to visualize transitions at a formidable level of detail, and to rationalize biochemically observed functions of transcription factors [22]. Resource table 2.2 summarizes all the factors involved in canonical transcription initiation, their subunit composition and their roles.

TBP

Transcription initiation complex assembly begins when TBP (TATA-box binding protein) binds to TATA or TATA-like elements in the genome [23]. TBP has a saddle-shaped structure, with a hydrophobic inner surface. Insertion of a β-sheet into the minor groove of its DNA recognition element widens the minor groove resulting in a 90° bend of the DNA, which is stabilized by intercalation of two TBP aromatic residues at the edges [24]. TBP is a subunit of the GTF TFIID (transcription factor IID), but can also function without the rest of the roughly 1.2 MDa TFIID complex.

TFIIA

TFIIA (transcription factor IIA) is not an essential GTF, but can stabilize the TBP-DNA interaction [25], by contacting DNA upstream of the TATA element, and the lower side of the TBP saddle [26].

TFIIB

Next, TFIIB (transcription factor IIB) binds to the TBP-DNA complex. The C-terminal part of TFIIB, called the B-core, and the N-terminal part, called the B-ribbon, play roles in stabilization of the TBP-DNA interaction, and RNAPII recruitment, respectively [27]. Oriented recognition by the B-core of B-recognition DNA elements

(BREs) upstream and downstream of the TATA-box may explain the directionality in the initiation complex assembly even though the TBP-DNA complex is pseudo-symmetrical [28]. The B-ribbon interaction with the dock domain of RNAPII tethers it to the TBP-DNA-TFIIB complex and facilitates its recruitment [29].

Upon RNAPII recruitment, a long linker region connecting the B-core and the B-ribbon of TFIIB is threaded through the RNAPII cleft [30]. The structure of the RNAPII-TFIIB complex revealed that, in the RNAPII cleft, the TFIIB linker forms two distinct elements; the B-reader and the B-linker elements. Whereas the B-linker helps to open DNA for insertion of single-stranded coding DNA into the RNAPII cleft, the B-reader helps to position this DNA for initiation of RNA synthesis, recognize the transcription start site (TSS), and then separates newly synthesized RNA from DNA after the addition of the 6th nucleotide, and directs it to the RNA exit channel [31].

TFIIF

RNAPII is recruited together with TFIIF (transcription factor IIF), which plays a role in stabilization of RNAPII and TFIIB in the PIC [32] and TSS selection [33]. TFIIF is composed of two conserved subunits (Tfg1 and Tfg2), and an additional one that is only present in yeast (Tfg3), which is not essential. Tfg1 and Tfg2 each have a dimerization domain, together constituting a dimerization module, which binds to the RNAPII protrusion. Both subunits additionally have a winged helix domain. The Tfg2 winged helix contacts DNA near the RNAPII cleft, as well as the B-ribbon of TFIIB, explaining its role in the TFIIB-RNAPII complex stabilization. On the other hand, the Tfg1 subunit extends into the RNAPII cleft, corresponding to its role in TSS recognition.

TFIIE

TFIIE (transcription factor IIE), is composed of two subunits, and binds the RNAPII clamp domain. Its main function is to recruit the TFIIH [22].

TFIIH

TFIIH (transcription factor IIH) is a 10-subunit complex composed of the translocase Ssl2 (XPB in human), the helicase Rad3 (XPD in human), the three-subunit kinase module Kin28-Ccl1-Tfb3 (CDK7-cyclin H-MAT1 in human) and other structural subunits [34]. TFIIH adopts a horse-shoe shaped structure, contacting TFIIE via Tfb3-Rad3, and downstream DNA via one of the two lobes of its translocase subunit Ssl2, pushed into place by two TFIIE helices on an extended loop [35]. The ATPase Ssl2 is proposed to open DNA by ATP-dependent ratcheting of its DNA-bound lobe against the second lobe, which is anchored in place within the rest of the TFIIH

structure. The main role of TFIIH is to open promoters by virtue of its ATPase [36], and to phosphorylate the RNAPII CTD resulting in promoter escape [37]. Although AT-rich promoters can spontaneously open *in vitro*, the majority require TFIIH *in vivo* [38]. This may be due to chromatinization, which is frequently absent in *in vitro* studies. Additionally, TFIIH has a function in DNA repair, unrelated to transcription [39].

Structure of the transcription Pre-initiation complex (PIC)

The complex of TBP, TFIIA, TFIIB, RNAPII and TFIIF on promoter DNA is called the core pre-initiation complex (core PIC or cPIC). Addition of TFIIE and TFIIH results in the pre-initiation complex (PIC). Before promoter DNA opening (if ATP is not added and the promoter is GC-rich), this is called a closed PIC, whereas a PIC with an open DNA bubble is called an open PIC. A PIC with an open bubble that has started to transcribe, thus contains a DNA-RNA hybrid with a short RNA chain is called an initially transcribing complex (ITC). Following the same pattern, an ITC that lacks TFIIE and TFIIH is called a core ITC (cITC).
Figure 2.3 shows the described complexes, 25 years in the making, from the first crystal structure of DNA-bound TBP, to the cryo-EM structure of a complete yeast PIC. Shown in this figure is the final structure of the complete yeast PIC [35], successively revealing different factors in the sequence of their recruitment, meant as a schematic visual aid, and not the true structures of intermediates that were solved over the years. Nevertheless, the structures of factors within the PIC and the intermediates in the PIC assembly process are highly resemblant.

When we started this study, TFIIH was not available, and therefore, what we refer to as a PIC in the following sections, is actually the cPIC plus TFIIE. This should be noted for all further analysis.

Table 2.2 | **Canonical transcription initiation factors.** CTD, C-terminal domain; NA, not available; Pol, RNA polymerase; TAF, TBP-associated factor; TBP, TATA-box-binding protein; TFIIA, transcription initiation factor IIA; TSS, transcription start site. * Archaeal homologue. ‡ Factor shared between Pol I, Pol II, and Pol III. § No known archaeal homologue. ǁ Component of TFIID, TFIIF and chromatin remodeling complexes. ¶ Approximate molecular weight. # TFG3 is a component of TFIID, TFIIF and chromatin remodeling complexes; the yeast-specific subunit is non-essential as part of TFIIF and as part of TFIID [22]

Factor	Gene name		Mass (kDa)	
	Yeast	Human	Yeast	Human
Pol II (RNAP*): transcribing enzyme				
RPB1	*RPO21*	*POLR2A*	191.1	217.2
RPB2	*RPB2*	*POLR2B*	138.8	133.9
RPB3	*RPB3*	*POLR2C*	35.3	31.4
RPB4	*RPB4*	*POLR2D*	25.4	16.3
RPB5‡	*RPB5*	*POLR2E*	25.1	24.6
RPB6‡	*RPO26*	*POLR2F*	17.9	14.5
RPB7	*RPB7*	*POLR2G*	19.1	19.3
RPB8‡	*RPB8*	*POLR2H*	16.5	17.1
RPB9	*RPB9*	*POLR2I*	14.3	14.5
RPB10‡	*RPB10*	*POLR2L*	8.3	7.6
RPB11	*RPB11*	*POLR2J*	13.6	13.3
RPB12‡	*RPB12*	*POLR2K*	7.7	7.0
Total (12 subunits)			513.6	516.7
TFIIA§: TBP stabilization and counteracts repressive effects of negative co-factors				
Large subunit	*TOA1*	*GTF2A1*	32.2	41.5
Small subunit	*TOA2*	*GTF2A2*	13.5	12.5
Total (2 subunits)			45.7	54.0
TFIIB: Pol II recruitment, TBP binding and TSS selection				
TFIIB (TFB*)	*SUA7*	*GTF2B*	38.2	34.8
TFIID: Pol II recruitment and promoter recognition				
TBP (TBP*): recognition of the TATA box	*TBP*	*TBP*	27.0	37.7
TAF1	*TAF1*	*TAF1*	120.7	212.7
TAF2	*TAF2*	*TAF2*	161.5	137.0
TAF3	*TAF3*	*TAF3*	40.3	103.6
TAF4	*TAF4*	*TAF4*	42.3	110.1
TAF5	*TAF5*	*TAF5*	89.0	86.8
TAF6	*TAF6*	*TAF6*	57.9	72.7
TAF7	*TAF7*	*TAF7*	67.6	40.3
TAF8	*TAF8*	*TAF8*	58.0	34.3
TAF9	*TAF9*	*TAF9*	17.3	29.0
TAF10	*TAF10*	*TAF10*	23.0	21.7
TAF11	*TAF11*	*TAF11*	40.6	23.3
TAF12	*TAF12*	*TAF12*	61.1	17.9
TAF13	*TAF13*	*TAF13*	19.1	14.3
TAF14ǁ	*TAF14*	*NA*	27.4	NA
Total (14 – 15 subunits)			1,200¶	1,300¶
TFIIE: recruitment of TFIIH and open DNA stabilization				
TFIIEα (TFE*)	*TFA1*	*GTF2E1*	54.7	49.5
TFIIEβ	*TFA2*	*GTF2E2*	37.0	33.0
Total (2 subunits)			91.7	82.5
TFIIF§: TSS selection and stabilization of TFIIB				
TFIIFα	*TFG1*	*GTF2F1*	82.2	58.2
TFIIFβ	*TFG2*	*GTF2F2*	46.6	28.4
TFG3#	*TAF14*	*NA*	27.4	NA
Total (2 – 3 subunits)			156.2	86.6

Factor	Gene name		Mass (kDa)	
	Yeast	Human	Yeast	Human
TFIIH§ (core): promoter opening and DNA repair				
Subunit 1 (p62)	*TFB1*	*GTF2H1*	72.9	62.0
Subunit 2 (p44)	*SSL1*	*GTF2H2*	52.3	44.4
Subunit 3 (p34)	*TFB4*	*GTF2H3*	37.5	34.4
Subunit 4 (p52)	*TFB2*	*GTF2H4*	58.5	52.2
Subunit 5 (p8)	*TFB5*	*GTF2H5*	8.2	8.1
XPD subunit: ATPase; DNA repair	*RAD3*	*ERCC2*	89.8	86.9
XPB subunit: ATPase; promoter opening	*SSL2*	*ERCC3*	95.3	89.3
Total (7 subunits)			414.5	377.3
TFIIH (kinase module): CTD phosphorylation				
Cyclin H	*CCL1*	*CCNH*	45.2	37.6
CDK7	*KIN28*	*CDK7*	35.2	39.0
MAT1	*TFB3*	*MNAT1*	38.1	35.8
Total (7 subunits)			118.5	112.4

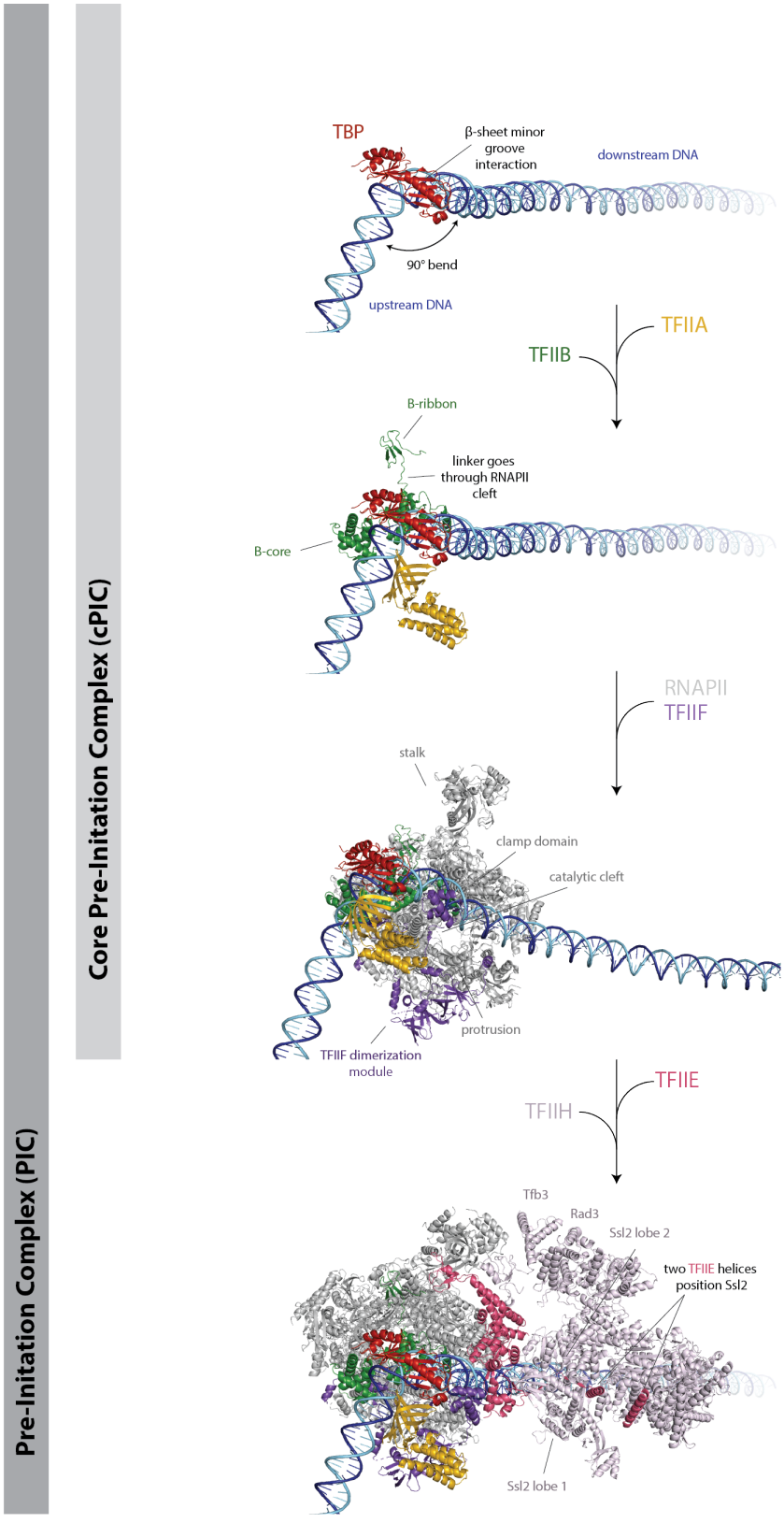

Figure 2.3 | Assembly of the Pre-Initation Complex.
The order of assembly of factors in the transcription Pre-Initiation Complex (PIC) is shown. Additionally, notable interactions of general transcription factors (GTFs) which relate to their function are highlighted.
All structures shown in this figure are derived from the structure of the complete S.cerevisiae PIC structure, PDB ID: 5OQJ.

Architecture of promoters

The genomic sites at which polymerases and associated factors assemble to initiate transcription are called promoters. The core promoter is defined as “the minimal DNA element required for basal transcription” [40]. Characteristic sequence elements distinguish core promoters; the TATA-box element is the recognition site for TATA-box binding protein (TBP); the initiator (INR) – which contains the transcription start site (TSS), the motif 10 element (MTE) and the downstream promoter element (DPE), together called the downstream core element (DCE) are additional recognition sites of the co-activator TFIID; and upstream and downstream TFIIB recognition elements (BRE_u and BRE_d) are recognition sites for the GTF TFIIB (found in higher eukaryotes). In TATA-containing promoters, TBP nucleates the assembly of the transcription pre-initiation complex (PIC), and this places the RNAPII active sites roughly 30 base pairs from the TATA element. In metazoans, this is the transcription start site (TSS) [41]. However, in yeast, the RNAPII scans 50 to 120 base pairs downstream of the TATA element before it initiates from a preferred AT-rich consensus sequence [42]. When fully assembled, the PIC covers approximately 60 base pairs of promoter DNA. Promoters occur in nucleosome-depleted regions (NDRs), which span roughly 140 base pairs of naked DNA, bounded by +1 and -1 nucleosomes [43]. The architecture of core promoters is schematically depicted in figure 2.4. adapted from [22].

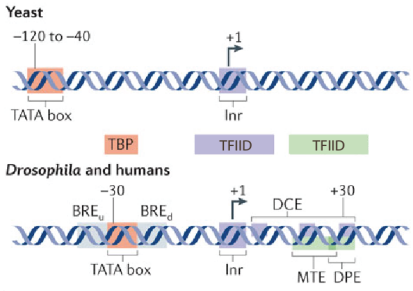

Figure 2.4 | Architecture of core promoters. Schematic depiction of core promoters in yeast and human, highlinghting characteristic DNA sequence elements. The TATA box binds TBP, BREs bind TFIIB and the Inr and the DCE contain TFIID binding sites. Transcription starts at the Inr.

2.2.4 Transcription activation

While possible *in vitro* from a DNA template, basal transcription does not occur *in vivo.* Virtually all RNAPII transcription *in vivo* is activated, and requires the binding of gene-specific transcription activators to DNA elements found upstream of promoters, known as upstream activation sequences (UASs) [44]. This is likely due to chromatinization, making the default state of genes "off" unless activated.

Architecture of upstream activation sequences (UASs)

UASs contain one or multiple recognition motifs for different transcription activators, and often allow for combinatorial control of gene activation. In yeast UASs are usually present within nucleosome-depleted regions (NDRs), or displayed on the surface of nucleosomes [45]. In human, UASs are called enhancers, and can operate from both 5' and 3' or promoters, whereas in yeast, they can only function if present on the 5' side [44].
UASs communicate with promoter regions by looping, and can thus achieve spatial proximity despite being remotely located on a linear DNA sequence [46]. Structural proteins, such as cohesin, support loop formation.

Transcription activators

The yeast genome database Yeastract [47] reports 118 defined transcription factors in the yeast genome. Transcription factors are characteristically modular, and often contain structurally and functionally distinct DNA-binding domains (DBDs) and activation domains (ADs). Based on their DNA binding domains, they can be classified into three main classes: zinc-stabilized, helix-turn-helix and zipper type [44]. The zinc-binding type can be further divided into; C2H2 zinc fingers, in which tetrahedral coordination of a zinc ion by two Cys and two His residues stabilizes the DBD; C6 zinc knuckles in which coordination of two zinc ions by six Cys residues stabilizes the DBD; and C4 or GATA type in which tetrahedral coordination by Cys residues stabilize the DBD. The zipper type include bZIP or leucine zippers, in which hydrophobic interaction between several Leu residues is involved in homodimerization of the DBD, and the bHLH type in which two amphipathic helices often result in heterodimerization [44]. Structures of representatives from each class, adapted from [44], are shown in figure 2.5 (adapted from [44]). The histidine deficiency response activator general control protein 4 (Gcn4), which we have used as a model in this study, is of the bZIP (leucine zipper) type.

Because of their modular nature, chimeras of DBDs of various factors with the very potent viral AD VP16, have often been employed as tool to study gene activation from various UASs [48].

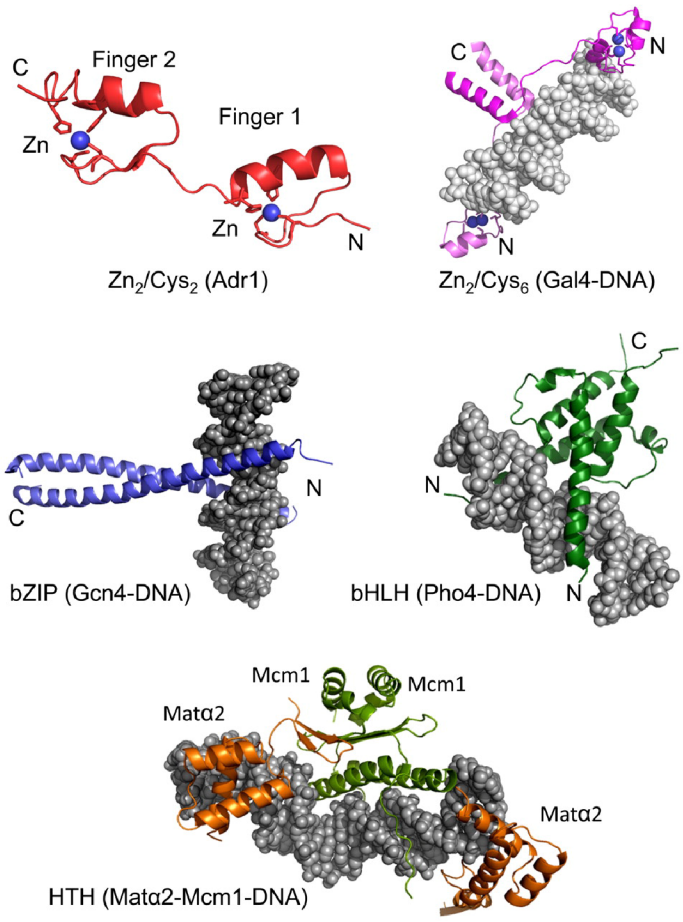

Figure 2.5 | Examples of DNA binding domains (DBDs) from different transcription activators. Representatives of transcription activators from the three types; zinc-stabilized, leucine zipper and the helix-turn-helix type are shown. Figure adapted from S.Hahn,2011.

Mechanism of activator function

The commonly accepted mechanism of activator function is physical recruitment. This is based on the observation that more coactivators, RNAPII and GTFs were found on genes upon gene induction [49],[50],[51]. Recently, several transcription activators have been shown to undergo liquid-liquid phase separation by virtue of their disordered activation domains, and this has been proposed as a general mechanism for transcription activation [52].

Transcription coactivators

Before PIC assembly, UAS-bound activators recruit huge multisubunit coactivator complexes called TFIID and SAGA (Spt–Ada–Gcn5 acetyltransferase), which are both responsible for delivering TBP to promoters to nucleate PIC assembly [53].

TFIID is made up of TBP and 14 TBP-associated factors (TAFs), which hold together via highly recurrent histone fold domains. TFIID binds promoters at elements upstream and downstream of the TBP binding site forming an arched structure, and the mechanism by which it deposits TBP remains unknown [54]. Moreover, whether coactivators deposit TBP to recruit PIC factors, and leave, or whether they remain bound and perform downstream functions in the PIC assembly progression awaits elucidation. One possibility is that the TFIID arch extends over the PIC and is therefore a part of the PIC structure.

The composition of SAGA is highly similar to that of TFIID, sharing a lot of the same TAF subunits, although it associates TBP less tightly [55]. Additionally, SAGA contains a histone acetyl transferase (HAT) subunit called Gcn5, which participates in gene activation by priming chromatin remodeling to deplete nucleosomes from downstream promoter regions.

SAGA binds at TATA-containing promoters, which make up only 20% of the yeast coding genome and are generally found at regulated, stress responsive genes. On the other hand, TFIID binds the majority of promoters, which lack a TATA element, and contain TATA-like AT-rich elements instead [56]. The exact roles of TFIID and SAGA, and the events that occur at activating sequences before PIC assembly are among the biggest open questions in transcription initiation. They have remained thus far elusive in part because they are mediated by huge, multisubunit complexes that are not straightforward to isolate, and in part because these events are frequently governed by “fuzzy” unstructured micromolar-affinity interactions, making them challenging to capture.

The Mediator complex

Contrary to what was observed *in vivo,* UAS-bound activators failed to stimulate transcription by purified PIC components from a DNA template *in vitro*, indicating that there is a missing component [57]. A tour-de-force of genetics and biochemistry in the 1990s led to the identification of this missing component, when an activity was isolated that rendered purified PIC components responsive to stimulation by transcription activators [58]. Genetic screening contemporaneously identified this activity as belonging to a group of RNAPII CTD-interacting genes [59],[60]. This activity, which mediates between activators and the PIC, was thereafter fittingly named the “Mediator”.

Mediator acts universally on all protein-coding genes [61], and is a huge complex composed of 25 subunits in yeast, and 30 subunits in human [62]. The function and composition of Mediator are depicted in figure 2.6. The subunit composition is detailed in resource table 2.3. Early studies of its structural and functional

architecture allowed the distinction of four modules; the head, the middle, the tail and the kinase modules. Whereas the head and middle modules, together called the core Mediator (cMed), are essential for viability in yeast, the tail and kinase modules are not [63]. This means that, inasmuch as it is essential for general transcription, Mediator is a GTF, whereas its interaction with activators additionally gives it a coactivator function. The GTF function can be pinned down to the head and middle modules (cMed), while the tail module is responsible for the majority of Mediator-activator interactions in yeast [63].

Mediator conveys the activation signal from UAS-bound activators to the PIC by Mediator-dependent stabilization of the PIC, and stimulation of the activity of the TFIIH kinase (by up to 12 times *in vitro*), resulting in RNAPII CTD phosphorylation and promoter escape [57].

Table 2.3 | **Subunit composition of the Mediator complex.** * Metazoan specific subunits. ¶ Approximate molecular weight.

Factor	Gene name		Mass (kDa)	
	Yeast	Human	Yeast	Human
Head module				
MED6	*MED6*	*MED6*	32.8	28.4
MED8	*MED8*	*MED8*	25.2	29.1
MED11	*MED11*	*MED11*	13.3	13.1
MED17	*SRB4*	*MED17*	78.5	72.9
MED18	*SRB5*	*MED18*	34.3	23.7
MED20	*SRB2*	*MED20*	22.9	23.2
MED22	*SRB6*	*MED22*	13.9	22.2
MED28*	-	*MED28*	-	19.5
MED30*	-	*MED30*	-	20.3
Total (7 / 11 subunits)			220.8	252.4
Middle module				
MED1	*MED1*	*MED1*	64.3	168.5
MED4	*MED4*	*MED4*	32.2	29.7
MED7	*MED7*	*MED7*	25.6	27.2
MED9	*CSE2*	*MED9*	17.4	16.4
MED10	*NUT2*	*MED10*	17.9	15.7
MED19	*ROX3*	*MED19*	24.9	26.3
MED21	*SRB7*	*MED21*	16.1	15.6
MED31	*SOH1*	*MED31*	14.7	15.8
MED26*	-	*MED26*	-	65.4
Total (8 / 9 subunits)			213.1	380.6
Tail module				
MED2 / MED29	*MED2*	*MED29*	47.7	21.1
MED3 / MED27	*PGD1*	*MED27*	43.1	35.4
MED5 / MED24	*NUT1*	*MED24*	128.8	110.3
MED14	*RGR1*	*MED14*	123.4	160.6
MED15	*GAL11*	*MED15*	120.3	86.8
MED16	*SIN4*	*MED16*	111.3	96.8
MED23 *	-	*MED23*	-	156.5
MED25 *	-	*MED25*	-	78.2
Total (6 subunits)			574.6	745.7

Factor	Gene name		Mass (kDa)	
	Yeast	Human	Yeast	Human
Kinase module				
MED12 / MED12 or MED12L	*SRB8*	*MED12 or MED12L*	166.9	243.1 or 240.1
MED13 / MED13 or MED13L	*SSN2*	*MED13 or MED13L*	160.0	239.3 or 242.6
CDK8 / CDK8 or CDK19	*SSN3*	*CDK8 or CDK19*	62.8	53.3 or 56.8
CycC	*SSN8*	*CCNC*	37.8	33.2
Total (4 subunits)			427.5	570.8¶

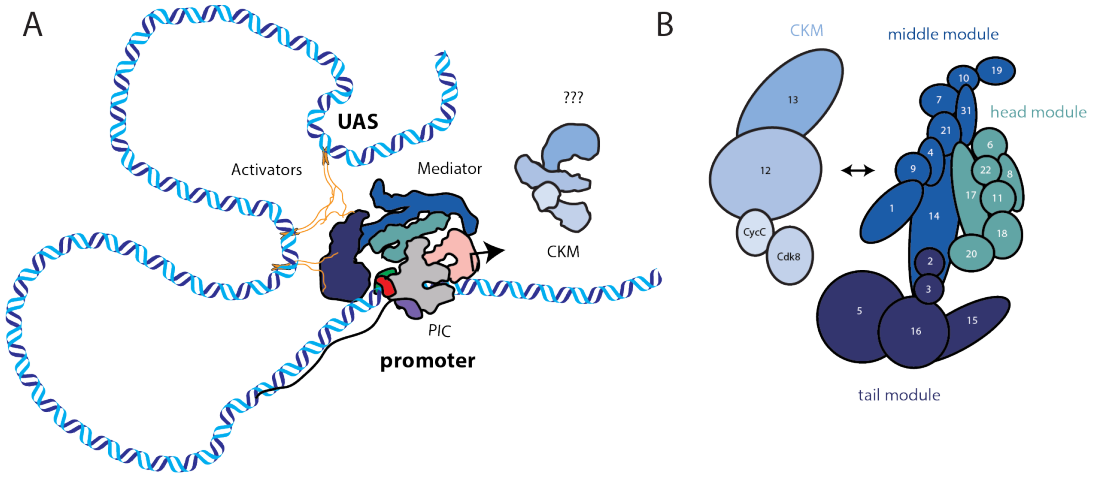

Figure 2.6 | Function and composition of the Mediator complex.
A, A cartoon depiction of Mediator function, bridging between activators at UASs and the assembled transcription machinery at promoters, to relay the activation signal. B, Composition of the Mediator complex. Numbered (#) subunits are named "Med#".

Mediator structural biology

Owing to its large size, flexibility and laborious preparation, attaining a high-resolution structure of the Mediator complex is still an ongoing endeavor, more than two decades after its first two-dimensional EM projection map [64]. Since then, a modular approach has been undertaken, solving piece by piece of the Mediator structure puzzle. Initially, single subunit structures and binary subunit interactions were solved [65]. More recently, the first structure of a complete Mediator module was demonstrated when the *S.pombe* head module structure was solved [66],[67]. Soon after, the crystal structure of the complete *S.pombe* core Mediator was solved at atomic resolution [68]. This structure allowed the accurate delineation of subunit assignment to the different modules, and illuminated the role of the long scaffolding subunit Med14, which traverses the length of Mediator, and acts as a backbone connecting the head, middle and tail modules together. Notably, the *S.pombe*

Mediator naturally lacks a tail module. Figure 2.7 shows a homology model of the *S.cerevisiae* cMed derived from the abovementioned structure, which we will use throughout this work for modeling different interactions. Structural elements that will be referred to later are also indicated.

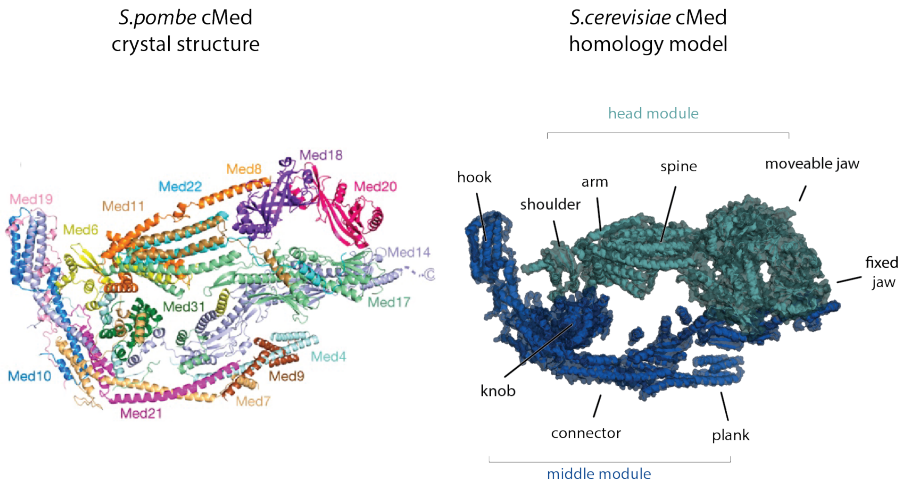

Figure 2.7 | Core Mediator (cMed) structure.
Left, crystal structure of *S.pombe* cMed allowed accurate identification of subunits and their locations (PDB ID: 5N9J). Right, homology model of *S.cerevisiae* cMed based on *S.pombe* structure, with key structural elements indicated.

Cryo-EM structures of free and RNAPII-bound *S.pombe* Mediator demonstrated a dramatic structural rearrangement that occurs upon binding [69]. Moreover, cryo-EM structures of the PIC-bound [35],[70] and cITC-bound cMed [71] uncovered the nature of the interaction of Mediator with the transcription initiation machinery and shed light on the GTF aspect of its function. Although not seen in these structures, the location of cMed indicates that it is positioned to possibly interact with the TFIIH kinase module, and thereby stimulate its activity. Moreover, together with the remainder of TFIIH, the Mediator hook domain creates a gulf that can cradle the RNAPII CTD and direct it towards the TFIIH kinase [35]. cMed interacts with RNAPII at two main interaction hubs; between the arm/spine of the cMed head module and the Rpb4/7 stalk of RNAPII, and between the moveable jaw of the cMed head module (Med18/Med20 heterodimer) and the dock of RNAPII (figure 2.8). Additionally, there is a transient interaction between the mobile plank of the cMed middle module and the foot of RNAPII.

Although the Mediator-PIC interaction has been extensively characterized, comparatively little is known about the other end of the PIC-Mediator-activator bridge. Whereas cMed is highly structured, disorder prevails in the activator-interacting tail module [72]. 118 annotated transcription activators in the yeast genome, means that the Mediator tail has *at least* 118 interaction partners. Disorder, which allows for sequence degeneracy, may be nature's economic solution to this problem, allowing the evolution of malleable interactions with a plethora of

unstructured activation domains. Indeed, this structural plasticity is a conserved part of Mediator function [73]. The ability of the mediator tail subunit Med15 to undergo liquid-liquid phase separation with the activation domains of various interaction partners is further testament to that [52].

The Mediator kinase module

The dissociable Cdk8-kinase module (CKM) of Mediator was identified in the same genetic screen for RNAPII CTD interactors as the other Mediator subunits, and co-purifies with them in some preparations [74]. Likewise, only a subpopulation of Mediator contains CKM *in vivo* [61]. Even though it is composed of only four subunits, the CKM is about the same size as cMed, and makes up almost a third by mass of the full Mediator complex. The CKM contains the kinase/cyclin pair Cdk8/CycC, which is the only catalytic activity within the Mediator complex [75],[76].

Like the other transcriptional kinases, Cdk8 phosphorylates the CTD of RNAPII [19]. Unlike the TFIIH kinase Cdk7, however, this is thought to be a repressive effect, occurring prior to PIC assembly [18]. Cdk8 additionally phosphorylates the activators Gcn4, Msn2, Phd1 and Ste12, resulting in their increased turnover, supporting the idea of its role as a repressive molecule [77]. On the other hand, it is required for complete activation of the activators Gal4, Skn7 and Sip4, contradicting that idea [77]. It has also been found to both activate and repress gene transcription in human [78].

Biochemical studies in human implicated a kinase-independent repression of transcription *in vitro* [79]. Recent reports have indicated that the CKM is not found on promoter sequences, but is found at UASs, as opposed to other Mediator subunits, which are found at both [80]. Although generally construed as repressive, counteracting the effect of Mediator, the exact role that the CKM plays is the subject of longstanding controversy.

The structure of the CKM and the CKM-Mediator are among the biggest open questions in transcription initiation. So far, the crystal structure of Cdk8/CycC from human has been solved [81], as a low-resolution map of the *S.cerevisiae* CKM is available [82], but there are no medium or high resolution structures of either complex.

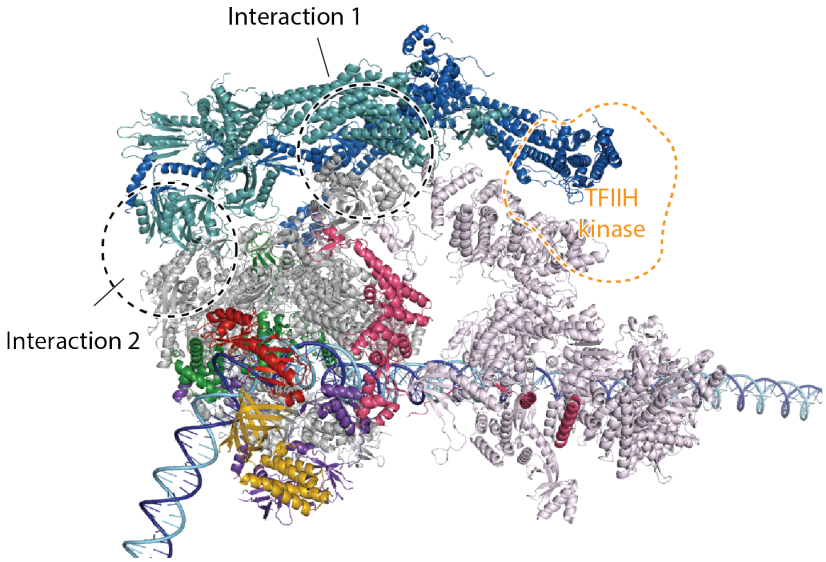

Figure 2.8 | Core Mediator (cMed) interaction with the PIC.
The cMed-PIC (PDB ID: 5OQM) structure shows interactions between the cMed arm and spine of the head module and the RNAPII stalk (interaction 1), as well as between the head moveable jaw and the RNAPII dock (interaction 2). The cMed hook domain is positioned in close proximity to TFIIH, where the TFIIH kinase is putatively present, showing that cMed-dependent stimulation of the TFIIH kinase may be effected by direct contact.

Phase separation

The observation that cells can concentrate proteins in membraneless compartments led to the rise of phase separation as a concept for the organization of cellular biochemistry, by confining reactions in liquid droplets that have phase separated from the cytoplasm [83]. These droplets are characterized by thermodynamic reversibility and are often composed of proteins of low sequence complexity. Various interactions are possible to maintain these droplets, including both structured and unstructured interactions, stabilized by electrostatic or hydrophobic contacts, between one or multiple proteins [84]. Cells can regulate the degree to which proteins phase separate by expending energy to pay off the entropic cost of their local enrichment, or by tuning post-translational modifications (PTMs), such as phosphorylations and methylations, which alter the solubility, affinity and valency of phase separating molecules.
In recent years, *in vitro* phase separation studies have emerged as a tool to study intrinsically disordered proteins, and learn about factors that may influence the behavior of phase-separating proteins and nucleic acids in the cell.

Components of transcription, such as the CTD of RNAPII [20], several Mediator subunits [85],[86], and transcription activators have been shown to undergo liquid-liquid phase separation in cells [52], and that this property relates to their characterized functions.

2.3 Aims of this study

The fundamental components of the transcription machinery are well understood. However, how this machinery is regulated in response to signaling remains largely obscure. Understanding gene regulation hinges on understanding the events that precede the assembly of transcriptional complexes. These include binding of activators to UASs, recruitment of coactivators, and signal transduction to the central transcription machinery.

Here, we aimed to understand the role that the Cdk8 kinase module (CKM) of the Mediator complex plays in transcription regulation; what complexes does it partake in, what are its phosphorylation targets, how does it interact with the rest of the Mediator complex, how does it affect transcription activators, and what does that mean about its enigmatic function. Furthermore, we aimed to solve the structures of the CKM and the CKM-cMed complex by cryo-electron microscopy to elucidate the nature of its interaction with Mediator, with the aim of deriving mechanistic insights from that.

To make that possible, we first needed to establish a recombinant expression and purification system for the *S.cerevisiae* CKM. After extensive trials, we successfully set up a novel method for its production, which is scalable and yields sufficient material of high quality for both functional and structural studies.

Using a combination of biochemical and structural techniques, we aimed to dissect the binding of CKM to the PIC and cMed. We set up exploratory phosphoproteomics studies to discover new targets of the CKM within the transcription machinery, and provided putative meanings for these phosphorylations using *in vitro* phase separation studies. Our findings will be presented in the following sections. From our data, we were able to venture a new model for CKM function. We were not successful at solving the structures of CKM or CKM-cMed. The outcomes of our trials and future directions will be presented in the next sections.

3 Materials

3.1 Vectors

Table 3.1 | **Vectors used in this study.** A compilation of the vectors used for cloning, which form the vector backbones of all recombined plasmids used in this study.

Plasmid	Source/vendor	Selection	Expression Host	Addgene number
438-A/B/C	Scott Gradia/ QB3 MacroLab	Amp Gen	Insect cells	55218 55219 55220
1B/C	Scott Gradia/ QB3 MacroLab	Kan	*E.coli* T7	29653 29654
pOPINE	Ray Owens/ In-Fusion	Amp	*E.coli* T7	26043
pET21	EMD Biosciences	Amp	*E.coli* T7	69741
pCOLADuet	Novagen(EMD Millipore)	Kan	*E.coli* T7	71406
pCDFDuet	EMD Biosciences	Strep	*E.coli* T7	71340
pETDuet	EMD Biosciences	Amp	*E.coli* T7	71146
pET28b	EMD Biosciences	Kan	*E.coli* T7	69865
pAHS3C	modified pET21	Amp	*E.coli* T7	[87]
6B	Scott Gradia/ QB3 MacroLab	Amp Neo	Mammalian	30125
mEGFP	Karel Svoboda/ ADDGENE	Amp	Mammalian	18696

3.2 Recombined plasmids

Table 3.2 | **Plasmids used in this study.** A compilation of all recombinant plasmids used, describing the genes they contain, fusion tags and their locations, linkers and vector backbones.

Factor/gene(s)	Residues	Tag	Vector	Selection	Source
CKM(A)/ *Sc*Med12 *Sc*Med13 *Sc*Cdk8 *Sc*CycC	1-1427 1-1420 1-555 1-323	- - N-His(x6)-MBP-TEV -	438-A	Amp Gen	this study
CKM(KD)/ *Sc*Med12 *Sc*Med13 *Sc*Cdk8(D286A) *Sc*CycC	1-1427 1-1420 1-555 1-323	- - N-His(x6)-MBP-TEV -	438-A	Amp Gen	this study
*Sc*Gcn4	1-281	N-His(x6)-thrombin	pET28b	Kan	H.Wang
mEGFP-Gcn4/ *Sc*Gcn4	1-281	N-His(x6)-TEV	1B	Kan	this study
mCherry-Med15/ *Sc*Med15	6-651	N-His(x6)-TEV	1B	Kan	this study
Med15_KIX123/ *Sc*Med15	1-238, 273-372, 484-651	N-His(x6)-MBP-N(x10)-TEV	1C	Kan	this study
TFIIA/ *Sc*Toa1(CO) *Sc*Toa2(CO)	1-94, 210-286 1-122	- C-His(x6)	pOPINE	Amp	[71]
*Sc*TBP	1-240	-	pOPINE	Amp	[71]
*Sc*TFIIB	1-345	C-His(x6)	pOPINE	Amp	[71]
TFIIF/ *Sc*Tfg1(CO) *Sc*Tfg2	1-735 1-400	N-His(x10)-Arg(x8)-SUMO-3C -	pAHS3C	Amp	[71]
TFIIE/ *Sc*Tfa1 *Sc*Tfa2	1-482 1-328	- C-His(x6)	pET21	Amp	[71]

Factor/gene(s)	Residues	Tag	Vector	Selection	Source
Med1,4,9/					
*Sc*Med1	1-566	N-His(x10)-Arg(x8)-SUMO-3C			
*Sc*Med4	1-284	-	pCDFDuet	Strep	[71]
*Sc*Med9	1-149	-			
cMedΔ4,9_1/	1-687	-			
*Sc*Med17	1-121	-			
*Sc*Med22	1-115	-			
*Sc*Med11 *Sc*Med6	1-295	-	pCOLADuet	Kan	[66]
*Sc*Med8 *Sc*Med20	1-223	-			
*Sc*Med18	1-210	-			
	1-307	-			
cMedΔ4,9_2/					
*Sc*Med31	1-127	-			
*Sc*Med10 *Sc*Med7	1-157	-	pCDFDuet	Strep	[66]
*Sc*Med21	1-222	-			
	1-140	-			
cMedΔ4,9_3/					
*Sc*Med19	1-220	-	pETDuet	Amp	[66]
*Sc*Med14	1-745	N-His(x10)			

Additionally, the following should be noted. The cMedΔ4,9 subunit sequences are present on three different plasmids (cMedΔ4,9_1, cMedΔ4,9_2 and cMedΔ4,9_3) co-transformed together into a single *E.coli* strain, which is maintained as a frozen stock.

CO means that the gene sequence had been codon optimized for the respective expression host. 3C and TEV refer to sequences encoding 3C protease and TEV protease cleavable linkers between the tag and the gene, respectively.

The mEGFP and mCherry tags were amplified from the mEGFP and 6B vectors (table 3.1), respectively. The mEGFP-Gcn4 and mCherry-Med15 sequences are connected via the artificially added linker sequence “GGSAGSGGSG”, which is not a part of the vector backbone.

3.3 DNA Scaffolds

DNA scaffolds used for immobilized template assays (ITAs) and other biochemical assays were modeled on the natural yeast HIS4 gene promoter, with modifications added for the intended application.

Sense and antisense strands were synthesized separately as Ultramers® from Integrated DNA Technologies (IDT), with the needed 5’ modifications.

Table 3.3 | **DNA scaffolds used in this study.** A compilation of the sense (top) and antisense (bottom) strands that were annealed together to obtain the DNA scaffolds used in this study, both shown in a 5' to 3' orientation. The experiments that the respective scaffolds were used for are indicated. The legend below the table explains the color-coding.

DNA scaffold name	Used in	Sense/antisense sequence (5' to 3')
Sc1	PIC ITA	5'-CGATATAGAAGGTAAGAAAAGGATATGACTATGAACAGTAGCACGCTG TGTATATAATAGCTATGGAACGTTCGATTCACCTCCGATGTGTGTTGTA CATACATAAAAATATCATAGCACAACTGCGCTGTGTAATAGTAATACAA TAGTCGGAAACCCATACACAGGGAAGATATCCGGTCCGTAGG-3' 5'-CCTACGGACCGGATATCTTCCCTGTGTATGGGTTTCCACTATTGTATTA CTATTACACAGCGCAGTTGTGCTATGATATTTTTATGTATGTACAACACA CATCGGAGGTGAATCGAACGTTCCATAGCTATTATATACACAGCGTGCT ACTGTTCATAGTCATATCCTTTTCTTACCTTCTATATCG-/biot/-3'
Sc3	Gcn4 ITA	5'-TAAGAAAAGGATATGACTCTGAACAGTAGCACGCACGCTGTGTAGCGA AACCCATACACAGGCAAGATATCCGGTCCGTAGG-3' 5'-CCTACGGACCGGATATCTTCCCTGTGTATGGGTTTCCCTACACAGCGTG CGTGCTACTGTTCAGAGTCATATCCTTTTCTTA-/biot/-3'
Sc4	Gcn4 kinase assay	5'-GCACAGTGACTCACGTTTTTTTATGACTCATTCGATATAGAAGGTAAG AAAAGGATATGACTCTGAACAGTAGCACGCACGCTGTGTAGCGAAAC CCATACACAGGCAAGATATCCGGTCCGTAGG-3' 5'-CCTACGGACCGGATATCTTCCCTGTGTATGGGTTTCCCTACACAGCGTG CGTGCTACTGTTCAGAGTCATATCCTTTTCTTACCTTCTATATCGAATGA GTCATAAAAAAACGTGAGTCACTGTGC-/biot/-3'
Sc5	Fluorescence Anisotropy+ Gcn4/DNA Droplet assay	5'-/FAM/-CATGACTCTG-3' 5'-CAGAGTCATG-3'

Gcn4 binding site
Linker + EcoRV restriction site
TATA Box…TSS
/modification/ (/biot/ = biotinylation, /FAM/= 6-FAM Fluorescein)

3.4 Chemicals

Chemicals were procured from Sigma-Aldrich, Roth, Thermo Fisher Scientific and Merck. It can be generally assumed that chemicals of the same grade from different qualified sources were used interchangeably. Situations where the source or grade of a chemical was significant will be specifically mentioned in the methods text.

3.5 Cell culture

3.5.1 *E.coli* strains

Table 3.4 | *E.coli* strains used in this study. Listing of the bacterial strains used in this study, together with their supplier and genotype.

Strain	Supplier	Genotype
XL1-Blue	Agilent	*recA1 endA1 gyrA96 thi-1 hsdR17 supE44 relA1 lac [F' proAB lacI^{q}ZΔM15 Tn10 (Tet^{r})]*
DH10EMBacY	Geneva biotech	*F^{-} mcrA Δ(mrr-hsdRMS-mcrBC) ϕ80dlacZΔM15 ΔlacX74 endA1 recA1 deoR Δ(ara, leu)7697 araD139 galU galK λ- rpsL nupG / bMON14272‡ yfp+/ pMON7124*
BL21-CodonPlus (DE3) RIL	Agilent	*E. coli B F^{-} ompT hsdS(r$_{B}^{-}$ m$_{B}^{-}$) dcm+ Tet^{r} E. coli gal λ (DE3) endA Hte [argU ileY leuW Cam^{r}]*
LOBSTR	Kerafast	*E. coli B F^{-} ompT hsdS(r$_{B}^{-}$ m$_{B}^{-}$) dcm+ Tet^{r} E. coli gal λ (DE3) endA Hte [argU ileY leuW Cam^{r}] (ArnA, SlyD knockout)*

3.5.2 S.cerevisiae strains

Table 3.5 | ***S.cerevisiae* strains used in this study.** Listing of the yeast strains used in this study for purification of endogenous *S.cerevisiae* protein complexes, together with their source and genotype.

Factor	Strain	Genotype	Source
RNAPII	BJ5464 Rpb3-His$_6$-Bio	*BJ5464; MATalpha; ura3-52 trp1 leu2-delta1 his3-delta200 pep4::HIS3 prb1-delta1.6R can1 GAL*	M. Kashlev[88]
Mediator (eMed)	BJ5464 Med16-TC6(MBP-TEV-4XProA), Med10-TC8(3HA-3C-Avi-10XHis), Med18-TAP	*BJ5464; MATalpha ura3-52 trp1 leu2-delta1 his3-delta200 pep4::HIS3 prb1-delta1.6R can1 GAL MED16::MED16-TC6-KanMX; MED10::MED10-TC8-natNT2, Med18::Med18-TAP-URA3*	S.Sainsbury

3.5.3 Insect cell lines

Table 3.6 | **Insect cell lines used in this study.** Listing of the insect cell lines used in this study together with their source of origin and vendors.

Cell line	Species	Source	Supplier
Sf9	*S.frugiperda*	Pupal ova(derived from strain *(IPLB-Sf21-AE)* [89]	Thermo Fisher Scientific
Sf21*(IPLB-Sf21-AE)*	*S.frugiperda*	Pupal ova [89]	Thermo Fisher Scientific
Hi5*(BTI-TN-5B1-4)*	*T.ni*	Pupal ova [90]	Expression Systems

3.5.4 Cell culture media

Table 3.7 | **Cell culture media and components.** Details of the media used for making liquid cultures or plates of bacterial, yeast and insect cells, together with their chemical composition and supplier.

Media	Culture type	Composition	Supplier
LB	*E.coli (liquid culture +plates)*	1% (w/v) tryptone, 0.5% (w/v) yeast extract, 0.5% (w/v) NaCl (1.5% (w/v) agar for plates)	homemade
YPD	*S.cerevisiae(liquid culture +plates)*	2% (w/v) peptone, 2% (w/v) glucose, 1.5% (w/v) yeast extract (1.8% (w/v) agar for plates)	homemade
SOB	*E.coli (liquid culture)*	2% (w/v) tryptone,0.5% (w/v) yeast extract,10mM NaCl, 2.5mM KCl	homemade
Gibco® Sf-900™ III SFM	*Sf9/Sf21 adherent and liquid culture*	Low-hydrolysate, serum-free, protein-free, animal origin-free insect cell culture medium	Thermo Fisher Scientific
ESF921™	*Hi5 liquid culture*	Serum-free, protein-free insect cell culture media, supplemented with L-glutamine and Kolliphor® P188	Expression Systems

3.5.5 Antibiotics and additives

Table 3.8 | **Antibiotics and additives to cell culture media.** Listing of antibiotics and additives used in cell culture media with their solvent, application, stock and final concentrations.

Substance	Added to	Stock concentration	Final concentration
Ampicillin (in water)	*E.coli culture+plates*	100 mg/mL	100 μg/mL
Kanamycin (in water)	*E.coli culture+plates*	50 mg/mL	50 μg/mL
Chloramphenicol (in 96% ethanol)	*E.coli culture+plates*	30 mg/mL	30 μg/mL
Gentamycin (in water)	*E.coli culture+blue-white selection plates*	10 mg/mL	10 μg/mL
Tetracycline (in water)	*E.coli culture+plates*	10 mg/mL	10 μg/mL
X-Gal (in DMSO)	*E.coli culture+blue-white selection plates*	150 mg/mL	150 μg/mL
IPTG (in water)	*E.coli culture+blue-white selection plates*	1M	0.1-1 mM
Streptomycin (in water)	*E.coli culture+plates*	30 mg/mL	30 μg/mL
X-tremeGENE™ 9 (in 80% ethanol)	Insect cell transfection	Not stated	1.5 μL/mL

3.6 Antibodies

3.6.1 Primary antibodies

Table 3.9 | **Primary antibodies used in this study.** Listing of primary antibodies used in this study, together with their target, supplier, dilution for western blot analysis, and the organism in which they were produced.

Antibody	Target	Supplier	Dilution	Production Organism
α-Gcn4	*Sc* Gcn4	Absolute Antibody C11L34	1:10,000	mouse
α-Srb4	*Sc* Med17	Abcam ab63812	1:5,000	rabbit
α-Ser2-P	RNAPII-CTD phosphorylated Ser2	D. Eick 3E10 [91]	1:60	rat
α-Ser5-P	RNAPII-CTD phosphorylated Ser5	D. Eick 3E8 [91]	1:60	rat
α-Ser7-P	RNAPII-CTD phosphorylated Ser7	D. Eick 4E12 [91]	1:10	rat
α-Tyr1-P	RNAPII-CTD phosphorylated Tyr1	D. Eick 3D12 [91]	1:7	rat

3.6.2 Secondary antibodies

Table 3.10 | **Secondary antibodies used in this study.** Listing of secondary antibodies used in this study, together with their target, supplier, dilution for western blot analysis, and the organism in which they were produced.

Antibody	Target	Supplier	Dilution	Production Organism
α-mouse-IgG-HRP	mouse IgG	Abcam ab5870	1:3,000	goat
α-rat-IgG-HRP	rat IgG	Sigma-Aldrich A9037	1:5,000	goat
α-rabbit-IgG-HRP	rabbit IgG	Santa Cruz	1:2,000	goat

3.7 Standard buffers and dyes

Table 3.11 | **Standard buffers and dyes.** Components of standard buffers and dyes that have been used throughout this study.

Buffer	Composition/source
SDS-PAGE loading dye	NuPAGE® 4X LDS loading buffer/Thermo Fisher Scientific
PBS	137 mM NaCl, 2.7 mM KCl, 10 mM Na_2HPO_4, pH 7.4, 1.76 mM KH_2PO_4, pH 7.4
TAE	5 mM EDTA, 2.5 M Tris-acetate, pH 8.0
Protease inhibitor cocktail	0.284 µg/ml leupeptin, 1.37 µg/ml pepstatin A, 0.17 mg/ml PMSF, 0.33 mg/ml benzamidine

4 Methods

4.1 DNA methods

Cloning strategies

To generate the DNA plasmid constructs for expression and purification of the proteins in this study in their respective heterologous expression systems, several cloning methods and vector systems were used. These included Ligation-Independent Cloning (LIC), In-fusion cloning and Gibson Assembly.

All steps were carried out at room temperature, unless otherwise indicated. All DNA constructs and intermediate DNA products were stored at -20°C. All water used in reactions was Milli-Q (Merck-Millipore) water, deionized and filter-sterilized through a 0.22 μm membrane filter, and additionally autoclaved. All bacterial cultures were grown at 37°C with vigorous shaking.

Vector digestion

For all the abovementioned methods, linearization of an acceptor plasmid with restriction endonucleases was needed. In digestion reactions, 20 μL of plasmid DNA (50 ng-2 μg) were mixed with 6 μL of the appropriate10X buffer (e.g. NEB CutSmart), 4 μL of restriction enzyme, made up to 60 μL with water, and incubated according to the commercial recommendations for the used restriction endonuclease at either 37°C or 25°C, for 1-3 hours or overnight. The linearized plasmid was then purified by gel extraction.

Insert generation by PCR

Genes or gene fragments of interest were amplified, either from genomic DNA, cDNA or a different plasmid, by polymerase chain reaction (PCR), using forward and reverse primers that define the beginning and the end of the sequence to be amplified.

Primer design

Forward and reverse PCR primers were designed such that they are identical to the 5' (beginning), and reverse complementary to the 3' (end), regions of the sequence to be amplified. As a rule of thumb, primers were designed to be between 12 and 30 nucleotides in length (of the template binding part), to have a melting temperature (T_m) between 55°C and 70°C, and to have a GC-content of 20-60% where possible.

Also, all primers were designed to end with (the 3'-most base) either a Guanine or a Cytosine.

For LIC cloning, 5' tags were added to the primers depending on the intended recipient vector. For insertion into the series-438 MacroBac insect cell transfer vectors (Macrolab), the tags v1 F and v1 rv (table) were added to the forward and reverse primers, respectively, for vectors 438-B and 438-C, whereas the tags vBac F and v1 rv were added for vector 438-A.

For insertion into the series-1 *E.coli* T7 expression vectors 1B and 1C (Macrolab), primer extensions v1 F and v1 rv were added to the forward and reverse primers, respectively.

Table 4.1 | **LIC tags added to primers.** Sequences of LIC tags added to the 5' ends of primers designed for cloning into the series-438 vectors.

LIC Tag	Sequence to be added 5' to PCR primers
v1 F	5'-TACTTCCAATCCAATGCA-3'
v1 rv	5'-TTATCCACTTCCAATGTTATTA-3'
vBac F	5'-TACTTCCAATCCAATCG-3'

For In-fusion cloning and Gibson assembly, where multiple fragments (or insert and linearized vector) were ligated, primers were designed such that they overlapped by at least 15 base pairs with each of the two fragments to be joined, and to have a T_m of at least 60°C.

Template DNA

When *S.cerevisiae* genomic DNA was used as a sequence template, it was first extracted from wild-type yeast colonies. Single colonies from a YPD plate, or cells from 100 µL of YPD culture at an OD_{600} of 0.4, were resuspended in 100 µL of 200 mM lithium acetate and 1% SDS. The cells were vortexed then incubated for 5 minutes at 70°C. 300 µL of 96% ethanol were added to precipitate the DNA. The mixture was briefly vortexed, and the DNA was pelleted by centrifugation at 15,000xg for 3 minutes. The supernatant was carefully removed, and the DNA pellet washed with 500 µL of 70% ethanol. Care was taken not to disrupt the pellet with shearing forces. The pellet was then dissolved in 100 µL of water (the water was added gently to the top and the DNA was allowed to dissolve without pipetting up and down). Debris was removed by centrifugation at 15,000xg for 1 minute. 1 µL of the clarified supernatant was used as a template for PCR reactions. This preparation was *not stored*, and prepared freshly before every use.

PCR reactions

In a typical PCR reaction, 1 μL of template DNA (50-100 ng), was mixed with 3 μL of 100 mM dNTP mix (dATP, dCTP, dGTP, dTTP - NEB), 3 μL of 100 μM forward primer, 3 μL of 100 μM reverse primer, 30 μL of 5x phusion polymerase buffer (NEB), and 0.5 μL of phusion polymerase enzyme (NEB), and made up to 150 μL with water. The 150 μL reaction was then divided into 3 (50 μL per PCR tube).

A typical PCR program had an initial template denaturation step at 95°C for 4 minutes, followed by an iterative program of denaturation (94°C for 45 seconds), annealing (55-60°C depending on the T_m of the designed primers, for 1 minute), and primer extension (72°C for 3 minutes). This was done for 30 iterations to amplify the product, followed by a final elongation step at 72°C for 10 minutes. A Tprofessional TRIO thermocycler (analytik jena) was used to vary the temperature as described.
The PCR extension time was adjusted according to the length of the sequence to be amplified, and the speed of the DNA polymerase used.

For difficult PCR reactions (particularly for genes approaching 5000 base pairs in length or longer), the reactions were optimized by: Applying a gradient of annealing temperatures, using different polymerases optimized for longer reactions such as Q5 (NEB) or Expand^{TM}20kb^{PLUS} (Sigma-Aldrich), addition of 1-10% DMSO or Betaine for better extension from GC-rich templates, or changing the PCR protocol to a two-step or touchdown PCR, where the annealing step was omitted, or set 5°C above the T_m and gradually reduced by 1-2°C per cycle, respectively.

Site-directed mutagenesis

Round-the-horn PCR (RTH PCR) was used to insert substitutions or deletions in a given sequence. In this method, the template is a circular plasmid, and primers are designed facing *away* from each other, and flanking the sequence to be modified. Thus the full plasmid sequence is amplified, *excluding* the sequence to be modified. The new, modified sequence is then encoded via an additional 5' overhang in one of the two primers, resulting in a product composed of a linearized copy of the template with the modification on one of its ends. 5'-phosphorylations on the primers allow re-circularization by ligation.

To perform round-the-horn PCR, the PCR reactions and programs were set up and optimized as previously described using Q5 (NEB) as a polymerase. 1 μL DpnI (NEB) was added per PCR reaction to digest the original template.
The product was circularized after purification by gel extraction, by incubation of 50 ng with 1 μL of T4 ligase (NEB) and 1 μL of 10X T4 ligase buffer (NEB) for 1 hour or overnight at room temperature. This could then be used to transform XL1-Blue cells.

Agarose gel electrophoresis for product size verification

1% (w/v) agarose was dissolved in 1x TAE buffer by boiling, and allowed to polymerize by cooling down. 3 μL of the DNA-intercalating stain Sybr™Safe (Invitrogen) per 50 mL of gel were mixed in the gel matrix to allow UV visualization of the DNA bands. Samples were loaded in the wells, together with a DNA ladder as a size fiducial, and the gels were run in an electrophoresis chamber. Gels were visualized using a GEL iX20 Imager system (Intas).

Gel extraction of product

Bands corresponding to the expected size were extracted from the gel by excising the gel area, and further processed using a QIAquick® gel extraction kit (QIAGEN) according to the commercial protocol, and finally eluted with water.

DNA quantification

DNA was quantified by absorbance measurement at a wavelength of 260 nm using a Nanodrop 2000 spectrophotometer (Thermo Scientific). The concentration was calculated from the absorbance measurement according to Beer's Law.

Combining vector and insert

For recombination by LIC cloning, vectors and inserts were treated separately with T4 polymerase supplemented with dGTP or dCTP, respectively. T4 polymerase is an enzyme that has conditional polymerase and exonuclease activities. In the absence of dNTPs, its exonuclease activity prevails, and vice versa. By addition of only one dNTP (either dCTP or dGTP), the T4 exonuclease chews back the ends of the linear fragments until it encounters the first G or C in the sequence, where its exonuclease activity gets inhibited due to the abundance of the complementary nucleotide. This creates complementary overhangs between vectors and inserts, which can then be annealed together.

In the T4 treatment reaction, a minimum of 50 ng of linearized vector or insert DNA were mixed with 2 μL of 10x T4 DNA polymerase buffer (Novagen), 1 μL of 100 mM DTT, 2 μL dNTP (dCTP for inserts and dGTP for vectors) and 0.4 μL of LIC-qualified T4 DNA polymerase (Novagen). The total reaction volume should not exceed 20 μL, and it is important to have roughly equal amounts (by mass) of vectors and inserts. The reaction was incubated for 40 minutes at room temperature, followed by an enzyme inactivation step at 75°C for 20 minutes. The reaction can then be stored at -20°C until needed.

T4-treated vectors and inserts were annealed by mixing together 2 µL from each reaction, and incubating at room temperature for 10 minutes. The entire reaction was used to transform 50-100 µL chemically competent XL1-Blue *E.coli* cells.

For recombination of fragments (whether vector and insert, or multiple pieces of insert) by In-fusion™ cloning, 10-100 ng of purified insert, and 100 ng of purified vector in a total of volume 9 µL were mixed with 1 µL 10X In-Fusion™ cloning reaction mix (Clontech), and incubated at 37°C for 15 minutes, followed by 15 minutes at 50°C. 2.5 µL of the cloning reaction were then used to transform 50-100 µL of XL1-Blue competent cells by heat shock.

For recombination of fragments (whether vector and insert, or multiple pieces of insert) by Gibson assembly, 0.02-0.5 pmols of fragment(s) + linearized vector in the case of 2-3 fragment assembly, or 0.2-1 pmols of fragments + linearized vector in the case of 4-6 fragment assembly, were mixed together with 10 µL 2X Gibson Assembly Master Mix (NEB), and the final volume adjusted to 20 µL with water. The samples were incubated at 50°C for 15 minutes for 2-3 fragment assembly, or 1 hour for 4-6 fragment assembly. 2 µL of the assembly reaction were then used to transform 5-alpha competent cells (NEB), by heat shock.

Preparation of chemically competent XL1-blue *E.coli* cells

Cells were streaked on LB plates and grown at 37°C. Single colonies were grown in a 50 mL overnight LB pre-culture. 1 mL of pre-culture was used to inoculate 250 mL SOB media with 10 mM magnesium chloride, and grown at 37°C until an OD_{600} of 0.5-0.7 was reached. The cells were collected by centrifugation at 3000xg for 10 minutes at 4°C, and then resuspended in 75 mL of chilled, sterile-filtered Inoue buffer (10 mM HEPES, pH 6.7, 250 mM potassium chloride, 15 mM calcium chloride, 55 mM manganese chloride). The cells were collected one more time by centrifugation, and then resuspended in 10 mL Inoue buffer. 700 µL DMSO were added dropwise with gentle swirling. The cells were aliquoted and flash frozen in liquid N_2.
All steps were performed on ice, in a cold room, or a chilled centrifuge.

Bacterial transformation by heat shock

For transformation of bacterial cells, competent cells (50-100 µL aliquots) were thawed on ice, and then mixed with 1 µL of purified vector, or the previously described amounts of cloning reactions, incubated on ice for 10-30 minutes, heat shocked at 42°C for 45-55 seconds, cooled down on ice for 2 minutes, and then given 1 mL of antibiotic-free LB for recovery, and outgrown for 45 minutes to up to 3 hours. Larger plasmids required longer recovery, and supplementation of the LB recovery media with 2% (w/v) sucrose.

For vector propagation, 150 μL of the outgrowth culture were plated. For all other purposes, cells from the entire outgrowth culture were plated after collection by centrifugation at 1000xg for 1 minute, removal of 950 μL of media, and resuspension in the remaining volume.

Isolation and verification of recombined plasmids

Single colonies were grown overnight in 50 mL LB cultures, and collected by centrifugation at 3148xg at 4°C for 10 minutes. Plasmid DNA was isolated using a QIAprep® Spin Miniprep kit (QIAGEN), up scaling the commercial protocol to apply on cells from 50 mL cultures instead of 5 mL.

The presence of inserts was verified first with restriction digestion, before sequencing the plasmids fully. All plasmids used in this study were sequenced before use to ensure absence of random mutations. Sequencing primers were designed to bind 800 base pairs apart in the forward direction to cover the entire length of genes, and 300 base pairs from the beginning of genes in the reverse direction, to cover the vector-insert transition.

Generation of polypromoter plasmids with multiple genes

The series-438 MacroBac insect cell transfer vectors are amenable to PmeI/SwaI LIC subcloning, which is a protocol developed by MacroLab based on the Biobricks™ recombination system that allows generation of cassettes with multiple ORFs [92]. In this protocol, an ORF-containing acceptor plasmid is linearized with SwaI, which cuts at a single site adjacent to the ORF, and a donor plasmid is digested with PmeI, which cuts at two sites, located on either side of the polyhedrin promoter-ORF-SV40 polyadenylation termination sequence. T4 treatment of the SwaI digested vector and the PmeI digested cassette gives them complementary sticky ends to allow ligation-independent annealing. The resultant plasmid contains two ORFs in tandem, each with their own promoter and terminator sequence. An unused SwaI site present within the incoming PmeI-digested cassette regenerates the SwaI site in the new plasmid, which also contains two unused PmeI sites, originating from the acceptor plasmid, now flanking the *two* ORFs. The regeneration of these sites allowed this process to be carried out reiteratively, each time adding one or multiple genes to the cassette in the same way.

The donor plasmid was digested with pmeI (NEB), and the acceptor plasmid with SwaI (NEB), according to the aforementioned vector digestion protocol, and purified by gel extraction. The donor and acceptor plasmids were treated with T4 polymerase, wherein the donor plasmid was treated as the insert and the acceptor

plasmid as the vector (as previously). The T4 treated plasmids were annealed together as previously described, and used to transform XL1-Blue *E.coli* cells.

A compilation of recombined plasmids with the cloning methods and primer sequences used to generate them

A list of plasmids generated in this study, together with the cloning method and the DNA templates used to generate them are shown in table 4.2. For referencing, clones are numbered. Clone numbers X/Y/Z in table 4.2, refer to the indicated ORFs cloned into acceptor vectors A/B/C, respectively.
Primer sequences for each primer set indicated in table 4.2 are shown in table 4.3.
Primers that contain LIC vector-binding sequences and template-binding sequences are indicated in bold face and regular, respectively. Primers that contain non-LIC vector-binding sequences and template-binding sequences are indicated in capital and small letters, respectively. Primers with PTMs are indicated between forward slashes.

Table 4.2 | **Plasmids cloned and cloning method.** A list of all plasmids cloned in this study, including the ORFs, the recipient vector, the cloning method used to recombine ORF-containing insert and linearized vector, and a cross-reference to the corresponding primers (table 4.3) designed to make that possible.

Clone #	ORF(s)	Cloning method	Template	Acceptor vector(s)	Primer sets
1/2	*Sc* Med12	LIC	genome	438-B/C	1
3/4/5	*Sc* Med13	LIC	genome	438-A/B/C	2
6	*Sc* Med13Δ	RTH-PCR	plasmid	438-A	3
7/8/9	*Sc* Cdk8	LIC	genome	438-A/B/C	4
10/11	*Sc* Cdk8 D286A	RTH-PCR	plasmid	438-B/C	5
12/13/14	*Sc* CycC	LIC	genome	438-A/B/C	6
15	*Sp* Med12	In-fusion/LIC	g-blocks (*T.ni* opt)	438-A	7
16	*Sp* Med13	In-fustion/LIC	g-blocks (*T.ni* opt)	438-A	8
17/18/19	*Sp* Cdk8	LIC	*Sp* cDNA	438-A/B/C	9
20/21/22	*Sp* CycC	LIC	*Sp* cDNA	438-A/B/C	10
23	mCh-Med15(6-651)	Gibson	plasmids	1B	11
24	GFP-Gcn4	Gibson	plasmids	1B	12
25	Med15_KIX123	Gibson	Plasmid	1C	13
26/27/28	*Sc* Cdk8 (ORF1) *Sc* CycC (ORF2)	Biobricks LIC subcloning	Plasmids	438-A/B/C	-
29	*Sc* CycC (ORF1) *Sc* Cdk8 (ORF2)	Biobricks LIC subcloning	Plasmids	438-A	-
30	*Sc* CycC (ORF1) *Sc* B-Cdk8 (ORF2)	Biobricks LIC subcloning	Plasmids	438-C	-
31/32	*Sc* CycC (ORF1) 438-B-*Sc* Cdk8 D286A (ORF2)	Biobricks LIC subcloning	Plasmids	438-A/B	-
33	*Sc* CycC (ORF1) 438-C-*Sc* Cdk8 (ORF2)	Biobricks LIC subcloning	Plasmids	438-A	-
34/35/36	*Sp* CycC (ORF1) *Sp* Cdk8 (ORF2)	Biobricks LIC subcloning	Plasmids	438-A/B/C	-
37	*Sc* Med12 (ORF1) *Sc* Med13 (ORF2)	Biobricks LIC subcloning	Plasmids	438-B	-
38/39	*Sc* Med13 (ORF1) *Sc* Med12 (ORF2)	Biobricks LIC subcloning	Plasmids	438-A/B	-

Clone #	ORF(s)	Cloning method	Template	Acceptor vector(s)	Primer sets
40	*Sc* Med12 (ORF1) 438-B- *Sc* Cdk8 (ORF2) *Sc* CycC (ORF3)	Biobricks LIC subcloning	Plasmids	438-A	-
41	*Sc* Med13 (ORF1) 438-B- *Sc* Cdk8 (ORF2) *Sc* CycC (ORF3)	Biobricks LIC subcloning	Plasmids	438-A	-
42	*Sc* Med13 (ORF1) *Sc* Med12 (ORF2) 438-B-*Sc* Cdk8 (ORF3) *Sc* CycC (ORF4)	Biobricks LIC subcloning	Plasmids	438-A	-
43	*Sc* Med13 (ORF1) *Sc* Med12 (ORF2) 438-B-*Sc* Cdk8 D286A (ORF3) *Sc* CycC (ORF4)	Biobricks LIC subcloning	Plasmids	438-A	-
44	*Sc* Med13 (ORF1) *Sc* Med12 (ORF2) 438-C-*Sc* Cdk8 (ORF3) *Sc* CycC (ORF4)	Biobricks LIC subcloning	Plasmids	438-A	-
45	*Sc* Med13 (ORF1) *Sc* Med12 (ORF2) 438-C-*Sc* Cdk8 D286A (ORF3) *Sc* CycC (ORF4)	Biobricks LIC subcloning	plasmids	438-A	-

Table 4.3 | **Primer sequences used for cloning.** A list of all primers used for cloning of the plasmids mentioned in table 4.2.

Primer sets	Sequences
1	5'-TACTTCCAATCCAATGCAAATAACGGTTCTGGTCGATACTT-3' (v1 F) 5'-TTATCCACTTCCAATGTTATTAATGTGGATTTTTCCTCTCAAAC-3' (v1 R) 5'-TACTTCCAATCCAATCGATGAATAACGGTTCTGGTCG-3' (vBac F)
2	5'-TACTTCCAATCCAATGCAAGTTCTGACGCTTCCACGTA-3' (v1 F) 5'-TTATCCACTTCCAATGTTATTATTTATCCGAGAGAATAATTGATGAA-3' (v1 R) 5'-TACTTCCAATCCAATCGATGAGTTCTGACGCTTCCAC-3' (vBac F)
3	/Phos/-5'-TTATCCACTTCCAATGTTATTAGGCAGCTGTTTGCTTTAATTGTATGAAATC-3' /Phos/-5'-TACTTCCAATCCAATCGATGACAATTTCAGAAAAAGAACAAGACATCTTAGATTTAATTGC-3'
4	5'-TACTTCCAATCCAATGCATATAATGGCAAGGATAGAGCACA-3' (v1 F) 5'-TTATCCACTTCCAATGTTATTATCTTCTGTTTTTCTTTCGAGATG-3' (v1 R) 5'-TACTTCCAATCCAATCGATGTATAATGGCAAGGATAGAGC-3' (vBac F)
5	/Phos/-5'-CTTTGAAACCCGCAAATATAATGGTGACCATAGA-3' /Phos/-5'-CTCGATGAAGCACCCAATTTTGATGAAGATACG-3'
6	5'-TACTTCCAATCCAATGCATCGGGGAGCTTCTGGACA-3' (v1 F) 5'-TTATCCACTTCCAATGTTATTAAATTGCAGATGCTGGTCTAAGA-3' (v1 R) 5'-TACTTCCAATCCAATCGATGTCGGGGAGCTTCTGG-3' (vBac F)
7	5'-TACTTCCAATCCAATGCAAGCAATCGAGATTCAGCAAAC-3' (v1 F) 5'-TTATCCACTTCCAATGTTATTACCAAAAGGTTGGCTCATACAA-3' (v1 R) 5'-TACTTCCAATCCAATCGATGAGCAATCGAGATTCAGCA-3' (vBac F)
8	5'-TACTTCCAATCCAATGCATCATATCAGGTGTGTTTTAAGAAAT-3' (v1 F) 5'-TTATCCACTTCCAATGTTATTAAGAGGTCACAGGATGTGTAATGTC-3' (v1 R) 5'-TACTTCCAATCCAATCGATGTCATATCAGGTGTGTTTTAAGA-3' (vBac F)
9	5'-TACTTCCAATCCAATGCAAAAGACGGTTATAAAATTATTGGGT-3' (v1 F) 5'-TTATCCACTTCCAATGTTATTAATTTCCTTTAAAACGTTTACTTTCG-3' (v1 R) 5'-TACTTCCAATCCAATCGATGAAAGACGGTTATAAAATTATTG-3' (vBac F)
10	5'-TACTTCCAATCCAATGCAGCAGCAAATTACTGG-3' (v1 F) 5'-TTATCCACTTCCAATGTTATTATTCAATATCCTCAAAATAAT-3' (v1 R) 5'-TACTTCCAATCCAATCGATGGCAGCAAATTACT-3' (vBac F)

Primer sets	Sequences
11	5'-CACCATGAAAACCTGTACTTCCAATCCAATatggtgagcaagggcgag-3' 5'-GCCGGAACCGCCGGAGCCCGCAGAACCGCCcttgtacagctcgtccatgcc-3' 5'-GGCGGTTCTGCGGGCTCCGGCGGTTCCGGCGTCCAAGACAAAGACACTCTGTCC-3' 5'-CTCGAATTCGGATCCGTTATCCACTTCCAATGTTAATTATTATTGTTTCCAGTAGAAGTAGTGCC-3'
12	5'-CACCATGAAAACCTGTACTTCCAATCCAATatggtgagcaagggcgag-3' 5'-GCCGGAACCGCCGGAGCCCGCAGAACCGCCcttgtacagctcgtccatgcc-3' 5'-GGCGGTTCTGCGGGCTCCGGCGGTTCCGGCATGTCCGAATATCAGCCAAGTTTATTTG-3' 5'-CTCGAATTCGGATCCGTTATCCACTTCCAATGTCAGCGTTCGCCAACTAATTTCTTTAATC-3'
13	5'-GATCGAGGAAAACCTGTACTTCCAATCCAATatgtctgctgctcctgtcc-3' (f1f) 5'-CAAAGGGTTGTTGTTCGCACTCTGTGCTTGTTGTTGCTGTAGC-3' (f1r) 5'-GCTACAGCAACAACAAGCACAGAGTGCGAACAACAACCCTTTG-3' (f2f) 5'-GGGAGGGCTGGTGCTGTTGGGCTCTCTGAAGGTTCGAG-3' (f2r) 5'-CTCGAACCTTCAGAGAGCCCAACAGCACCAGCCCTCCC-3' (f3f) 5'-CTCGAATTCGGATCCGTTATCCACTTCCAATATTATTattgtttccagtagaagtagtgcctg-3' (f3r)

Strand annealing of DNA scaffolds

To anneal the strands of DNA scaffold used in various experiments (table 3.3) together, sense and antisense strands were dissolved in DNA duplex buffer (30 mM HEPES, pH 7.5, 100 mM KOAc, 0.1 mM EDTA) to 100 μM. 2 μL of each were mixed and annealed by heating to 95°C for 10 minutes, followed by gradual cooling in steps of 2°C over approximately 30 minutes. Annealed DNA was later diluted in DNA duplex buffer to 100 nM.

4.2 Insect cell methods

Modifying baculoviral bacmids using insect cell transfer vectors

The series-438 MacroBac Insect cell transfer vectors are designed such that the ORF or multiple ORFs of interest are inserted in between Tn7L and Tn7R transposition elements that are recognized by the T7 transposase enzyme. As such, transformation in DH10αEMBacY cells, which is a strain stably carrying a baculoviral genome bacmid (bMON14272), and a helper plasmid (pMON7124) encoding the 4 enzymes of the T7 transposase system [93], allows site-specific transposition of the ORF cassette from the transfer plasmid into the baculoviral bacmid. The T7 attachment site on the bacmid is located within a LacZα gene, meaning that successful transposition events cause impaired β-galactosidase expression, and thus colonies appear white on X-Gal-IPTG-Gentamycin blue-white selection plates.

Preparation of electrocompetent DH10αEMBacY *E.coli* cells

Bacterial cells take up large DNA plasmids more efficiently by electroporation. Therefore, electrocompetent DH10αEMBacY cells were prepared. A single colony from a native selection plate (Amp-Kan-Tet) was grown in 5 mL of LB overnight at 37°C with the same antibiotics. 1 mL of overnight culture was added per 250 mL of SOB media supplemented with the same antibiotics, and the culture was grown further at 37°C until an OD_{600} of 0.5 to 0.7 was reached. The cells were spun down at 3128xg for 10 minutes at 4°C, and resuspended in 150 mL of chilled water. The centrifugation step was repeated twice, the second time resuspending in 5 mL of chilled 10% (v/v) glycerol, and the final time resuspending in 5 mL of chilled 5% (v/v) glycerol. The cells were aliquoted and flash frozen in liquid N_2.

Transformation by electroporation

100 μL of electrocompetent DH10αEMBacY cells were mixed with 250-1000 ng of insect cell transfer plasmid in a Gene®/Micro™ Pulser cuvette of 0.1 cm width (Bio-Rad), and then subjected to an electric pulse of 25 μF and 1.8 kV using a MicroPulser Electroporator (Bio-Rad). 1 mL of antibiotic-free LB media was added and the cells were transferred to a 15 mL culture tube, and recovered for 5 hours at 37°C. 30 μL of cell culture was then plated on X-Gal-IPTG-Gentamycin plates, and grown at 37°C for 18-20 hours. White colonies on blue-white selection plates were picked, and restreaked one more time on X-Gal-IPTG-Gentamycin plates. Colonies that remained white were used to inoculate 10 mL LB-Gentamycin cultures, which were used for bacmid DNA isolation.

Isolation and storage of bacmid DNA

Glycerol stocks were made from bacmid cultures for future bacmid preparations, by mixing 750 μL of 70% glycerol with 750 μL of culture in cryotubes, and stored at -80°C. Bacmids were isolated from DH10αEMBacY by alkaline lysis and isopropanol precipitation. For the subsequent steps, buffers from a QIAprep® Spin Miniprep kit (QIAGEN) were used, but not the columns. Absolute ethanol was used to prepare all ethanol-containing solutions (the quality of the ethanol was critical to avoid undesired re-dissolution of precipitated DNA).

The cells from 10 mL cultures were divided into 2x 5mL and collected by centrifugation at 3128xg for 10 minutes. The supernatant was removed, and the pellets resuspended in 250 μL of resuspension buffer P1 (50 mM Tris, pH 8.0, 10 mM EDTA, 50 mM glucose, 0.1 mg.mL DNAse-free Rnase-A) and transferred to 1.5 mL tubes (eppendorf). 250 μL of lysis buffer P2 (0.2 M NaOH, 1% SDS) was added, followed by 350 μL of neutralization buffer N3 (4M KOAc pH 5.5). Cell debris was

removed by centrifugation at 21,130xg for 15 min. The supernatant was transferred to fresh 1.5 mL tubes, and further clarified by centrifugation at 21,130xg for 15 min. Finally, 750 μL of the supernatant were transferred to fresh 1.5 mL tubes to which 750 μL of Isopropanol were added. Isopropanol precipitation was carried out overnight at -20°C.

To collect the precipitated bacmid DNA, samples were centrifuged at 21,130xg for 30 min at 4°C. To wash the pellet, 500 μL of 70% ethanol were added gently to the top of the pellet (without resuspension). The samples were centrifuged again at 21,130xg for 15 min at 4°C. The supernatant was removed and the wash and centrifugation steps repeated one more time. Finally, 30 μL of 70% ethanol were added to completely cover the bacmid pellet for storage at -20°C. The remaining half of the bacmid prep was dissolved in 100 μL of water, and used as a PCR template to verify the presence of the genes of interest before transfection.

Insect cell culture

Sf9, Sf21 and Hi5 insect cells were constantly maintained in liquid culture. Sf9 and Sf21 cells were maintained in Gibco® Sf-900™ III SFM media (Thermo Fisher Scientific), whereas Hi5 cells were maintained in ESF921™ media (Expression Systems). Cells were maintained at a density of $1E^6$ cells/mL in culture, optimally diluting the cells with media once every 24 hours. Stock cultures were never diluted below $0.3E^6$ cells/mL and never allowed to overgrow above $3E^6$ cells/mL, and were transferred to fresh flasks once every 3-4 days. Cultures were maintained in a dark windowless climate-controlled room at 27°C with constant shaking at 60 rpm in dedicated Innova® 44 Incubator Shakers (New Brunswick). All steps involving open cultures (addition or removal of media, addition of viruses and withdrawal of samples) were carried out in sterile conditions under a UV-sterilized laminar flow hood. All flasks and serologicals brought under the hood were thoroughly wiped with 70% ethanol first. Glass flasks were washed with 5% acetic acid, twice with milli-Q water, autoclaved once with water, and once without, before re-using.

The flask to culture volume ratio did not exceed 1:10 for Sf9 and Sf21 cultures, and 1:5 for Hi5 cultures. After infection with viruses, cells could be divided into fresh flasks if they were still doubling, but never after proliferation arrest.

All viruses were stored at 4°C in the dark, for up to one year, and not frozen.

Cell density, mean and peak diameter, and cell viability were measured using a CASY® Modell TT Cell Counter and Analyzer System, according to the commercial protocol for insect cells. Uninfected Sf9, Sf21 and Hi5 cells had an average viability range of 85-95%. Sf9 cells had a mean diameter of around 16 μm, which increased upon infection. Sf21 and Hi5 cells had a mean diameter of 20-22 μm.

Sf9 cell transfection (V0 production)

To produce the first viruses (V0) from isolated bacmid DNA, the storage ethanol was gently removed from the top of the bacmid pellet, and the tube was left open for 10 minutes under a laminar flow hood to ensure complete evaporation of the storage solution. 20 μL of water were added to the top of the pellet with as little agitation as possible. 20 minutes were allowed for the pellet to dissolve in water (without mixing).

A transfection master mix containing 10 μL of Xtreme Gene 9 transfection reagent (Roche) and 100 μL of Gibco® Sf-900™ III SFM media (Thermo Fisher), per bacmid to be transfected, was prepared. After dissolution, 200 μL of Sf-900 III media and 100 μL of transfection master mix were added gently to each bacmid without mixing, and allowed to sit for 60 minutes.

3 mL of Sf9 cell culture at a cell density of $1E^6$ cells/mL were pipetted per well in 5 out of 6 wells in sterile 6-well plates (Greiner). 3 mL of media were added to the 6^{th} well as a contamination control. 150 μL of the transfection reagent-bacmid mix were added dropwise per well. Two V0's were made per construct. Plates were incubated for 2-3 days. The cells adhered to the bottom of the wells, and the infectious supernatant (the V0 virus) was collected and stored.

Virus propagation in Sf9 or Sf21 cell culture (V1)

150 μL – 3 mL of V0 virus were added to 25 mL of Sf21 or Sf9 cell culture at a cell density adjusted to $1E^6$ cells/mL, depending on the strength of the V0 virus. Cells should divide at least once before the day of proliferation arrest (DPA), but this can also take up to 4 days. Cells were grown for an additional 2-3 days after DPA, and harvested when their viability dropped below 90%, but was still above 80%. The mean cell diameter should have increased by 3-6 μm by the time of harvest, indicating virus uptake. Viruses were harvested by centrifugation at 500xg for 20 minutes. The infectious supernatant (V1 virus) was stored. The cell pellets were used to perform V1 expression test pull-downs.

Monitoring virus progression

In addition to the baculoviral genome, the isolated bacmids (modified bMON14272) contained an EYFP (enhanced yellow fluorescent protein) reporter gene. This allowed monitoring of infection status and virus production efficiency by observing or measuring YFP fluorescence. For V0 viruses, this was done by looking at the plates under the appropriate fluorescence objective filter on an Axiovert inverted microscope (Zeiss). Optimal transfection resulted in a “starry night” pattern of fluorescence.
For V1 and V2 viruses, cells were collected from 1 mL of virus-treated cultures by centrifugation at 500xg for 10 minutes at 4°C. The media was discarded, and the cells were resuspended in 200 μL of PBS, 100 μL of which were transferred into a black 96-well plate with clear round bottoms (Greiner) and measured using an Infinite® M1000 Pro micro-plate reader (Tecan) using a λ-excitation of 514 nm and a λ-emission of 527 nm. An increase in detected fluorescence over the infection period confirmed successful infection.

V1 expression test pull-downs

Expression test pull-downs from V1 cell pellets, using Ni-NTA agarose (QIAGEN) or amylose beads (NEB), were used to screen for protein expression and solubility from many constructs before large-scale protein production (V2).
Cells from 25 mL V1 culture were resuspended in 1 mL lysis buffer (300 mM NaCl, 20 mM HEPES pH 7.4, 30 mM Imidazole, 1 mM DTT, 10% (v/v) glycerol and 1x protease inhibitor cocktail), and sonicated with a 5-second pulse duration (0.5 seconds on, 0.5 seconds off) and amplitude of 10%. A 30 μL sample was taken from the lysate, and the lysate was clarified by centrifugation at 21,130xg for 30 min at 4°C. A 30 μL sample was taken from the supernatant. The supernatant was then transferred to 250 μL of bead slurry, which had been washed 3 times with 1 mL of water, and 3 times with 1 mL of lysis buffer, and resuspended in 500 μL of lysis buffer (by centrifugation at 1000xg for 1 minute between washes). Protein was allowed to bind to the beads for 30 minutes. The pellet was resuspended in 1 mL of lysis buffer, of which a 30 μL sample was taken.

The flowthrough was collected by centrifugation (1000xg for 1 minute at 4°C), and a 30 μL sample was taken. The beads were washed 3 times with 1 mL of lysis buffer (by centrifugation at 1000xg for 1 minute at 4°C between washes). 40 μL of elution buffer (300 mM NaCl, 20 mM HEPES pH 7.4, 500 mM Imidazole (or 100 mM maltose for amylose-bead pulldowns), 1 mM DTT, 10% (v/v) glycerol and 1x protease inhibitor cocktail) were added to the beads, incubated at room temperature for 1 minute, and then a 30 μL sample was taken.

The volume-normalized samples taken from the lysate, supernatant and pellet, as well as the flowthrough, wash, elution and bead samples, were analyzed by SDS-PAGE, allowing assessment of protein expression and solubility from different constructs.

Protein expression in Hi5 insect cells (V2)

To start Hi5 expression cultures, Hi5 stock cell culture was expanded to 200 mL in a 1 L flask on day 1. On day 2, Hi5 cells were expanded to 2X 300 mL in 2X 3 L flasks. On day 3, if the cell count had reached $1E^6$ cells/mL, V1 virus was added in a 1:2500 ratio of virus to culture. On day 4, cells (which should have doubled) were diluted back to $1E^6$ cells/mL by direct addition of 300 mL of media per flask. This day is ideally also the DPA. If not, cells were continually diluted back to $1E^6$ cells/mL until the DPA was reached. On day 5 (first day after DPA), cells showed a 3-4 μm increase in mean and peak diameters. On day 6 or day 7, cells experienced a rapid drop in viability to below 80%. When this happened, cells were harvested by centrifugation at 238xg for 30 minutes at 4°C, resuspended in 20 mL of the lysis buffer to be used for purification, and flash frozen in liquid N_2.

YFP fluorescence was measured everyday after DPA to monitor infection. When establishing new expressions, 1 mL samples were additionally taken each day after DPA and analyzed by SDS-PAGE to determine the time needed for sufficient expression, but not degradation, of the proteins of interest.

This protocol was for the preparation of a total of 1.2 L of Hi5 protein expression culture (V2) and can be scaled up as needed.

4.3 Protein methods

Preparation of chemically competent BL21 (DE3 RIL), Rosetta, or LOBSTR cells for protein expression

For protein expression in *E.coli*, chemically competent BL21, Rosetta or LOBSTR cells were prepared in the same way as described for XL1-blue, but with additional chloramphenicol in the selection plates and cultures.
Owing to their variability, individual expression protocols will be detailed under the method sections for each of the purified proteins.

Large-scale yeast fermentation culture for isolation of endogenous complexes

Genetically modified yeast strains were used for isolation of endogenous complexes. The doubling time for a given strain was first determined by successive OD_{600} measurement in a small-scale 2 L YPD culture, and plotting a growth curve.
For large-scale fermentation cultures, a colony was used to inoculate a 200 mL YPD preculture with the appropriate antibiotics, which was grown overnight at 30°C. Based on the calculated doubling time, the appropriate volume of preculture was used to inoculate a 2 L culture, such that an OD_{600} of 2.5 was reached within 7-10 hours. This is the minimum starting cell concentration, which could then be used to inoculate a 250 L fermentation culture in an INFORS-HT fermenter in YPD media and the appropriate antibiotics. A sample was checked under a microscope before inoculating the fermenter to ensure absence of bacterial contamination.

Cell lysis methods

For protein purification, insect cells were lysed by sonication for 1-2 minutes, with a pulse duration of 0.4 seconds on, 0.6 seconds off and an amplitude of 30%, using a model 250 Branson Digital Sonifier® (Marshall Scientific), whereas *E.coli* cells were lysed for 15-20 minutes, with a pulse duration of 0.4 seconds on, 0.6 seconds off and an amplitude of 40-60%. All sonication was carried out in beakers made of metal or non-insulating material on ice, in a cold room.

Yeast cells were lysed by bead beating using 0.5 mm dia. glass beads and a BeadBeater (Biospec Products). The metal chamber was filled half with glass beads, and half with yeast cells resuspended in ice-cold lysis buffer, and gently mixed with a glass rod to remove air bubbles. The chamber was then placed in an ice-water jacket in the cold room, and onto the BeadBeater motor base. The BeadBeater was run for 30-second intervals, and 90-second pauses allowing renewal of the ice jacket, for a total of 90 minutes.

Protein buffers and handling

All protein handling steps were carried out at 4°C, in the cold room, or using pre-cooled equipment. The pH of buffers was always adjusted after mixing of all buffer components, and taking into consideration the temperature-dependence of the buffering substance. For 5X and 10X buffers (for example, for sucrose gradients or *in vitro* biochemical reactions) the pH was adjusted at 5X or 10X. Please note, that this may not exactly correspond to the pH under 1X conditions.

SDS-PAGE

Analysis of purified proteins based on molecular weight was done by addition of 4X NuPAGE® LDS sample buffer (Invitrogen) to protein samples, boiling at 95°C for 5 minutes, and loading onto pre-cast gradient NuPAGE® 4-12% Bis-Tris Protein Gels (Invitrogen) together with a Precision Plus Protein™ prestained standard (Bio-rad), as a molecular weight fiducial. The electrophoretic setup was assembled in XCell SureLock™ Mini-Cell chambers (Thermo Fisher Scientific). Proteins were separated on the gel based on their elecrtokinetic properties, by applying a voltage of 150-200V (Biometra Standard Powerpack 25) for 30-60 minutes in a 1X MES or MOPS running buffer (Invitrogen). Gels were stained with InstantBlue™ (Expedeon), destained with water, and scanned with an Epson Perfection V800 flatbed scanner (Epson).

Native-PAGE

Electromobility shift assays and assessment of crosslinking and the behavior of protein compexes were carried out using Native (SDS-free) PAGE. Samples were mixed with 20-30% (v/v) glycerol, and loaded onto NativePAGE™ 3-12% BisTris pre-cast gels (Invitrogen) which had been pre-run for 1 hour at 150 V. Gels were then run at 90 V for 4-6 hours, and visualized by InstantBlue™ (Expedeon) staining, or, in the case of fluorescent proteins, using the appropriate filter on a Typhoon FLA 9500 scanner (GE).

Chromatographic methods

All automated chromatographic methods were carried out using an ÄKTATM Pure protein purification system (GE healthcare). The commercial recommendations for pressures, flow rates and storage of columns and resins were observed. In cases where alteration of these parameters was significant to the protein purification method in question, the values will be specifically mentioned. Otherwise, standard values can be assumed. In cases where complexes were assembled on gel filtration for cryo-EM grid preparation, a Superose™ 6 Increase 3.2/300 column on an ÄKTAmicro™ system was used.

Sucrose gradient ultracentrifugation

A 5X buffer was prepared as needed, and mixed with water and 50% (w/v) sucrose to prepare a buffered heavy solution (30% (w/v) sucrose) and light solution (10% (w/v) sucrose). Roughly 2.5 mL of light solution were transferred to a 4 mL Thinwall Ultra-Clear™ centrifugation tube (Beckman Coulter), and then heavy solution was added to the bottom of the light solution using a FINE-JECT 5-cm syringe needle (Henke-Sass-Wolf) until the meniscus reached the middle mark. A BioComp

Gradient Master 108 (BioComp Instruments) was used to mix the two solutions to make a 10-30% sucrose gradient. Up to 140 μL of sample could be added to the top of the sucrose gradient. The gradients were ultracentrifuged in an SW60 Ti rotor (Beckman Coulter) at 175,000xg for 16 hours at 4°C. After centrifugation, gradients were fractionated into 200 μL fractions by gentle pipetting from the top. The same pipette tip was used for all fractions.

Bioinformatic tools

Gene sequences were obtained from the Saccharomyces Genome Database (SGD) [94]. Protein paramaters (molecular weight, pI and molar extinction coefficient) were calculated using ExPASy ProtParam [95]. For large complexes and protein fusions, sequences were simply concatenated for parameter calculation. Protein domains and secondary structure were found or predicted using the HHPred, PSIPred and Quick2D bioinformatics toolkit [96]. IUPred was used for disorder prediction [97].
Alignment of sequences was carried out using ClustalW [98].

Phos-Tag™ Gels

Phos-Tag™ SDS-PAGE was used to detect phosphorylation of proteins [99]. In this method, Phos-Tag™ (Wako Chemicals), a large molecule (chelating two zinc or manganese ions), which was structurally modeled on an alkaline phosphatase catalytic domain to specifically bind phosphorylated residues (S/T/Y and H/D/K), is used to selectively retard the electromobility of phosphorylated proteins in PAGE. This allows a clear shift to be seen between phosphorylated and unphosphorylated proteins, and between different phosphorylated forms.
SuperSep™ Phos-Tag™ (50 μmol/L), 7.5% 17-well pre-cast polyacrylamide gels (FujiFilm) were used to detect phosphorylation in kinase assays where no phosphosite-specific antibodies were available. The gels were run in a running buffer (100 mM MOPS pH 7.8, 0.1% (w/v) SDS, 5 mM Sodium Bisulfite) freshly diluted from a 5X stock, and freshly adding Sodium Bisulfite solution (from a 500 mM stock solution stored in the dark at 4°C) before use. Care was taken to avoid EDTA in samples, sample loading dyes and running buffers, which would compete away the divalent metal cations from the Phos-Tag™ chemical. Gels were run as normal SDS-PAGE gels. For blotting, gels were washed in a 10 mM EDTA solution for 10 minutes, three times, and then once in EDTA-free transfer buffer before blotting.

Western Blot Analysis

Western blot analysis was used to specifically detect proteins using antibodies against proteins or tags. SDS-PAGE was carried out as described, the gels were not stained, and electric voltage was used to transfer proteins onto polyvinylidene

fluoride (PVDF) or nitrocellulose membranes, using the wet blotting or semi-dry Turbo blotting methods.

For semi-dry Turbo blotting, gels were placed onto a PVDF membrane, sandwiched between three filter papers pre-wetted with transfer buffer from both sides using the pre-assembled Trans-Blot® Turbo™ Mini PVDF Transfer Packs (Bio-Rad). 25 V and 2.5 A of electricity were then applied for 7 minutes using a Trans-Blot® Turbo™ Blotting System (Bio-Rad).

For wet blotting, a piece of Amersham ™ Protran™ 0.2μm nitrocellulose (GE Life Sciences) or 0.45 μm PVDF transfer membrane (Thermo Scientific) was cut out, together with 6 pieces of similarly sized Rotilabo®-Blotting papers thick 1.0mm, and arranged as described into a an XCell II ™ Blot Module (Thermo Fisher Scientific), and submerged in 1X NuPAGE® Transfer buffer (Invitrogen) in 10% ethanol, placed in an XCell SureLock™ Mini-Cell chamber (Thermo Fisher Scientific), and subjected to an electrical voltage of 30 V for 1 hour using a Standard Powerpack 25 (Biometra). For Phos-Tag™ gels, this was carried out at 15 V overnight at 4°C to ensure transfer from the retarding matrix. PVDF membranes were activated with ethanol prior to blotting.

Membranes were blocked with 5% (w/v) milk solution in PBS-T (1X PBS, 0.1% TWEEN 20) for 30 minutes at room temperature, and then the appropriate dilution of primary antibody in 6 mL of 2.5% (w/v) milk solution in PBS-T was added and incubated for 1 hour at room temperature, or overnight at 4°C. Membranes were washed 3 times for 5 minutes with PBS-T once more, and the appropriate dilution of secondary antibody in 6 mL of 0.1%(w/v) milk solution in PBS-T was added and incubated for 1 hour at room temperature or overnight at 4°C. Finally, Membranes were washed again 3 times for 5 minutes with PBS-T, and developed by adding and mixing the two components provided by the Pierce™ Enhanced Chemi-Luminescence Western Blotting Substrate kit (Thermo Fisher Scientific). Membranes were imaged using the chemiluminescence filter on an Advanced Fluorescent Imager (Intas). For all blots where comparisons are presented, images were taken with identical settings of exposure time and signal integration.

Fluorescent-labeling of proteins

For fluorescent-labelling, proteins were first dialyzed into a thiol-free reducing environment (TCEP, no DTT or β-ME).100 μL of protein were incubated with 10 μL of Alexa fluor 647 maleimide reactive dye (Thermo Fisher Scientific) at 10 mg/mL in a ratio of 20:1 pmol of dye to protein for 2 hours at room temperature and away from light. Excess dye was removed first by dialysis overnight in at least 1000X buffer volumes, and then additionally by using a 7K MWCO 0.5 mL Zeba™ Spin Desalting Column (Thermo Fisher Scientific) which had been blocked with 2% (w/v) gelatin solution and washed 10 times with protein buffer before applying the protein.

4.3.1 Mass spectrometry

Protein identification and phosphosite mapping

Mass Spectrometry was used to confirm the identity of purified proteins. M. Raabe and A. Kühn of the H. Urlaub department (Max Planck Institute for Biophysical Chemistry, Göttingen) carried out the measurement and analysis, following standard protocols of in-gel trypsin digestion and extraction [166], peptide enrichment by size exclusion and analysis using an LTQ-Orbitrap Velos or Q-Exactive mass spectrometer (Thermo Fisher Scientific). For phosphosite mapping, samples were treated the same way but enriched for phosphopeptides after gel extraction. Data sets were analyzed with Mascot [167] against the NCBI non-redundant proteome database.

Cross-linking/mass spectrometry

80 μg of CKM-cMed in roughly 100 μL were dialyzed overnight into lower salt buffer (20 mM HEPES pH 7.6, 250 mM KOAc, 10% (v/v) glycerol, 5 mM β-ME) to allow complex formation, then crosslinked with bis-sulfo(succinimidyl) suberate (BS3), stored in powder form (BS3, No-weight Format, Thermo Fisher Scientific) and dissolved in buffer freshly before use to a 30 mM stock, to a final concentration of 0.1 mM BS3. Crosslinked samples were separated by Native-PAGE (20 μg per lane) and species corresponding to the full CKM-cMed complex were excised from the gel (2 lanes) and treated by in-gel digestion with trypsin as described [166]. Briefly – the excised gel bands were cut to 1 mm^2 pieces, reduced with 10 mM DTT, alkylated with 55 mM iodoacetamide and digested with trypsin (Sigma-Aldrich) overnight. Tryptic peptides were extracted, dried and reconstituted in a solution containing 2 % (v/v) acetonitrile and 0.05% (v/v) TFA and subjected to liquid chromatography-tandem mass spectrometry (LC-MS/MS). LC-MS/MS analyses were performed on a Q Exactive HF-X hybrid quadrupole-orbitrap mass spectrometer (Thermo Scientific) coupled to a Dionex Ultimate 3000 RSLCnano system. The peptide mixture from

each gel lane was loaded on a Pepmap 300 C18 column (Thermo Fisher) at a flow rate of 10 µl/min in buffer A (0.1% (v/v) formic acid) and washed for 3 min with buffer A. The sample was separated on an in-house packed C18 column (30 cm; ReproSil-Pur 120Å, 1.9 µm, C18-AQ; inner diameter, 75 µm) at a flow rate of 300 nl/min. Sample separation was performed over 120 min using a buffer system consisting of 0.1% (v/v) formic acid (buffer A) and 80% (v/v) acetonitrile, 0.08% (v/v) formic acid (buffer B). The main column was equilibrated with 5% B before application of the peptide mixture to the column and the column was washed for 3 min with 5% B. Peptides were eluted with a linear gradient over 105 min from 10-45 % B (replicates 1-3) or 15-50 % B (replicate 4), followed by an 8 min gradient from 90-95 % B and re-equilibration for 4 min at 5 % B. Eluting peptides were analyzed in positive mode using a data-dependent top 20-acquisition methods. MS1 and MS2 resolution were set to 120,000 and 30,000 FWHM, respectively, and AGC targets were $5*10^5$ and $2*10^5$. Precursors selected for MS2 (scan range *m/z* 380-1580) were fragmented using 30% normalized, higher-energy collision-induced dissociation (HCD) fragmentation. Allowed charge states of selected precursors were +3 to +7 (replicates 1, 2, 4) or +2 to +7 (replicate 3) Further MS/MS parameters were set as follows: isolation width, 1.4 *m/z*; dynamic exclusion, 10 sec; max. injection time (MS1/MS2), 60 ms/200 ms. The lock mass option (*m/z* 445.12002) was used for internal calibration.

The .raw files of all replicates from both lanes were searched by the software pLink 2, version 2.3.1 [168] against a customized protein database containing the expressed proteins. Protein-protein crosslinks were filtered with a 1 % FDR and plotted using xiNET [169]. Manual validation of identified crosslinks was performed by a selection of 8 crosslinks between cMed subunits, mapping them onto the *S.cerevisiae* cMed homology model derived from the *S.pombe* crystal structure (PDB ID: 5N9J). Atomic distances were measured between α-carbon atoms of crosslinked residues using PyMol.

4.3.2 Light microscopy methods

mPEGylation of glass slides

To ensure inertness of the underlying glass substrate to phase-separated droplets, glass slides were passivated with mPEG silane before use following the method from [170]. Glass microscope slides (Thermo Scientific) were washed with 5% Hellmanex solution (VWR) for 4 hours, and then rinsed with Milli-Q water and allowed to dry in a fume hood. The slides were then etched in 1M NaOH for 1 hour, rinsed extensively with Milli-Q water, and dried again in a fume hood. 2x 80 µL drops of 25 mg/mL mPEG-silane (Nanosoft polymers) in 95% ethanol were pipetted on to the glass slides and allowed to stand overnight. The slides were rinsed once with 95% ethanol

and thoroughly with Milli-Q water, and allowed to dry completely in a fume hood for 3-4 hours before use.

Fluorescence microscopy

Images of liquid droplets on glass slides were taken using a Leica DM6000B inverted fluorescence microscope fitted with the following objective filter cubes and excitation wavelengths (Exc):
A4(UV): Exc 360/40, BGR(UV): Exc 420/30;495/15;570/20, GFP(blue): Exc 470/40, L5(blue): Exc BP 480/40, N3(green): Exc BP 546/12, 60R (red): Exc HQ 630/20x

All images were taken through the 63X magnification water-immersion objective. Images of liquid droplets of unlabeled proteins were taken using the Differential Interference Contrast (DIC) setting. GFP-tagged or FAM-labeled proteins were imaged through the GFP filter cube. mCherry or Alexa Fluor 647-labelled proteins were imaged through the 60R filter cube. There was no bleedthrough signal between the GFP and the 60R filter cubes. For all images where comparisons are presented, settings of magnification, exposure time, gain and intensity were kept constant between the different images.

4.3.3 Electron microscopy methods

Sample fixation

Electron Microscopy (EM) samples were usually fixated by chemical crosslinking. Batch crosslinking was done with bis-sulfo(succinimidyl) suberate (BS3) or glutaraldehyde. BS3 was stored in powder form (BS3, No-weight Format, Thermo Fisher Scientific) and dissolved in buffer freshly before use to a 30 mM stock. The appropriate volume of BS3 to reach the desired final concentration was added to the bottom of a 1.5 mL tube (eppendorf), and the larger volume of the protein sample was rapidly pipetted on top, to ensure fast and complete mixing. Batch crosslinking with glutaraldehyde was done similarly, using a 25% EM grade glutaraldehyde aqueous solution (Electron Microscopy Sciences). Ampoules were opened once, aliquoted, flash-frozen in liquid N_2 and stored at -80°C. Aliquots were only used once.

The majority of samples were crosslinked in a sucrose gradient using the GraFix method [100]. Sucrose gradients were prepared as previously described, but with addition of glutaraldehyde in the heavy sucrose solution to the desired final glutaraldehyde concentration in the gradient.

Quenching

Glutaraldehyde was quenched after crosslinking by addition of 25-50 mM of aspartate, or an apartate/lysine/tris mixture, and incubation on ice for 15 minutes. BS3 was quenched with 0.1 M tris buffer and 0.01 M ammonium bicarbonate.

EM Grids

For negative stain EM, commercial carbon-coated copper mesh grids (S160-4; Plano), were used. For cryo-EM, carbon grids; Quantifoil® R 1.2/1.3 Cu 300 mesh or Quantifoil® 2/1 Cu 200 mesh, or gold grids; UltrAuFoil® R 2/2 Au 200 mesh, were used.

Grids with continuous carbon support were either made by pre-floating carbon foil onto the surface of a water reservoir and fishing it from below with a Quantifoil® carbon grid, or by directly floating the carbon foil onto the surface of the sample before freezing. Pre-floated carbon grids were a kind gift from Carrie Bernecky. Carbon foil was either homemade using a Leica EM ACE600 carbon evaporator at approximately 3 nm in thickness, or was a kind gift from Holger Stark.

Glow discharging

Negative stain EM grids were glow discharged using a PELCO easiGlow™ glow discharger (Ted Pella) for 45 seconds at 25 mA and 0.39 mbar. Cryo-EM carbon grids were glow discharged for 80 seconds, and gold grids for 160 seconds with the same settings. Pre-floated continuous carbon grids were glow discharged as holey carbon grids. Continuous carbon grids made by floating carbon foil on the sample were not glow discharged.

Negative staining

5 μL of sample were pipetted onto the surface of a carbon-coated copper grid, and incubated for 30 seconds to 2 minutes, depending on the sample concentration. The sample was blotted away using a Whatman™ filter paper (GE Life Sciences). Two 20 μL drops of water and three 20 μL drops of 2% uranyl formate solution were pipetted onto a piece of Parafilm® (Bemis Flexible Packaging). The grid was picked up with tweezers, and placed face-down on each of the water droplets and the excess water was blotted away, and then on each of the uranyl formate drops, where it was held for 20 seconds (a total of 60 seconds). Finally, the excess stain was either blotted away, or incubated for an additional 20 seconds to 1 minute, depending on the required degree of staining.

Cryo-EM

Buffer exchange

After GraFix, buffer was exchanged into the chosen freezing buffer to remove the high concentration of sucrose. Dialysis was done using Slide-A-Lyzer® MINI Dialysis Devices, 3.5K MWCO, 2 mL (Thermo Fisher Scientific) or Slide-A-Lyzer® MINI Dialysis Units, 20K MWCO, 0.1 mL (Thermo Fisher Scientific). Alternatively, buffer was exchanged using Zeba™ Spin Desalting Columns, 7K MWCO, 0.5 mL (Thermo Fisher Scientific), by washing them twice with freezing buffer, once with a 2% gelatin solution, followed by 10 times with freezing buffer, before applying the protein sample.
We noticed that when dialyzing into freezing buffers containing detergents with low critical micelle concentrations (CMC) such as Lauryl Maltose Neopentyl Glycol (LMNG, Anatrace), that the detergent did not pass through the dialysis membrane. Therefore, for these samples we either added the detergent directly to the dialyzed sample before freezing, or used the spin column buffer exchange method.
We also noticed that, although it doesn't pass through the dialysis membrane, that the volume expansion during dialysis (which was generally at least 3 to 4 times) resulting in undesired dilution of the sample, was significantly counteracted in the presence of LMNG in the dialysis buffer to almost no expansion at all. This can be explained by the osmotic effect caused by the inability of micelles to permeate the dialysis membrane, and may be used as a trick to minimize volume expansion during dialysis.

Plunge freezing

Cryo-EM grids of samples were made by sample application followed by automated plunge freezing into a cryogen tank of liquid ethane immersed in a liquid N_2 reservoir, using an FEI Vitrobot™ (Thermo Fisher Scientific). Whatman™ filter papers (circular, 55 mm diameter) were placed in the vitrobot chamber 30 minutes before freezing to equilibrate their moisture content. The humidity of the vitrobot chamber was set to 100% and the temperature to 4°C. A glow-discharged grid was placed on the tweezer, which was in turn fixed on the vitrobot tweezer holder and withdrawn into the temperature and humidity controlled vitrobot chamber. 3-4 μL of sample were pipetted onto one side of the grid. The grid was plunged into the ethane vitrification media, quickly transferred to liquid N_2 and stored. All handling, transfer and storage steps were carried out in liquid N_2 or liquid N_2 atmosphere conditions.

Imaging (Neg stain and Cryo)

Negative stain grids were imaged on a CM120 (Phillips) electron microscope with a lanthanum hexaboride (LaB_6) cathode, and a spherical aberration of 6.7 mm. 4K X 4K TIFF Micrographs were taken at a magnification of SA 52,000X.

Cryo-EM grids were imaged on an FEI Titan Krios (Thermo Fisher Scientific) fitted with a K2 summit camera and a GIF energy filter, at a magnification of SA 105,000X (1.37 Å/pix) or SA 130,000X (1.05 Å/pix).

The CKM cryo-EM dataset was imaged on an FEI Titan Krios (Thermo Fisher Scientific) fitted with a Falcon III camera, and without a GIF, at a magnification of SA 130,000X. The built-in EPU software was used to set up automated image collection from holes.

Image Processing

Negative stain images were binned by a factor of 2 (4.4 Å/pix), and particle picking was carried out in EMAN2 [101], with a box size of 88 pix and a particle size of 60 pix. Picked particle coordinates were exported. Particle extraction, Contrast Transfer Function (CTF) estimation and 2D classification were carried out in Relion 1.4. The particle mask diameter used was 300 Å. 2D classification was run for 50 iterations, to sort the particles into 100 2D classes, with a regularization parameter (T) of 2. 3D *ab initio* model building was carried out using CryoSparc [102], using picked particles from all the good 2D classes.

Cryo-EM micrographs were pre-processed (Motion correction, CTF estimation and Auto-picking) using the on-the-fly pre-processing pipeline Warp [35]. Particles were then extracted unbinned (1.06 Å/pix) and processed in Relion 2.0 [103]. The particle mask diameter used was 260 Å, and the box size was 290 pix. 2D classification was run for 50 iterations, to sort the particles into 100 2D classes, with a regularization parameter (T) of 2. The best 2D classes were selected, and 3D classification into 5 classes was carried out using the *ab initio* model of CKM as an input reference. 2D projections from the best 3D class obtained were used to train the Relion autopicker on a small selection of micrographs, and write a Figure of Merit map, which was then used to guide re-picking particles more accurately from the entire dataset. Several rounds of 2D and 3D classification were carried out with varying parameters of offset search step and range, as well as changing the input model to one of the 3D volumes obtained from 3D classification. Additionally several rounds of homogeneous and heterogeneous refinement were done. There was no improvement in the 3D model.

4.3.4 Purified proteins

Mediator Cdk8 Kinase module (CKM A or KD)

Clones number 44 for CKM(A) and 45 for CKM(KD) in table 4.2 were the final constructs used for making viruses. V0 and V1 viruses were made in Sf9 cells as described. V0 viral load was titrated (250 μL, 500 μL, 1000 μL and 2000 μL). V1 from the V1 culture with the highest YFP fluorescence read 2 days after DPA was used to infect Hi5 cells in a 1:2500 ratio of V1 to Hi5 culture. Cells were harvested 3-4 days after DPA, with daily monitoring of viability (which should not drop below 75% at this stage).

Pellets from 2.4 L of Hi5 insect cell culture, frozen in lysis buffer (20 mM HEPES pH 7.6, 400 mM KOAc, 10% (v/v) glycerol, 5 mM β-ME, 1X PI) were thawed in a temperate water bath, lysed by sonication for 2X 1 min, with a pulse duration of 0.4 seconds on, 0.6 seconds off and an amplitude of 30%. The lysate was clarified by centrifugation at 27,000 rpm in an A27-8x50 rotor (Thermo Scientific).

60 mL of amylose beads slurry (NEB) were equilibrated with lysis buffer. Supernatant containing CKM was added to the equilibrated beads, and bound with nutation for 1.5 hours. The flowthrough was collected by centrifugation of the beads (1000xg for 5 minutes) or by gravity flow (PolyPrep gravity flow columns, Bio-Rad). The beads were washed with lysis buffer, by adding 3 resin volumes of lysis buffer, resuspending the beads, and centrifugation, or by gravity flow. This was repeated 3 times. Finally, 2 resin volumes of elution buffer (20 mM HEPES pH 7.6, 400 mM KOAc, 10% (v/v) glycerol, 5 mM β-ME, 100 mM maltose, 1X PI) were added. The beads were incubated with elution buffer for 15 minutes, and the eluate was collected by gravity flow. It is not possible to perform this step using an automated chromatography system. Moreover, MBPTrap (GE healthcare) columns, showed a dramatically lowered complex-binding capacity.

The eluate was diluted 3:1 (eluate to buffer) dropwise with IEX buffer A (20 mM HEPES pH 7.6, 10% (v/v) glycerol, 5 mM β-ME), bringing the salt concentration down to 300 mM KOAc. (This salt concentration was determined by dropwise dilution until first precipitation). The protein was then loaded onto a HiTrapQ HP (1 mL) column (GE Healthcare), equilibrated with 30% IEX buffer B (20 mM HEPES pH 7.6, 10% (v/v) glycerol, 1 M KOAc, 5 mM β-ME), and eluted with a salt gradient from 30% to 100% buffer IEX B over 20 column volumes (20 mL). A steep elution gradient in this step is critical. The protein-containing fractions were pooled and concentrated using an Amicon Ultra-15 centrifugal filter with a 10 kDa MWCO, spun at 2700 rpm for 8-minute intervals. Using this type of centrifugal filter (despite the huge discrepancy in the cutoff value compared to the size of the complex) was critical, It is

not clear why. The complex was dialyzed overnight into gel filtration buffer (20 mM HEPES pH 7.6, 400 mM KOAc, 10% (v/v) glycerol, 5 mM β-ME), and then run on size-exclusion chromatography on a Superose™ 6 Increase (10/300) column (GE Healthcare). It is important to concentrate the complex *before* the dialysis step, and not after. Dialysis was critical for stability on any subsequent sizing step. Up to 800 *μ*g of CKM were obtained per purification. Alternatively, the complex was applied onto a sucrose gradient, as previously described, and the buffer was exchanged before use.
The complex was flash frozen in liquid N_2 after dialysis, provided a sizing step was to be carried out before further use (gel filtration or sucrose gradient ultracentrifugation). Otherwise, the complex was purified freshly before use.

Core Mediator (cMed)

Recombinant core Mediator (cMed) was expressed and purified as two separate subcomplexes, cMedΔ4,9 (containing the subunits Med17, Med18, Med6, Med8, Med20, Med22, Med11, Med19, Med7, Med21, Med10, Med31, and His(x10) Med14(1-745)) and the Med1,4,9 heterotrimer, that were later reconstituted on gel filtration.
cMedΔ4,9 was expressed in BL21 (DE3 RIL) cells. A 200 mL preculture in LB-Amp-Strep-Kan-Cam was grown overnight at 37°C. 24 L (12x 2L LB cultures) were grown by inoculating each with 15 mL of overnight culture, and the appropriate amount of antibiotics. Cultures were grown at 37°C until an OD_{600} of 0.7 was reached (3-4 hours). The flasks were then cooled on ice for 30 minutes, and the incubator shakers were cooled down to 18°C. Cultures were induced with 0.5 mM IPTG and grown for 20-24 hours at 18°C, and harvested by centrifugation at 6000 rpm in a F9-6X1000 LEX rotor (Thermo Scientific) for 10 minutes. Cell pellet from 8 L of culture was used per purification.

Med1,4,9 was likewise expressed in BL21 (DE3 RIL) cells. A 200 mL preculture in LB-Strep-Cam was grown overnight at 37°C. 12 L (6x 2L LB cultures) were grown by inoculating each with 25 mL of overnight culture, and the appropriate amount of antibiotics at 37°C until they reached an OD_{600} of 0.7 and were then similarly cooled down and induced with 0.5 mM IPTG, grown for 20-24 hours at 18°C, and harvested. Cell pellet from 4 L of culture was used per purification.

For purification of cMedΔ4,9, the cell pellet was resuspended in 80 mL of lysis buffer (25 mM HEPES pH 7.5, 400 mM KOAc, 10% (v/v) glycerol, 2 mM DTT, 1X PI, 30 mM imidazole), sonicated for 15 minutes (45% amplitude, 0.4 seconds on, 0.6 seconds off), and clarified by centrifugation for 60 minutes (27,000 rpm in an A27-8x50 rotor (Thermo Scientific)). The supernatant was filtered through a Millex® 0.45 *μ*m PVDF syringe filter unit (Millipore), and then loaded onto a 5 mL HisTrap HP

column (GE Healthcare) which had been equilibrated with 3 column volumes of lysis buffer. The column was then washed with 5 column volumes of lysis buffer. Contaminants were washed off with a 0-21% elution buffer (25 mM HEPES pH 7.5, 400 mM KOAc, 10% (v/v) glycerol, 2 mM DTT, 500 mM imidazole) gradient over 10 column volumes, and the complex was eluted with a step elution to 100% elution buffer over 10 column volumes. Protein-containing fractions were pooled, and diluted with 3 volumes of IEX buffer A (25 mM HEPES pH 7.5, 100 mM KCl, 10% (v/v) glycerol, 2 mM DTT, 1 mM EDTA). 100 μL of 5 mg/mL 3C protease were added and incubated for 3 hours at 4°C. The protein was then loaded onto a 1 mL HiTrap Q HP column (GE Healthcare), which had been equilibrated with 10 column volumes of IEX buffer A. The complex was eluted with a 0-30% salt gradient of IEX buffer B (25 mM HEPES pH 7.5, 2000 mM KCl, 10% (v/v) glycerol, 2 mM DTT, 1 mM EDTA) over 200 column volumes at a flow rate of 0.75 mL/min. The complex was pooled and concentrated to 3 mg/mL (An E1% value of 7.6 was taken for concentration measurement). The complex was flash frozen in liquid N_2.

For purification of Med1,4,9, cell pellet was processed in exactly the same way until 3C protease tag cleavage, and was then loaded onto a MonoQ 5/50 GL column (GE Healthcare), which had been equilibrated with 10 column volumes of IEX buffer A. The trimer was eluted with a 0-30% salt gradient of IEX buffer B over 150 column volumes at a flow rate of 0.75 mL/min. The complex was pooled and concentrated to 1.7 mg/mL (An E1% value of 7.0 was taken for concentration measurement). The complex was flash frozen in liquid N_2.

cMedΔ4,9 and Med1,4,9 were mixed together in a 1:1.5 molar ratio, and loaded onto a Superose 6 10/30 Increase column (GE Healthcare) run at 0.3 mL/min and taking 0.2 mL fractions, to resolve the cMed complex from the excess trimer. Fractions containing the full complex were pooled and concentrated in a 50K or 100K MWCO Vivaspin® 6 centrifugal concentrator (Sartorius) at 15°C, to 3-6 mg/mL and used directly or flash frozen (minimization of concentration time as much as possible has a large impact on the yield). 300-700 μg of pure cMed were obtained per purification.

Endogenous Mediator (eMed)

Endogenous Mediator was purified using a standard TAP-tag purification. A 300 g pellet of cells from *S.cerevisiae* fermentation culture frozen in a 2:1 volume ratio of cells to TEV extraction buffer (50 mM HEPES pH 7.6, 250 mM KOAc, 1 mM EDTA, 10% (v/v) glycerol, 1X PI, 1 mM DTT) was thawed in a 30°C water bath, then transferred together with 220 mL of glass beads into a BeadBeater chamber, and lysed by bead beating for 90 minutes. The glass beads were removed, and the required volume of 5M KOAc at pH 7.6 was added to bring the final KOAc concentration to 600 mM. The lysate was centrifuged for 1 hour at 12,000 rpm in an

F14-6x250y rotor (Thermo Scientific), and then untracentrifuged for 2 hours at 42,000 rpm in a Ti45 rotor (Beckman Coulter).
2X 4 mL resin volume of IgG-sepharose beads slurry (GE Healthcare) were washed twice with 40 mL of TEV extraction buffer (with 5 minutes of nutation, and then spinning for 5 minutes at 3128xg between washes).
The clarified supernatant was added to the equilibrated IgG beads and allowed to bind overnight at 4°C with nutation.
The beads were collected by centrifugation (3128xg for 8 minutes), the flowthrough removed, and the beads washed 3 times with TEV extraction buffer, and once with TEV extraction buffer + 0.1% NP-40 (NP-40 Sufact-Amps™, Thermo Fisher Scientific). Note that using detergent of high quality is essential for this purification. The beads were resuspended to roughly 10 mL with TEV extraction buffer + 0.1% NP-40. 340 μg of TEV protease were added, and incubated with nutation for 3 hours at room temperature. The beads were collected, and the eluate (around 6 mL) saved (E1). Two more 6 mL buffer elutions with TEV extraction buffer (E2, and E3) were done. Elution fractions were pooled, and calcium chloride was added to a final concentration of 3 mM. 2X 1.4 mL of calmodulin resin (IBA) was washed 3 times with calmodulin binding buffer (50 mM HEPES pH 7.6, 250 mM KOAc, 1 mM EDTA, 10% (v/v) glycerol, 1X PI, 1 mM DTT, 3 mM $CaCl_2$, 1 mM imidazole, 0.01% NP-40). The Mediator-containing IgG elutions were added to the equilibrated calmodulin resin and allowed to bind overnight at 4°C with nutation.

On the following day, the beads were collected (3128xg, 8 minutes), washed twice with 12 mL of calmodulin wash buffer 1 (50 mM HEPES pH 7.6, 250 mM KOAc, 1 mM EDTA, 10% (v/v) glycerol, 1 mM PMSF, 1 mM TCEP, 3 mM $CaCl_2$, 1 mM imidazole, 0.1% NP-40), twice with 12 mL of calmodulin wash buffer 2 (50 mM HEPES pH 7.6, 250 mM KOAc, 1 mM EDTA, 10% (v/v) glycerol, 1 mM PMSF, 1 mM TCEP, 3 mM $CaCl_2$, 1 mM imidazole, 0.01% NP-40), and then transferred to a 10 mL gravity flow column (Bio-Rad). The wash buffer was allowed to flow out, and 6x 0.8 mL of elution buffer ((50 mM HEPES pH 7.6, 250 mM KOAc, 1 mM EDTA, 10% (v/v) glycerol, 1 mM PMSF, 1 mM TCEP, 3 mM EGTA, 1 mM imidazole, 0.01% NP-40) were added and collected (E1-E5). Fractions were analyzed by SDS-PAGE. Complex-containing fractions were pooled and concentrated in a 100K MWCO Vivaspin® 6 centrifugal concentrator (Sartorius), and quantified using Bradford assay (Pierce™ Coomassie Plus (Bradford) Assay reagent – Thermo Fisher Scientific) against a BSA standard curve.

Elutions were used directly or kept at 4°C for 1 day but not frozen. This complex is not freeze-thaw stable (we noticed by sucrose gradient ultracentrifugation comparing fresh sample, versus sample after freeze-thaw). 100-200 μg of purified eMed were obtained per purification.

Gcn4

BL21 (DE3) RIL chemically competent cells were transformed with the plasmid, and used to inoculate a 200 mL preculture in LB medium with the appropriate antibiotics. The 200 mL preculture was then diluted to 2L on the following morning with LB and the appropriate antibiotics. Cells were induced when they reached an OD_{600} of 0.5-0.6 by adding 0.5 mM IPTG and were harvested 4 hours later. Pellets were resuspended in 20 mL of lysis buffer (20 mM HEPES, pH 7.4, 500 mM NaCl, 20 mM Imidazole, 1x PI, 1 mM β-ME) and flash frozen until needed.

Pellets were thawed and sonicated for 15 minutes at 40% amplitude with a pulse of 0.4 s on and 0.6 s off. The lysate was clarified by centrifugation at 20,000 rpm for 45 minutes. 2mL of approximately 50% Ni-NTA agarose slurry (washed once with water, and once with 5 volumes of lysis buffer, then resuspended in 2 mL of lysis buffer) was added per 2L of culture. 1 hour of nutation was allowed for binding at 4°C. The beads were spun down at 500xg for 2 minutes, and then washed 4 times with lysis buffer, before adding 5 mL of elution buffer (20 mM HEPES, pH 7.4, 500 mM NaCl, 500 mM Imidazole, 1x PI, 1 mM β-ME), and incubating for 10 minutes at 4°C. The eluate (E1) was collected by spinning down the beads, and this was repeated twice (E2 and E3). E1, E2 and E3 were combined and diluted 1:5 with buffer A (20 mM HEPES, pH 7.4, 1 mM EDTA, 10% glycerol) to bring down the salt concentration to 100 mM. The eluate was then loaded onto a 5 mL HiTrap Heparin (GE healthcare) column equilibrated in 10% buffer B (20 mM HEPES, pH 7.4, 1 mM EDTA, 10% glycerol, 1M KCl), using a sample pump connected to an ÄKTA pure system (GE healthcare) at 3 mL/min. The fractions were analyzed with SDS-PAGE using a MES buffer. Fractions containing Gcn4 were pooled and concentrated using a 50 mL 10,000 MWCo Amicon® concentrator by centrifugation at 3000xg for 30 minute intervals at 4°C. The total concentration time was 2.5-3 hours. The final protein concentration was determined to be 8 mg/mL (258 μM) using an extinction coefficient value of 11,460 and a molecular weight of 31,000 Da.

GFP-Gcn4

LOBSTR chemically competent cells were transformed with the mEGFP-Gcn4 plasmid, and used to inoculate a 200 mL preculture in LB medium with the appropriate antibiotics. The preculture was diluted 1:30 in 2L on the following morning with LB and the appropriate antibiotics. Cells were grown 1.5 hours at 16°C and then induced with 1 mM IPTG and were incubated for 5 hours at 37°C. Pellets were frozen until needed.

His-mEGFP-Gcn4 was purified following the same buffers and protocol as for His-Gcn4. After elution from Heparin, fractions containing purified protein were pooled

and dialyzed into buffer D (20 mM HEPES, pH 7.4, 300 mM NaCl, 10% glycerol, 1mM TCEP). Fractions were then concentrated to 23 mg/mL (396 μM) and flash frozen.

mCherry-Med15

LOBSTR cells were transformed with the mCherry-Med15 plasmid, and one colony was used to inoculate a 200 mL preculture in LB medium and the appropriate antibiotics. The following morning, cultures were diluted 1:30 in 500 mL LB medium with the appropriate antibiotics. Cultures were grown at 16°C, and induced with 1 mM IPTG after 1.5 hours, irrespective of their O.D.600. The temperature was raised to 37°C and the cultures were grown for an additional 5 hours after induction. Cells were harvested, flash frozen, and stored at -80°C until needed.

For protein purification, cell pellet from a total of 2L of culture was resuspended in 15 mL of Ni-binding buffer (50 mM Tris, pH 7.5, 500 mM NaCl, 10 mM Imidazole, 1 mM β-ME, 1x PI), and lysed by sonication using a pulse amplitude of 40% and duration of 0.4 s on, 0.6 s off, for a total time of 10 minutes. Lysate was clarified by centrifugation at 27,000 rpm for 30 minutes. Supernatent was then added to 2 mL Ni-NTA agarose slurry (Qiagen) that had been washed once with water, and once with 5 CV of lysis buffer, and nutated for 1 hour at 4°C. The flowthrough was collected by spinning down the beads at 500x g for 2 minutes. 15 CV of Ni-binding buffer were then added to resuspend the beads, and the slurry was transferred to a gravity flow column. The protein was eluted with 2 CV E50 (50 mM Tris, pH 7.5, 500 mM NaCl, 50 mM Imidazole, 1mM β-ME, 1x PI), followed by 2 CV E100 (50 mM Tris, pH 7.5, 500 mM NaCl, 100 mM Imidazole, 1mM β-ME, 1x PI), then 3 CV E250 (50 mM Tris, pH 7.5, 500 mM NaCl, 250 mM Imidazole, 1mM β-ME, 1x PI). The fractions were visualized by SDS-PAGE in MES buffer. Fractions containing the protein were pooled and concentrated in a 15 mL Amicon® centrifugal filter (Merck-Millipore) with a 50,000 MWCO by centrifugation at 3300 rpm for 15 minute intervals until the volume was reduced to 150 μL. It was then dialyzed overnight in 1L dialysis buffer (20 mM HEPES, pH 7.4, 300 mM NaCl, 10% glycerol, 1 mM TCEP) using a 2 mL Slide-A-Lyzer MINI dialysis device, 3.5 MWCO (Thermo). Concentration was calculated based on parameters computed using the ExPASy ProtParam tool; molar extinction coefficient of 58,790 and a molecular weight of 102 kDa. Note that the concentration is approximate due to the partial purity of the protein purified in this method (which was adapted from [52]).

Med15_KIX123

The plasmid was used to transform BL21 (DE3 ril) chemically competent cells. One colony was used to inoculate a 200 mL preculture in LB medium with the appropriate

antibiotics. 20 mL were then taken and diluted to 2L with LB and the appropriate antibiotics. Cells were induced with 0.5 mM IPTG when they reached an OD_{600} of 0.5-0.6, and harvested after 3 hours of induction. Cells were flash frozen and stored at – 80°C until use.

Cell pellet from 3L of culture was resuspended in 90 mL of Ni-binding buffer (50 mM HEPES, pH 7.0, 500 mM NaCl, 40 mM Imidazole, 10% glycerol, 1x PI, 1 mM β-ME) and sonicated for 10 minutes, with an amplitude of 40% and a pulse duration of 0.4s on, 0.6s off. The lysate was then clarified by centrifugation at 27,000 rpm for 40 minutes. 2x 2 mL Ni-NTA agarose beads slurry (Qiagen) were washed once with 5 CV of water, and once with 5 of CV Ni-binding buffer by spinning at 500x g for 2 minutes between washes, and resuspended in 2x 2mL Ni-binding buffer. Clarified lysate was added to the beads, and nutated for 1 hour at 4°C for binding. Flowthrough was collected by spinning down the beads at 500x g for 2 minutes. The beads were washed 3 times, each with 5 CV of Ni-binding buffer, by spinning at 500x g for 2 minutes between washes. 20 mL elution buffer (50 mM HEPES, pH 7.0, 500 mM NaCl, 500 mM Imidazole, 10% glycerol, 1x PI, 1 mM β-ME) were added to the beads, and nutated for 10 minutes. The elution was collected by centrifugation, and 30 mL of Heparin buffer A (50 mM HEPES, pH 7.0, 10% glycerol, 1x PI, 1 mM β-ME) were added to the eluate to bring down the salt concentration to 200 mM NaCl.

The eluate was then loaded onto a 5 mL HiTrap Heparin (GE healthcare) column equilibrated in 20% buffer B (50 mM HEPES, pH 7.0, 10% glycerol, 1M NaCl, 1x PI, 1 mM β-ME), using a sample pump connected to an ÄKTA pure system (GE healthcare) at 3 mL/min. The column was then washed with 5 column volumes of 20% buffer B, and eluted in a gradient of 20 – 50% buffer B over 10 column volumes, followed by a step of 100% buffer B for 5 column volumes. Fractions were analyzed by SDS-PAGE in MES buffer. Fractions containing the protein were pooled and concentrated in a 15 mL Amicon® centrifugal filter (Merck-Millipore) with a 50,000 MWCO by centrifugation at 3300 rpm for 15 minute intervals until the volume was reduced to 150 μL. The sample was then dialyzed overnight in 1L dialysis buffer (50 mM HEPES, pH 7.0, 10% glycerol, 300 mM NaCl, 1 mM TCEP) using a 2 mL Slide-A-Lyzer MINI dialysis device, 3.5 MWCO (Thermo). The sample was concentrated again using a 0.5 mL Amicon® centrifugal filter (Merck-Millipore) with a 50,000 MWCO at 5,500 rpm for 15 minute intervals to a final concentration of 17.3 mg/mL (170 μM). Values were calculated using a molar extinction coefficient of 89,300 and a molecular weight of 102 kDa (the MBP tag was not cleaved).

CTD of RNAPII

GST-tagged RNAPII CTD was purified as in [20].

RNAPII and transcription initiation factors

RNAPII and the GTFs; TFIIA, TBP, TFIIB, TFIIF and TFIIE were purified essentially as previously described [87] with the help of Carina Burzinsky.

Kinase assays

Two reactions were set up with active versus dead CKM in a total volume of 20 μL. The appropriate volume of components were pipetted to have 10 μM GST-hCTD, 0.4 μM CKM(A or KD),1X of 5X buffer (100 mM HEPES pH 7.5, 1.5M KOAc, 25 mM β-ME),10 mM $MgCl_2$ and [10 mM ATP – added later] in the final reaction. The volume was brought up to 20 μL with water.

All components except for ATP were mixed together on ice, and then transferred to a 30°C heat block, with 300 rpm shaking (eppendorf ThermoMixer C). Tubes with 8 μL 4x LDS buffer were prepared for quenching by denaturation of protein reaction components. 1 μL of the starting reaction was transferred to the time point 0 quenching tube. Then, ATP was added, and 2 μL samples from the reaction were taken and quenched after 5, 10, 20, 30, 60 and 120 minutes.

1 μL from each time point, for both the CKM(A) and CKM(KD) reactions, was run in MES buffer on an SDS-PAGE gel and blotted with the CTD Ser5 phosphosite specific antibody. The same was repeated for blotting with CTD Ser2, Ser7 and Tyr1 phosphosite specific antibodies (a kind gift from Dirk Eick).

The RNAPII kinase assay was performed in exactly the same way, but using roughly 6.5 μM RNAPII in the reaction, which had been dephosphorylated by treatment with λ-phosphatase for 1 h at 4°C before gel filtration within the standard RNAPII purification.

The Gcn4 kinase assay was peformed essentially as described, but using 13 μM of His(x6)-Gcn4 and 0.5 μM CKM(A) in the kinase reaction, or 13 μM His(x6)-Gcn4 + 20 μM scaffold DNA (sc3).

Immobilized-Template Assay

40 μL of Dynabeads® MyOne™ Streptavidin T1 beads (Life Technologies) per planned reaction (x) = Y μL were transferred to a 2 mL tube (eppendorf). Using a

DynaMag™ magnetic rack (Life technologies), buffer was removed. Beads were washed three times with Y µL of streptavidin binding buffer (20 mM HEPES pH 7.5, 150 mM KOAc, 5-10% glycerol, 5 mM BME, 10 mM MgCl2, 0.05% NP40), and then resuspend in Y - x µL buffer, with x µL of biotinylated scaffold DNA (sc1) at 40 µM. Beads were incubated with DNA for 25 minutes at 25°C, and washed once with Y µL of streptavidin binding buffer to remove excess scaffold, and resuspend in Y µL. Resuspended beads were divided into 40 µL per reaction tube.

Seven reactions were set up; (1) Scaffold + CKM(KD), (2) Scaffold + cMed, (3) Scaffold + cMed-CKM(KD), (4) Scaffold + PIC factors + cMed, (5) Scaffold + PIC factors + cMed-CKM(A), (6) Scaffold + PIC factors + cMed-CKM(A) +ATP, (7) Scaffold + PIC factors + cMed-CKM(KD) + ATP.

For PIC-containing reactions, the PIC factors were mixed such that 40 pmol each of TFIIA, TFIIB and TBP, 10 pmol of RNAPII, 20 pmol of TFIIF and 60 pmol of TFIIE are present per reaction. The volumes required for 4 reactions were mixed together, made up to 40 µL with buffer, or with buffer – volume of additional components. For reactions (4), (5), (6) and (7), 10 µL of PIC mix was added. To reaction (1), 15 pmol of CKM(KD) were added. To reaction (2) and (4), 22.5 pmol of cMed were added. To reactions (3),(5),(6) and (7), 15 pmol CKM(A or KD as indicated) and 22.5 pmol cMed, dialyzed to lower salt buffer (20 mM HEPES pH 7.6, 250 mM KOAc, 10% (v/v) glycerol, 5 mM β-ME) to allow complex formation, were added. To reactions (6) and (7), ATP to a final concentration of 2.5 mM was added.

Reactions were pipetted into the respective tubes, and the final volume was adjusted to 40 µL with streptavidin binding buffer, and incubated for 10 minutes at 25°C. Buffer was removed from the beads and the reactions added to the respective tubes, mixed and incubated at 25°C for 45 minutes.
The flowthrough (unbound) was collected, and the beads were washed 3 times with streptavidin binding buffer. 24.5 µL of streptavidin binding buffer + 0.5 µL of 100 U/µL EcoRV-HF® (NEB) were added per tube, and incubated at 28°C for 75 minutes to allow the restriction enzyme to cleave off the DNA from the beads.10 µL and 5 µL of 4x LDS loading dye were added to the unbound and elution fractions, respectively. Fractions were analyzed by SDS-PAGE.

CKM Phosphoproteomics of the PIC

Buffers and experimental setup were exactly as described for the immobilized template assay, with the only difference being that 15 pmol per reaction of cMed were added (in a 1:1 ration with CKM), instead of 22.5 pmol.
Three reactions were set up; (1) scaffold + cMed + PIC, (2) scaffold + cMed + PIC + [CKM(A) + ATP] later, (3) cMed + PIC + CKM(A) + ATP + [scaffold] later

The difference between reaction (2) and (3) is that, in reaction (2) PIC-cMed was first assembled on the DNA scaffold, washed, and then CKM(A) was added, whereas in reaction (3) PIC components were incubated with CKM(A) and ATP first on ice for 30 minutes, before adding in the bead-bound scaffold for the assembly reaction.

All unbound and elution fractions were run on an SDS-PAGE gel. Full lanes from the gel were cut out, the proteins were extracted, digested, phosphor-enriched and subjected to mass spectrometric analysis to identify phosphorylations on PIC components.

CKM-cMed-PolII competition assay

Storage buffer was removed from 400 μL of amylose magnetic beads (NEB) using a magnetic rack in a 2 mL eppendorf tube, and the beads were washed once with 400 μL of water, and then blocked with 600 μL of 1 mg/mL BSA solution in binding buffer 1 (20 mM HEPES, pH 7.5, 300 mM KOAc, 10% glycerol, 5 mM β-ME) at 37°C for 20 minutes with vigorous shaking. The blocking solution was then removed and the beads were washed 3 times with binding buffer 1. 440 μg of CKM(KD) in storage buffer (240 μL) were adjusted to a total volume of 800 μL, and then added to the beads, and shaken at 800 rpm for 1 hour at 4°C to bind MBP-tagged CKM to the blocked amylose beads. After binding, the flowthrough was discarded, and the beads were washed twice with binding buffer 1, then twice with binding buffer 2 (20 mM HEPES, pH 7.5, 250 mM KOAc, 10% glycerol, 5 mM β-ME to lower the salt concentration in preparation for the addition of cMed. 880 μg (360 μL) of cMed (2x molar ratio compared to CKM) adjusted to 800 μL in binding buffer 2 were added and shaken together at 800 rpm with the amylose-CKM beads at 4°C. After binding, the flowthrough was discarded and the beads were washed 12 times with 400 μL of binding buffer 2 (the number of washes had been previously determined in a preliminary experiment where all washes were blotted with the same antibody used in this experiment to determine the times after which equilibrium is reached – there was always a trace of cMed detected, but after about 10 washes, the level of detected cMed became constant). All previous steps were carried out in a single tube. After the washes, the beads were then resuspended in 410 μL of binding buffer 2. The beads were then divided into 50 μL of resuspended beads per tube. Six solutions with varying concentrations of polymerase were prepared. 0, 0.2, 0.4, 1, 2 and 10 μL, respectively, of purified RNAPII at 9.45 μM were adjusted to 200 μL in binding buffer 2. This corresponded to a molar excess of RNA-polymerase II over bead-bound CKM-cMed of 0x, 0.5x, 2x, 5x, 10x, and 50x, respectively, approximated from the theoretical binding capacity of the amylose beads based on their binding to MBP5-paromysinΔSal. CKM-cMed-amylose beads were incubated with polymerase at room temperature for 1 hour with shaking. The beads were then removed, and 30 μL from the 200 μL wash volume were taken and mixed with 10 μL of 4x LDS loading

dye. 18 μL were then loaded onto a 4-12% SDS-PAGE gel (NuPAGE) run in MES buffer. The gel was then blotted onto a nitrocellulose membrane (Biorad) and then probed with anti-Srb4 antibody.

Droplet assays

CTD:
0.18 μL (0.02 μL + 0.15 μL) of $MgCl_2$ (1M)-ATP (100 mM, pH 7.4), 1.5 μL of CKM(A) or CKM(KD) - at 4.2 mg/mL (ca. 8.7 μM) and 3.85 μL of GST-yCTD at 130 μM were mixed and incubated together at 30°C for 4 hours. 26% dextran solution in water was diluted to 20% such that the final solution contained 20 mM HEPES (pH 7.4) and 175 mM NaCl. 2 μL of the CTD-CKM(A) and the CTD-CKM(KD) reactions were then directly mixed with 8 μL of the 20% dextran solution. The final mixture contained 16% dextran, 20 mM HEPES pH 7.4 and 200 mM NaCl.

TFIIF:
3.85 μL of purified TFIIF (5.7 mg/mL) were mixed with 1.5 μL of CKM(A) or CKM(KD) and 0.18 μL of $MgCl_2$-ATP. The reactions were incubated for 4 hours at 30°C to ensure complete phosphorylation. 2 μL from each reaction were mixed with 8 μL 20% dextran solution in HEPES, pH 7.4 and 100 mM NaCl, so that the final droplet buffer conditions were 16% dextran and 120 mM NaCl.

Gcn4 with FAM-DNA:
DNA strands at 100 μM in DNA duplex buffer (30 mM HEPES pH 7.5, 150 mM KOAc, 0.1 mM EDTA) were annealed as described previously in a total volume of 4 μL. 1 μL of annealed DNA was then diluted with 9 μL of water, to a final concentration of 10 μM. 3 μL of purified His-Gcn4 at a concentration of 258 μM were mixed with 3 uL of 10 μM annealed DNA scaffold diluted in water, such that the His-Gcn4 concentration was brought down to approximately 130 μM, and the final salt concentration was 150 mM NaCl. In the control reaction, 1 μL DNA duplex buffer mixed with 9μL water substituted annealed DNA. 10 minutes on ice were allowed for binding. 1 uL of 20% dextran (2.85% in the final droplet formation buffer) in 100 mM NaCl, HEPES pH 7.4, was gently mixed with each reaction to avoid the introduction of any air bubbles.

mCherry-Med15 with GFP-Gcn4:
1.925 μL of purified GFP-Gcn4 adjusted to 81 μM in dilution buffer were mixed with 1.925 μL of purified mCh-Med15 (81 μM), 1.5 μL CKM(A) or CKM(KD) and 0.18 μL $MgCl_2$-ATP. The reactions were incubated for 4 hours at 30°C to ensure complete phosphorylation. The tubes were then centrifuged for 5 minutes at 4°C at 15,000 rpm. 3 μL of each reaction were mixed with 3 μL of 20% dextran solution in 100 mM

NaCl, HEPES pH 7.4. As such, the final conditions in the droplet formation buffer were 200 mM NaCl, 10% dextran and 30 μM of each of the two proteins.

8 μL (CTD) or 5 μL (all others) of the droplet solutions were pipetted on to the surface of an mPEGylated glass slide, covered with a cover slip, and the edges were sealed. The slides were then imaged using an inverted fluorescence microscope in differential interference contrast mode, or using the appropriate filter cube.

Fluorescence anisotropy of Gcn4-DNA

Buffer 1 (20 mM HEPES, pH 7.6, 300 mM KOAc, 10% glycerol)
Buffer 2 (20 mM HEPES, pH 7.6, 300 mM KOAc, 5 mM BME)
Buffer 3 (5X buffer 2: 100 mM HEPES, pH 7.6, 1.5 M KOAc, 25 mM BME)
Buffer 4 (2X assay buffer: 20 mM HEPES, pH 7.6, 300 mM KOAc, 10% glycerol, 0.2 mg/mL BSA)
DNA duplex buffer (30 mM HEPES, pH 7.5, 100 mM KOAc, 0.1 mM EDTA)

5'- 6-FAM (Carboxyfluorescein) labeled sense strand and unlabeled antisense strand were dissolved in DNA duplex buffer to 100 μM. After annealing, DNA was diluted in DNA duplex buffer to 100 nM.

Preparation of phosphorylated and unphosphorylated Gcn4:
400 μL of amylose magnetic beads (NEB) were divided equally between two 2-mL eppendorf tubes. The storage buffer was removed and the beads were washed once with 200 μL buffer 1. 400 μL of 1 mg/mL BSA in buffer 1 were then added to each tube, and incubated for 20 minutes at 37°C to block the beads. The beads were then washed twice with buffer 1 and twice with buffer 2. In the first tube, the beads were resuspended in 95 μL buffer 2 and 5 μL of active CKM at 4.2 mg/mL (21 μg) were added. In the second tube, the beads were resuspended in 90.14 μL buffer 2 and 9.86 μL kinase dead CKM at 2.13 mg/mL (21 μg) were added. After a one-hour incubation period at 4°C to immobilize the complex on the beads, any excess unbound CKM was washed away by washing the beads ten times with 200 μL buffer 2. This is important because the differential affinity of the kinase dead mutant and the active kinase to the substrate may influence the outcome of the anisotropy experiment. The immobilized enzyme was then used to phosphorylate Gcn4 (or not, in the case of the kinase dead mutant) in a phosphorylation reaction with 50 μL of 258 μM Gcn4, 20 μL of buffer 3, 2 μL of 100 mM $MgCl_2$, 2 μL of 100 mM ATP (pH 7.4) and 26 μL of water. The reaction was incubated for 4 hours at 30°C, and then overnight at 4°C to ensure complete phosphorylation which might be slower due to the restricted mobility of the enzyme. An additional 1 μL of 100 mM ATP (pH 7.4) was added at approximately half time.

The beads were removed using a magnetic rack, the supernatants were transferred to fresh tubes, and the process was repeated again to ensure the complete removal of the beads.

Fluorescence Measurement:
Phosphorylated and unphosphorylated Gcn4 were diluted in a log(0.5) dilution series. 13.6 μL from each supernatant were transferred to 30 μL of buffer 2. 13.6 μL of that were then, in turn, transferred further to 30 μL of buffer 2, and so on. In this way, 12 different concentrations were prepared, with the first one being the supernatant without any dilution, and the last one buffer only with no added protein.

In each well, 7.5 μL of phosphorylated or unphosphorylated Gcn4 of the respective dilution were mixed with 2 μL of DNA at 100 nM, 3 μL of water, and 12.5 μL of buffer 4 (the final assay conditions contained 150 mM potassium acetate, 0.2 mg/mL BSA, 8 nM DNA and Gcn4 at the respective concentration). 18 μL of the 25 μL reactions were then transferred to 384-well plates, and fluorescence was measured with an excitation wavelength of 470 nm and bandwidth of 5 nm, and an emission wavelength of 518 nm and bandwidth of 20 nm. A gain value of 75 and a Z-position of 26050 μm were set, and measurement was carried out on a TECAN Infinite M1000 Pro multi-well plate reader.

Fluorescence intensity was measured in triplicate for each Gcn4 concentration to average out pipetting errors. Fluorescence polarization (FP) and anisotropy (r) were calculated according to the following equations;

$$FP = \frac{I\parallel - I\perp}{I\parallel + I\perp}$$

$$r = \frac{I\parallel - I\perp}{IT}$$

Where $I\parallel$ is the fluorescence intensity in the parallel direction
$I\perp$ is the fluorescence intensity in the perpendicular direction
IT is the total fluorescence intensity

Mean fluorescence anisotropy was plotted against log(Gcn4 concentration) for phosphorylated and unphosphorylated Gcn4. Curves were fitted using the fitting equation from Reference.

Electromobility shift assay of Med15_KIX123 and GFP-Gcn4

0.58 μL of GFP-Gcn4 at 130 μM were mixed with 0.5 μL of CKM(A) or CKM(KD) at 4.2mg/mL, 0.7 μL Mg-ATP and 2 μL CKM buffer. The reactions were incubated for 2 hours at 30°C to ensure complete phosphorylation. After the completion of the reaction, the volumes were adjusted to 100 μL with dilution buffer, to adjust the final concentration of GFP-Gcn4 to 0.75 μM.
To verify phosphorylation, 5 μL from each reaction were loaded onto a Phos-Tag gel (Wako Chemicals). The gel was run at 130 V for 2.5 hours at room temperature, and then imaged through the EGFP channel on a Typhoon FLA 9500 biomolecular imager (GE healthcare).

MBP-M15KIX123 was diluted in a 2-fold dilution series in dilution buffer from 3.75 μM to 117 nM. 3 μL of phosphorylated or unphosphorylated GFP-Gcn4 were mixed with 3 μL MBP-M15KIX123 dilution or dilution buffer only, and allowed to bind for 10 minutes on ice. 2 μL 70% glycerol were added to each tube, and the samples were loaded onto a (pre-run for 1h at 150 V) 3-12% Bis-tris Native PAGE gel (NuPAGE), and run at 120 V in 1X NativePAGE buffer for 5 hours at 4°C. The gel was then imaged through the EGFP channel on a Typhoon FLA 9500 biomolecular imager (GE healthcare).

5 Results

5.1 PART I: SAMPLE PREPARATION

5.1.1 A strategy for recombinant expression and purification of CKM

A major hurdle towards solving the structure of the Mediator Cdk8-kinase module (CKM), whether on its own or together with the core Mediator complex (cMed), and towards its thorough biochemical characterization, was obtaining sufficient amounts of pure, homogeneous and stoichiometric complex. Here, we were able to solve this problem by establishing and optimizing a heterologous expression system for the *S.cerevisiae* CKM in insect cells. We chose *S.cerevisiae* as a model organism, consistent with all previous efforts to elucidate *S.cerevisiae* transcription initiation complexes [87].

We chose insect cells as the expression host to accommodate the large size and elaborate interaction interfaces of the complex that likely require chaperone-assisted folding, as well as post-translational modifications. Moreover, overexpression of active kinases is notoriously toxic to *E.coli* [104].

5.1.2 Cloning of the complete *S.cerevisiae* CKM on a single vector

We cloned the *S.cerevisiae* CKM (which contains the four subunits Med12, Med13, Cdk8 and Cyclin C) from genomic DNA into insect cell transfer vectors. In situations where individual genes were too large to be amplified all at once from genomic DNA, fragments were amplified separately and stitched back together by homologous-recombination-based cloning. All the DNA sequences used were the natural sequences from the *S.cerevisiae* genome (not codon-optimized for the insect cell expression host). We found that expression of the complex was only possible when all subunits were assembled together on a single vector.

The final transfer plasmid approached 20,000 base pairs in length (figure 5.1), and encoded an N-terminal Polyhistidine-Maltose Binding Protein (MBP)- fusion tag on the Cdk8 subunit connected via a flexible linker containing a TEV protease cleavage site. All remaining subunits were untagged. Two versions of the plasmid were made; the first encodes a wild-type Cdk8 subunit, and the second encodes a kinase-dead mutant, in which a crucial aspartate residue in the catalytic center (D286) was mutated to an alanine, with the remainder otherwise identical. Wild-type CKM is henceforth designated ‘CKM(A)’, and the catalytically inactive mutant, ‘CKM(KD)’. The sequence containing all genes was transferred onto a baculoviral bacmid, which was isolated and used to transfect Sf9 insect cells to package the first viruses (V_0),

which were further propagated in Sf9 cells (V_1) to reach the appropriate titer for protein expression.

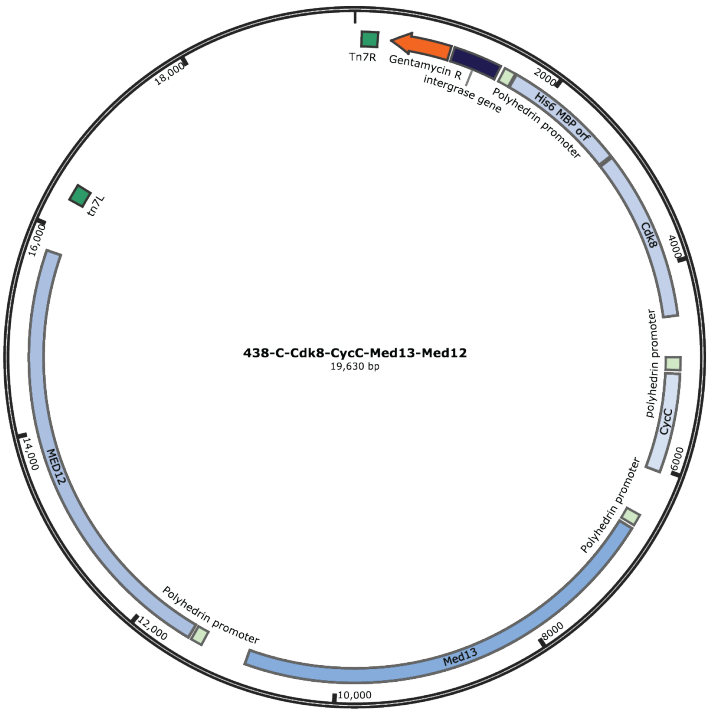

Figure 5.1 | CKM expression construct containing the CKM subunits Med12, Med13, Cdk8 (or Cdk8 D286A) and CycC, each with its own promoter, and the 438-C insect cell transfer vector backbone, providing an N-terminal His(x6)-MBP-TEV fusion to the Cdk8 subunit.

5.1.3 A baculovirus expression vector system for CKM

CKM(A) and CKM(KD) were expressed in the Hi5 insect cell line. We found that modulating the strength of the V1 expression virus is imperative for adequate expression. Fresh virus (not older than three months) should always be used. On the other hand, virus that was too strong resulting in a too-rapid drop in insect cell viability was also detrimental to expression. In this case, it was necessary to lower the initial viral load to allow enough time for expression of the larger subunits. Expression over 4-5 days, such that the cells double on the first day after infection and then arrest proliferation, with the viability remaining above 80% for at least three more days before harvest, was optimal.

Expression was also tested in Sf9 cells, which may confer different post-translational modifications than Hi5 cells, but this provided no observable advantage on the level of expression or purification.

5.1.4 A purification strategy yielding pure, stoichiometric CKM

We established a novel purification method for recombinant CKM yielding pure and stoichiometric complex. In order to set up this method, we tested a range of salts and salt concentrations for insect cell lysis. We found that a range of 350-450 mM potassium acetate in the lysis buffer strikes a good balance between solubility and stability of the complex. Nickel affinity capture using a Polyhistidine tag (His(x6)) on the N-terminus of Cdk8 isolated an intact complex, but the complex disintegrated upon gradient imidazole elution on an ÄKTA chromatography purification system. Batch binding and step elution, on the other hand, allowed stable elution of CKM, but the complex was unstable on all forms of subsequent ion exchange chromatography (cation exchange, anion exchange, or heparin resins) due to its sensitivity to salt, which lead to persistent protein and nucleic acid contamination that could not be resolved. Although unsuccessful, these trials indicated that the N-terminus of the Cdk8 subunit allows accessible and non-disruptive tagging.

Having exhausted most conventional purification resins, we resorted to re-cloning the complex to introduce a His(x6)-MBP tag to the N-terminus of Cdk8. Affinity enrichment on amylose resin with maltose elution reproduced the capture of an intact complex, further validating the suitability of this tagging position even for larger tags. Adding a nickel-affinity capture step before or after the amylose affinity capture conferred no detectable advantage. Presence of a solubility tag allowed lowering of the salt concentration to a minimum of 285 mM potassium acetate for subsequent ion exchange, below which the complex visibly precipitated. Tag cleavage also resulted in precipitation of the complex and was therefore omitted.

In our final purification protocol (figure 5.2), cells are lysed in 400 mM potassium acetate followed by affinity capture of CKM on amylose beads and maltose elution. This led to stably eluting CKM together with an overstoichiometric Cdk8-CycC subcomplex. The salt concentration was then lowered to 300 mM potassium acetate by direct dilution for binding to an anion exchange column. This resolved the overstoichiometric Cdk8-CycC subcomplex, which did not bind the anion exchange column at this salt concentration. The complex was then eluted by a *steep gradient* from the anion exchange column (from 300 mM to 1M potassium acetate over 20 mL), and then dialyzed back into 400 mM potassium acetate, before sizing by gel filtration or sucrose gradient ultracentrifugation, in the same salt concentration. It is important to note that using a shallow salt elution gradient or omission of the dialysis step results in total disintegration of the complex upon size exclusion chromatography. A partially overlapping chaperone (hsc70) contamination leads to wasting about a third of the eluting gel filtration peak. On the other hand, this contamination was completely resolved if a sucrose gradient was used instead

(figure 5.2 B), but this necessitates an additional buffer exchange step before further processing.

Using our method, purification from 1.2 L of Hi5 insect cell culture yields 200-300 μg of pure CKM(A), and 400-600 μg of pure CKM-KD. This purification method can be scaled up to up to double the yield when 2.4 L of insect cell culture are used per purification.

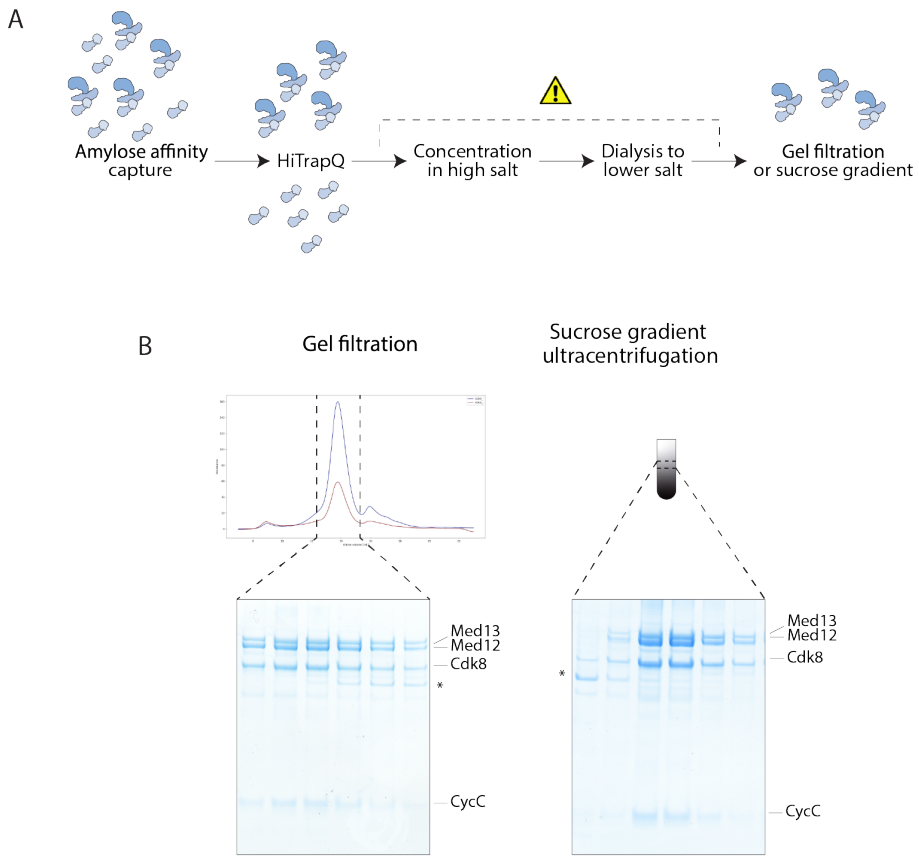

Figure 5.2 | A novel purification strategy for recombinant CKM.
A, Schematic depiction of our CKM purification strategy, starting with amylose affinity capture, which pulls down a mixture of full complex and an overstoichiometric Cdk8-CycC subcomplex, followed by anion exchange chromatography, which resolves this subcomplex, concentration in high salt, dialysis to low salt, and a final sizing step. Steps we found to be crucial to the stability of the complex are indicated with an exclamation sign. B, Gel filtration chromatography and sucrose gradient ultracentrifugation both show an intact complex. A chaperone contaminant, marked by an asterisk, is better resolved by sucrose gradient ultracentrifugation.

5.1.5 Design of a catalytically inactive CKM

To catalytically inactivate the Cdk8 subunit of CKM, we designed a mutant in which an aspartate residue in the catalytic cleft, which is highly conserved among all cyclin-dependent kinases (CDKs) [105], was replaced by an alanine residue. By virtue of its negatively charged side chain, this aspartate can coordinate one of the two magnesium ions in the cleft, which in turn bind the α and β phosphates of the incoming ATP substrate, to allow subsequent transfer of the γ phosphate to the phosphorylation target [106]. Based on co-crystallization with ADP, this residue was identified as Asp 127 in Cdk2 shown in figure 5.3 (PDB ID: 4I3Z). To find this residue in Cdk8, we aligned the sequences of human Cdk2 and *S.cerevisiae* Cdk8, and found the corresponding aspartate to be Asp 286. Therefore, in our kinase dead CKM complex, CKM(KD), the Cdk8 subunit is replaced by a Cdk8 D286A mutant.

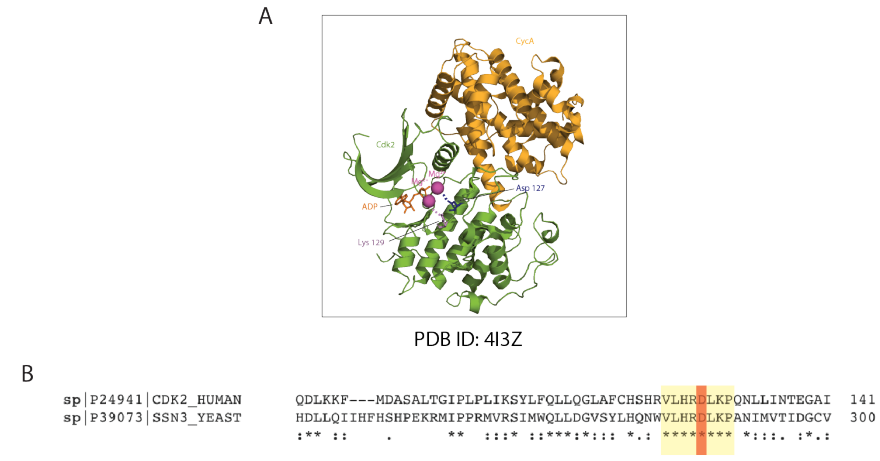

Figure 5.3 | Design of a catalytically inactive Cdk8 mutant.
A, Structure of human Cdk2/CycA co-crystallized with ADP (PDB ID: 4I3Z) shows the coordination of essential magnesium ions by the residues Asp 127 and Lys 129. B, Sequence alignment of human Cdk2 and *Sc* Cdk8 identifies the corresponding catalytic aspartate on Cdk8 as Asp 286.

5.1.6 Verification of the integrity of recombinant CKM

Recombinant CKM is catalytically active on known substrate

A hallmark of correct folding of recombinant complexes is their ability to fulfill their catalytic function. Therefore, we tested the ability of our recombinantly purified CKM(A) to phosphorylate the C-terminal domain (CTD) of Rpb1, the largest subunit of RNA polymerase II (RNAPII), which is one of its known phosphorylation targets [19]. To do that, we used purified human Glutathione-S-Transferase tagged CTD (which has an identical heptad repeat sequence to the yeast CTD sequence (YSPTSPS), but contains 52 repeats of the heptad instead of 26). GST-CTD was mixed and incubated with 25-fold less CKM(A) or CKM(KD) by molar ratio, and supplemented with ATP and magnesium ions. Samples were taken over definite time

intervals, and immunoblotted using CTD phosphosite-specific antibodies against Serine 5, Serine 2, Serine 7 or Tyrosine 1(figure 5.4 A). The appearance, and increase in intensity along the reaction coordinate, of bands that correspond to the various CTD phosphorylation sites confirms the activity of our recombinant CKM(A). Furthermore, their absence when the same was carried out using CKM(KD) instead of CKM(A), confirms that our chosen active site mutation successfully abolished Cdk8-kinase activity. In addition to the purified CTD, we also confirmed activity using the complete, endogenously purified RNAPII as a substrate, which had been treated with lambda-phosphatase prior to the reaction to remove any endogenous phosphorylations on its CTD (figure 5.4 B).

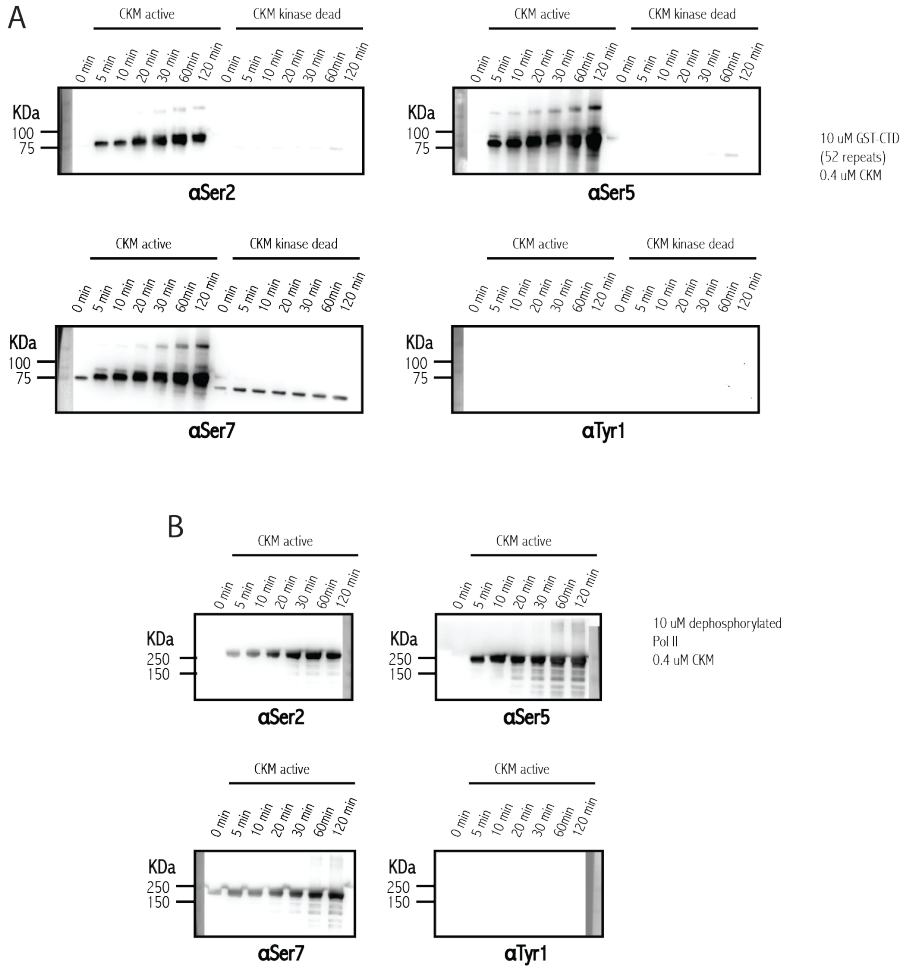

Figure 5.4 | Verification of catalytic activity of recombinantly purified CKM on RNAPII CTD.
A, Wild-type recombinantly purified CKM(A) is catalytically active, as shown by increase in phosphorylation of one of its known phosphorylation targets, the RNAPII CTD, along the reaction coordinate, as opposed to its kinase dead counterpart CKM(KD). αSer2, αSer5, αSer7 and αTyr1 refer to the RNAPII CTD phosphosite specific antibodies on Ser 2,5,7 and Tyr 1, respectively, that were used for blot detection in the respective assays.
B, The same holds true when complete endogenously purified RNAPII is used as a substrate instead of CTD.

Negative stain electron microscopy of recombinant CKM is consistent with endogenous CKM

While generally an essential validation for recombinant purifications, the catalytic activity of the CKM accounts for only approximately 25% by mass of the complex. The remaining 75% constitutes the large polypeptides Med12 and Med13, which are challenging to express, and the first to be affected by suboptimal expression conditions. Furthermore, the recombinant expression of these subunits in yeast had never been reported. Therefore, to verify the integrity of our purified particle, and the efficacy of the purification setup that we established, we performed negative stain electron microscopy. CKM(KD) was purified as described, concentrated after gel filtration, then fixated with glutaraldehyde during sucrose gradient ultracentrifugation according to the GraFix protocol [100]. Fractions containing CKM were then quenched with aspartate and incubated on carbon-foil-coated EM grids, and stained with uranyl formate. The grids showed homogeneous particles, evenly distributed over the surface of the grid with no aggregation even at high particle densities (figure 5.5 A). Approximately 300 micrographs were collected, from which 60,000 particles were picked, and used to perform 2D classification in RELION and 3D *ab initio* model building in CryoSparc.

The 2D classes showed that the majority of the particles were intact, confirming the homogeneity and quality of the sample (figure 5.5 B). There was a clear preferential orientation as shown by the abundance of side views compared to top views, which is not unexpected given the elongated shape of the particle. The *ab initio* 3D model calculated from the picked particles, and not biased by any input model, generated an elongated volume with three prominent wedges forming an overall shape similar to the capital letter “E” (figure 5.5 C,D), which is consistent with the low resolution cryo-EM densities reported for endogenously purified CKM [82],[107]. This indicated that recombinant expression and purification of CKM improved its yield and purity, gave us more control over biochemical conditions, and facilitated generation of mutants, while still preserving the overall architectural integrity of the complex.
Knowing this, we were able to proceed with confidence about the quality of our preparation.

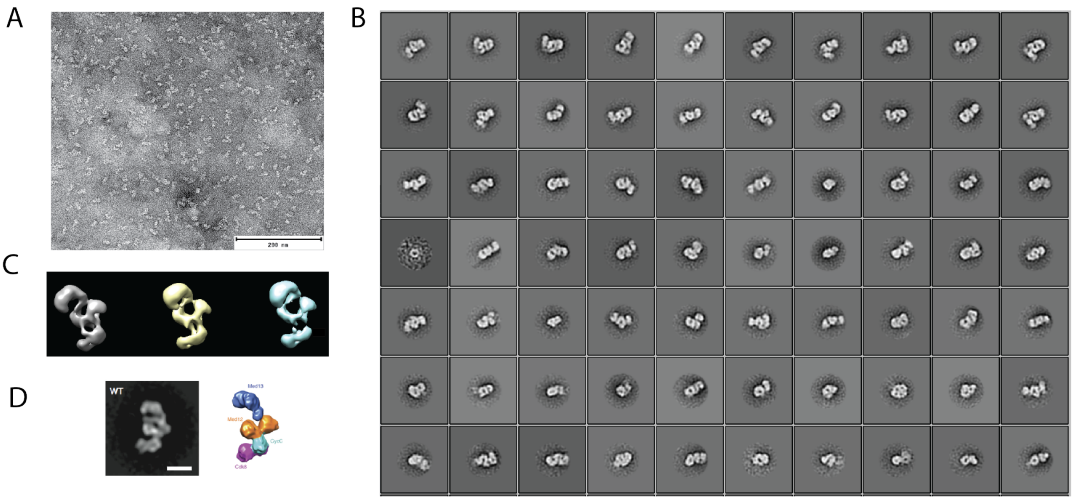

Figure 5.5 | Negative stain EM of recombinantly purified CKM.
A, Micrograph of CKM fixed in uranyl formate shows dense, homogeneous distribution of particles. B, 2D classes calculated from 60,000 picked CKM particles show a high degree of homogeneity, with the most occupied classes containing intact complex. C, 3D *ab initio* model building from all good particles shows an overall shape consistent with the previously reported (EMDB 5588) architecture of endogenously purified CKM, validating our recombinant purification.

5.1.7 Purified proteins toolbox

For both structural biology and biochemical characterization studies, which will be encountered in the following sections, several additional proteins and multi-protein complexes were purified. All the proteins used in this study are *S.cerevisiae* proteins. These include the 16-subunit core Mediator, cMed, comprising the Mediator head and middle modules, the 20-subunit endogenous Mediator, eMed, comprising the Mediator head, middle and tail modules, and different parts of the Mediator tail subunit Med15, the subunit implicated in numerous Mediator-activator interactions. Additionally, the activator General control protein 4 (Gcn4) the C-terminal domain of Rpb1 (CTD), and the pre-initiation complex components; general transcription factors (GTFs) and RNAPII, all of which are involved in the interplay of factors that regulate transcription initiation, were needed (figure 5.6).

CKM (A or KD) was expressed and purified from insect cells. cMed was expressed and purified from *e.coli* as two separate subcomplexes; Med1,4,9 and cMedΔ4,9, and then reconstituted on gel filtration using a protocol modified from [71] to allow stoichiometric incorporation of the Med1 subunit.
eMed was purified from a genetically modified yeast strain by a standard TAP-tag purification. All other factors were expressed and purified in *e.coli* yielding purified protein quantities in the order of milligrams. RNAPII and the GTFs were purified by Carina Burzinsky [71].

5.1.8 Complex formation of CKM with cMed

The binding of CKM to cMed was evident by a shift in the complex-containing fractions to higher density fractions upon sucrose gradient ultracentrifugation (figure 5.7). However, the complex was not gel-filtration-stable, without prior hyperstabilization by chemical crosslinking. Moreover, this complex could only form under lower salt conditions than those optimal for either of CKM or cMed separately.

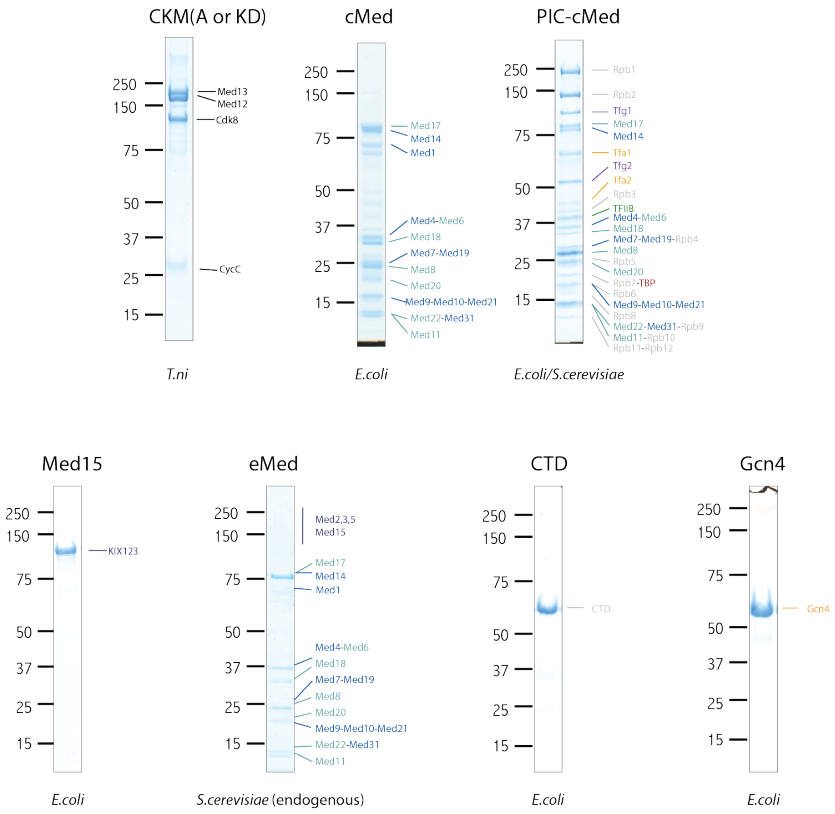

Figure 5.6 | Purified proteins toolbox.
Repertoire of proteins purified in this study for structural analyses and *in vitro* biochemical studies.

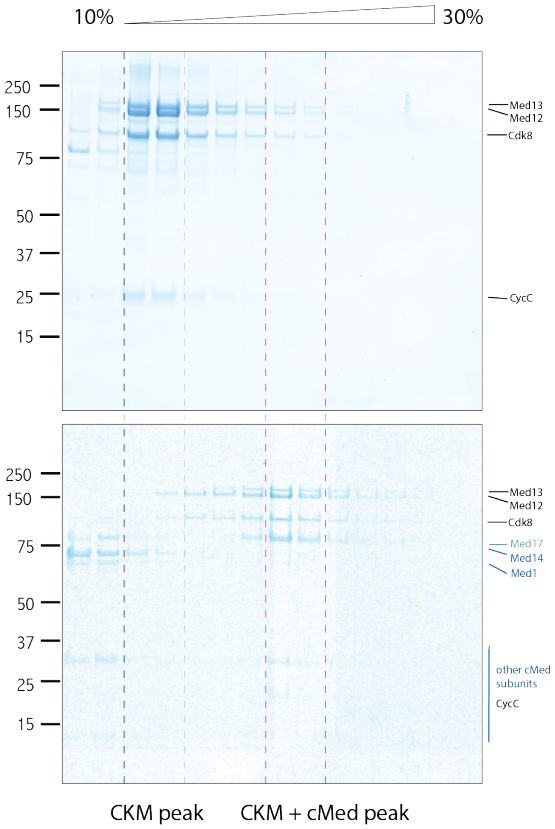

Figure 5.7 | CKM-cMed binding on a sucrose gradient.
Although not gel filtration stable, the binding of CKM to cMed is evident by a shift to higher density fractions on sucrose gradient ultracentrifugation. The CKM-cMed complex is about double the mass of CKM and cMed, separately.

5.2 PART II: CHARACTERIZATION OF CKM-CMED BINDING IN THE CONTEXT OF TRANSCRIPTION INITIATION

5.2.1 CKM is not a part of the transcription pre-initiation complex

Having isolated CKM, and CKM-cMed, we asked whether these complexes participate in the transcription pre-initiation complex (PIC). To approach this question, we set up an immobilized template assay (ITA) using a DNA scaffold containing a promoter sequence modeled on the yeast HIS4 promoter, with a TATA-box and a transcription start site (TSS), as a platform for PIC assembly. Biotinylation on the 3' end allowed immobilization of the template on streptavidin beads, and an EcoRV restriction site downstream of the promoter sequence allowed elution by endonuclease cleavage. CKM(A or KD) in the presence or absence of ATP were incubated on the immobilized template together with purified cMed and purified PIC components; RNAPII and the general transcription factors TFIIA, TFIIB, TFIIE, TFIIF and the TFIID subunit TBP. Excess factors were washed away, and the DNA template was eluted by restriction digestion from the beads. The elutions were then analyzed by SDS-PAGE to investigate what remained bound to promoter DNA (figure 5.8).

CKM alone showed no background binding to the DNA template, but some unspecific binding was seen in the presence of cMed. In the presence of the PIC components, cMed bound stoichiometrically to the PIC, but CKM binding did not exceed background levels, indicating that CKM is excluded from the PIC, whereas cMed binds to the PIC. Moreover, this was so, irrespective of whether active kinase-containing complex CKM(A) or the dead mutant CKM(KD) were used, demonstrating that this effect is predominantly a steric, structural effect, rather than an effect mediated by Cdk8-kinase activity.

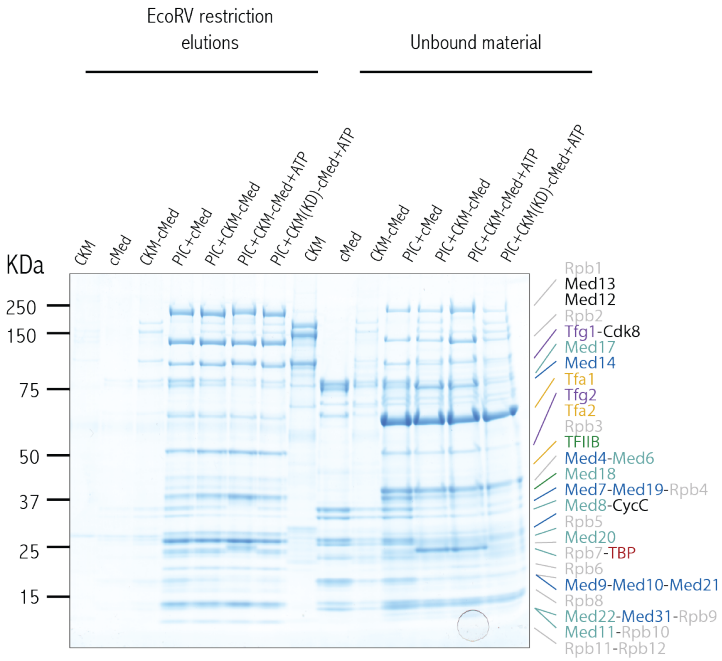

Figure 5.8 | CKM does not bind to the PIC.
Immobilized template assay of the transcription pre-initation complex (PIC) assembled from purified components shows that the CKM does not bind to the PIC above background levels, and that this effect does not depend on Cdk8-kinase activity.

5.2.2 CKM directly competes with RNAPII for Mediator binding

To investigate whether the CKM-cMed and the cMed-RNAPII complexes are mutually exclusive, we performed an *in vitro* competition assay with purified CKM, cMed and RNAPII. In this assay, we took advantage of the MBP-tag on the CKM complex to immobilize it on amylose beads. Having determined that the exclusion of the CKM from the PIC is a structural effect, we used CKM(KD). After binding of CKM to beads, overstoichiometric amounts of cMed were added to ensure binding saturation. The beads were then copiously washed to remove any unbound cMed. Finally, wash buffer with increasing concentrations of RNAPII was added, and the washes were analyzed by western blot analysis using an antibody against Med17 (alternatively called Srb4 in yeast), one of the subunits of cMed. Presence in the washes of increasing amounts of Med17, hence cMed, correlating to increasing added RNAPII is an indication that RNAPII competes with CKM for cMed binding (figure 5.9). The first lane is a buffer control, where no RNAPII was added. As an additional control, the same experiment was carried out, without addition of cMed. The rationale behind this control was to ensure that the observed effect is not simply due to trace amounts of co-purifying cMed subunits from the RNAPII endogenous purification, resulting in an increasing signal as RNAPII is added in increasing concentrations, or from a cross-reactivity of the antibody to any of the other experimental components. This experiment provides corroborating evidence in

support of the notion that cMed can interact with the CKM or with RNAPII, but not with both simultaneously, and allowed us to identify RNAPII as the PIC component responsible for preventing the incorporation of the CKM into the PIC.

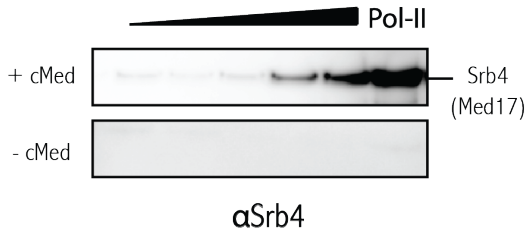

Figure 5.9 | CKM directly competes with RNAPII for cMed binding. Biochemical competition assay, where bead-bound CKM was washed with increasing amounts of RNAPII, and the washes probed with an αSrb4 (Med17) antibody, one of the cMed subuints, shows that RNAPII directly competes with CKM for cMed binding.

5.2.3 A shared binding interface of CKM and RNAPII on Mediator accounts for their mutually exclusive binding behavior

To investigate the mode of binding of CKM to cMed, we performed crosslinking-mass spectrometric analysis (XL-MS) of the CKM-cMed complex. To do that, CKM and cMed were mixed together in a 1:1 ratio, dialyzed into lower salt to allow the complex to form, and then crosslinked with 1 mM bis(sulfo)succinimidyl suberate (BS3), after having titrated the crosslinker concentration to a concentration just below complete crosslinking. The crosslinked complex was then run on a native gel to separate the CKM-cMed complex from the two component sub-complexes. CKM-cMed was extracted from the gel, trypsin digested, enriched for crosslinked peptides and subjected to mass spectrometric analysis. The analysis was carried out with a false discovery rate (FDR) cutoff of 1%. The generated crosslinking network (figure 5.10 A), showed extensive crosslinking within the CKM and cMed subcomplexes, but also several high confidence crosslinks between CKM and cMed.

To validate the interaction map, crosslinks between cMed subunits, for which the structure is already known, were mapped onto the structure. Crosslinks used for validation are shown on the interaction map in black, together with the measured atomic distances (figure 5.10 A; 5.11 A). The appearance of many crosslinks within the expected distance constraints confirmed the validity of the crosslinking network (figure 5.11 A).

In addition to crosslinks within cMed, several high confidence crosslinks between CKM and cMed were found. These crosslinks were mapped onto the cMed structure

(figure 5.10 B), and are indicated by red spheres, and corresponding red lines on the interaction network. Crosslinks that could not be mapped exactly, due to their presence in flexible regions that were not visible in the structure, were mapped to the closest structured residue and are indicated by pink spheres, and corresponding pink lines on the interaction network. This means that pink spheres indicate approximate crosslinking locations, and red spheres indicate exact locations, whereas both pink and red spheres refer to high confidence crosslinks. Dashed lines connected to the spheres indicate the complementary residues on CKM. Crosslinks for which more than one unique match was found are emphasized in bold face.

An overwhelming majority of crosslinks between CKM and cMed fall on the RNAPII-binding face of cMed, with a larger number of crosslinks to the cMed middle module, than to the head. In particular, a clustering of crosslinking sites to the CKM subunits Med12 and Med13 is seen on the knob and hook domains of cMed. On the other hand, Cdk8 and CycC contact the head module spine and moveable jaw, respectively.

In figure 5.11 B, the RNAPII-cMed interaction within the PIC is shown. RNAPII is rendered with low opacity to allow seeing through the polymerase into the polymerase-Mediator interfaces. These interaction interfaces are between the Rpb4/7 stalk of the polymerase and arm/spine domain of the cMed head module, between the polymerase dock and the moveable jaw of the cMed head module (made up of the Med18/Med20 heterodimer), and an additional transient interaction between the polymerase foot and the mobile plank domain (Med4/Med9) of the cMed middle module (not shown). These interfaces contain conserved residues, and suggest a conserved nature of the RNAPII-mediator interaction across species. The presence of crosslinks directly on, and in close spatial proximity to, these interfaces, as shown in figure 5.11 B, is unequivocal proof of mutually exclusive binding. Moreover, it provides a structural framework to explain the observed biochemical competition behavior, by demonstrating that RNAPII and CKM share an overlapping binding surface on cMed.

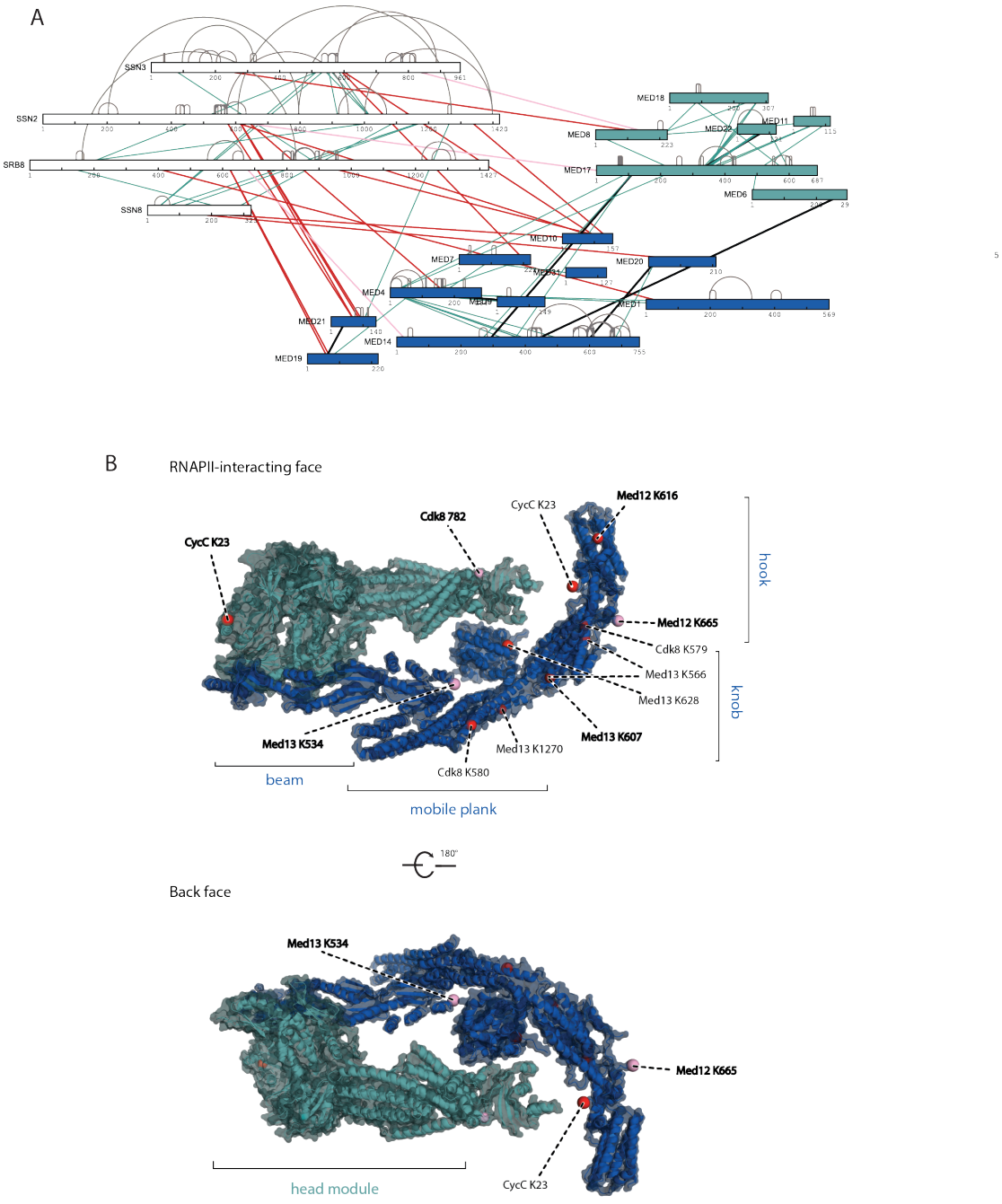

Figure 5.10 | Structural analysis of CKM-cMed binding by XL-MS.
A, Crosslinking network of CKM-cMed shows extensive contacts between the two complexes (highlighted in red and pink). B, Mapping crosslinks onto the cMed structure (homology model based on *S.pombe* Mediator structure PDB ID 5N9J) shows that the majority of crosslinks occur on the RNAPII-interacting interface, clustering on the hook, knob and mobile plank domains of the cMed middle module and extending all the way to the head module moveable jaw. Red spheres indicate exact crosslinking locations of high-confidence crosslinks, whereas pink spheres indicate approximate locations of high confindence crosslinks. The complementary CKM residues are indicated by dashes lines connected to the spheres. Crosslinks for which more than one unique match was found are indicated in bold face.

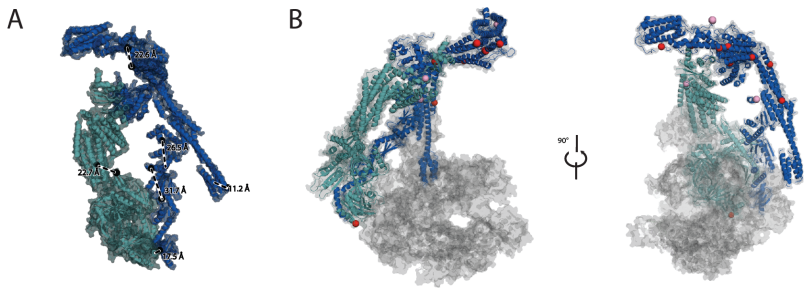

Figure 5.11 | RNAPII and CKM binding to cMed cannot occur simultaneously.
A, Crosslinks within cMed, for which a structure is available, appear within the expected atomic distances, thereby validating the shown crosslinking network (figure 5.10). B, Overlay of RNAPII onto cMed on which CKM crosslinks have been mapped n their PIC binding conformation (PDB ID: 5OQM, other factors hidden and RNAPII was rendered with low opacity.) . Pink and red spheres mean the same as in figure 5.10. The visibility of CKM crosslink sites through the translucent RNAPII density confirms mutually exclusive binding between CKM and cMed, and cMed and RNAPII.

5.3 PART III: CKM IN VITRO PHOSPHOPROTEOMICS

Having established the structural effect of CKM in steric occlusion of cMed from binding to RNAPII and the PIC, we asked what is the function of the kinase activity of CKM? To address this question, we first set up a series of exploratory studies to identify novel phosphorylation targets of the CKM within transcription initiation complexes. Once targets are identified, questions can then be posed about the specific functions of these phosphorylations.

5.3.1 CKM undergoes extensive autophosphorylation

By comparing phosphosites on CKM(KD) and CKM(A), by phosphopeptide enrichment and mass spectrometry, we found that CKM undergoes extensive autophosphorylation. We mapped the phosphosites onto the CKM subunits (figure 5.12). Based on their localization probability, phosphosites were divided into two classes; p(STY) class I contains phosphosites with a localization probability greater than or equal to 0.75, whereas p(STY) class II contains phosphosites with a localization probability between 0.25 and 0.75. Phosphorylations found only in the CKM(A) sample, but not in the CKM(KD) sample, and therefore attributed to autophosphorylation, are represented in orange. Dark orange represents those sorted into p(STY) class I, and light orange represents those sorted into p(STY) class II. Phosphorylations found in the CKM(KD) sample as well are represented in teal, with dark and light teal likewise representing phosphorylations sorted into p(STY) class I and II, respectively. Phosphorylations present in both samples are deposited by the insect cell expression host during recombinant expression. A large number of autophosphorylations occur on the long unstructured insertion of over 500 amino acids within the Med13 subunit. Notably, this region constitutes a large part of the interface involved in binding to cMed, and is conserved from yeast to human.

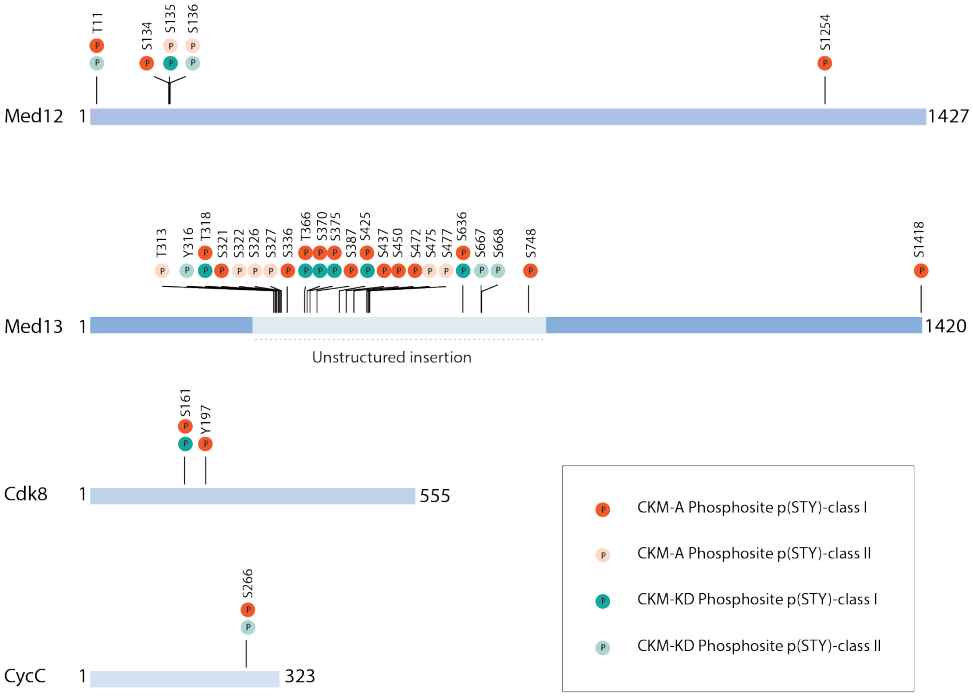

Figure 5.12 | CKM undergoes extensive autophosphorylation.
Comparison of phosphorylation sites on CKM(A) and CKM(KD) shows additional phosphorylation sites present only in the CKM(A) sample (orange), indicating autophosphorylation. Particularly, the long unstructured insertion in Med13 is targeted. Phosphosites in p(STY)-class I have a localization probablity above 0.75, whereas those in p(STY)-class II have a localization probability between 0.25 and 0.75.

5.3.2 CKM phosphoproteomics of the PIC

To explore the phosphorylation targets of CKM within the PIC, we set up an experiment similar to the previously described immobilized template assay, using the same DNA template. In this experiment, three reactions were set up. In the first reaction, purified PIC components; RNAPII and the general transcription factors TFIIA, TFIIB, TFIIE, TFIIF and the TFIID subunit TBP, as well as cMed were mixed together with the immobilized template, washed, and eluted by restriction digestion. In the second reaction, PIC-cMed was similarly assembled on the immobilized template, excess components were washed, and then CKM(A) and ATP were added and incubated together with the pre-assembled PIC, and eluted by restriction digestion. In the third reaction, the PIC components and cMed were incubated with CKM(A) and ATP *before* addition of the immobilized template (I.e. before PIC assembly). Box 5.1, shows a schematic depiction of the experimental concept. The elution fractions from the first, second and third reactions are called E1, E2 and E3, respectively. The unbound fractions from the first and third reactions are called U1 and U3, respectively. The unbound fraction from the second reaction before addition of CKM(A) is called U2, and after the addition of CKM(A) is called U2-2.

Box 5.1 | PIC in vitro phosphoproteomics experimental design. Schematic depiction of the experimental setup for *in vitro* phosphoproteomic analysis of the PIC, showing how the PIC factors (RNAPII and GTFs) were processed, and which fractions were taken for phosphopeptide enrichment and mass spectrometry.

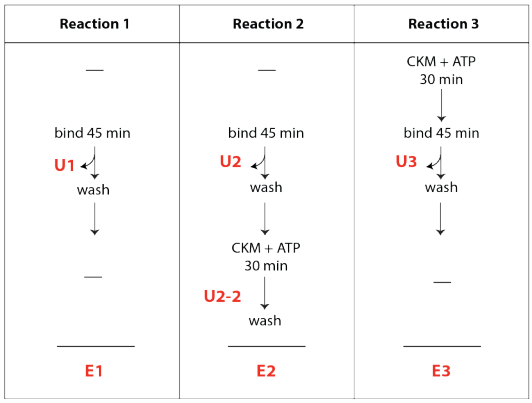

We separately identified and mapped the phosphosites in each of the unbound fractions (U1, U2, U2-2 and U3) and the elution fractions (E1, E2 and E3).
Phosphorylations present in U2-2, U3 or E2, E3 but not in U1, U2 or E1 (where no CKM was added), are henceforth designated "CKM-dependent" phosphorylations. Among these, two groups were clearly discernable. The first group includes phosphorylations that are present in both U (U2-2,U3) and E (E2,E3) fractions; i.e. CKM-dependent phosphorylations that do not inhibit binding to the PIC. The second group includes phosphorylations that appear consistently only in U fractions but not in E fractions; i.e. CKM-dependent phosphorylations that inhibit binding to the PIC. To simplify the analysis of this complex, multiprotein system, only phosphorylations for which the localization probability was greater than 0.75 were considered. Our findings are detailed in the following sections.

CKM phosphorylates Mediator and impairs its binding to the PIC

Phosphorylations on cMed were found exclusively in the U3 fraction, but not in other unbound or elution fractions, indicating that these sites are a) not accessible when mediator is bound to the PIC, and b) inhibit subsequent binding to the PIC. Mapping these phosphorylations onto cMed within the known PIC structure [35] revealed sites on the hook and knob domains of the mediator middle module (figure 5.13). In addition, sites were found on the arm domain of the head module (Med8 and Med17) in close proximity to the Rpb4/7 stalk of the RNAPII, one of the main interaction hubs between mediator and the RNAPII, and on the scaffolding subunit Med14, close to the head module jaws, which also contact RNAPII. Furthermore, phosphorylation sites were found on the mobile plank domain of the mediator, which forms a transient interface with the RNAPII foot.

The interfaces between Mediator and RNAPII are hydrophilic in nature. Presence of phosphorylations at, and close to, the Mediator-RNAPII interaction interfaces, resulting in dramatically altered surface chemistry in these regions, may explain why CKM-phosphorylated cMed is excluded from the PIC.

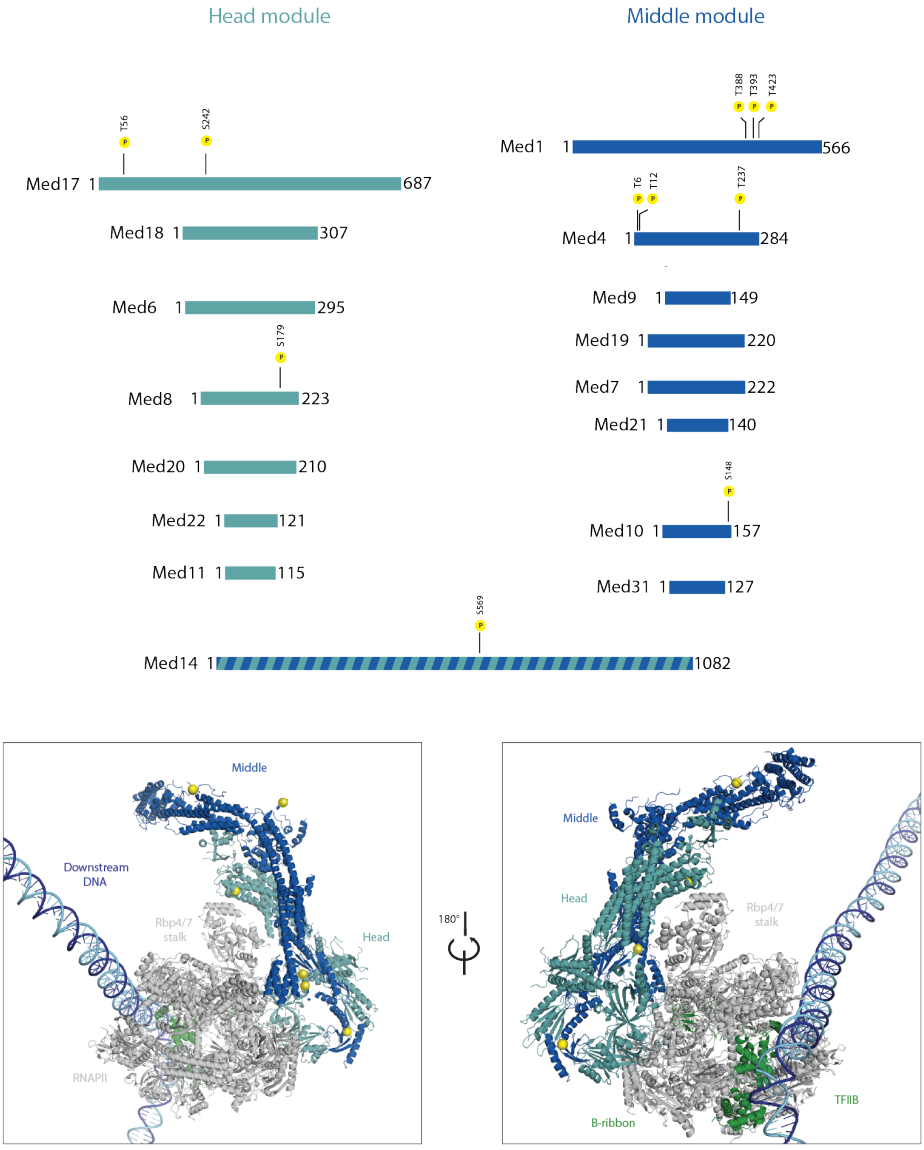

Figure 5.13 | CKM-dependent phosphorylations that inhibit PIC binding.
High confidence CKM- dependent phosphorylations that inhibit binding to the PIC, mapped on the PIC structure were found to occur on subunits of the Mediator complex, at or close to binding interfaces between RNAPII and Mediator.

CKM phosphorylates PIC components TBP and TFIIF and does not affect their PIC binding

Other CKM-dependent phosphorylation sites found on components of the PIC appeared in both unbound (U2-2,U3) and elution (E2,E3) fractions. I.e. these phosphorylations did not interfere with PIC binding. Those were found on the TFIID subunit TBP, which defines the assembly site for transcription initiation, and the largest subunit of general transcription factor TFIIF, which intimately associates with RNAPII (figure 5.14). Note that, the smallest subunit of TFIIF (Tfg3), which is highly unstructured, has been omitted from our preparations for ease of expression. Additionally, the CKM also phosphorylates the C-terminal domain (CTD) of Rpb1 on serines 2, 5 and 7, which is not detected in MS-based phosphosite mapping due to the absence of trypsin digestion sites on the CTD, but has been shown earlier by immunoblotting (please refer to section 5.1.5)

Mapping these phosphosites onto the known PIC structure [35] revealed that they were located exclusively on unstructured loops (indicated by dashed lines in the same color as the factor of interest) that were not visible in the structure. The presence of these phosphorylations on flexible loops that extend from the PIC, and do not take part in structured interfaces, explains why their presence does not perturb the assembly of the PIC. Not only that, but it also explains why these phosphorylations can be deposited by the CKM indiscriminately, whether it has free access to the PIC components (U3,E3), or receives a pre-assembled PIC as a substrate (U2-2, E2).

Seeing as these phosphorylations do not influence PIC assembly, this calls into question what their function may be.

5.3.3 PIC components form liquid-like droplets that dissolve upon CKM phosphorylation

To address the question of the function of CKM-dependent phosphorylations that appear in unstructured regions of PIC components, and do not influence PIC binding, we resorted to liquid-liquid phase separation studies. At high concentrations, many intrinsically disordered proteins are known to undergo liquid-liquid phase separation. We asked whether this was true for the PIC components *in vitro*, and whether phoshphorylations deposited by CKM may have an effect on this phenomenon.

To examine the effect of CKM-dependent CTD phosphorylation on its phase separation propensity, we mixed N-terminal GST tagged yeast CTD (GST-yCTD) at a high concentration, which had been pre-treated with 25-fold less of either CKM(KD) or CKM(A) and ATP, with dextran (figure 5.15). As a high molecular weight substance, dextran acts as a crowding agent that simulates the crowded environment in the cell by engaging a large number of solvent molecules, and

thereby increasing the effective concentration of the protein of interest (solvent exclusion effect). The presence of liquid droplets of GST-yCTD when it is pre-treated with kinase dead CKM, and the absence thereof when GST-yCTD is pre-treated with active CKM, demonstrates that CKM-dependent phosphorylation of the Rpb1 CTD dissolves these condensates.

Likewise, TFIIF pre-treated with CKM(KD) versus CKM(A) showed a similar pattern, albeit less stark (figure 5.15). These observations indicate that CKM-dependent phosphorylation of PIC components attenuates their phase separation.

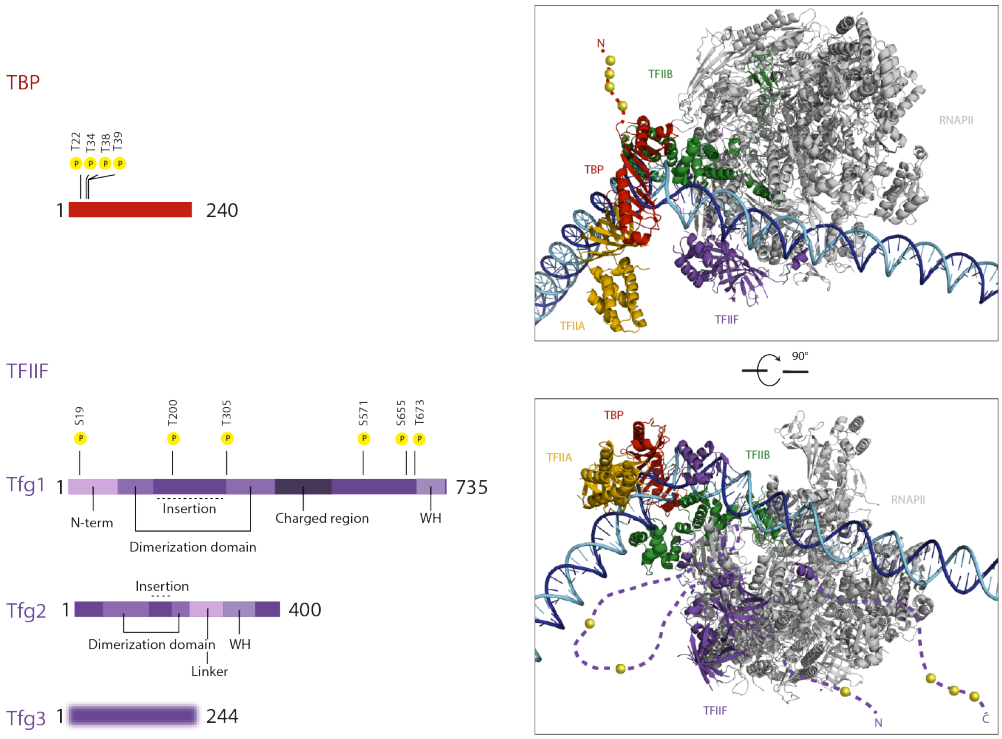

Figure 5.14 | CKM-dependent phosphorylations that do not inhibit PIC binding.
Mapping of high confidence CKM- dependent phosphorylations that do not inhibit binding to the PIC on the PIC structures (PDB ID 5OQM) shows that they are mostly located in protruding unstructured loops, explaining why they do not inhibit PIC binding.

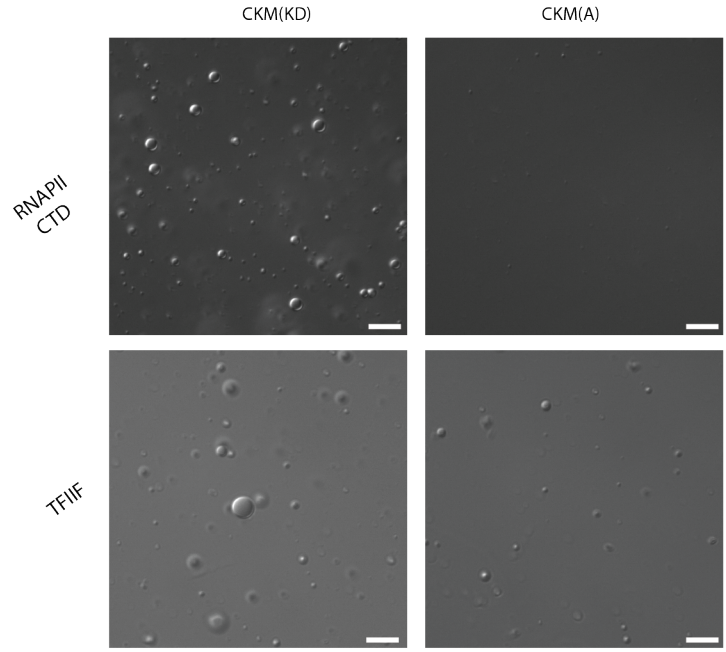

Figure 5.15 | Cdk8 phosphorylation of PIC components attenuates their phase separation.
Images of phase separated PIC components RNAPII CTD (top) and TFIIF (bottom) treated with kinase dead (left) or active (right) CKM show that Cdk8 phosphorylation reduces their ability to form liquid droplets. The scale bar length is 10 µm.

5.4 PART IV: CHARACTERIZATION OF THE FUNCTION OF THE CKM IN ACTIVATOR-DEPENDENT TRANSCRIPTION

5.4.1 CKM targets the activator Gcn4 for phosphorylation

Several transcription activators, particularly ones involved in response to stress and nutrient deficiency, are known targets of the CKM kinase Cdk8 [77], committing them to proteasomal degradation. At upstream activating sequences, chromatin-bound activators recruit the Mediator complex, which in turn contacts the PIC on promoters to activate transcription by stimulating promoter escape. In *in vitro* biochemical binding terms, this means that activators at upstream activating sequences are part of a ternary interaction; contacting DNA on one side, and Mediator on the other. We asked whether phosphorylation of activators by CKM has an effect on this DNA-activator-Mediator ternary interaction, schematically depicted in figure 5.16 A.

Apart from global turnover effects, we asked what are the direct effects of CKM-dependent phosphorylation of activators. To address that, we purified the yeast activator General control protein 4 (Gcn4), one of the best-characterized yeast activators. Gcn4 is a typical activator, with a distinct structured DNA-binding domain, and a long, disordered activation domain. We set up a kinase assay to test *in vitro* phosphorylation of Gcn4 by CKM. Figure 5.16 B shows that Gcn4 phosphorylation by

Cdk8 can be recapitulated *in vitro*, and can occur on free or DNA-bound Gcn4 as a substrate, with no visible effect on the kinetics of the phosphorylation reaction.

Having established CKM-dependent phosphorylation of Gcn4 *in vitro,* we went on to investigate the effect this may have on the DNA-activator-Mediator ternary interaction. To approach this problem, we divided it into its two binary components.

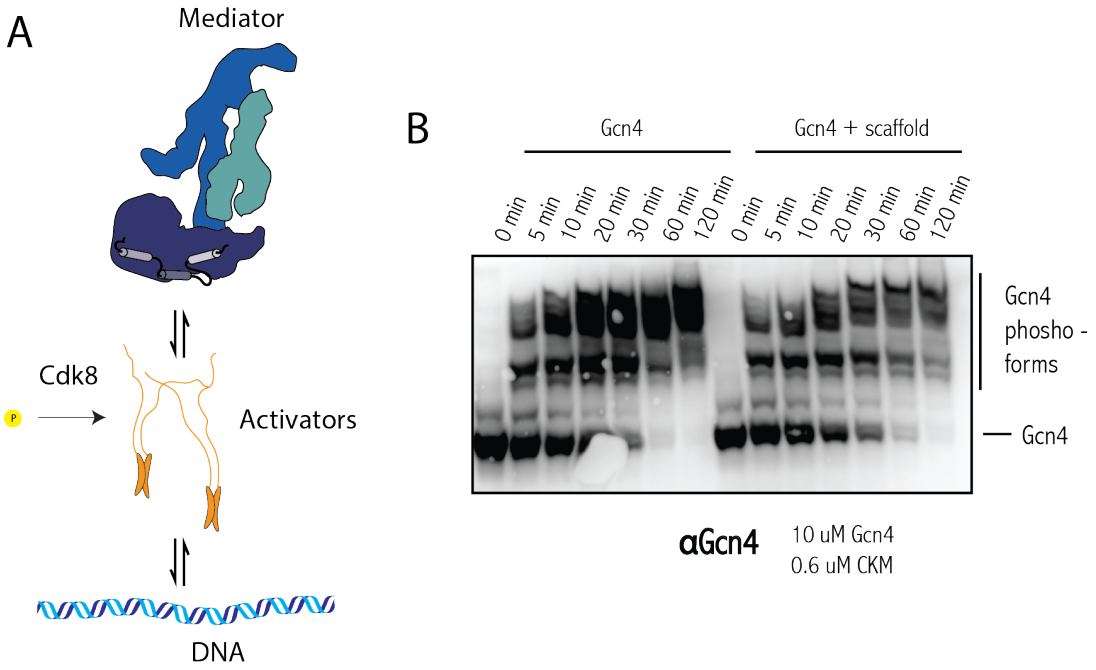

Figure 5.16 | Cdk8 phosphorylation of the activator Gcn4 can be recapitulated in vitro.
A, Schematic depiction of the Mediator-activator-DNA ternary interaction, and the addressed role of Cdk8. B, Purified Gcn4 is phosphorylated by purified CKM *in vitro* into various phospho-forms. This can happen whether Gcn4 is free or DNA-bound, and the reaction kinetics do not seem to be affected by DNA binding.

CKM phosphorylation of Gcn4 impairs its genomic binding

First, we investigated the effect of CKM phosphorylation on the ability of activators to bind their cognate binding sites on DNA (figure 5.17). To do that, we employed a combination of complementary assays. On an immobilized template assay, we used a DNA template modeled on the upstream sequence adjacent to the yeast HIS4 promoter, which contains five binding sites for the activator Gcn4 in the natural sequence. We used a truncated version, which contained only three Gcn4 binding sites with a biotinylation on the 3' side. The DNA scaffold was immobilized on streptavidin beads, and Gcn4 was bound to the DNA scaffold, the unbound excess Gcn4 was washed away, and then the Gcn4-DNA complex was incubated with CKM(A or KD), and ATP (figure 5.17 B), and then eluted by restriction digestion. Strikingly, we saw a remarkable reduction in affinity upon phosphorylation, indicating that CKM phosphorylation can actively dislodge Gcn4 from its genomic binding site.

This could be confirmed by measurement of the affinity of CKM-phosphorylated versus unphosphorylated Gcn4 to a fluorescein-labelled DNA scaffold containing a Gcn4 binding site by fluorescence anisotropy, which showed that unphosphorylated Gcn4 had close to double the affinity to DNA than its phosphorylated counterpart (figure 5.17 C). Please note that the K_d values presented here are not meaningful in absolute terms, but only in relative terms, due to the nature of the experimental setup, which allowed only relative concentrations to be determinable (please refer to the methods section for experimental details).

Mapping the phosphorylation sites by phosphopeptide enrichment and mass spectrometry revealed sites within the disordered activation domain of Gcn4, as well as one site in the DNA-binding domain (figure 5.17 E). Mapping this site onto the crystal structure of the Gcn4 DNA-binding domain (DBD) [108], showed that it occurs within the highly hydrophobic interface of the leucine zipper formed by dimerization of the DBDs of two Gcn4 molecules, providing a potential explanation for the loss of affinity to DNA upon phosphorylation.

Gcn4 and other activators with low complexity activation domains have been shown to undergo liquid-liquid phase separation *in vitro* and *in vivo* [52]. To test the effect of DNA-binding on droplet formation, we mixed Gcn4 with or without fluorescein-labelled DNA containing a Gcn4 binding site with dextran, as previously described. DNA was incorporated into Gcn4 droplets, as evident by detection of green fluorescence within the droplets, and resulted in markedly bigger droplets than Gcn4 alone (figure 5.17 D). Having separately shown that CKM phosphorylation of Gcn4 impairs its DNA binding, and that DNA binding enhances liquid droplet formation, it can be inferred that CKM phosphorylation attenuates Gcn4-DNA phase separation.

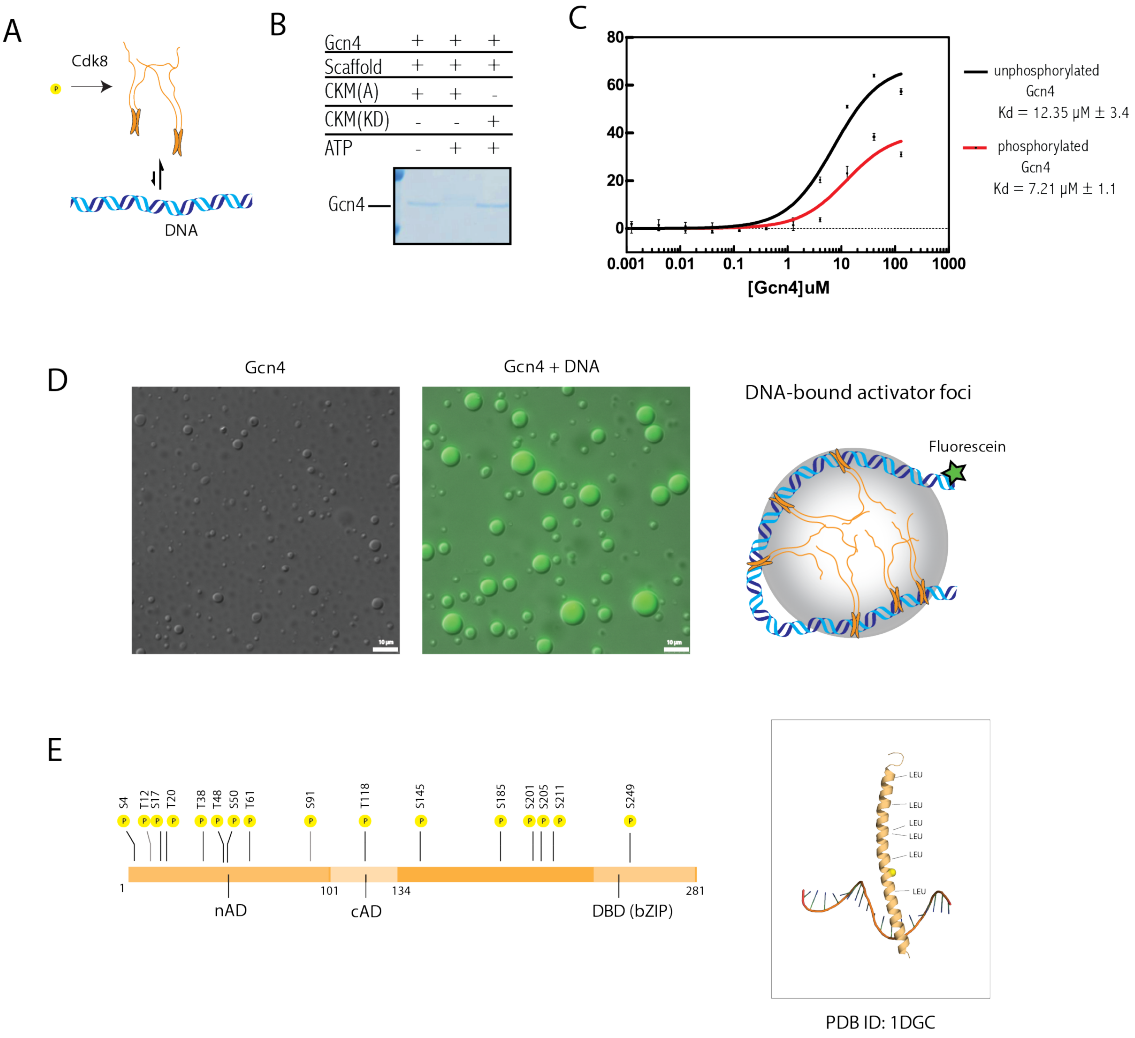

Figure 5.17 | The activator Gcn4 loses affinity to DNA as a result of Cdk8-kinase activity.
A, Schematic depiction of the interaction addressed. B, Immobilized-template assay shows that the template retention of phosphorylated Gcn4 is lower than unphosphorylated Gcn4. C, The loss of affinity of phosphorylated Gcn4 to DNA compared to unphosphorylated Gcn4 was measured by fluorescence anisotropy.
D, Gcn4 forms liquid droplets that incorporate and are enhanced by DNA, implying that Cdk8 phosphorylation may disrupt these foci.
E, Mapping of the Cdk8 phosphorylation sites onto Gcn4 identifies sites throughout the activation domain as well as one site in the DNA-binding domain which may disrupt dimerization of the leucine-zipper, explaining the loss of affiinty.

CKM phosphorylation impairs the interaction of Mediator with activators and dissolves activator/mediator liquid droplets

Next, we looked at the interaction between activators and Mediator (figure 5.18). Our recombinant cMed does not contain the tail module, which is responsible for the majority of activator-Mediator interactions in yeast, and contains many characteristic low complexity sequences, which impart a high degree of structural plasticity, which is conserved from yeast to human. Technically, this also means that this Mediator

module is difficult to recombinantly express and purify. Owing to the difficulty of performing biochemical studies with the minute amounts of purified endogenous Mediator that contains a tail module, we resorted to recombinantly expressing and purifying only the part of the complex that has been reported to interact with the Gcn4 activator. We capitalized on the wealth of knowledge available about the Gcn4-Mediator interaction, which has been meticulously characterized by heteronuclear single quantum coherence spectroscopy and XL-MS [109]. This study showed that Gcn4 binds the Mediator tail subunit Med15 at four distinct structured binding domains called KIX, ABD1, ABD2 and ABD3, which are interspersed between disordered polyglutamine (polyQ) and polyglutamine/polyalanine (polyQ/A) linkers. The binding of the Gcn4 activation domain to *all* of the Med15 structured domains led to the description of this interaction as a “fuzzy free-for-all” rather than a defined interaction.

Knowing that the four Med15 structured domains are sufficient for Gcn4 binding, we purified a Med15 variant, Med15_KIX123, where we removed all the polyQ and polyQ/A linkers and concatenated the four binding domains together. To test the effect of CKM-phosphophorylation of Gcn4 on the binding of Gcn4 to Med15, we performed an electrophoretic mobility shift assay (EMSA), in which a constant amount of phosphorylated or unphosphorylated GFP-tagged Gcn4 was titrated against increasing concentrations of Med15_KIX123. We found that phosphorylation of Gcn4 weakens this interaction (figure 5.18 B).

It has also been reported that Gcn4 and Med15 undergo liquid-liquid phase separation and colocalize in the same droplets [52]. To test the effect of Gcn4 phosphorylation on Med15-Gcn4 phase separation (figure 5.18 C), we reproduced the experiment in this study, by purifying the N-terminal half of Med15 (residues 6-651), this time with its polyQ and polyQ/A linkers, with an mCherry fusion tag. We purified mCherry-Med15 as in [52]. This purification is crude - expression levels are minute due to the extensive polyQ and Q/A linkers - but the presence of a fluorescent tag allowed unambiguous detection of the protein.

We incubated a 1:1 mix of GFP-Gcn4 and mCherry-Med15 with CKM(KD or A) and ATP, and then added dextran and visualized the formed phase-separared droplets under a fluorescence microscope. Our results show that phosphorylation by CKM attenuated these droplets (figure 5.18 C).

Taken together, the weakening of the Med15-Gcn4 interaction, and the shrinkage of Med15-Gcn4 droplets, upon CKM phosphorylation, is an indication of CKM-mediated release of Mediator at upstream activating sequences, and a resolution of local Mediator-activator foci (figure 5.18 D).

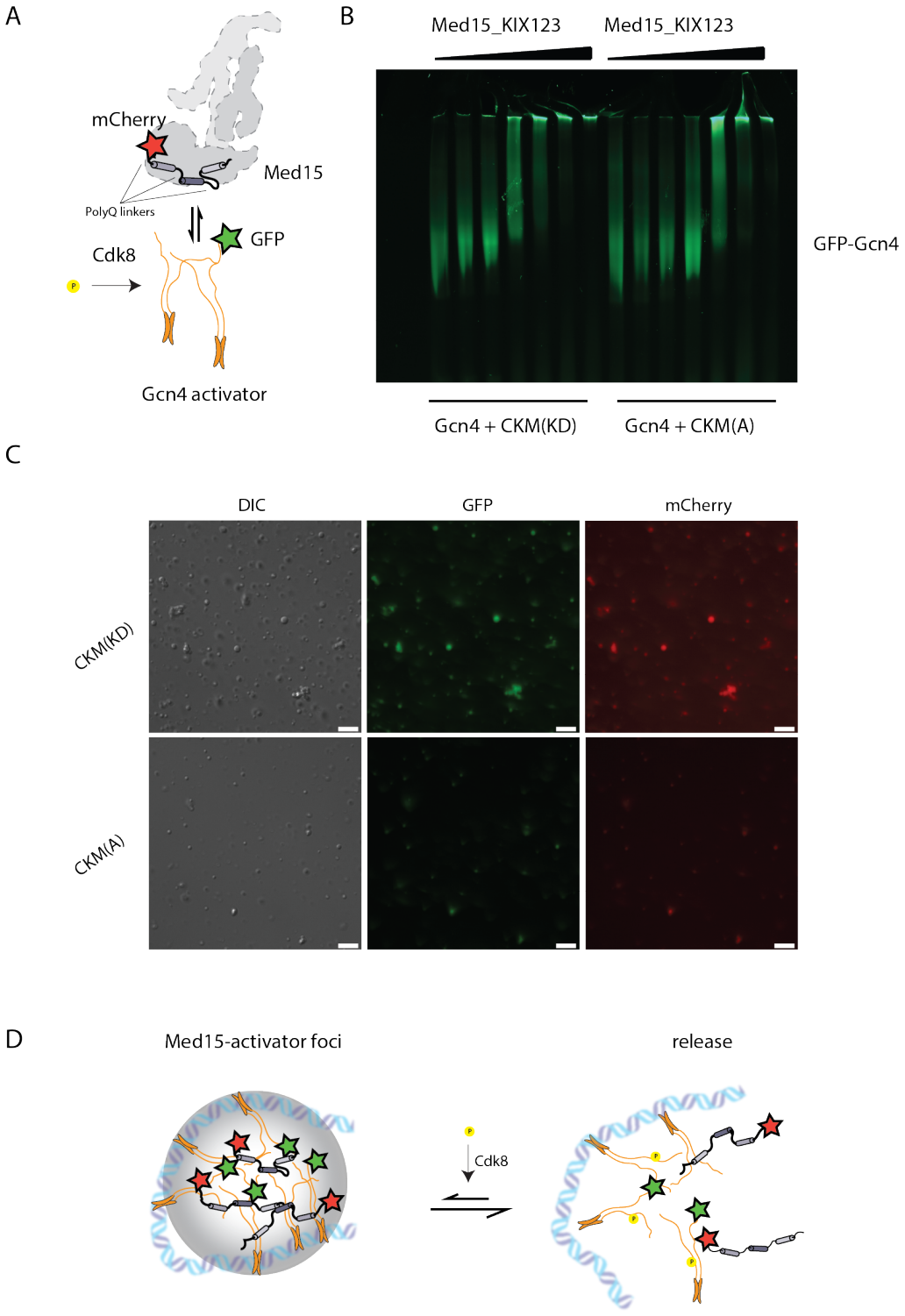

Figure 5.18 | Mediator-activator phase separation is disrupted as a result of Cdk8-kinase activity.
A, Schematic depiction of the interaction addressed, and the experimental concept.
B, Electromobility shift assay of GFP-tagged Gcn4 with increasing added Med15_KIX123(mutant with all polyQ linkers removed) using Gcn4 that has been subjected to Cdk8 phosphorylation or not, shows that Cdk8 phosphorylation disrupts the Mediator-activator interaction. C, Phase separation of mCherry-Med15 (here including polyQ regions) with GFP-Gcn4 is attenuated upon Cdk8 phosphorylation. The scale bar length is 10 µm. D, Schematic depiction of the effect of Cdk8 phosphorylation of Mediator-activator foci.

5.5 PART V: CRYO-EM OF CKM AND CKM-CMED

The structure of CKM, both in isolation and in complex with cMed, has endured as one of the big open questions in the Mediator structure field. The current study confirms the magnitude of the challenge that this task presents.

In the following sections, the attempts we made to solve the structure of CKM and the CKM-cMed complex will be presented, as well as an analysis of what can be learned from these trials. The majority of our efforts focused on finding good cryo-EM grid conditions for both complexes, which was the major bottleneck for further progress. Significant improvements were seen, but despite extensive trials, we were not able to solve either of these structures at this time. We hope that the experience gathered through our attempts, however, will provide the foundational knowledge to guide future studies, and narrow down the conditions needed for cryo-EM of these complexes.

5.5.1 Cryo-EM of CKM

The general strategy for preparation of cryo-EM grids of CKM was to purify the complex, crosslink it in batch or GraFix, and to apply a sizing and/or buffer exchange step to bring the complex to the desired freezing buffer conditions. Parameters at each of these steps were varied.

Trials to obtain homogeneous single particles of CKM are presented in tabular form (table 5.1 and 5.2), describing the main altered parameters and their outcomes. To navigate these tables, the following information is given. All numbers, apart from values of pH, refer to concentration in mM units. The non-standard abbreviations GA, conc., sp.col., dial., sucr., phosph., cont., GeFi, and exch. stand for glutaraldehyde, concentration, spin desalting column, dialysis, sucrose, phosphorylation, continuous, gel filtration and exchange, respectively. ‘Jbf’ means added just before freezing.

Experiments are numbered from 1 through 55. The columns headed ‘crosslinking’, ‘quencher’ and ‘GraFix’ describe whether samples were crosslinked or not, and in what conditions (crosslinker/quencher identity and concentration, and in batch or GraFix). ‘Buffer exchange’ refers to the method used to remove excess quencher and/or sucrose after crosslinking, when the last step before freezing was not gel filtration. Conditions in which gel filtration and GraFix are checked mean that CKM was first applied on gel filtration chromatography as a part of its purification protocol, and then applied to GraFix for fixation. Conditions in which gel filtration is not checked were conditions where the gel filtration step in the purification protocol was omitted, and GraFix was used for concomitant sizing and fixation. Conditions in

which neither is checked mean that the sample was used directly after ion exchange chromatography.

'Concentration' refers to concentration of the sample in spin filter concentrators *after* crosslinking and buffer exchange. Due to the huge loss of protein observed, compared to only marginal increase in concentration, this was frequently omitted.

'Detergent' and 'additives' refer to added potentially stabilizing substances; the nonionic detergent LMNG, the ATP transition-state analogue (ADP•BeF_3), a small percentage of sucrose intentionally left over from GraFix by incomplete buffer exchange, or glycerol added to the freezing buffer. 'Lower LMNG' refers to the LMNG concentration when LMNG was added to the dialysis buffer. We noticed, by comparing negative stain grids of LMNG-containing samples prepared by dialysis versus spin column, that detergent micelles were present in the latter only, implying that the detergent does not efficiently pass through dialysis membranes. Therefore, we do not know the final LMNG concentration in these conditions, but grids prepared in the same way were assumed to have the same final concentration.

Phosphorylation and auto-phosphorylation refer to addition of an active Cdk8-CycC subcomplex during the CKM(KD) purification, or ATP before the final step of CKM(A) purification, to impart phosphorylations on the complexes, to alter their surface charge distribution.

Finally, the salt, pH and the version of CKM used (A or KD), and type of cryo-EM grid used are also stated. For pH's 7.6-8.4, HEPES buffer was used, whereas Tris and BisTris was used for pH 8.5 and 6.5, respectively.

Heavy aggregation of CKM on cryo-EM grids compared to negative stain grids

Heavy aggregation of CKM paritcles on cryo-EM grids was a recurrent outcome of our trials under most standard conditions. This was as opposed to negative stain grids, where particles distributed homogeneously when applied directly after GraFix, or showed only minor aggregation when applied after buffer exchange.

Systematic solution condition testing

To check whether aggregation was a problem occurring already in solution before grid preparation, we systematically screened different buffering components using the ProteoPlex technology [110].
Characteristically shaped two-state thermal unfolding curves without an early shoulder confirmed that there were no aggregates in solution under the used

conditions. Furthermore, the results showed that, while the standard condition at pH 7.6 was among the top four best conditions, lowering the pH to about 6.5 had a superior stabilizing effect.

Table 5.1 | Cryo-EM grid conditions tested for the CKM complex.

Exp	pH	cross-linking	quencher	salt	GraFix	GeFi	buffer exch.	conc.	detergent	activity	additive	extra note	grid type
1	7,6	0,075% GA	Asp	350 KOAc	yes	yes	dial.	yes		KD			1.2/1.3 C
2	7,6	no		350 KOAc		yes	dial.	no		KD			1.2/1.3 C
3	7,6	0.05% GA, batch	Asp	350 KOAc		yes	dial.	no		KD			1.2/1.3 C
4	7,6	0.075% GA, batch	Asp	350 KOAc		yes	dial.	no		KD			1.2/1.3 C
5	7,6	0,05% GA	Asp	350 KOAc	yes	yes	dial.	no		KD		phosph.	1.2/1.3 C
6	7,6	0,05% GA	Asp	350 KOAc	yes	yes	dial.	no		KD		phosph.	cont.C (1.2/1.3)
7	6,5	0.02% GA	Asp	400 KOAc	yes	no	sp.col.	no	0,01% LMNG	KD			2/1 C
8	6,5	0.08% GA	Asp	400 KOAc	yes	no	sp.col.	no	0,01% LMNG	KD			2/1 C
9	6,5	0.045% GA	Asp	400 KOAc	yes	no	sp.col.	no	0,01% LMNG	KD			2/1 C/ Au 2/2
10	6,5	0.045% GA	Asp	400 KOAc	yes	no	sp.col.	no	0,01% LMNG	KD	1.5% sucr.		2/1 C/ Au 2/2
11	6,5	0.045% GA	Asp	400 KOAc	yes	no	short dial.	no	lower LMNG	KD	1.5% sucr.		2/1 C/ Au 2/2
12	6,5	0.045% GA	Lys/tris/Asp	400 KOAc	yes	no	sp.col.	no	0,01% LMNG	KD			2/1 C/ Au 2/2
13	6,5	0.045% GA	Lys/tris/Asp	400 KOAc	yes	no	sp.col.	no	0,01% LMNG	KD	1.5% sucr.		2/1 C/ Au 2/2
14	6,5	0.045% GA	Lys/tris/Asp	400 KOAc	yes	no	short dial.	no	lower LMNG	KD	1.5% sucr.		2/1 C/ Au 2/2
15	6,5	0.045% GA	Asp	400 KOAc	yes	no	sp.col.	no	0,01% LMNG	A	ADP.BeF3	auto-phosph.	2/1 C
16	6,5	0.045% GA	Asp	400 KOAc	yes	no	sp.col.	no	0,01% LMNG	A	1.5% sucr./ADP.BeF3	auto-phosph.	2/1 C
17	6,5	0.045% GA	Asp	400 KOAc	yes	no	short dial.	no	lower LMNG	A	1.5% sucr./ADP.BeF3	auto-phosph.	2/1 C
18	6,5	0.045% GA	Asp	400 KOAc	yes	no	short dial.	no	0,01% LMNG	A	1.5% sucr./ADP.BeF3	auto-phosph.	2/1 C
19	6,5	0.01% GA	Asp	400 KOAc	yes	no	sp.col.	no	0,01% LMNG	KD	1.5% sucr.		2/1 C
20	6,5	0.01% GA	Asp	400 KOAc	yes	no	sp.col.	no	0,01% LMNG	KD	1.5% sucr.		2/1 C
21	6,5	0.01% GA	Asp	400 KOAc	yes	no	short dial.	no	lower LMNG	KD	1.5% sucr.		2/1 C
22	6,5	0.01% GA	Asp	400 KOAc	yes	no	short dial.	no	0,01% LMNG	KD	1.5% sucr.		2/1 C

Exp	pH	cross-linking	quencher	salt	GraFix	GeFi	buffer exch.	conc.	detergent	activity	additive	extra note	grid type
23	6,5	0.01% GA	Asp	400 KOAc	yes	no	sp.col.	no	0,01% LMNG	A	1.5% sucr./ADP.BeF3	auto-phosph.	2/1 C
24	6,5	0.01% GA	Asp	400 KOAc	yes	no	sp.col.	no	0,01% LMNG	A	1.5% sucr./ADP.BeF3	auto-phosph.	2/1 C
25	6,5	0.01% GA	Asp	400 KOAc	yes	no	short dial.	no	lower LMNG	A	1.5% sucr./ADP.BeF3	auto-phosph.	2/1 C
26	6,5	0.01% GA	Asp	400 KOAc	yes	no	short dial.	no	0,01% LMNG	A	1.5% sucr./ADP.BeF3	auto-phosph.	2/1 C
27	6,5	no		400 KOAc	yes	no	sp.col.	no	0,01% LMNG	KD	1.5% sucr.		2/1 C
28	6,5	no		400 KOAc	yes	no	sp.col.	no	0,01% LMNG	KD	1.5% sucr.		2/1 C
29	6,5	no		400 KOAc	yes	no	short dial.	no	lower LMNG	KD	1.5% sucr.		2/1 C
30	6,5	no		400 KOAc	yes	no	short dial.	no	0,01% LMNG	KD	1.5% sucr.		2/1 C
31	7,6	0.5 BS3, batch	ABC/tris	350 KOAc		ÄKTA micro	none	no		KD		phosph.	1.2/1.3 C
32	7,6	0.5 BS3	Asp	400 KOAc		ÄKTA micro	none	no		A		auto-phosph.	2/1 C
33	8,4	0.5 BS3	Asp	400 KOAc		ÄKTA micro	none	no		A		auto-phosph.	2/1 C
34	8,4	0.5 BS3	Asp	300 KOAc		ÄKTA micro	none	no		A		auto-phosph.	2/1 C
35	8,4	0.5 BS3	Asp	250 KOAc		ÄKTA micro	none	no		A		auto-phosph.	2/1 C
36	8,4	0.5 BS3	Asp	250 KCl		ÄKTA micro	none	no		A		auto-phosph.	2/1 C
37	8,4	0.5 BS3	Asp	150 KCl		ÄKTA micro	none	no		A		auto-phosph.	2/1 C
38	8,4	0.02% GA	Asp	400 KOAc	yes	no	sp.col.	no	0,01% LMNG	KD			2/1 C/ Au 2/2
39	8,4	0.02% GA	Asp	400 KOAc	yes	no	sp.col.	no	0.001% LMNG	KD			2/1 C
40	8,4	0.04% GA	Asp	400 KOAc	yes	no	sp.col.	no	0.001% LMNG	KD			2/1 C
41	8,4	0.04% GA	Asp	400 KOAc	yes	no	sp.col.	no	0.01% LMNG	KD			2/1 C
42	8,4	0.04% GA	Asp	400 KOAc	yes	no	sp.col.	no	0.001% LMNG	KD	1.5% sucr.		2/1 C
43	8,4	0.04% GA	Asp	400 KOAc	yes	no	sp.col.	no	0.01% LMNG	KD	1.5% sucr.		2/1 C
44	6,5 to 8,4	0.04% GA	Asp	400 KOAc	yes	no	sp.col.	no	0.001% LMNG	KD			2/1 C
45	6,5 to	0.04% GA	Asp	400 KOAc	yes	no	sp.col.	no	0.01% LMNG	KD			2/1 C

Exp	pH	cross-linking	quencher	salt	GraFix	GeFi	buffer exch.	conc.	detergent	activity	additive	extra note	grid type
	8,4												
46	6,5	0.04% GA	Asp	400 KOAc	yes	no	sp.col.	no	0.001% LMNG	KD			2/1 C
47	6,5	0.04% GA	Asp	400 KOAc	yes	no	sp.col.	no	0.01% LMNG	KD			2/1 C
48	7,8	0.02% GA	Asp	400 KOAc	no	no	dial.	no		KD	2.5% glycerol	high conc 1 mg/mL	2/1 C
49	7,8	0.02% GA	Asp	400 KOAc	no	no	dial.	no	0.01% LMNG	KD	2.5% glycerol	0.25 mg/mL, dil+LMNG jbf	2/1 C
50	7,8	0.02% GA	Asp	400 KOAc	no	no	dial.	no		KD	2.5% glycerol	0.25 mg/mL, dil jbf	cont.C (1.2/1.3)
51	8	0.02% GA	Asp	400 KOAc	no	no	dial.	no		KD	2.5% glycerol	high conc 1 mg/mL	2/1 C
52	8	0.02% GA	Asp	400 KOAc	no	no	dial.	no	0.01% LMNG	KD	2.5% glycerol	0.25 mg/mL, dil+LMNG jbf	2/1 C
53	8	0.02% GA	Asp	400 KOAc	no	no	dial.	no		KD	2.5% glycerol	0.25 mg/mL, dil jbf	cont.C (1.2/1.3)
54	8,5	0.02% GA	Asp	400 KOAc	no	no	dial.	no		KD	2.5% glycerol	high conc 1 mg/mL	2/1 C
55	8,5	0.02% GA	Asp	400 KOAc	no	no	dial.	no	0.01% LMNG	KD	2.5% glycerol	0.25 mg/mL, dil+LMNG jbf	2/1 C

Table 5.2 I Results of screening of conditions in table 5.1.

Exp	Result	Exp	Result	Exp	Result	Exp	Result	Exp	Result
1	aggregated	13	aggregated	25	aggregated	37	single dots/ fallen apart, low contrast	49	low contrast
2	aggregated	14	aggregated	26	aggregated	38	homogeneous single particles	50	low contrast
3	aggregated	15	aggregated	27	aggregated	39	grainy/denatured	51	low contrast
4	aggregated	16	aggregated	28	aggregated	40	grainy/denatured	52	low contrast
5	aggregated	17	aggregated	29	aggregated	41	grainy/denatured	53	low contrast
6	aggregated	18	aggregated	30	aggregated	42	grainy/denatured	54	low contrast
7	clustered	19	aggregated	31	aggregated	43	grainy/denatured	55	low contrast
8	aggregated	20	aggregated	32	aggregated	44	grainy/denatured		
9	aggregated	21	aggregated	33	single dots/ fallen apart, low contrast	45	grainy/denatured		
10	aggregated	22	aggregated	34	single dots/ fallen apart, low contrast	46	grainy/denatured		
11	aggregated	23	aggregated	35	single dots/ fallen apart, low contrast	47	grainy/denatured		
12	aggregated	24	aggregated	36	single dots/ fallen apart, low contrast	48	low contrast		

Effect of pH

At pH 7.6 and 6.5, despite being the most favorable solution conditions, CKM particles invariably aggregated on cryo-EM grids. On the other hand, at pH 8.4, single particles were seen. This points to pH as the single most influential parameter for CKM aggregation on cryo-EM grids.

To reconcile the discrepancy between the optimal pH for stability (6.5), and the only pH where there is no aggregation on cryo-EM grids (8.4), in experiments 44 and 45, we performed the GraFix step at a pH of 6.5, and then changed the pH to 8.4 only in the final buffer exchange step, but this resulted in complete denaturation of the complex on grids.

In conditions where grids were prepared directly after ion exchange chromatography, to arrive at a pH of 8.4 for freezing, the pH of the high salt ion exchange buffer B was adjusted to 8.4. Coincidentally, we noticed that this pH/salt elution washed away an overlapping chaperone and resulted in a drastic improvement of the CKM yield.

Effect of crosslinker concentration

At different pH conditions, the concentration of crosslinker added to the GraFix heavy sucrose solution made a remarkable difference on particles' tendency to aggregate. This necessitated titration of crosslinker concentration in GraFix, and the use of the minimum sufficient concentration to fixate the complex. We noticed that at different pH's, this concentration varied for the same crosslinker (figure 5.19 A).

Effect of buffer exchange method and detergents

Dialysis as the final buffer exchange step consistently resulted in disintegration of the complex. On the other hand, using a blocked spin desalting column resulted in intact particles in some conditions.

Figure 5.19 B shows micrographs of CKM crosslinked with the minimum titrated crosslinker concentration (for the respective pH) at pH 6.5 versus pH 8.4, using the same buffer exchange method, demonstrating the dramatic effect of pH. Panel B shows the difference between two grids at pH 8.4, where one was prepared by crosslinking followed by gel filtration, in contrast to GraFix followed by spin desalting column buffer exchange, highlighting the effect of different buffer exchange methods. All micrographs are low-pass filtered for visual clarity.

Our findings place pH at the top of the parameter influence hierarchy, as the parameter to be optimized first. Next, the use of gentler biochemical preparation conditions (GraFix instead of gel filtration), and faster buffer exchange, seems to be important for delicate complexes like the CKM. Finally, the use of a mild detergent such as LMNG may help prevent particle denaturation at the air-water interface.

A cryo-EM grid condition with homogeneous single particles of CKM

Condition number 38 in table 5.1 was the only condition that showed a homogeneous distribution of single particles of CKM, and was reproducible across different preparations.
Preliminary data collection and processing showed that particles only partially aligned in 2D using standard EM processing software, and further collection and processing, and/or grid optimization, which was beyond the scope of this work, is required.

5.5.2 Cryo-EM of CKM-cMed

In addition to CKM on its own, structural investigation of the mode of binding of CKM to cMed would provide valuable insights into the function of the CKM complex in the context of transcription initiation. We asked whether CKM within the CKM-cMed complex demonstrates more stable behavior on cryo-EM grids, particularly because the long unstructured insertion in the CKM subunit Med13 is involved in the CKM-cMed binding surface, according to our XL-MS findings and previous reports [82]. Moreover, this region harbors Molecular Recognition Features (MoRFs), which are sequences that are bioinformatically predicted to have a high propensity for protein-protein interaction, and may acquire structure in the presence of a binding partner [73].

The quality of our recombinant cMed preparation had been previously verified in the context of the PIC [35],[71]. Despite being present in roughly 15% of the classes only, it could be resolved to a local resolution of around 8-9 Å.
However, the cMed sample showed a high degree of aggregation behavior on EM grids, when on its own, in the absence of the globular stabilizing polymerase core.

The general strategy was assembly of the CKM-cMed complex by mixing and dialysis into lower salt, crosslinking in batch followed by sizing, or in GraFix, buffer exchange and grid preparation. At each of these steps, parameters were varied. Similarly structured tables to the ones for CKM, tables 5.3 and 5.4, present a compilation of the tested cryo-EM grid conditions for the CKM-cMed complex, and their results.

The same givens as for the CKM tables can be assumed, with the following addenda. Experiments are numbered from 1 through 43. GeFi refers to gel filtration *after* the assembly and crosslinking of the CKM-cMed complex. 'ATP(before)' means ATP was added and incubated before the final sizing step, to allow for auto-phoshphorylation of the complexes, but was washed away and no longer present in the final freezing buffer. 'Gradient (no Fix)' means that the complex was assembled and crosslinked in batch, and then applied onto a sucrose gradient which did not contain any additional crosslinker, to separate the full complex from its component subcomplexes. TEV then GraFix means that TEV protease was added to the assembled complex to cleave off the MBP tag on CKM, before application on GraFix. The MBP tag on CKM is normally uncleavable when CKM is on its own because the complex precipitates, but can be cleaved in the presence of cMed.

In conditions 42 and 43, endogenously purified complete Mediator complex eMed (containing the head, middle and tail modules) was used instead of cMed, and assembled with recombinant CKM-KD and the tail-interaction activator Gcn4.

So far, no homogeneous particle condition for CKM-cMed has been found, but conditions at pH 6.5 showed the highest promise.

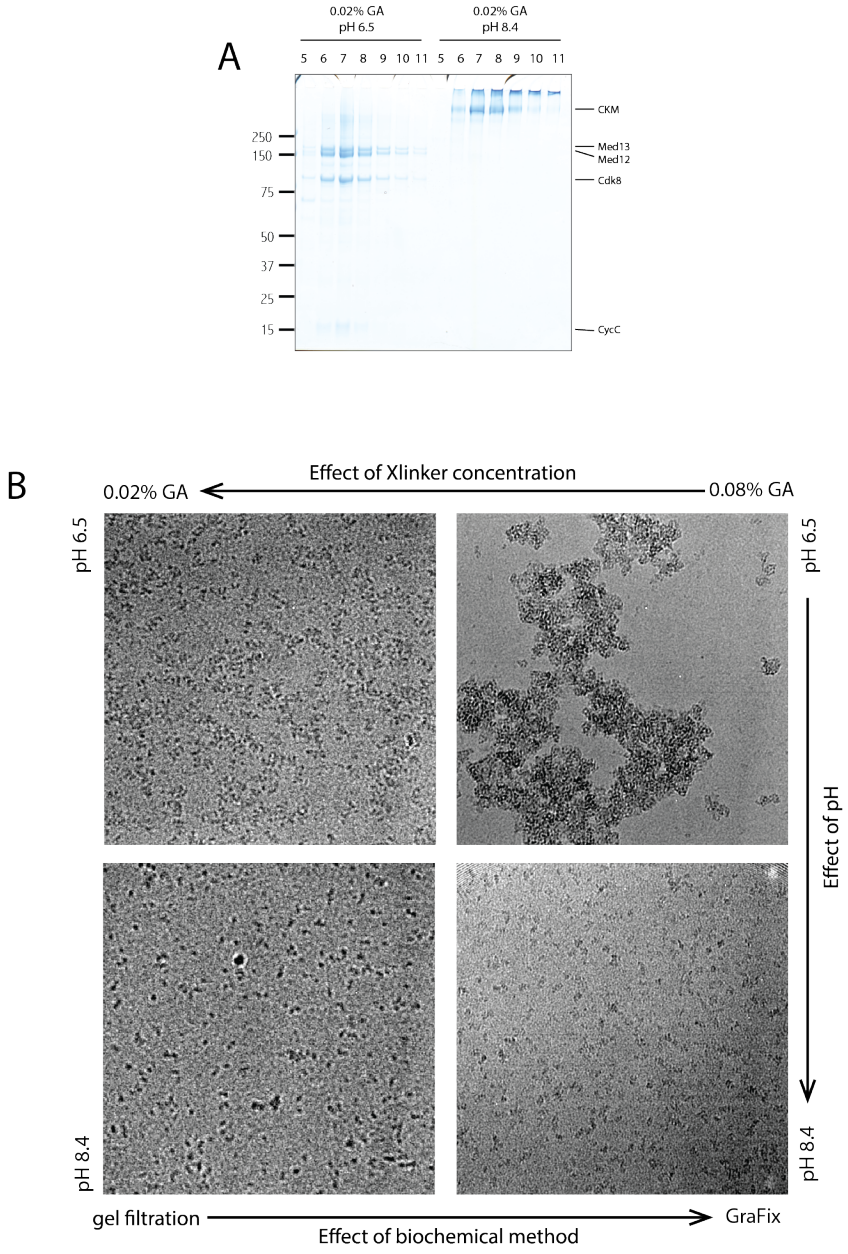

Figure 5.19 | Cryo-EM of CKM.
A, GraFix fractions of CKM showing that the same concentration of glutaraldehyde only slightly crosslinks CKM at pH 6.5, but completely crosslinks it at pH 8.4, highlighting the need to titrate crosslinker concentration for each pH. B, Influence of different parameters on particle aggregation on cryo-EM grids of CKM in vitreous ice. The top two panels show grids of CKM at pH 6.5, varying only the concentration of crosslinker in GraFix. From top to bottom, the pH is varied, with the crosslinker concentration kept constant at the minimal concentration needed for crosslinking *at the respective pH,* (i.e. not the same absolute value), highlighting the drastic effect of varying the pH on aggregation behaviour. The two bottom panels, show the difference between preparing the complex by gel filtration (left) or GraFix and spin column buffer exchange (right). Due to a high degree of interdependence between the varied parameters, these are not segregated effects, but allow us to draw important conclusions about CKM behaviour on cryo-EM grids nevertheless. Namely, pH is the single most influential parameter that determines particle aggregation, and should be optimized first. Next, at the right pH, biochemical method of complex preparation before freezing and buffer exchangecan make the difference between completely damaged (bottom left) or intact (bottom right) single particles. Conditions for top left, top right, bottom left and bottom right are conditions number 7, 8, 32 and 38 in table 5.1, respectively.

Table 5.3 I Tested cryo-EM grid conditions for the CKM-cMed complex.

Exp	pH	crosslinking	quencher	salt	GraFix	GeFi	buffer exch.	conc.	detergent	activity	additive	grid type
1	7,6	0,075% GA	Asp	250 KOAc	TEV then grafix	yes	dial.	no		KD		1.2/1.3 C
2	7,6	0.5 BS3 batch	ABC/tris	250 KOAc		ÄKTA micro	none	no		KD		2/1 C
3	7,6	0.5 BS3 batch	ABC/tris	250 KOAc		ÄKTA micro	none	no		KD		2/1cont. C
4	7,6	0.5 BS3 batch	tris only	250 KOAc	gradient(no Fix)	no	dial.	no	0.01% NP40	KD		2/1 C
5	7,6	0.5 BS3 batch	tris only	250 KOAc	gradient(no Fix)	no	dial.	no	0.01% NP40	KD		1.2/1.3 C
6	7,6	0.5 BS3 batch	tris only	250 KOAc	gradient(no Fix)	no	dial.	no	1% glycerol	KD		2/1 C
7	7,6	0.5 BS3 batch	tris only	250 KOAc	gradient(no Fix)	no	dial.	no	1% glycerol	KD		1.2/1.3 C
8	7,6	0.5 BS3 batch	tris only	250 KOAc	gradient(no Fix)	no	dial.	no	0.01% NP40	KD		2/1 cont. C
9	7,6	0.5 BS3 batch	tris only	250 KOAc	gradient(no Fix)	no	dial.	no	1% glycerol	KD		2/1 cont. C
10	7,6	0.5 BS3 batch	tris only	250 KOAc		ÄKTA micro	none	no	0.02% NP40	A	ATP(before)	2/1 C
11	7,6	0.5 BS3 batch	tris only	250 KOAc		ÄKTA micro	none	no	0.02% NP40	A	ATP(before)	2/1 cont.C
12	7,6	0.5 BS3 batch	tris only	250 KOAc		ÄKTA micro	none	no	0.03% NP40	A	ATP(before)	2/1 C
13	7,6	0.5 BS3 batch	tris only	250 KOAc		ÄKTA micro	none	no	0.03% NP40	A	ATP(before)	2/1cont. C
14	7,6	0.5 BS3 batch	tris only	250 KOAc		ÄKTA micro	none	no	0.04% NP40	A	ATP(before)	2/1 C
15	7,6	0.5 BS3 batch	tris only	250 KOAc		ÄKTA micro	none	no	0.04% NP40	A	ATP(before)	2/1 cont.C
16	8,4	0.5 BS3 batch	tris only	250 KOAc		ÄKTA micro	none	no		A	ATP(before)	2/1 C
17	8,4	0.5 BS3 batch	tris only	250 KOAc		ÄKTA micro	none	no	0.01% NP40	A	ATP(before)	2/1 C
18	7,6	0.03% GA	Asp	200 KOAc	TEV then grafix	no	sp.col.	no	0.01% LMNG	KD		2/1 C
19	7,6	0.03% GA	Asp	200 KOAc	TEV then grafix	no	sp.col.	no	0.01% LMNG	KD		2/1cont. C
20	8,4	0.03% GA	Asp	200 KOAc	TEV then grafix	no	sp.col.	no	0.01% LMNG	KD		2/1 C
21	8,4	0.03% GA	Asp	200 KOAc	TEV then grafix	no	sp.col.	no	0.01% LMNG	KD		2/1cont. C
22	6,5	0.03% GA	Asp	250 KOAc	yes	no	sp.col.	no	0.01% LMNG	KD		2/1 C
23	6,5	0.03% GA	Asp	250 KOAc	yes	no	sp.col.	no	0.001% LMNG	KD	1% sucr.	2/1 C
24	6,5	0.5 BS3 batch	tris only	250 KOAc	gradient(no Fix)	no	sp.col.	no	0.01% LMNG	KD		2/1 C

Exp	pH	crosslinking	quencher	salt	GraFix	GeFi	buffer exch.	conc.	detergent	activity	additive	grid type
25	6,5	0.5 BS3 batch	tris only	250 KOAc	gradient(no Fix)	no	sp.col.	no	0.001% LMNG	KD	1% sucr.	2/1 C
26	6,5	no		250 KOAc	yes	no	sp.col.	no	0.01% LMNG	KD		2/1 C/ Au 2/2
27	6,5	no		250 KOAc	yes	no	sp.col.	no	0.01% LMNG	KD	1% glycerol	2/1 C/ Au 2/2
28	6,5	0.03% GA	Lys	250 KOAc	yes	no	sp.col.	no	0.01% LMNG	KD		2/1 C/ Au 2/2
29	6,5	0.03% GA	Lys	250 KOAc	yes	no	sp.col.	no	0.01% LMNG	KD	1% glycerol	2/1 C/ Au 2/2
30	6,5	0.03% GA	Asp/tris/Lys	250 KOAc	yes	no	sp.col.	no	0.01% LMNG	KD	1.5% sucr.	2/1 C/ Au 2/2
31	6,5	0.03% GA	Asp/tris/Lys	250 KOAc	yes	no	sp.col.	no	0.01% LMNG	KD	1.5% sucr.	2/1 cont.C
32	6,5	0.03% GA	Asp/tris/Lys	250 KOAc	yes	no	short dial.	no	lower LMNG	KD	1.5% sucr.	2/1 C/ Au 2/2
33	6,5	0.03% GA	Asp/tris/Lys	250 KOAc	yes	no	short dial.	no	lower LMNG	KD	1.5% sucr.	2/1cont. C
34	6,5	0.05% GA	Asp	250 KOAc	yes	no	sp.col.	no	0.01% LMNG	KD	1.5% sucr.	2/1 cont.C
35	6,5	0.05% GA	Asp	250 KOAc	yes	no	sp.col.	no	0.01% LMNG	KD	1.5% sucr.	2/1 C
36	6,5	0.05% GA	Asp	250 KOAc	yes	no	short dial.	no	0.01% LMNG	KD	1.5% sucr.	2/1 cont.C
37	6,5	0.05% GA	Asp	250 KOAc	yes	no	short dial.	no	lower LMNG	KD	1.5% sucr.	2/1 C
38	6,5	0.05% GA	Asp	250 KOAc	yes	no	short dial.	no	0.01% LMNG	KD	1.5% sucr.	2/1 C
39	8,4	0.05% GA	Asp	250 KOAc	yes	no	sp.col.	no	0.01% LMNG	KD	1.5% sucr.	2/1 C
40	8,4	0.05% GA	Asp	250 KOAc	yes	no	short dial.	no	lower LMNG	KD	1.5% sucr.	2/1 C
41	8,4	0.05% GA	Asp	250 KOAc	yes	no	short dial.	no	0.01% LMNG	KD	1.5% sucr.	2/1 C
42	7,9	0.03% GA batch	Asp	250 KOAc	gradient(no Fix)	no	dial.	no		KD/eMed/ Gcn4	1.5% sucr.	2/1 cont.C
43	7,9	0.03% GA batch	Asp	251 KOAc	gradient(no Fix)	no	sp.col.	no		KD/eMed/ Gcn4	1.5% sucr.	2/1 cont.C

Table 5.4 I Results of screening of conditions in table 5.3.

Exp	Result	Exp	Result	Exp	Result
1	empty	16	aggregated	31	aggregated
2	huge aggregates	17	empty	32	aggregated
3	huge aggregates	18	small particles/empty	33	aggregated
4	huge aggregates	19	small particles/empty	34	Nothing seen on carbon
5	huge aggregates	20	small particles/empty	35	heavy aggregates
6	huge aggregates	21	small particles/empty	36	Nothing seen on carbon
7	huge aggregates	22	aggregated	37	heavy aggregates
8	huge aggregates	23	aggregated	38	heavy aggregates
9	huge aggregates	24	aggregated	39	denatured
10	grainy	25	aggregated	40	denatured
11	grainy	26	empty/grainy/aggreg	41	denatured
12	grainy	27	empty/grainy/aggreg	42	empty/proteasomes
13	grainy	28	empty/grainy/aggreg	43	Strange circles around 20 nm in diameter with protein on edges.
14	grainy	29	empty/grainy/aggreg		
15	grainy	30	aggregated		

6 Discussion

In this study, we demonstrated a new method for the heterologous expression and purification of the *S. cerevisiae* Mediator Cdk8 kinase module (CKM) in insect cells, and validated this method by testing the catalytic activity and structural integrity of our recombinant particle. 3D reconstruction from negative stain images of CKM purified according to our method was consistent with previously published densities of endogeneously purified *S.cerevisiae* CKM [82],[107], meaning that our method markedly improved the yield and homogeneity, facilitated generation of mutants, and provided rigorous control over biochemical conditions, while still preserving the architectural integrity of the complex.

We found that the CKM did not bind cMed-PIC assembled *in vitro* from purified components on template DNA containing a promoter sequence. Using a biochemical competition assay, we confirmed that CKM directly competes with RNAPII for cMed binding. Moreover, by conducting XL-MS on the CKM-cMed complex, we could offer an explanation for these observations by showing that the CKM binds to cMed on the RNAPII-interacting face, which would sterically block the cMed-RNAPII (hence cMed-PIC) interaction.

Furthermore, we investigated the role of the Cdk8-kinase activity of the CKM. By comparing active and kinase dead CKM, we found that CKM undergoes extensive autophosphorylation. We set up an exploratory *in vitro* phosphoproteomics study to seek out novel targets of CKM phosphorylation within the PIC, which identified the general transcription factors (GTFs) TFIIF and TBP as novel targets, apart from the previously identified C-terminal repeat domain (CTD) of the RNAPII. These phosphorylations did not affect the binding of these factors to the PIC, but attenuated their phase separation. On the other hand, we found phosphorylations deposited by CKM on cMed that appear to weaken the interaction of cMed with the PIC.

Next, we looked at the effect that CKM phosphorylation of activators has on their binding to the genome, and to Mediator, by a combination of biochemical binding experiments and phase separation studies. We found that CKM phosphorylation disrupts activator-DNA and activator-Mediator association, and resolves their condensates.

Lastly, we tried to solve the structure of CKM and CKM-cMed by cryo-EM, but were not successful. In the following sections, we will discuss the implications of our findings and how they relate to published data, and propose a new integrative model of CKM function. Additionally, we will discuss new experiments that are needed to

substantiate this model and guide future directions for both functional and structural studies.

The structural effect of CKM

The observation that CKM is not a part of the transcription Pre-Inititation Complex (PIC) formed on immobilized DNA templates, and that it directly competes with RNAPII for Mediator binding, corroborates a growing body of evidence pointing towards a similar conclusion. A recent mass spectrometry-based interactomics study of the *S. cerevisiae* Mediator complex revealed interactions between Mediator with GTFs and RNAPII when the core Mediator (cMed) subunit Med17 was used for co-immunoprecipitation from yeast cells, but a striking lack thereof when the CKM subunit Med13 was used instead, supporting the idea that the binding of CKM to Mediator abolishes interactions with the PIC [111].

Furthermore, although previous studies had been inconclusive, showing overlaps between all Mediator subunits [112],[113], and even Mediator complex association with gene bodies [61],[114],[115],[37] the latest chromatin immunoprecipitation (ChIP) studies of the Mediator complex in *S. cerevisiae* provided clear insights into the composition of Mediator complexes and their differential localization on the genome. In ChIP-seq experiments, DNA-bound proteins are physically captured onto their genomic locus in cells by formaldehyde crosslinking. Using an antibody against the protein of interest, the protein-DNA complex is precipitated, fragmented, the crosslinks reversed, and the associated DNA fragment sequenced and mapped back to the genome to identify the genomic locus from which it originates. This gives rise to protein occupancy profiles as a function of genomic location; in which mapped sequences and the number of sequencing reads denote positions and amplitudes, respectively. Many years of Mediator ChIP experiments had been confounded with antibodies of poor specificity, making it difficult to draw unambiguous conclusions. The advent of highly specific antibodies, and the discovery that inhibition of the TFIIH kinase kin28 to block RNAPII escape was needed to retain Mediator long enough at promoters to obtain a ChIP signal [37],[116], imbued the latest Mediator ChIP studies with unprecedented clarity. In two recent studies, ChIP of various Mediator subunits showed that while the Mediator head, middle and tail modules were found on both upstream activating sequences (UAS's) and promoter sequences, the CKM was found exclusively on UAS's, implying that ejection of the CKM is necessary before Mediator-PIC interactions can take place [80],[117].

Similar observations of mutual exclusivity from low-resolution structural studies in the yeast *S.pombe* [118], and *in vitro* biochemical reconstitution of transcription from chromatinized templates in human [79], suggest that what we observe is a core, conserved feature of CKM function, rather than a peculiarity.

Our crosslinking/mass spectrometry analysis of a highly purified CKM-cMed complex provides an underlying structural framework to account for these observations, by showing that CKM binding spans the entire length of the RNAPII-binding face of the Mediator complex from the middle module hook domain to the head module jaw domains, and thereby sterically blocks RNAPII binding when present. This is in agreement with averaged 2D EM images of *S.cerevisiae* CKM-Mediator which showed longitudinal binding in the majority of classes [82]. In contrast, human CKM reportedly showed a different binding mode to Mediator, where it was anchored to a protrusion of the Mediator tail module via the Med13 subunit only, with the rest of CKM extending perpendicularly [82],[79]. Due to their poor resolution, however, these studies, like all Mediator EM structural studies before 2014, completely misassigned the Mediator modules, and should therefore be interpreted with caution [119].

Collectively, our data, and others', converge on the following mechanistic take-home message: at gene promoters where the CKM is present, CKM binding to Mediator at UAS's prevents the interaction of Mediator with RNAPII and the assembled transcription initiation machinery on promoters by physical occlusion, independent of the kinase function. Release of Mediator from CKM binding is necessary for the interaction of Mediator with the RNAPII initiation machinery, to stimulate transcription by stabilizing the PIC and by stimulating the TFIIH kinase [120], which phosphorylates the CTD of RNAPII resulting in promoter escape [10].

The kinase activity of CKM

Apart from its structural effect, the CKM contains a Cdk/cyclin pair, which is the only catalytic activity within the Mediator complex. Like the TFIIH kinase kin28 (or Cdk7 in human), the CKM kinase Cdk8 targets the CTD of RNAPII for phosphorylation at serines 2 and 5, according to immunoblot assays [76], and at serine 5 only, according to more reliable mutagenesis studies, where the serine residues in question were mutated to alanines, and the effect of that on phosphorylation was probed [18]. This is consistent with what we observed using our CKM preparations. Besides the RNAPII CTD, we identified two additional targets of the Cdk8 kinase within the PIC complex; the TFIID subunit TBP, and TFIIF. Phosphorylation by Cdk8 did not affect the ability of these factors to bind to the PIC. However, they lowered the propensity of TFIIF, and the RNAPII CTD to undergo liquid-liquid phase separation. We have not yet tested the effect of TBP phosphorylation. We also found novel Cdk8-dependent phosphorylations on cMed that inhibited its binding to the PIC.

Further reported CKM phosphorylation targets in yeast include a variety of gene-specific transcription activators, such as the histidine deficiency response activator

Gcn4 and the multistress response regulator Msn2, committing them to proteasomal degradation, and nuclear exclusion, respectively [121]. In response to nutrient limitation, yeast cells grow pseudohyphae and transition to a filamentous type. Cdk8 was found to phosphorylate two key activators involved in this process, Ste12 and Phd1, similarly marking them for increased turnover, and preventing this transition [122],[123]. Conversely, Cdk8 phosphorylation of a transcriptional regulator of gluconeogenesis, Sip4, was found to be necessary for activation of transcription [124]. Likewise, Cdk8 phosphorylation of the stress responsive activator Skn7 is needed for gene activation [125], and Cdk8 phosphorylation of Gal4 is necessary for galactose-inducible transcription [126],[127],[128],[129],[130].

We found that Cdk8 phosphorylation can actively disengage Gcn4 from its cognate UAS binding site, and that this may be due to a phosphorylation in its DNA-binding domain leucine zipper, disrupting essential hydrophobic contacts needed for homodimerization [131]. Additionally, we found that Cdk8 phosphorylation of Gcn4 decreases its binding to Mediator. The Gcn4-Mediator interaction is dependent on hydrophobic contact, despite the acidic nature of the Gcn4 acitvation domain [132]. Given that, it is not surprising that phosphorylation may disrupt this interaction. Lastly, we found that the CKM undergoes Cdk8-dependent autophosphorylation at its Mediator binding interface, which hints at a possible Cdk8-dependent release of CKM from the CKM-cMed complex.

Phase separation

Although an age-old concept, a recent renaissance of phase separation as a paradigm for compartment-free organization of cellular biochemistry was met with a surge of enthusiasm. The attractiveness of this model lies in its potential to explain how cells control biochemical reactions in space and time, alter their kinetics, and prevent undesired crosstalk [133]. In particular, transcription-related complexes have been shown to phase separate, and these condensates were found near actively transcribing regions of the genome [85]. Phase separation of RNAPII has been attributed to its disordered CTD [20]. In our study, we showed that the effect of Cdk8 phosphorylation on CTD phase separation *in vitro* was identical to that observed upon its phosphorylation by the TFIIH kinase Cdk7 [20]; phosphorylated CTD could no longer form condensates. We also showed that the GTF TFIIF can phase separate *in vitro*, and that this is also attenuated upon Cdk8 phosphorylation. Given the intimate association between RNAPII and TFIIF [134],[87], and their co-recruitment [32], it is imaginable that the two can share a condensate, although this has not been tested *in vitro* or *in vivo*. The effect of Cdk8 phosphorylation on the abovementioned PIC condensates can be interpreted in multiple ways. Depending on whether phosphorylation occurs before or after assembly of the PIC, attenuation of condensates can either repress transcription by undermining recruitment, or

activate it by liberating assembled PIC complexes from anchoring condensates, as construed for the Cdk7 kinase [20].

Furthermore, the Mediator complex has been shown to form phase separated condensates *in vivo*, which overlap with RNAPII condensates intermittently [85],[86]. Mediator was also found in condensates with the activators oct4, Gcn4 and the estrogen receptor [52]. Long disordered activation domains, a salient feature of many activators, were found to be responsible for their phase separation capacity. This led the authors to conclude that, because activation domains are required for gene activation *and* for phase separation, transcription factors *therefore* "activate genes through the phase-separation capacity of their activation domains". Conspicuously absent logical link notwithstanding, this study provided the basis for a view of Mediator and activators as liquid condensates at UAS's. We reproduced essentially the same experiment shown in this study, using the N-terminal half of the Mediator tail subunit Med15 and Gcn4 as a model for Mediator-activator phase separation, and tested the effect of Cdk8 kinase activity on these condensates. Remarkably, we found that Cdk8 phosphorylation of Gcn4 attenuates these condensates. Once again, whether this is interpreted as disruption or release, depends on the timing and extent of occurrence. In contrast, we did not observe any effect of Cdk8 phosphorylation on pure Gcn4 droplets.

Experimental drawbacks

In this work, we identified and mapped various phosphorylation events using phophopeptide enrichment-mass spectrometry. Mass spectrometry is a powerful tool to assay phosphosites on proteins. However, while instructive about positions of phosphosites, all information about stoichiometry is lost. That is to say, if a rare phosphorylation occurs only a few times on a particular residue, whereas an abundant phosphorylation occurs many times on another residue, they will appear as equals, provided they are both present above the detection threshold, and have the same localization probability within a digested peptide. This should be kept in mind when considering phosphorylation data in general, but even more so for *in vitro* phosphorylation data, where the exposure of purified substrates to kinases in high concentrations may result in unspecific phosphorylations, particularly in unstructured loops.

Another consideration pertains to phase separation studies. The fact that some proteins exhibit phase separation behavior in a highly purified system *in vitro*, owing to the physicochemical properties of their disordered regions, does not necessarily mean that such liquid droplets have any physiological relevance. Rather, these experiments give us first clues about what to look for *in vivo*. Moreover, some *in vitro* condensates were found to unspecifically incorporate other phase-separating

components. To this end, we have supplemented all multi-component phase separation data that we show in this work with classical biochemical binding experiments such as electrophoretic mobility shift assays or fluorescence anisotropy experiments.

It is not inconceivable that parts of our observations are *in vitro* artifacts, which occur due to missing important contextual influences, or unnaturally shifted equilibria. Therefore, as with any *in vitro* biochemical study, we advise the reader to take the outcomes of these experiments with a healthy dose of skepticism, and with a backdrop of information provided from functional studies, and emphasize that, unless reinforced by concurring observations *in vivo*, this data is not inherently meaningful.

The value of our experiments, however, comes from their ability to isolate direct effects in a controlled environment, which is not possible *in vivo*. Another point of consideration is that our *in vitro* biochemical experiments reveal *natures* of effects, and not the *extents* to which they occur. For example, phosphorylation often elicits a certain function whereas hyperphosphorylation frequently marks the end of this effect (as has been shown for the RNAPII CTD [135]), and this cannot be distinguished in our experiments. Information about extents is implicit, and can only be derived from the intersection between biochemical and functional observations. Ultimately, a coalition of the two is needed to paint a complete picture, which is why we have drawn on *in vivo* functional studies in building our model, and suggest more functional studies to validate it. Keeping all of the above in mind, we will present what we believe is a fitting interpretation of our data.

An integrative model of CKM function

Since its discovery [75], several models have been put forth to describe the function of CKM throughout the various stages of data availability, with the majority describing it as a general repressive molecule. One model in this direction aptly describes the CKM in analogy to a ‘rheostat’ [79]. In this model, CKM controls the degree to which transcription is activated, in much the same way that the resistance in a rheostat controls the passage of electric current. The kinase activity supports the structural effect, and together the two act as a repressive taskforce; the structural effect by steric blockage of the Mediator-RNAPII interaction, and the kinase by phosphorylating the RNAPII CTD before PIC assembly [18], rendering it transcription-incompetent [135],[136], and by phosphorylating various activators and increasing their turnover [121],[123],[122]. In this way, the CKM acts a resistor against uncontrolled transcription, and the cell can control the degree of resistance by controlling the level of CKM expression. Viewed from this angle, our data confirmed the steric effect in a purified system and provided a structural explanation for it, on the one hand, and contributed additional novel mechanisms by which the

kinase activity can exert its repressive influence, on the other. These constitute impairing the ability of the cell to concentrate polymerases, and the PIC factor TFIIF, needed for transcription, phosphorylating Mediator to inhibit its RNAPII binding, and dissolving activator-DNA and activator-Mediator condensates. A new version of the rheostat model extended to include our findings is presented in figure 6.1. According to this model, a dynamic balance between transcriptional activation and repression dictates transcriptional output.

While appealing in its simplicity, however, we argue that this model is inadequate insofar as it fails to account for the *numerous gene-activating* effects that have been also observed as a result of Cdk8 phosphorylation. Indeed, the discovery of the Cdk8 kinase was driven by the realization that mutating it led to decreased galactose induction from a GAL promoter [75].

The notion of CKM as a purely repressive molecule originates from an early study of its interaction with the RNAPII CTD [18]. The experimental cornerstone underlying this idea was the observation that the Cdk8 kinase ostensibly phosphorylated the RNAPII CTD *before* PIC assembly *in vitro*, whereas the activating TFIIH kinase could only do that *after* PIC assembly. However, this has since been refuted, because high quality preparations of the TFIIH kinase readily phosphorylate the RNAPII CTD *in vitro* without the need for prior PIC assembly (Thesis Schilbach 2017).

Moreover, in the same study, surprisingly, using nuclear extract could not reproduce the same effect; pre-incubating the transcription machinery in nuclear extract from Cdk8 active or inactive mutant strains with ATP invariably did *not* repress transcription, indicating that the reported effect does not occur *in vivo*, and calling into question the relevance of this finding. Furthermore, this argues that Cdk8 is inhibited under normal conditions in cells.

The authors also justified a repressive effect of Cdk8 on grounds of artificial recruitment experiments. Fusion of active or inactive Cdk8 to the DNA-binding domain LexA to forcibly recruit it to a LexA binding sequence upstream of a reporter gene showed that the active kinase repressed reporter expression compared to the wild-type, whereas the inactive one did not. Although seemingly straightforward, interpretation of artificial recruitment experiments has proven to be only deceptively simple. Huge discrepancies in the outcomes of these experiments have been observed, depending on the nature of the reporter, its presence on a plasmid versus genomic integration [137], the presence or absence of overexpression of the fusion [138], the exact position of the fusion tag on the protein [139], as well as the need for chromatin marks or remodeling [140]. Moreover, the absence of a repressive structural influence, which we are now fairly certain of, in the Cdk8 artificial

recruitment experiment shown in this study is a strong indication that Cdk8 alone was being recruited rather than the full CKM complex, creating an unnatural context.

We thus demonstrate that the basis for the view of Cdk8 as purely repressive kinase was not foolproof, and the evidence for it is weak at best. Indeed, another study showed that both the Cdk8 and the Cdk7 kinases are functionally redundant *in vitro* and *in vivo*, because only inhibition of both simultaneously resulted in maximal inhibition of transcription as measured by ChIP occupancy of RNAPII on genes [19]. Furthermore, apart from the reported repressive effects of the Cdk8 kinase *in vivo* [18],[121],[123],[122], diverse studies showed additional activating effects in both yeast [124],[125],[126],[127],[128],[129], and human [141],[142],[143],[144], on a scale that can no longer be dismissed.

We do not doubt that the CKM has a repressive aspect to its function. However, in light of both our own findings, and the new data that has become available since then, we beg to differ from the traditional repressive model. Instead, we propose a new model of CKM function, which unifies the two seemingly contradicting observations of CKM-mediated activation and repression in a single explanatory scheme: a conditional repression model of CKM function.

Our model (figure 6.2) stipulates that, at the genes on which CKM is present (highly regulated genes), activators, Mediator and the transcription machinery are assembled at UASs and *poised for activation*, but prevented from premature firing under normal conditions by the presence of CKM. In these complexes, the Cdk8 kinase is inactive. Upon signaling, the Cdk8 kinase is activated, and phosphorylation results in rapid release of this UAS condensate, freeing the Mediator block, and concomitantly activating transcription and promoter escape (by RNAPII CTD phosphorylation). As such, rapid actuation of *preset programs* of gene transcription can take place in response to stress or developmental signals. These programs are encoded in a) the localization of CKM on a certain subset of genes, and b) the specific response of gene-specific activators to phosphorylation by the Cdk8 kinase. For example, the Gal4 activator requires phosphorylation by Cdk8 to be functional [128], whereas phosphorylation of Gcn4 removes it from its binding site (this study) and targets it to degradation [121].

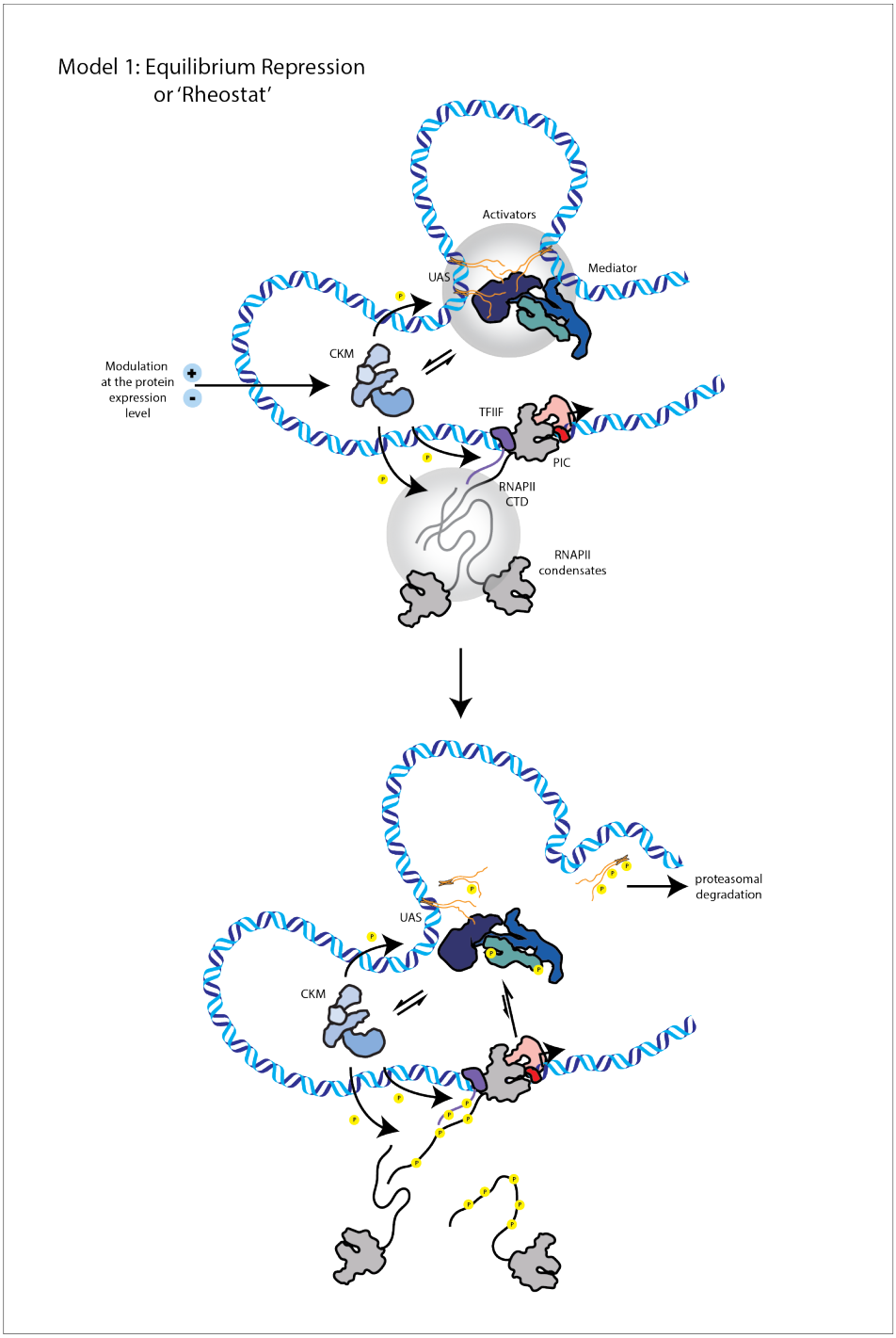

Figure 6.1 | Equilibrium repression, or 'rheostat' model of CKM function.
In this model, the steric function of CKM binding to Mediator acts in conjunction with its kinase function. The steric function blocks the interaction of Mediator with the PIC, to prevent the activation of the TFIIH kinase, CTD phosphorylation and promoter escape. The Cdk8 kinase phosphorylates RNAPII CTD, dissolving RNAPII condensates, as well as TFIIF. Furthermore, it phosphorylates activators, disrupting their interaction with DNA, and with Mediator, and dissolves DNA-activator-Mediator condensates, and commits activators to proteasomal degradation. In this model, the protein expression levels of CKM are modulated to bring about repressive effects by the described mechanisms to fine-tune transcriptional output. This can be responsive to signalling.

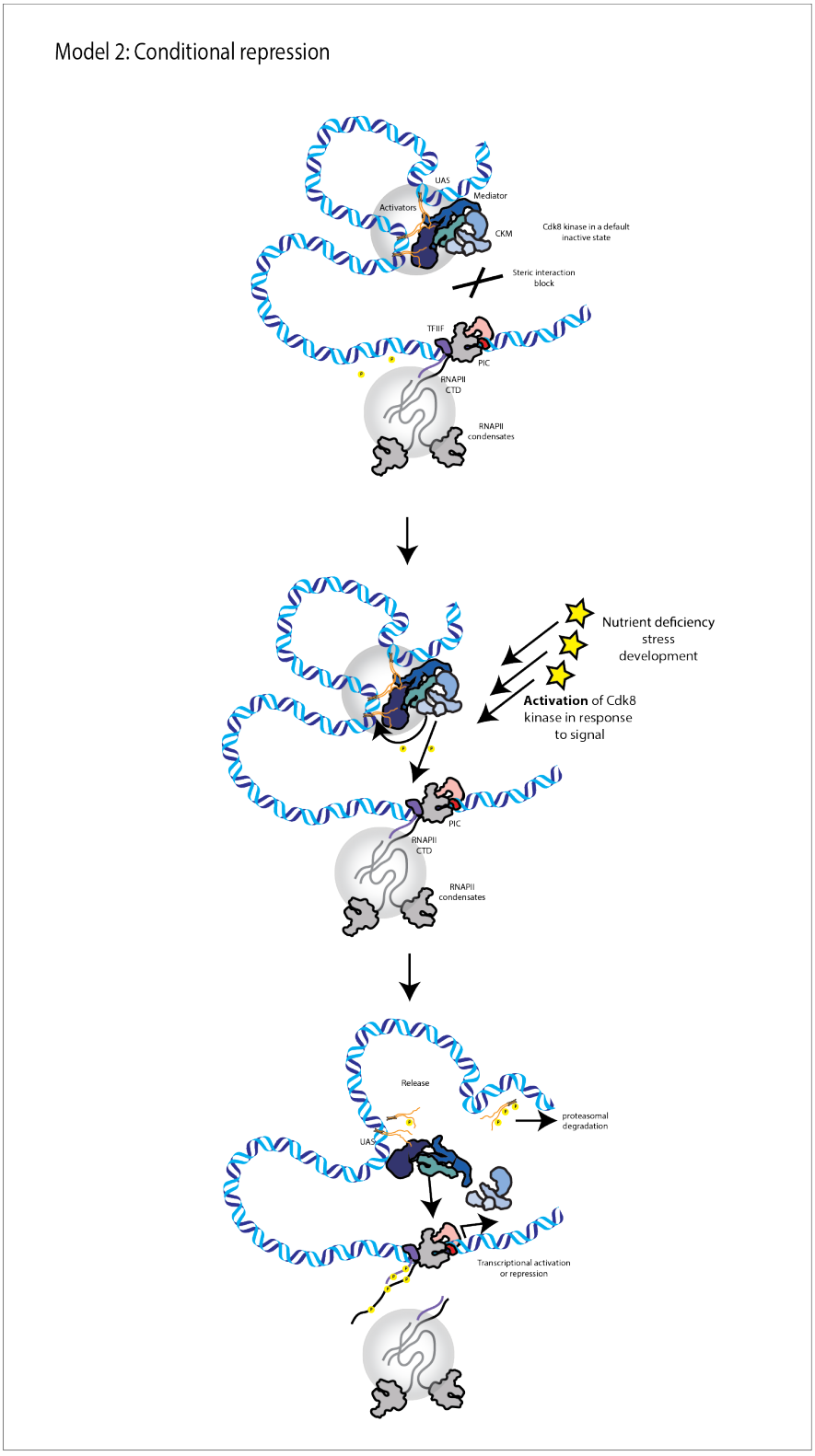

Figure 6.2 | Conditional repression model.
This model postulates that on CKM-dependent genes, activators and Mediator are pre-assembled, together with CKM in a kinase-inhibited form, preventing activation by steric blockage of the RNAPII-Mediator interaction. This way, these genes are poised for activation. Upon receiving a signal, the kinase of CKM is activated, and releases Mediator from the Mediator-activator condensate. Furthermore, it brings about gene-specific effects by phosphorylating gene-specific transcription factors, either committing them to degradation, or further activation, depending on the nature of the transcription activator. As such, CKM allows the rapid actuation of pre-defined transcriptional programs in response to environmental cues.

CKM is thus a *conditional* repressor, preventing activation until the time is right. Our model emphasizes a *duality* in the CKM function; a general repressive kinase-independent function by virtue of its bulky structure; and a kinase-dependent release function followed by gene-specific downstream effects mediated by the interaction of the CKM with different transcription activators as substrates, which triggers gene-specific effects within pre-defined transcription programs. We propose that stress, development, and nutrient status signaling switch from the former mode (repression) to the latter (release), because the CKM targets activators involved in response to these stimuli, and because CKM has been found to be directly under the influence of signaling pathways, such as the Ras/PKA [145] and the Wnt-β-catenin [146] pathways. Notably, these pathways target residues on Med13 and Med12, respectively, implying an allosteric transmission of the signal through the CKM complex to the kinase, in our model. This idea is consistent with the characterized function of Mediator as a central processor of signals, receiving environmental inputs, and processing them into transcriptional outputs; other subunits of the Mediator complex are targeted by the thyroid, insulin, fatty acid sensing, stress, and infection response signaling pathways [62],[147].

Moreover, we believe that such a model in which kinase activation brings about a discrete, rapid effect, is more fitting to the nature of phosphorylation as a post-translational modification (PTM), which results in a dramatically altered chemical microenvironment, than a model in which phosphorylation is involved in a mildly tuned dynamic equilibrium effect.

Because stress and development response genes that would need to be amenable to this form of activation, also need to be activated in a controlled and time-limited manner *by necessity*, prolonged phosphorylation of activators by CKM would *also* mark the end of the activation cycle, rendering these genes refractory to further stimulation, and committing the activators to subsequent ubiquitylation and proteasomal degradation.

The co-recruitment of CKM and Mediator to UASs supports our idea of pre-assembly [80],[117]. The transience of the interaction between CKM and Mediator, as shown by ChIP-re-ChIP experiments, supports our idea that CKM can sometimes be released from the CKM-Mediator complex [61]. In these experiments, Mediator ChIP fractions were ChIPed once more using an antibody against CKM. A discrepancy in their relative occupancy is evidence for transience (whereas a stable interaction would show an equal occupancy for both).

Furthermore, the absence of global effects on gene expression upon Cdk8 inhibition supports our idea of conditional, rather than global, repression [148]. Similarly, the upregulation of certain gene products, and the downregulation of others, upon Cdk8

inhibition supports our idea of reprogramming, although this has only been shown conclusively so far in human [143]. Also, the observation that Cdk8 in nuclear extract is not able to phosphorylate the RNAPII CTD supports our idea that Cdk8 is normally inhibited [18]. Our model would also explain the non-lethality of CKM mutants under normal conditions [148], but only under non-permissive conditions such as cold-sensitivity, when Cdk8 activation would be needed to initiate response programs
All of the above is ample evidence that our conditional repression hypothesis is worth entertaining, but perhaps the strongest argument yet is the uncoupling between Mediator binding and transcription activation, as evident by its indiscriminate ChIP localization to active *and* inactive genes [61]. Following the same rationale, the constitutive presence of some activators on the UASs of some of their target genes, even though these genes are *not constitutively active* further attests to the notion of uncoupling [149],[44]. This means that there must be a player repressing this activation until needed. As opposed to repression by heterochromatinization, repressive histone marks, or more committing forms of repression, this argues for a form of repression that is dependent on the underlying genes being active (have activators bound to their UASs), and ready to quickly switch to a transcribing state. We argue that this player is the CKM, and its responsiveness to signaling brings about this switch.

Composite effects such as the one we propose for the CKM function are hard to detect. What is empirically observed are the divergent outcomes. Our new model resolves the paradox of two seemingly opposite outcomes, and provides a new and exciting possibility to understand transcriptional reprogramming in response to signals of stress, development and nutrient availability. One of the most important selection pressures that direct evolution is the ability to rapidly adapt to a changing environment, and we propose that the CKM can contribute to making that possible, explaining its relatively early occurrence in evolution (for a “repressive” molecule), and its conservation from yeast to human [150].

Naturally, our model is not free of shortcomings. Notably, we cannot explain our own observation of phosphorylations on Mediator that inhibit its PIC binding and what role that could play. It is plausible that auxiliary factors are involved, which are not present in our preparations, such as phosphatases, which confer an additional level of regulation, and can extend this model, but we cannot comment on that at this time. Additionally, if true, our model begs the question, what activates the Cdk8 kinase? This needs further investigation. Moreover, gene activation can still be incorporated into the equilibrium repression model as a secondary effect. Direct repression of genes that alter the expression of downstream genes in a negative or positive way may still be able to give rise to specific transcriptional programs. Equilibrium repression can also be refined into a local equilibrium repression model due to gene-specific CKM recruitment, to explain the lack of global effects. The key point that

distinguishes our model and cannot be incorporated as an extension to the equilibrium repression model, is the notion of stable Mediator-CKM-activator complexes at UASs, and their signaling-induced kinase-dependent release, and the resulting paradigm of rapid activation. Both models are hypothetical, contain the same number of assumptions, and have unique advantages. To determine which one is closer to the truth, the arbiter will undoubtedly be functional data.

Experiments needed to test this model

Our model generates hypotheses about CKM function concerning recruitment and release, which can be translated into experimental questions. If our idea is true that the uncoupling between the presence of activators and Mediator at UASs from activation of transcription is a function of CKM presence, then ChIP occupancy of CKM should correlate with lack of activation from genes at which Mediator and activators are present.

Moreover, if our idea is true that the activity of the Cdk8 kinase releases this block, then inhibition of the Cdk8 kinase should increase the residence time of CKM at UASs, manifested by an increase in the amplitude of its ChIP peak at a given genomic locus. This can be tested using an analogue-sensitive version of the Cdk8 kinase. The analogue-sensitive (AS) kinase technology is based on engineering a space-creating mutant in a kinase's ATP binding pocket [151]. This allows specific inhibition of the kinase if an ATP analogue with a bulky adduct is used, while still allowing it to function normally under normal conditions. Comparing CKM occupancy profiles from inhibited and uninhibited Cdk8-AS would answer this question.

Next would be to test whether that correlates to the effect of environmental stresses such as starvation or heat shock. If our model holds true, then directly following a pressure, CKM occupancy at UASs should drop, and be re-established when conditions normalize. This effect should disappear if the residues involved in signal transduction are mutated.

While the localization of CKM relative to other mediator subunits on some gene promoters has recently been shown, to our knowledge, its genome-wide localization has not been thoroughly characterized. If our idea of preset programs activated by the CKM kinase is true, then CKM should be found on the specific subset of genes that are affected by its Cdk8 kinase activity. On the other hand, global presence of CKM on genes would rather support subtle global effects as is in the equilibrium repression model. This can be tested by ChIP and next generation sequencing of the associated genomic fragments.

After testing effects on CKM localization, we would need to test effects on the transcriptomic level. Some knowledge about that is already available from yeast and human, which gives us the knowledge resource to ask targeted questions. Knowing that some genes are positively regulated while others are negatively regulated upon Cdk8 inhibition, the question is whether this happens directly or indirectly, and what are the mechanisms. To test whether the effects of the Cdk8 kinase on transcription are direct or indirect, the UAS of one upregulated, and one downregulated gene can be taken as an example. Fusing this UAS to a reporter gene on a plasmid, and transforming yeast cells from strains of active or inactive kinase, would allow us to study the effect of the *identity* of the activator, on the response to Cdk8 kinase activity. If upregulation and downregulation are direct effects, then reporter expression should decrease upon kinase inhibition in the case of upregulated genes, and vice versa. A deviation from this pattern would indicate that upregulation or downregulation are secondary effects.

Newer technologies also allow direct detection of newly transcribed mRNA by exposing cells to 4-thiouridine (4SU) [152]. This labels newly transcribed mRNA, which incorporates the modified Uridine. Total RNA can then be extracted, and the newly transcribed mRNA selectively isolated by biotinylation and streptavidin affinity purification. In this way, more accurate information about transient upregulation and downregulation of genes upon Cdk8 inhibition can be obtained as opposed to studies of total mRNA, which had been previously reported [148]. These newly synthesized transcripts can subsequently be reverse transcribed, and upregulation and downregulation from specific genes of interest can be assayed using primers against those transcripts to perform quantitative PCR.

If we find that, indeed, upregulation and downregulation are direct effects of Cdk8 kinase inhibition, this would raise the question of how activators on upregulated and downregulated genes differ to bring about these disparate outcomes. So far, we studied Gcn4 in binding and phase separation assays with Mediator and DNA. To answer this question, we would need to study at least one additional activator from a gene that is affected in the opposite way, to investigate how that compares to the effects on DNA binding, Mediator binding and phase separation, that we observed for Gcn4.

Also eminently missing from our *in vitro* data so far is a true functional readout. This can be attained by reconstituting activated transcription from a DNA template, using all the purified components, which we can now produce. Using a DNA template containing a UAS, a TATA-box and a TSS, the transcription machinery can be supplemented with nucleotides and allowed to transcribe. In the presence of Mediator (eMed) and activators, transcription from the template should be stimulated. Pre-incubating activators with immobilized active CKM would allow us to assay

phosphorylations deposited by CKM, without the physical presence of CKM. This would make it possible to disentangle the structural effect, which we have now elaborately characterized, from the kinase effect, highlighting the unique advantage of our *in vitro* system. In case eviction of activators from DNA is an inadvertent hyperphosphorylation effect, we can study the effect of phosphorylations in the activation domain only (excluding the ones in the DBD) by using a phosphomimetic mutant of the activator. Due to chemical similarity to phosphorylations, serine residues that are targeted for phosphorylation (which we have identified by mass spectrometry) can be mutated to aspartates, and the effect of that on the stimulation of transcription assayed.

Additionally, if the CKM is found on some genes, and not on others in ChIP experiments, this can be hypothesized to be due to an affinity of CKM to certain gene-specific activators, but not others. We can test this idea using our established *in vitro* CKM purification, to test binding to various activators, and see if this mirrors its *in vivo* distribution. If so, this will provide a mechanism for its asymmetric presence on genes, and further support our idea of pre-defined transcription programs. Collectively, these experiments will help us solve the mechanism of gene-specific effects brought about by CKM.

Last, but not least, to validate our phase separation paradigm, we need to find these components together in the same droplets *in vivo*. This can be done by fluorescent labeling and live cell imaging of CKM and Mediator, activators and RNAPII, to see whether they localize to the same droplets, and how this is affected by inhibition of the Cdk8 kinase. If what we observe *in vitro* is true, then Cdk8 inhibition should stabilize activator-Mediator-CKM droplets, and the reverse should happen in response to environmental cues. For this, the yeast system is no longer applicable, because the yeast nucleus is too small, and a switch to human cells would be necessary. This will be facilitated by genome editing techniques that can now be routinely used to manipulate proteins of interest, for example, by insertion of a fluorescent fusion tag.

Structural and unstructural biology of CKM and CKM-cMed

The initial goal of this study was to solve the structures of CKM and CKM-cMed, with the aim of elucidating the mode of binding of CKM to Mediator, in order to derive mechanistic implications about its function. Highly homogeneous samples, as demonstrated by negative stain EM, could be obtained from the recombinant expression and purification setup we established. Although still limiting, the substantial improvement in the yield of recombinant CKM, as opposed to endogenously purified CKM [82], has made it possible for the first time to thoroughly, and systematically optimize biochemical conditions. Nevertheless, despite achieving

significant milestones to this end, we have been unsuccessful at solving either structure so far. Knowledge from our trials can hopefully inform future work, and narrow down the conditions needed to be tested.

Systematic testing of conditions for the CKM sample showed a pH of 6.5 as the most stable solution pH. However, the only single particle condition we found for CKM on cryo-EM grids was at pH 8.4. On the contrary, we did not find any homogeneous particle conditions for the CKM-cMed complex. Learning from these trials, we now believe that the CKM-cMed sample is not the most stable for structural characterization.

Guided by the results of our biochemical experiments, we believe that the UAS complex of CKM, Mediator and activators may be the stable form of this complex, especially considering reports about huge allosteric structural rearrangements in the Mediator complex brought about by activator binding [119]. Endogenously purified Mediator, containing a tail module, an activator bound to a DNA scaffold containing a UAS sequence, and CKM with an inactive kinase, would make up our new complex. Re-thinking our structural target based on our new model of CKM function may hold the key to obtaining a stable sample, that is amenable to structural characterization by cryo-EM.

Preliminary attempts to assemble the complex in this way, using a biotinylated scaffold with a single Gcn4 binding site on beads were not successful, but western blot analysis proved that the recruitment was possible, only inefficient. This means that, in principle, our idea could work, and can be made more efficient by increasing the concentration of the sample, lowering the salt, or artificially adding more activator binding sites to the UAS.

The aggregation problem

A common feature of our cryo-EM grids was heavy aggregation. Normally, particles may aggregate on grids if they are damaged during biochemical purification resulting in partial exposure of buried hydrophobic interiors. This is exacerbated by the stabilizing effect that the hydrophobic air-water interface has on these metastable forms [153]. However, the realization that CKM still aggregated in its most stable solution condition, after the sample passed all quality control checks, including negative stain EM, may be an indication that what we observe is an inherent behavior of the CKM sample. Of its approximately 500 KDa mass, more than 100 KDa is composed of a long unstructured insertion in the subunit Med13. Indeed, we found that the CKM complex undergoes liquid-liquid phase separation under a variety of conditions, when mixed with the crowding agent dextran (figure 6.3). Shifting the pH to a high pH, at which all the acidic groups are charged, and the basic

groups are not, imparting a net negative charge to the particle, was the only solution we found to reversing this behavior. Another alternative would be truncating this insertion, but this is only possible for the CKM sample, because this region is directly involved in Mediator binding, and would impair the CKM-cMed interaction if removed.

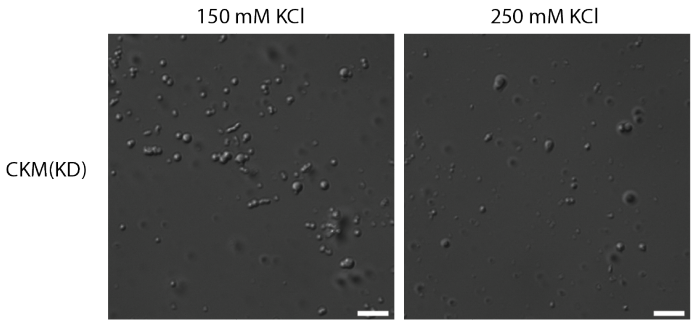

Figure 6.3 | CKM undergoes liquid-liquid phase separation.
CKM phase separates when mixed with the crowding agent dextran, highlighting the preponderence of disordered regions in its structure. The scale bar length is 10 µm.

CKM from yeast to human

Macromolecular machines have a conserved functional essence within the eukaryotic lineage. Using the yeast system makes it possible to abstract the fundamental principles governing gene regulation, from a simpler system where the functional essence is less convoluted by higher levels of regulation. The relative ease of genetic manipulation and molecular biology techniques is likely to maintain the yeast model at the forefront of discovery for years to come. Nonetheless, there are additional metazoan-specific effects that diversify possibilities of regulation.

Similar to the yeast system, human CKM showed a kinase-independent effect that inhibits transcription [79], and phosphorylates the RNAPII CTD [154]. Also like in yeast, the RNAPII CTD phosphorylation was not possible with endogenous CKM, implying that the Cdk8 is kept normally in an inactive state. On top of that, additional metazoan-specific targets of Cdk8 have been identified; the TFIIH cyclin H, resulting in repression, and the histone H3, resulting in activation [154]. The discovery of a specific inhibitor for the human Cdk8 kinase has allowed its targeted inhibition [155]. Using this inhibitor, an exhaustive proteomic study characterized the effect of human Cdk8 inhibition, and found groups of targets that increased or decreased, but there were no marked global effects [143]. Like in yeast, the human Cdk8 was also found to play a role in activation of sugar utilization responses [141], and hypoxia-induced responses [142]. Conversely, it was found to repress super-enhancer associated genes [156], among a variety of other targets. This disparity in repression and activation is highly reminiscent of the yeast system, indicating a general, conserved functional modality that our conditional repression model attempts to explain.

Moreover, genetic experiments in *S.cerevisiae, C.elegans* and *D.melanogaster*, show that deletion of the CKM has no impact on cell viability (yeast), but is detrimental to organismal viability [148],[157],[158], highlighting a powerful evolutionary advantage given by the presence of CKM due to a conferred responsiveness to environmental signals; in this case, developmental cues that are crucial to multicellularity.

Clinical implications

Understanding how the CKM works has important implications for human disease. Mutations in CKM subunits have been linked to neurodevelopmental diseases, such as X-linked mental retardation, and to the development and progression of cancers, such as colorectal carcinomas, uterine leiomas, breast cancers and melanomas [159]. The survival of tumors is contingent on their ability to utilize sugar by aerobic glycolysis, and to respond to hypoxia. It becomes clear then, from our viewpoint of CKM function, that the CKM is advantageous to tumours, and helps them respond better to the stresses and deficiencies they face. Indeed, Cdk8 has been identified as an oncogene, which is dysregulated in many cancers [144],[160], and development of Cdk8-targetting drugs is currently underway [161],[162].

Cdk8 is an appealing drug target, compared to the other transcriptional kinases CDK7 and CDK9, against whom drugs are also under development [163], because inhibition of CDK8 allows targeting specific transcriptional programs, as opposed to global transcription. On the other hand, targeting CDK7 and CDK9, which targets global transcription, is likely to be more cytotoxic, but to also have devastating side effects, like the overwhelming majority of cytotoxic anticancer drugs. Understanding CKM function will undoubtedly open up new avenues for therapeutic intervention, in which therapeutic advantage might be accessible without the associated toxicity.

Future perspectives

To truly understand gene activation, we have to get comfortable with disorder. Nuclear magnetic resonance (NMR) techniques such as heteronuclear single quantum coherence spectroscopy (HSQC) are powerful for studying unstructured interactions in isolation at single amino acid resolution.

Phase separation studies are also likely to remain instrumental. However, their low exploratory potential may rapidly become a hindrance. In the early days of biochemical purification, isolation of complexes with varying degrees of stringency allowed the discovery of novel interactors. Similarly, fractionation of cellular compartments allowed the isolation and identification of their contents. A major

limitation with phase separation studies is the lack of a physical separation principle to allow the isolation of droplets. Chromatographic methods necessarily resolve phase separated droplets, and density-based methods are unfruitful because liquid droplets, usually transient and in the order of only a few micrometers in diameter, are not sufficiently dense, or distinguishable from one another.

So far, the gold standard for phase separation studies has been reconstitution of droplets using purified components and crowding agents, complemented by finding the same effect when this component is labeled and imaged in live cells. While informative, this also means that one always gets only exactly what one set out to look for, and nothing more. How can we find out what *else* is in these droplets? The need for development of methods to make that possible is likely to motivate future research.

One idea could be to optimize proximity labeling live-cell proteomics methods for this problem. Proximity labeling is based on tagging a protein of interest with an enzymatic activity, such as a modified ascorbate peroxidase, engineered to use biotin-phenol as a substrate [164]. Because the product is a radical (biotin phenoxy radical), this creates rapidly reacting and short-lived biotin labels, which selectively target only proteins in the direct vicinity of the tagged bait in a spatially and temporally resolved manner. Subsequent proteomic analysis would then allow the identification of the labeled proteins. This method has been implemented to study events at neuronal synapses [165], and may also prove useful for purposes of phase separation studies.

7 Bibliography

1. Crick, F., *Central dogma of molecular biology.* Nature, 1970. **227**(5258): p. 561.
2. Luger, K., et al., *Crystal structure of the nucleosome core particle at 2.8 Å resolution.* Nature, 1997. **389**(6648): p. 251.
3. Eberharter, A. and P.B. Becker, *Histone acetylation: a switch between repressive and permissive chromatin: Second in review series on chromatin dynamics.* EMBO reports, 2002. **3**(3): p. 224-229.
4. Clapier, C.R. and B.R. Cairns, *The biology of chromatin remodeling complexes.* Annual review of biochemistry, 2009. **78**: p. 273-304.
5. Hurwitz, J., *The discovery of RNA polymerase.* Journal of Biological Chemistry, 2005. **280**(52): p. 42477-42485.
6. Brueckner, F., J. Ortiz, and P. Cramer, *A movie of the RNA polymerase nucleotide addition cycle.* Current opinion in structural biology, 2009. **19**(3): p. 294-299.
7. Vannini, A. and P. Cramer, *Conservation between the RNA polymerase I, II, and III transcription initiation machineries.* Molecular cell, 2012. **45**(4): p. 439-446.
8. Cramer, P., D.A. Bushnell, and R.D. Kornberg, *Structural Basis of Transcription: RNA Polymerase II at 2.8 Ångstrom Resolution.* Science, 2001. **292**(5523): p. 1863-1876.
9. Armache, K.-J., H. Kettenberger, and P. Cramer, *Architecture of initiation-competent 12-subunit RNA polymerase II.* Proceedings of the National Academy of Sciences, 2003. **100**(12): p. 6964-6968.
10. Buratowski, S., *Progression through the RNA polymerase II CTD cycle.* Molecular cell, 2009. **36**(4): p. 541-546.
11. Max, T., M. Søgaard, and J.Q. Svejstrup, *Hyperphosphorylation of the C-terminal repeat domain of RNA polymerase II facilitates dissociation of its complex with mediator.* Journal of Biological Chemistry, 2007. **282**(19): p. 14113-14120.
12. Fabrega, C., et al., *Structure of an mRNA capping enzyme bound to the phosphorylated carboxy-terminal domain of RNA polymerase II.* Molecular cell, 2003. **11**(6): p. 1549-1561.
13. Ng, H.H., et al., *Targeted recruitment of Set1 histone methylase by elongating Pol II provides a localized mark and memory of recent transcriptional activity.* Molecular cell, 2003. **11**(3): p. 709-719.
14. Komarnitsky, P., E.-J. Cho, and S. Buratowski, *Different phosphorylated forms of RNA polymerase II and associated mRNA processing factors during transcription.* Genes & development, 2000. **14**(19): p. 2452-2460.
15. Mosley, A.L., et al., *Rtr1 is a CTD phosphatase that regulates RNA polymerase II during the transition from serine 5 to serine 2 phosphorylation.* Molecular cell, 2009. **34**(2): p. 168-178.
16. Peterlin, B.M. and D.H. Price, *Controlling the elongation phase of transcription with P-TEFb.* Molecular cell, 2006. **23**(3): p. 297-305.
17. Viladevall, L., et al., *TFIIH and P-TEFb coordinate transcription with capping enzyme recruitment at specific genes in fission yeast.* Molecular cell, 2009. **33**(6): p. 738-751.

18. Hengartner, C.J., et al., *Temporal regulation of RNA polymerase II by Srb10 and Kin28 cyclin-dependent kinases.* Molecular cell, 1998. **2**(1): p. 43-53.
19. Liu, Y., et al., *Two Cyclin-Dependent Kinases Promote RNA Polymerase II Transcription and Formation of the Scaffold Complex.* Molecular and Cellular Biology, 2004. **24**(4): p. 1721-1735.
20. Boehning, M., et al., *RNA polymerase II clustering through carboxy-terminal domain phase separation.* Nature structural & molecular biology, 2018. **25**(9): p. 833.
21. Sayre, M.H., H. Tschochner, and R.D. Kornberg, *Reconstitution of transcription with five purified initiation factors and RNA polymerase II from Saccharomyces cerevisiae.* Journal of Biological Chemistry, 1992. **267**(32): p. 23376-82.
22. Sainsbury, S., C. Bernecky, and P. Cramer, *Structural basis of transcription initiation by RNA polymerase II.* Nature Reviews Molecular Cell Biology, 2015. **16**: p. 129.
23. Nikolov, D.B., et al., *Crystal structure of TFIID TATA-box binding protein.* Nature, 1992. **360**(6399): p. 40.
24. Kim, Y., et al., *Crystal structure of a yeast TBP/TATA-box complex.* Nature, 1993. **365**(6446): p. 512.
25. Imbalzano, A.N., K.S. Zaret, and R.E. Kingston, *Transcription factor (TF) IIB and TFIIA can independently increase the affinity of the TATA-binding protein for DNA.* Journal of Biological Chemistry, 1994. **269**(11): p. 8280-8286.
26. Tan, S., et al., *Crystal structure of a yeast TFIIA/TBP/DNA complex.* Nature, 1996. **381**(6578): p. 127.
27. Buratowski, S. and H. Zhou, *Functional domains of transcription factor TFIIB.* Proceedings of the National Academy of Sciences, 1993. **90**(12): p. 5633-5637.
28. Lagrange, T., et al., *New core promoter element in RNA polymerase II-dependent transcription: sequence-specific DNA binding by transcription factor IIB.* Genes & development, 1998. **12**(1): p. 34-44.
29. Bushnell, D.A., et al., *Structural basis of transcription: an RNA polymerase II-TFIIB cocrystal at 4.5 Angstroms.* Science, 2004. **303**(5660): p. 983-988.
30. Kostrewa, D., et al., *RNA polymerase II–TFIIB structure and mechanism of transcription initiation.* Nature, 2009. **462**(7271): p. 323.
31. Sainsbury, S., J. Niesser, and P. Cramer, *Structure and function of the initially transcribing RNA polymerase II–TFIIB complex.* Nature, 2013. **493**(7432): p. 437.
32. Rani, P.G., J.A. Ranish, and S. Hahn, *RNA polymerase II (Pol II)-TFIIF and Pol II-mediator complexes: the major stable Pol II complexes and their activity in transcription initiation and reinitiation.* Molecular and cellular biology, 2004. **24**(4): p. 1709-1720.
33. Khaperskyy, D.A., et al., *Functions of Saccharomyces cerevisiae TFIIF during transcription start site utilization.* Molecular and cellular biology, 2008. **28**(11): p. 3757-3766.
34. Compe, E. and J.-M. Egly, *TFIIH: when transcription met DNA repair.* Nature Reviews Molecular Cell Biology, 2012. **13**: p. 343.
35. Schilbach, S., et al., *Structures of transcription pre-initiation complex with TFIIH and Mediator.* Nature, 2017. **551**(7679): p. 204-209.

36. Holstege, F., P. Van der Vliet, and H. Timmers, *Opening of an RNA polymerase II promoter occurs in two distinct steps and requires the basal transcription factors IIE and IIH.* The EMBO journal, 1996. **15**(7): p. 1666-1677.
37. Wong, Koon H., Y. Jin, and K. Struhl, *TFIIH Phosphorylation of the Pol II CTD Stimulates Mediator Dissociation from the Preinitiation Complex and Promoter Escape.* Molecular Cell, 2014. **54**(4): p. 601-612.
38. Dienemann, C., et al., *Promoter Distortion and Opening in the RNA Polymerase II Cleft.* Mol Cell, 2019. **73**(1): p. 97-106.e4.
39. Kokic, G., et al., *Structural basis of TFIIH activation for nucleotide excision repair.* bioRxiv, 2019: p. 628032.
40. Smale, S.T. and J.T. Kadonaga, *The RNA Polymerase II Core Promoter.* Annual Review of Biochemistry, 2003. **72**(1): p. 449-479.
41. Miller, G. and S. Hahn, *A DNA-tethered cleavage probe reveals the path for promoter DNA in the yeast preinitiation complex.* Nat Struct Mol Biol, 2006. **13**(7): p. 603-10.
42. Hampsey, M., *Molecular genetics of the RNA polymerase II general transcriptional machinery.* Microbiol Mol Biol Rev, 1998. **62**(2): p. 465-503.
43. Bernstein, B.E., et al., *Global nucleosome occupancy in yeast.* Genome Biol, 2004. **5**(9): p. R62.
44. Hahn, S. and E.T. Young, *Transcriptional Regulation in Saccharomyces cerevisiae: Transcription Factor Regulation and Function, Mechanisms of Initiation, and Roles of Activators and Coactivators.* Genetics, 2011. **189**(3): p. 705-736.
45. Li, B., M. Carey, and J.L. Workman, *The role of chromatin during transcription.* Cell, 2007. **128**(4): p. 707-719.
46. Bulger, M. and M. Groudine, *Functional and Mechanistic Diversity of Distal Transcription Enhancers.* Cell, 2011. **144**(3): p. 327-339.
47. Teixeira, M.C., et al., *YEASTRACT: an upgraded database for the analysis of transcription regulatory networks in Saccharomyces cerevisiae.* Nucleic Acids Res, 2018. **46**(D1): p. D348-d353.
48. Hirai, H., T. Tani, and N. Kikyo, *Structure and functions of powerful transactivators: VP16, MyoD and FoxA.* The International journal of developmental biology, 2010. **54**(11-12): p. 1589-1596.
49. Kuras, L. and K. Struhl, *Binding of TBP to promoters in vivo is stimulated by activators and requires Pol II holoenzyme.* Nature, 1999. **399**(6736): p. 609.
50. Li, X.-Y., et al., *Enhancement of TBP binding by activators and general transcription factors.* Nature, 1999. **399**(6736): p. 605.
51. Weake, V.M. and J.L. Workman, *Inducible gene expression: diverse regulatory mechanisms.* Nature Reviews Genetics, 2010. **11**(6): p. 426.
52. Boija, A., et al., *Transcription factors activate genes through the phase-separation capacity of their activation domains.* Cell, 2018. **175**(7): p. 1842-1855. e16.
53. Bryant, G.O. and M. Ptashne, *Independent recruitment in vivo by Gal4 of two complexes required for transcription.* Mol Cell, 2003. **11**(5): p. 1301-9.
54. Louder, R.K., et al., *Structure of promoter-bound TFIID and model of human pre-initiation complex assembly.* Nature, 2016. **531**(7596): p. 604.

55. Han, Y., et al., *Architecture of the Saccharomyces cerevisiae SAGA transcription coactivator complex.* The EMBO journal, 2014. **33**(21): p. 2534-2546.
56. Basehoar, A.D., S.J. Zanton, and B.F. Pugh, *Identification and distinct regulation of yeast TATA box-containing genes.* Cell, 2004. **116**(5): p. 699-709.
57. Kim, Y.-J., et al., *A multiprotein mediator of transcriptional activation and its interaction with the C-terminal repeat domain of RNA polymerase II.* Cell, 1994. **77**(4): p. 599-608.
58. Koleske, A.J. and R.A. Young, *An RNA polymerase II holoenzyme responsive to activators.* Nature, 1994. **368**(6470): p. 466.
59. Carlson, M., *Genetics of transcriptional regulation in yeast: connections to the RNA polymerase II CTD.* Annual review of cell and developmental biology, 1997. **13**(1): p. 1-23.
60. Nonet, M.L. and R.A. Young, *Intragenic and extragenic suppressors of mutations in the heptapeptide repeat domain of Saccharomyces cerevisiae RNA polymerase II.* Genetics, 1989. **123**(4): p. 715-724.
61. Andrau, J.-C., et al., *Genome-Wide Location of the Coactivator Mediator: Binding without Activation and Transient Cdk8 Interaction on DNA.* Molecular Cell, 2006. **22**(2): p. 179-192.
62. Allen, B.L. and D.J. Taatjes, *The Mediator complex: a central integrator of transcription.* Nature Reviews Molecular Cell Biology, 2015. **16**: p. 155.
63. Conaway, R.C. and J.W. Conaway, *Function and regulation of the Mediator complex.* Current opinion in genetics & development, 2011. **21**(2): p. 225-230.
64. Asturias, F.J., et al., *Conserved Structures of Mediator and RNA Polymerase II Holoenzyme.* Science, 1999. **283**(5404): p. 985-987.
65. Verger, A., D. Monté, and V. Villeret, *Twenty years of Mediator complex structural studies.* Biochemical Society Transactions, 2019: p. BST20180608.
66. Lariviere, L., et al., *Structure of the Mediator head module.* Nature, 2012. **492**(7429): p. 448-51.
67. Robinson, P.J.J., et al., *Structure of the Mediator Head module bound to the carboxy-terminal domain of RNA polymerase II.* Proceedings of the National Academy of Sciences, 2012. **109**(44): p. 17931-17935.
68. Nozawa, K., T.R. Schneider, and P. Cramer, *Core Mediator structure at 3.4 Å extends model of transcription initiation complex.* Nature, 2017. **545**: p. 248.
69. Tsai, K.L., et al., *Mediator structure and rearrangements required for holoenzyme formation.* Nature, 2017. **544**(7649): p. 196-201.
70. Robinson, P.J., et al., *Structure of a Complete Mediator-RNA Polymerase II Pre-Initiation Complex.* Cell, 2016. **166**(6): p. 1411-1422.e16.
71. Plaschka, C., et al., *Architecture of the RNA polymerase II–Mediator core initiation complex.* Nature, 2015. **518**: p. 376.
72. Nagulapalli, M., et al., *Evolution of disorder in Mediator complex and its functional relevance.* Nucleic Acids Res, 2016. **44**(4): p. 1591-612.
73. Toth-Petroczy, A., et al., *Malleable machines in transcription regulation: the mediator complex.* PLoS Comput Biol, 2008. **4**(12): p. e1000243.

74. Taatjes, D.J., et al., *Structure, function, and activator-induced conformations of the CRSP coactivator.* Science, 2002. **295**(5557): p. 1058-1062.
75. Liao, S.-M., et al., *A kinase–cyclin pair in the RNA polymerase II holoenzyme.* Nature, 1995. **374**(6518): p. 193.
76. Borggrefe, T., et al., *A complex of the Srb8,-9,-10, and-11 transcriptional regulatory proteins from yeast.* Journal of Biological Chemistry, 2002. **277**(46): p. 44202-44207.
77. Nemet, J., et al., *The two faces of Cdk8, a positive/negative regulator of transcription.* Biochimie, 2014. **97**: p. 22-27.
78. Malik, S. and R.G. Roeder, *The metazoan Mediator co-activator complex as an integrative hub for transcriptional regulation.* Nature reviews. Genetics, 2010. **11**(11): p. 761-772.
79. Knuesel, M.T., et al., *The human CDK8 subcomplex is a molecular switch that controls Mediator coactivator function.* Genes & development, 2009. **23**(4): p. 439-451.
80. Jeronimo, C., et al., *Tail and kinase modules differently regulate core mediator recruitment and function in vivo.* Molecular cell, 2016. **64**(3): p. 455-466.
81. Schneider, E.V., et al., *The structure of CDK8/CycC implicates specificity in the CDK/cyclin family and reveals interaction with a deep pocket binder.* J Mol Biol, 2011. **412**(2): p. 251-66.
82. Tsai, K.L., et al., *A conserved Mediator-CDK8 kinase module association regulates Mediator-RNA polymerase II interaction.* Nat Struct Mol Biol, 2013. **20**(5): p. 611-9.
83. Hyman, A.A., C.A. Weber, and F. Julicher, *Liquid-liquid phase separation in biology.* Annu Rev Cell Dev Biol, 2014. **30**: p. 39-58.
84. Alberti, S., *Phase separation in biology.* Curr Biol, 2017. **27**(20): p. R1097-r1102.
85. Cho, W.-K., et al., *Mediator and RNA polymerase II clusters associate in transcription-dependent condensates.* Science, 2018. **361**(6400): p. 412-415.
86. Sabari, B.R., et al., *Coactivator condensation at super-enhancers links phase separation and gene control.* Science, 2018. **361**(6400): p. eaar3958.
87. Plaschka, C., et al., *Transcription initiation complex structures elucidate DNA opening.* Nature, 2016. **533**(7603): p. 353.
88. Sydow, J.F., et al., *Structural basis of transcription: mismatch-specific fidelity mechanisms and paused RNA polymerase II with frayed RNA.* Molecular cell, 2009. **34**(6): p. 710-721.
89. Vaughn, J., et al., *The establishment of two cell lines from the insectspodoptera frugiperda (lepidoptera; noctuidae).* In vitro, 1977. **13**(4): p. 213-217.
90. Wickham, T., et al., *Screening of insect cell lines for the production of recombinant proteins and infectious virus in the baculovirus expression system.* Biotechnology progress, 1992. **8**(5): p. 391-396.
91. Chapman, R.D., et al., *Transcribing RNA polymerase II is phosphorylated at CTD residue serine-7.* Science, 2007. **318**(5857): p. 1780-1782.
92. Gradia, S.D., et al., *MacroBac: new technologies for robust and efficient large-scale production of recombinant multiprotein complexes*, in *Methods in enzymology*. 2017, Elsevier. p. 1-26.

93. Waddell, C.S. and N.L. Craig, *Tn7 transposition: recognition of the attTn7 target sequence.* Proceedings of the National Academy of Sciences, 1989. **86**(11): p. 3958-3962.
94. Cherry, J.M., et al., *SGD: Saccharomyces genome database.* Nucleic acids research, 1998. **26**(1): p. 73-79.
95. Gasteiger, E., et al., *Protein identification and analysis tools on the ExPASy server*, in *The proteomics protocols handbook*. 2005, Springer. p. 571-607.
96. Zimmermann, L., et al., *A completely reimplemented MPI bioinformatics toolkit with a new HHpred server at its core.* Journal of molecular biology, 2018. **430**(15): p. 2237-2243.
97. Dosztányi, Z., et al., *IUPred: web server for the prediction of intrinsically unstructured regions of proteins based on estimated energy content.* Bioinformatics, 2005. **21**(16): p. 3433-3434.
98. Thompson, J.D., T.J. Gibson, and D.G. Higgins, *Multiple sequence alignment using ClustalW and ClustalX.* Current protocols in bioinformatics, 2003(1): p. 2.3. 1-2.3. 22.
99. Kinoshita, E., E. Kinoshita-Kikuta, and T. Koike, *Separation and detection of large phosphoproteins using Phos-tag SDS-PAGE.* Nature protocols, 2009. **4**(10): p. 1513.
100. Kastner, B., et al., *GraFix: sample preparation for single-particle electron cryomicroscopy.* Nature methods, 2008. **5**(1): p. 53.
101. Tang, G., et al., *EMAN2: an extensible image processing suite for electron microscopy.* Journal of structural biology, 2007. **157**(1): p. 38-46.
102. Punjani, A., et al., *cryoSPARC: algorithms for rapid unsupervised cryo-EM structure determination.* Nature methods, 2017. **14**(3): p. 290.
103. Scheres, S.H., *RELION: implementation of a Bayesian approach to cryo-EM structure determination.* Journal of structural biology, 2012. **180**(3): p. 519-530.
104. Berger, I., D.J. Fitzgerald, and T.J. Richmond, *Baculovirus expression system for heterologous multiprotein complexes.* Nature biotechnology, 2004. **22**(12): p. 1583.
105. Echalier, A., et al., *An inhibitor's-eye view of the ATP-binding site of CDKs in different regulatory states.* ACS chemical biology, 2014. **9**(6): p. 1251-1256.
106. Yu, L., et al., *Role of Mg2+ ions in protein kinase phosphorylation: insights from molecular dynamics simulations of ATP-kinase complexes.* Molecular Simulation, 2011. **37**(14): p. 1143-1150.
107. Wang, X., et al., *Structural flexibility and functional interaction of Mediator Cdk8 module.* Protein & cell, 2013. **4**(12): p. 911-920.
108. König, P. and T.J. Richmond, *The X-ray structure of the GCN4-bZIP bound to ATF/CREB site DNA shows the complex depends on DNA flexibility.* Journal of molecular biology, 1993. **233**(1): p. 139-154.
109. Tuttle, L.M., et al., *Gcn4-mediator specificity is mediated by a large and dynamic fuzzy protein-protein complex.* Cell reports, 2018. **22**(12): p. 3251-3264.
110. Chari, A., et al., *ProteoPlex: stability optimization of macromolecular complexes by sparse-matrix screening of chemical space.* Nature methods, 2015. **12**(9): p. 859.

111. Uthe, H., J.T. Vanselow, and A. Schlosser, *Proteomic Analysis of the Mediator Complex Interactome in Saccharomyces cerevisiae.* Scientific Reports, 2017. **7**: p. 43584.
112. Fan, X., D.M. Chou, and K. Struhl, *Activator-specific recruitment of Mediator in vivo.* Nature structural & molecular biology, 2006. **13**(2): p. 117.
113. Fan, X. and K. Struhl, *Where does mediator bind in vivo?* PloS one, 2009. **4**(4): p. e5029.
114. Zhu, X., et al., *Genome-Wide Occupancy Profile of Mediator and the Srb8-11 Module Reveals Interactions with Coding Regions.* Molecular Cell, 2006. **22**(2): p. 169-178.
115. Paul, E., et al., *Genome-wide association of mediator and RNA polymerase II in wild-type and mediator mutant yeast.* Molecular and cellular biology, 2015. **35**(1): p. 331-342.
116. Jeronimo, C. and F. Robert, *Kin28 regulates the transient association of Mediator with core promoters.* Nature structural & molecular biology, 2014. **21**(5): p. 449.
117. Petrenko, N., et al., *Mediator Undergoes a Compositional Change during Transcriptional Activation.* Molecular Cell, 2016. **64**(3): p. 443-454.
118. Elmlund, H., et al., *The cyclin-dependent kinase 8 module sterically blocks Mediator interactions with RNA polymerase II.* Proceedings of the National Academy of Sciences, 2006. **103**(43): p. 15788-15793.
119. Tsai, K.-L., et al., *Subunit Architecture and Functional Modular Rearrangements of the Transcriptional Mediator Complex.* Cell, 2014. **157**(6): p. 1430-1444.
120. Kim, Y.J., et al., *A multiprotein mediator of transcriptional activation and its interaction with the C-terminal repeat domain of RNA polymerase II.* Cell, 1994. **77**(4): p. 599-608.
121. Chi, Y., et al., *Negative regulation of Gcn4 and Msn2 transcription factors by Srb10 cyclin-dependent kinase.* Genes & development, 2001. **15**(9): p. 1078-1092.
122. Nelson, C., et al., *Srb10/Cdk8 regulates yeast filamentous growth by phosphorylating the transcription factor Ste12.* Nature, 2003. **421**(6919): p. 187.
123. Raithatha, S., et al., *Cdk8 regulates stability of the transcription factor Phd1 to control pseudohyphal differentiation of Saccharomyces cerevisiae.* Molecular and cellular biology, 2012. **32**(3): p. 664-674.
124. Vincent, O., et al., *Interaction of the Srb10 kinase with Sip4, a transcriptional activator of gluconeogenic genes in Saccharomyces cerevisiae.* Molecular and cellular biology, 2001. **21**(17): p. 5790-5796.
125. Lenssen, E., et al., *The Ccr4-not complex regulates Skn7 through Srb10 kinase.* Eukaryotic cell, 2007. **6**(12): p. 2251-2259.
126. Hirst, M., et al., *GAL4 is regulated by the RNA polymerase II holoenzyme-associated cyclin-dependent protein kinase SRB10/CDK8.* Mol Cell, 1999. **3**(5): p. 673-8.
127. Rohde, J.R., J. Trinh, and I. Sadowski, *Multiple Signals Regulate GALTranscription in Yeast.* Molecular and cellular biology, 2000. **20**(11): p. 3880-3886.

128. Sadowski, I., C. Costa, and R. Dhanawansa, *Phosphorylation of Ga14p at a single C-terminal residue is necessary for galactose-inducible transcription.* Molecular and cellular biology, 1996. **16**(9): p. 4879-4887.
129. Sadowski, I., et al., *GAL4 is phosphorylated as a consequence of transcriptional activation.* Proceedings of the National Academy of Sciences, 1991. **88**(23): p. 10510-10514.
130. Ansari, A.Z., et al., *Transcriptional activating regions target a cyclin-dependent kinase.* Proceedings of the National Academy of Sciences, 2002. **99**(23): p. 14706-14709.
131. Hope, I. and K. Struhl, *GCN4, a eukaryotic transcriptional activator protein, binds as a dimer to target DNA.* The EMBO journal, 1987. **6**(9): p. 2781-2784.
132. Brzovic, P.S., et al., *The acidic transcription activator Gcn4 binds the mediator subunit Gal11/Med15 using a simple protein interface forming a fuzzy complex.* Molecular cell, 2011. **44**(6): p. 942-953.
133. Banani, S.F., et al., *Biomolecular condensates: organizers of cellular biochemistry.* Nature reviews Molecular cell biology, 2017. **18**(5): p. 285.
134. Chen, Z.A., et al., *Architecture of the RNA polymerase II–TFIIF complex revealed by cross-linking and mass spectrometry.* The EMBO journal, 2010. **29**(4): p. 717-726.
135. Lu, H., et al., *The nonphosphorylated form of RNA polymerase II preferentially associates with the preinitiation complex.* Proceedings of the National Academy of Sciences, 1991. **88**(22): p. 10004-10008.
136. Chesnut, J., J. Stephens, and M. Dahmus, *The interaction of RNA polymerase II with the adenovirus-2 major late promoter is precluded by phosphorylation of the C-terminal domain of subunit IIa.* Journal of Biological Chemistry, 1992. **267**(15): p. 10500-10506.
137. Gaudreau, L., et al., *Transcriptional activation by artificial recruitment in yeast is influenced by promoter architecture and downstream sequences.* Proceedings of the National Academy of Sciences, 1999. **96**(6): p. 2668-2673.
138. Cheng, J.X., M. Gandolfi, and M. Ptashne, *Activation of the Gal1 gene of yeast by pairs of'non-classical'activators.* Current biology, 2004. **14**(18): p. 1675-1679.
139. Wang, X., et al., *Proteolytic instability and the action of nonclassical transcriptional activators.* Current Biology, 2010. **20**(9): p. 868-871.
140. Ryan, M.P., et al., *Artificially recruited TATA-binding protein fails to remodel chromatin and does not activate three promoters that require chromatin remodeling.* Molecular and cellular biology, 2000. **20**(16): p. 5847-5857.
141. Galbraith, M.D., et al., *CDK8 kinase activity promotes glycolysis.* Cell reports, 2017. **21**(6): p. 1495-1506.
142. Galbraith, M.D., et al., *HIF1A employs CDK8-mediator to stimulate RNAPII elongation in response to hypoxia.* Cell, 2013. **153**(6): p. 1327-1339.
143. Poss, Z.C., et al., *Identification of mediator kinase substrates in human cells using cortistatin A and quantitative phosphoproteomics.* Cell reports, 2016. **15**(2): p. 436-450.

144. Chen, M., et al., *CDK8/19 Mediator kinases potentiate induction of transcription by NFκB.* Proceedings of the National Academy of Sciences, 2017. **114**(38): p. 10208-10213.
145. Chang, Y.-W., S.C. Howard, and P.K. Herman, *The Ras/PKA Signaling Pathway Directly Targets the Srb9 Protein, a Component of the General RNA Polymerase II Transcription Apparatus.* Molecular Cell, 2004. **15**(1): p. 107-116.
146. Kim, S., et al., *Mediator Is a Transducer of Wnt/β-Catenin Signaling.* Journal of Biological Chemistry, 2006. **281**(20): p. 14066-14075.
147. Miller, C., et al., *Mediator Phosphorylation Prevents Stress Response Transcription During Non-stress Conditions.* Journal of Biological Chemistry, 2012. **287**(53): p. 44017-44026.
148. Holstege, F.C., et al., *Dissecting the regulatory circuitry of a eukaryotic genome.* Cell, 1998. **95**(5): p. 717-728.
149. Jakobsen, B.K. and H.R. Pelham, *Constitutive binding of yeast heat shock factor to DNA in vivo.* Mol Cell Biol, 1988. **8**(11): p. 5040-2.
150. Bourbon, H.-M., *Comparative genomics supports a deep evolutionary origin for the large, four-module transcriptional mediator complex.* Nucleic acids research, 2008. **36**(12): p. 3993-4008.
151. Lopez, M.S., J.I. Kliegman, and K.M. Shokat, *The logic and design of analog-sensitive kinases and their small molecule inhibitors.* Methods Enzymol, 2014. **548**: p. 189-213.
152. Garibaldi, A., F. Carranza, and K.J. Hertel, *Isolation of Newly Transcribed RNA Using the Metabolic Label 4-Thiouridine.* Methods in molecular biology (Clifton, N.J.), 2017. **1648**: p. 169-176.
153. Glaeser, R.M. and B.-G. Han, *Opinion: hazards faced by macromolecules when confined to thin aqueous films.* Biophysics reports, 2017. **3**(1-3): p. 1-7.
154. Knuesel, M.T., et al., *The human CDK8 subcomplex is a histone kinase that requires Med12 for activity and can function independently of mediator.* Mol Cell Biol, 2009. **29**(3): p. 650-61.
155. Cee, V.J., et al., *Cortistatin A is a High-Affinity Ligand of Protein Kinases ROCK, CDK8, and CDK11.* Angewandte Chemie International Edition, 2009. **48**(47): p. 8952-8957.
156. Pelish, H.E., et al., *Mediator kinase inhibition further activates super-enhancer-associated genes in AML.* Nature, 2015. **526**(7572): p. 273.
157. van de Peppel, J., et al., *Mediator expression profiling epistasis reveals a signal transduction pathway with antagonistic submodules and highly specific downstream targets.* Molecular cell, 2005. **19**(4): p. 511-522.
158. Boube, M., et al., *Drosophila homologs of transcriptional mediator complex subunits are required for adult cell and segment identity specification.* Genes & Development, 2000. **14**(22): p. 2906-2917.
159. Spaeth, J.M., N.H. Kim, and T.G. Boyer, *Mediator and human disease.* Seminars in Cell & Developmental Biology, 2011. **22**(7): p. 776-787.
160. Firestein, R. and W.C. Hahn, *Revving the Throttle on an Oncogene: CDK8 Takes the Driver Seat.* Cancer Research, 2009. **69**(20): p. 7899-7901.
161. Philip, S., et al., *Cyclin-Dependent Kinase 8: A New Hope in Targeted Cancer Therapy?* J Med Chem, 2018. **61**(12): p. 5073-5092.

162. Crown, J., *CDK8: a new breast cancer target.* Oncotarget, 2017. **8**(9): p. 14269-14270.
163. Hamdan, F.H. and S.A. Johnsen, *Perturbing Enhancer Activity in Cancer Therapy.* Cancers (Basel), 2019. **11**(5).
164. Trinkle-Mulcahy, L., *Recent advances in proximity-based labeling methods for interactome mapping.* F1000Research, 2019. **8**: p. F1000 Faculty Rev-135.
165. Chung, C.Y., et al., *In Situ Peroxidase Labeling and Mass-Spectrometry Connects Alpha-Synuclein Directly to Endocytic Trafficking and mRNA Metabolism in Neurons.* Cell Syst, 2017. **4**(2): p. 242-250.e4.
166. Shevchenko, A., Tomas, H., Havlis, J., Olsen, J.V. and Mann, M. (2006) *In-gel digestion for mass spectrometric characterization of proteins and proteomes* Nature Protocols 2006 **1**(6), 2856-60.
167. Cottrell, J. S. & London, U. *Probability-based protein identification by searching sequence databases using mass spectrometry data*. electrophoresis **20**, 3551-3567 (1999)
168. B. Yang, Y. J. Wu, M. Zhu, S. B. Fan, J. Lin, K. Zhang, S. Li, H. Chi, Y. X. Li, H. F. Chen, S. K. Luo, Y. H. Ding, L. H. Wang, Z. Hao, L. Y. Xiu, S. Chen, K. Ye, S. M. He, M. Q. Dong, *Identification of cross-linked peptides from complex samples*. Nat. Methods **9**, 904–906 (2012)
169. Combe, C. W., Fischer, L. & Rappsilber, J. *xiNET: Cross-link Network Maps With Residue Resolution*. Mol Cell Proteomics **14**, 1137–1147 (2015).
170. Banani, S. F., Lee, H. O., Hyman, A. A., & Rosen, M. K. (2017). *Biomolecular condensates: organizers of cellular biochemistry*. Nature reviews Molecular cell biology, **18**(5), 285

8 List of figures

Figure 2.1 Key aspects of the RNAPII structure.
Figure 2.2 The RNAPII transcription cycle.
Figure 2.3 Assembly of the Pre-Initation Complex.
Figure 2.4 Architecture of core promoters.
Figure 2.5 Examples of DNA binding domains (DBDs) from different transcription activatiors.
Figure 2.6 Function and composition of the Mediator complex.
Figure 2.7 Core Mediator (cMed) structure.
Figure 2.8 Core Mediator (cMed) interaction with the PIC.
Box 5.1 PIC in vitro phosphoproteomics experimental design.
Figure 5.1 CKM expression construct.
Figure 5.2 A novel purification strategy for recombinant CKM.
Figure 5.3 Design of a catalytically inactive Cdk8 mutant.
Figure 5.4 Verification of catalytic activity of recombinantly purified CKM on RNAPII CTD.
Figure 5.5 Negative stain EM of recombinantly purified CKM.
Figure 5.6 Purified proteins toolbox.
Figure 5.7 CKM-cMed binding on a sucrose gradient.
Figure 5.8 CKM does not bind to the PIC.
Figure 5.9 CKM directly competes with RNAPII for cMED binding.
Figure 5.10 Structural analysis of CKM-cMed binding by XL-MS.
Figure 5.11 RNAPII and CKM binding to cMed cannot occur simultaneously.
Figure 5.12 CKM undergoes extensive autophosphorylation.
Figure 5.13 CKM-dependent phosphorylations that inhibit PIC binding.
Figure 5.14 CKM-dependent phosphorylations that do not inhibit PIC binding.
Figure 5.15 Cdk8 phosphorylation of PIC components attenuates their phase separation.
Figure 5.16 Cdk8 phosphorylation of the activator Gcn4 can be recapitulated in vitro.
Figure 5.17 The activator Gcn4 loses affinity to DNA as a result of Cdk8-kinase activity.
Figure 5.18 Mediator-activator phase separation is disrupted as a result of Cdk8-kinase activity.
Figure 5.19 Cryo-EM of CKM.
Figure 6.1 Equilibrium repression, or ‘rheostat’ model of CKM function.
Figure 6.2 Conditional repression model.
Figure 6.3 CKM undergoes liquid-liquid phase separation.

9 List of tables

Table 2.1 Transcriptional kinases.
Table 2.2 Canonical transcription initiation factors.
Table 2.3 Subunit composition of the Mediator complex.
Table 3.1 Vectors used in this study.
Table 3.2 Plasmids used in this study.
Table 3.3 DNA scaffolds used in this study.
Table 3.4 *E.coli* strains used in this study.
Table 3.7 Cell culture media and components.
Table 3.8 Antibiotics and additives to cell culture media.
Table 3.9 Primary antibodies used in this study.
Table 3.10 Secondary antibodies used in this study.
Table 3.11 Standard buffers and dyes.
Table 4.1 LIC tags added to primers.
Table 4.2 Plasmids cloned and cloning method.
Table 4.3 Primer sequences used for cloning.
Table 5.1 Cryo-EM grid conditions tested for the CKM complex.
Table 5.2 Results of screening of conditions in table 5.1.
Table 5.3 Tested cryo-EM grid conditions for the CKM-cMed complex.
Table 5.4 Results of screening of conditions in table 5.3.

10 List of abbreviations

1E6	one million	exch.	exchange
Å	Ångstrom	EYFP	enhanced yellow fluorescent protein
ABC	ammonium bicarbonate	FAM	Fluorescein amidite
Amp	ampicillin	FDR	false discovery rate
ATP	adenosine triphosphate	GA	glutaraldehyde
Au	gold	GC	Guanine Cytosine
biot	biotin	Gcn4	general control protein 4
BS3	bis(sulfosuccinimidyl)suberate	GeFi	gel filtration, size exclusion chromatography
BSA	bovine serum albumin	Gen	gentamycin
C	carbon	GFP	green fluorescent protein
CDK	cyclin-dependent kinase	GraFix	gradient fixation
cDNA	complementary DNA	HEPES	2-[4-(2-hydroxyethyl)piperazin-1- yl]ethanesulfonic acid
CKM(A) / CKM(KD)	Cdk8 kinase module (active) / (kinase dead)	HSQC	heteronuclear single quantum coherence
cMed	core Mediator complex	IgG	immune globulin G
conc.	concentration	IPTG	isopropyl-β-D-1-thiogalactopyranoside
cont.	continuous	ITA	immobilized template assay
CTD	C-terminal domain	Jbf	just before freezing
CTF	contrast transfer function	Kan	kanamycin
dATP	deoxyadenosine triphosphate	KOAc	potassium acetate
dCTP	deoxycytidine triphosphate	LB	lysogeny broth/Luria-Bertani broth
dGTP	deoxyguanosine triphosphate	LIC	ligation independent cloning
dil.	dilution	LMNG	Lauryl maltose-neopentyl glycol
DMSO	dimethyl sulfoxide	MBP	maltose-binding protein
dNTP	deoxynucleoside triphosphate	mCh	mCherry
DPA	ay of proliferation arrest	MES	2-(N-morpholino)ethanesulfonic acid
DTT	dithiothreitol	MOPS	3-(N-morpholino)propanesulfonic acid

EGTA	ethylene glycol-bis(β-aminoethyl ether)-*N*,*N*,*N*′,*N*′-tetraacetic acid	N_2	nitrogen
EM	electron microscopy	NaOH	sodium hydroxide
Ni-NTA	nickel-nitrilotriacetic acid	Tm	melting temperature
OD_{600}	optical density at 600 nm	TSS	transcription start site
PAGE	polyacrylamide gel electrophoresis	v/v	volume per volume
PBS	phosphate buffered saline	w/v	weight per volume
PCR	polymerase chain reaction	X-Gal	5-bromo-4-chloro-3-indolyl-β-D- galactopyranoside
phosph.	phosphorylation	XL-MS	crosslinking-mass spectrometry
pI	protein inhibitor	YFP	yellow fluorescent protein
PIC	pre-initiation complex	YPD	yeast extract peptone dextrose
PMSF	phenylmethylsulfonyl fluoride	β-ME	β-mercaptoethanol
RNAPII	RNA polymerase II	λ-emission	wavelength of emission
SDS	sodium dodecyl sulfate	λ-excitation	wavelength of excitation
SOB	Super Optimal Broth		
Sp. col.	spin column		
sucr.	sucrose		
TAE	tris-acetate-EDTA		
TCEP	tris(2-carboxyethyl)phosphine hydrochloride		
Tet	tetracyclin		
TEV	tobacco etch virus		

11 Curriculum vitae

Sara Osman

Date of birth	September 15th. 1991
Place of birth	Abu Dhabi, United Arab Emirates
Nationality	Egyptian
Address	Am Fassberg 11, MPI-BPC 37077 Göttingen Germany

Languages

Arabic	Mother Tongue
English	Bilingual proficiency
German	Intermediate
French	Basic

Education

06/2015 – present	**PhD student in Molecular Biology and Biochemistry** Prof. Dr. Patrick Cramer Laboratory Department of Molecular Biology Max Planck Institute for Biophysical Chemistry, Göttingen, Germany
09/2013 – 03/2015	**M.Sc. Molecular Biology (Grade: 1.6; max 1.0, min 5.0)** Georg-August-University of Göttingen, IMPRS for Molecular Biology, Germany
10/2008 – 06/2013	**B.Sc. Pharmacy and Biotechnology with highest honors (Grade: 0.73; max 0.7, min 5.0)** German University in Cairo, Egypt
09/1995 – 07/2008	**International General Certificate for Secondary Education (IGCSE)** **A-levels in Physics, Chemistry, Biology and Mathematics (Grade: A)** Al-Nahda National School, Abu Dhabi, U.A.E

Fellowships and Awards

08/2013 – 08/2014	**Stipend of the International Max Planck Research School**
10/2008 – 06/2013	**Academic scholarship of the German University in Cairo**
07/2011	**German University in Cairo Academic Excellence Award**
07/2009	**German University in Cairo Academic Excellence Award**
03/2007	**University of Cambridge International Examinations Award for** **Outstanding Academic Achievement** top IGCSE O-level score in Middle East region

Work experience

09/2013 – present	**Freelance writer at Nature Middle East** Contributor writing short Research Highlights and occasionally features

12 Supplementary information

Supplementary table 1 | CKM autophosphorylation. Phosphosite data for CKM(A) and CKM(KD).

Protein	Localization prob	Localization prob 1_A	Localization prob 2_KD	Number of Phospho (STY)	Amino acid	Sequence window	Positions
SSN8	0,98455	0,98455	0,526607	1	S	ASAASEAIRDPKNSSSPVQIAFNRFMAESLV	266
SSN2	1	1	0,999744	1;2	S	YHSVQETNKISPKDFSPNFTGIDKLMLSPSD	375
SSN2	0,972798	0,972798		1	S	DDPVPTPPAIEHKPVSPDKIGTFTADYSKPN	86
SSN3	0,249905		0,249905		S	SFSPLQKEEALNFDISMADLSSSEEEEDEEE	649
SSN3	0,249905		0,249905		S	QKEEALNFDISMADLSSSEEEEDEEENGSSD	654
SSN3	0,249905		0,249905		S	KEEALNFDISMADLSSSEEEEDEEENGSSDE	655
SSN3	0,249905		0,249905		S	EEALNFDISMADLSSSEEEEDEEENGSSDED	656
SSN2	0,306655		0,306655		S	DLSSSEEEEDEEENGSSDEDLKSLNVRDDMK	667
SSN2	0,366075		0,366075		S	LSSSEEEEDEEENGSSDEDLKSLNVRDDMKP	668
SSN2	0,924879	0,924879		1	S	KEGTLEQREQNENLPSDKSDSMVDKELFGED	472
SSN2	0,333333	0,333333			S	TLEQREQNENLPSDKSDSMVDKELFGEDEDE	475
SSN2	0,333333	0,333333			S	EQREQNENLPSDKSDSMVDKELFGEDEDEDL	477
SSN2	1	1	0,999988	1	S	NNVDNKYKSGGKFSFSPLQKEEALNFDISMA	636
SSN2	1	1		1	S	SAATVHTATSSSIILSDK_____	1418
SSN2	0,986309	0,986309		1	S	NSIWKIPQNDIPQTESPLKTVDSSIQPIESN	748
SSN2	1	1	1	1;2	S	SQPASYHSVQETNKISPKDFSPNFTGIDKLM	370
SSN2	1	1	1	1	S	FNDRKQTTVSNDLENSPLKTELEANGRSLEK	425
SSN2	0,992258	0,992258		1	S	KDFSPNFTGIDKLMLSPSDQFAPAFLNTPNN	387
SSN2	0,865812	0,865812		2	S	DFIQLKQTAAYRTPGSSGVLSSNIAGTNPLS	321
SSN2	0,562273	0,562273		2	S	FIQLKQTAAYRTPGSSGVLSSNIAGTNPLSS	322

Protein	Localization prob	Localization prob 1_A	Localization prob 2_KD	Number of Phospho (STY)	Amino acid	Sequence window	Positions
SSN2	0,260776	0,260776			S	KQTAAYRTPGSSGVLSSNIAGTNPLSSDGAY	326
SSN2	0,260776	0,260776			S	QTAAYRTPGSSGVLSSNIAGTNPLSSDGAYT	327
SSN2	0,779415	0,779415		1;2	S	SSGVLSSNIAGTNPLSSDGAYTEQFQHYKNN	336
SSN2	1	1		1	S	LENSPLKTELEANGRSLEKVNNSVSKTGSVD	437
SSN2	1	1		1	S	GRSLEKVNNSVSKTGSVDTLHNKEGTLEQRE	450
SSN2	0,764029	0,764029		1	T	NSISSQPASYHSVQETNKISPKDFSPNFTGI	366
SSN2	0,344364	0,344364			T	QDALDAIDDFIQLKQTAAYRTPGSSGVLSSN	313
SSN2	0,998002	0,998002	0,990374	1;2	T	AIDDFIQLKQTAAYRTPGSSGVLSSNIAGTN	318
SSN2	0,259825		0,259825		Y	LDAIDDFIQLKQTAAYRTPGSSGVLSSNIAG	316
SSN3	1	1		1	S	EGVTPGRIRTTREDVSPHYNSQKQTLIKKPL	161
SSN3	0,933817	0,933817		1	Y	IKKFKTEKDGVEQLHYTGISQSACREMALCR	197
Srb8	0,758594	0,758594		1	S	ITLTDHRKETWLHELSSSHTSLVKIGKFIPH	134
Srb8	0,773182	0,384809	0,773182	1	S	TLTDHRKETWLHELSSSHTSLVKIGKFIPHG	135
Srb8	0,709471	0,688173	0,709471	1	S	LTDHRKETWLHELSSSHTSLVKIGKFIPHGL	136
Srb8	0,888208	0,888208		1	S	IFQRIIADLSADKPTSPFIDSICKLFDKISF	1254
Srb8	0,993738	0,993738		1	T	_____MNNGSGRYLLTPPDDLHPYVPSSKPQ	11

Supplementary table 2 | **PIC phosphorylation.** Phosphosite data from PIC phosphorylation experiments (sample names as in box 5.1 – results section).

Protein	Localization prob L1_U1	Localization prob L2_U2	Localization prob L3_U3	Localization prob L4_U2-2	Localization prob L5_E1	Localization prob L6_E2	Localization prob L7_E3	#	Amino acid	Sequence window
Tfg1			0,999991	0,999804		0,999784	0,999968	1	S	TKAVDSSNNASNTVPSPIKQEEGLNSTVAER
Tfg1			1	0,999626		0,999994	0,999891	1	S	NPYLSESDIENKENESPVKKEEDSDTLSKSK
Tfg1			1	0,999883		0,999643	0,99995	1	S	RNPPGSRNGGGPTNASPFIKRDRMRRNFLRM
Tfg1			0,999321	0,98876		0,999939	0,99973	1	T	SGTVSLNNTVKDGSQTPTVDSVTKDNTANGV
Tfg1			0,97065					1	T	YDGKEVTNEPEFEEGTMDPLADVAPDGGGRA
Tfg1			0,949803					1	T	KQEEGLNSTVAEREETPAPTITEKDIIEAIG
Tfg1			0,870167			0,792241		1	T	KKILKSFPEGEWNPQTTKAVDSSNNASNTVP
TBP						0,910154		1	T	DPNTRQVWENQNRDGTKPATTFQSEEDIKRA
TBP			0,990353	0,91441		0,814498	0,964492	1	T	RQVWENQNRDGTKPATTFQSEEDIKRAAPES
TBP			0,803405	0,492888		0,982904	0,960264	1	T	QVWENQNRDGTKPATTFQSEEDIKRAAPESE
TBP						1			T	LKEFKEANKIVFDPNTRQVWENQNRDGTKPA
Med1			0,903503						T	PFSTSTKDKNSSTSNTEPIPRSNRHGSVVEA
Med10			0,772781			0,804041		1	S	FPELKEPVEDIIKRTSPIDNVSNTH_____
Med1			0,949028					1	S	PDYQAPFSTSTKDKNSSTSNTEPIPRSNRHG
Med1			0,969232					1	S	ASRRRRSSTNKSKRPSITEAMMLKEEGLQQF
Med8			0,983969					1	S	RNEYGKHDFKNEESLSEEHASLLVRDSKPSK
Med14			0,985137					1	S	KIDKPIRTQVNTGGESVVKKEDNKYAIAGNN
Med17			0,766662					1	T	PTSDEPVPESAGKADTSIRLEGDELENKTKK; PTSDEPVPESTGKADTSIRLEGDELENKTKK
Med4			0,983566					1	T	SQSEEQKGQMAKKEGTPKTDSFIFDGTAKEV
Med4			0,946425					1	T	_____MSVQDTKAVEFSMGHIRSSSV
Med17			0,98068					1	S	LLLSGVKESTGMSSMSPFLRKVVKPSSLNSD; LLLSSVKESTGMSSMSPFLRKVVKPSSLNSD
Med4			1					1	S	____MSVQDTKAVEFSMGHIRSSSVSLVAEA

Supplementary table 3 | **Gcn4 phosphorylation.** Phosphosite data from Gcn4 phosphorylation by CKM.

Protein	Localization prob	Sequence window	Position
Gcn4	1	NSVVKKSHHVGKDDESRLDHLGVVAYNRKQR	4
Gcn4	0,925088	FIKTEEDPIIKQDTPSNLDFDFALPQTATAP	5
Gcn4	1	RLDHLGVVAYNRKQRSIPLSPIVPESSDPAA	3
Gcn4	1	LGVVAYNRKQRSIPLSPIVPESSDPAALKRA	5
Gcn4	0,871314	NRKQRSIPLSPIVPESSDPAALKRARNTEAA	11
Gcn4	1	LQRMKQLEDKVEELLSKNYHLENEVARLKKL	6
Gcn4	0,990454	SEYQPSLFALNPMGFSPLDGSKSTNENVSAS	16
Gcn4	0,972318	GFSPLDGSKSTNENVSASTSTAKPMVGQLIF	7

Supplementary table 4 | CKM-cMed crosslinks. P1 and R1 refer to residue on protein 1, P2 and R2 refer to residue on protein 2, and Score refers to the score of the crosslink.

P1	R1	P2	R2	Score	P1	R1	P2	R2	Score
splP47822lMED21_YEAST	100	splP47822lMED21_YEAST	93	12,38	splP47822lMED21_YEAST	100	splP47822lMED21_YEAST	93	10,31
splP47822lMED21_YEAST	100	splP47822lMED21_YEAST	93	12,17	splP38782lMED6_YEAST	282	splP19263lMED14_YEAST	417	12,06
splP47822lMED21_YEAST	100	splP47822lMED21_YEAST	93	8,56	splP47822lMED21_YEAST	100	splP47822lMED21_YEAST	93	16,30
splP47822lMED21_YEAST	100	splP47822lMED21_YEAST	93	12,01	splP47822lMED21_YEAST	100	splP47822lMED21_YEAST	93	14,05
splP47822lMED21_YEAST	100	splP47822lMED21_YEAST	93	12,16	splP25648lSRB8_YEAST	88	splP47821lSSN8_YEAST	262	14,75
splP47822lMED21_YEAST	100	splP47822lMED21_YEAST	93	8,06	splP47822lMED21_YEAST	100	splP47822lMED21_YEAST	93	12,49
splP47822lMED21_YEAST	100	splP47822lMED21_YEAST	93	13,39	splP32585lMED18_YEAST	280	splP32569lMED17_YEAST	333	7,30
splP47822lMED21_YEAST	100	splP47822lMED21_YEAST	93	11,69	splP39073lSSN3_YEAST	574	splP39073lSSN3_YEAST	580	10,95
splP47822lMED21_YEAST	100	splP47822lMED21_YEAST	93	10,54	splP25648lSRB8_YEAST	888	splP25648lSRB8_YEAST	823	6,30
splP47822lMED21_YEAST	100	splP47822lMED21_YEAST	93	10,02	splP19263lMED14_YEAST	594	splP19263lMED14_YEAST	610	6,63
splP47822lMED21_YEAST	100	splP47822lMED21_YEAST	93	14,32	splP19263lMED14_YEAST	726	splP19263lMED14_YEAST	667	9,45
splP47822lMED21_YEAST	100	splP47822lMED21_YEAST	93	11,66	splP19263lMED14_YEAST	436	splP19263lMED14_YEAST	418	7,99
splP47822lMED21_YEAST	100	splP47822lMED21_YEAST	93	12,15	splP32569lMED17_YEAST	608	splP32569lMED17_YEAST	555	7,43
splP39073lSSN3_YEAST	550	splP39073lSSN3_YEAST	580	9,67	splP47822lMED21_YEAST	100	splP47822lMED21_YEAST	93	10,60
splP25648lSRB8_YEAST	888	splP25648lSRB8_YEAST	823	9,16	splP32570lMED22_YEAST	2	splP32569lMED17_YEAST	324	13,16
splP47822lMED21_YEAST	100	splP47822lMED21_YEAST	93	10,50	splP39073lSSN3_YEAST	550	splP47821lSSN8_YEAST	23	9,11
splP47822lMED21_YEAST	100	splP47822lMED21_YEAST	93	12,20	splQ99278lMED11_YEAST	68	splQ99278lMED11_YEAST	61	7,51
splP47822lMED21_YEAST	100	splP47822lMED21_YEAST	93	9,25	splP32570lMED22_YEAST	82	splP32570lMED22_YEAST	2	7,27
splP47822lMED21_YEAST	100	splP47822lMED21_YEAST	93	8,58	splP25648lSRB8_YEAST	888	splP25648lSRB8_YEAST	823	5,89
splP47822lMED21_YEAST	100	splP47822lMED21_YEAST	93	8,02	splP32570lMED22_YEAST	9	splP32569lMED17_YEAST	333	7,68
splP32585lMED18_YEAST	68	splP32569lMED17_YEAST	589	11,62	splP32585lMED18_YEAST	280	splP32570lMED22_YEAST	2	8,02
splP47822lMED21_YEAST	100	splP47822lMED21_YEAST	93	8,90	splP39073lSSN3_YEAST	39	splP39073lSSN3_YEAST	43	15,26
splP47822lMED21_YEAST	100	splP47822lMED21_YEAST	93	10,95	splP39073lSSN3_YEAST	530	splP39073lSSN3_YEAST	550	9,98
splP47822lMED21_YEAST	100	splP47822lMED21_YEAST	93	10,33	splP47822lMED21_YEAST	75	splP38931lSSN2_YEAST	607	15,83

P1	R1	P2	R2	Score	P1	R1	P2	R2	Score
splP47822lMED21_YEAST	100	splP47822lMED21_YEAST	93	13,43	splP47822lMED21_YEAST	100	splP47822lMED21_YEAST	93	7,63
splP38931lSSN2_YEAST	607	splP47822lMED21_YEAST	100	12,56	splP47822lMED21_YEAST	100	splP47822lMED21_YEAST	93	13,32
splP47822lMED21_YEAST	100	splP47822lMED21_YEAST	93	8,50	splQ12343lMED4_YEAST	138	splQ12343lMED4_YEAST	147	10,07
splP47822lMED21_YEAST	100	splP47822lMED21_YEAST	93	5,26	splP47822lMED21_YEAST	100	splP47822lMED21_YEAST	93	9,90
splP47822lMED21_YEAST	100	splP47822lMED21_YEAST	93	12,49	splP38304lMED8_YEAST	191	splP32570lMED22_YEAST	2	5,41
splP47822lMED21_YEAST	100	splP47822lMED21_YEAST	93	11,23	splP39073lSSN3_YEAST	804	splP39073lSSN3_YEAST	823	3,44
splP19263lMED14_YEAST	697	splP19263lMED14_YEAST	663	12,43	splP39073lSSN3_YEAST	550	splP39073lSSN3_YEAST	580	10,60
splP25648lSRB8_YEAST	632	splP25648lSRB8_YEAST	665	12,51	splQ99278lMED11_YEAST	68	splQ99278lMED11_YEAST	61	7,22
splP47822lMED21_YEAST	100	splP47822lMED21_YEAST	93	13,73	splP32585lMED18_YEAST	280	splP32570lMED22_YEAST	2	6,31
splP47822lMED21_YEAST	100	splP47822lMED21_YEAST	93	11,90	splP47822lMED21_YEAST	100	splP47822lMED21_YEAST	93	7,51
splP47822lMED21_YEAST	100	splP47822lMED21_YEAST	93	12,31	splP47822lMED21_YEAST	100	splP47822lMED21_YEAST	93	12,62
splP47822lMED21_YEAST	100	splP47822lMED21_YEAST	93	8,99	splP47822lMED21_YEAST	100	splP47822lMED21_YEAST	93	8,39
splP38931lSSN2_YEAST	457	splP38931lSSN2_YEAST	440	16,57	splP47822lMED21_YEAST	100	splP47822lMED21_YEAST	93	11,18
splP47822lMED21_YEAST	100	splP47822lMED21_YEAST	93	8,32	splP39073lSSN3_YEAST	550	splP38931lSSN2_YEAST	919	8,43
splP32585lMED18_YEAST	68	splP32569lMED17_YEAST	589	11,39	splP32569lMED17_YEAST	349	splQ99278lMED11_YEAST	89	16,45
splP47822lMED21_YEAST	100	splP47822lMED21_YEAST	93	8,03	splP32585lMED18_YEAST	280	splP32569lMED17_YEAST	333	7,26
splP39073lSSN3_YEAST	820	splP39073lSSN3_YEAST	782	9,41	splP32569lMED17_YEAST	319	splP32569lMED17_YEAST	427	8,87
splP38931lSSN2_YEAST	414	splP38931lSSN2_YEAST	440	5,82	splP47822lMED21_YEAST	100	splP47822lMED21_YEAST	93	9,48
splP32569lMED17_YEAST	333	splP32570lMED22_YEAST	2	11,06	splP32569lMED17_YEAST	78	splP32569lMED17_YEAST	71	5,71
splP47822lMED21_YEAST	100	splP47822lMED21_YEAST	93	7,58	splQ12343lMED4_YEAST	64	splQ12343lMED4_YEAST	2	3,46
splP19263lMED14_YEAST	418	splQ12343lMED4_YEAST	2	7,85	splP19263lMED14_YEAST	697	splP19263lMED14_YEAST	663	5,63
splP47822lMED21_YEAST	100	splP47822lMED21_YEAST	93	9,59	splP47822lMED21_YEAST	100	splP47822lMED21_YEAST	93	8,35
splP47822lMED21_YEAST	100	splP47822lMED21_YEAST	93	9,96	splP47822lMED21_YEAST	100	splP47822lMED21_YEAST	93	7,31
splP32570lMED22_YEAST	9	splP32569lMED17_YEAST	333	8,15	splP39073lSSN3_YEAST	574	splP39073lSSN3_YEAST	550	10,75
splP32569lMED17_YEAST	333	splP32570lMED22_YEAST	2	13,42	splP47822lMED21_YEAST	100	splP47822lMED21_YEAST	93	12,57
splP19263lMED14_YEAST	418	splQ12343lMED4_YEAST	2	8,92	splP47822lMED21_YEAST	100	splP47822lMED21_YEAST	93	10,61

P1	R1	P2	R2	Score	P1	R1	P2	R2	Score
splP47822IMED21_YEAST	100	splP47822IMED21_YEAST	93	9,38	splP47822IMED21_YEAST	100	splP47822IMED21_YEAST	93	10,58
splP25648ISRB8_YEAST	888	splP25648ISRB8_YEAST	823	6,85	splQ99278IMED11_YEAST	68	splQ99278IMED11_YEAST	61	10,99
splP19263IMED14_YEAST	594	splP19263IMED14_YEAST	610	6,87	splP32569IMED17_YEAST	68	splP32569IMED17_YEAST	71	7,66
splP19263IMED14_YEAST	549	splP19263IMED14_YEAST	591	7,96	splP32585IMED18_YEAST	280	splP32569IMED17_YEAST	333	6,35
splP19263IMED14_YEAST	360	splQ12343IMED4_YEAST	2	6,81	splQ99278IMED11_YEAST	68	splQ99278IMED11_YEAST	61	6,15
splP38931ISSN2_YEAST	607	splP47822IMED21_YEAST	93	6,16	splP47822IMED21_YEAST	100	splP47822IMED21_YEAST	93	7,43
splP39073ISSN3_YEAST	820	splP39073ISSN3_YEAST	782	9,76	splP47822IMED21_YEAST	100	splP47822IMED21_YEAST	93	8,55
splP32569IMED17_YEAST	333	splP32570IMED22_YEAST	2	12,60	splP32570IMED22_YEAST	82	splP32570IMED22_YEAST	2	7,14
splP38304IMED8_YEAST	191	splP32570IMED22_YEAST	2	11,78	splP19263IMED14_YEAST	549	splP19263IMED14_YEAST	610	8,04
splP39073ISSN3_YEAST	820	splP39073ISSN3_YEAST	782	8,19	splP32569IMED17_YEAST	386	splP32569IMED17_YEAST	427	10,03
splP47822IMED21_YEAST	100	splP47822IMED21_YEAST	93	7,73	splP32569IMED17_YEAST	608	splP32569IMED17_YEAST	555	9,95
splP33308IMED9_YEAST	78	splQ12343IMED4_YEAST	2	6,35	splP47822IMED21_YEAST	100	splP47822IMED21_YEAST	93	10,48
splP47822IMED21_YEAST	100	splP47822IMED21_YEAST	93	10,43	splP47822IMED21_YEAST	100	splP47822IMED21_YEAST	93	10,71
splP39073ISSN3_YEAST	820	splP39073ISSN3_YEAST	782	14,38	splP38782IMED6_YEAST	282	splP19263IMED14_YEAST	417	7,91
splP25648ISRB8_YEAST	888	splP25648ISRB8_YEAST	823	8,45	splP25648ISRB8_YEAST	899	splP25648ISRB8_YEAST	901	20,72
splP47822IMED21_YEAST	100	splP47822IMED21_YEAST	93	7,80	splP25648ISRB8_YEAST	888	splP25648ISRB8_YEAST	823	4,90
splP19263IMED14_YEAST	697	splP19263IMED14_YEAST	663	9,48	splP47822IMED21_YEAST	100	splP47822IMED21_YEAST	93	15,12
splP47822IMED21_YEAST	100	splP47822IMED21_YEAST	93	14,29	splP47822IMED21_YEAST	100	splP47822IMED21_YEAST	93	7,03
splP32569IMED17_YEAST	333	splP32570IMED22_YEAST	2	8,75	splP38304IMED8_YEAST	191	splP32570IMED22_YEAST	2	7,24
splP19263IMED14_YEAST	591	splP19263IMED14_YEAST	674	7,47	splP19263IMED14_YEAST	678	splP19263IMED14_YEAST	667	7,48
splP39073ISSN3_YEAST	729	splP39073ISSN3_YEAST	782	10,48	splP39073ISSN3_YEAST	820	splP39073ISSN3_YEAST	782	7,61
splP19263IMED14_YEAST	360	splQ12343IMED4_YEAST	2	5,79	splP25648ISRB8_YEAST	899	splP25648ISRB8_YEAST	901	10,55
splP47822IMED21_YEAST	100	splP47822IMED21_YEAST	93	11,11	splP32569IMED17_YEAST	608	splP32569IMED17_YEAST	601	4,60
splP39073ISSN3_YEAST	550	splP39073ISSN3_YEAST	580	7,64	splP47822IMED21_YEAST	100	splP47822IMED21_YEAST	93	9,63
splP39073ISSN3_YEAST	550	splP39073ISSN3_YEAST	580	10,20	splP47822IMED21_YEAST	100	splP47822IMED21_YEAST	93	6,58
splP38931ISSN2_YEAST	414	splP38931ISSN2_YEAST	440	5,72	splP19263IMED14_YEAST	591	splP19263IMED14_YEAST	674	5,90

P1	R1	P2	R2	Score	P1	R1	P2	R2	Score
splP32569IMED17_YEAST	333	splP32570IMED22_YEAST	2	6,97	splP32569IMED17_YEAST	333	splP32570IMED22_YEAST	2	14,38
splP39073ISSN3_YEAST	550	splP39073ISSN3_YEAST	580	8,27	splP47822IMED21_YEAST	100	splP47822IMED21_YEAST	93	7,17
splP25648ISRB8_YEAST	899	splP25648ISRB8_YEAST	901	15,82	splP19263IMED14_YEAST	678	splP19263IMED14_YEAST	667	6,45
splP47822IMED21_YEAST	100	splP47822IMED21_YEAST	93	10,03	splP32569IMED17_YEAST	333	splP32569IMED17_YEAST	324	13,36
splP19263IMED14_YEAST	417	splQ12343IMED4_YEAST	2	9,60	splP39073ISSN3_YEAST	820	splP39073ISSN3_YEAST	782	11,30
splP47822IMED21_YEAST	100	splP47822IMED21_YEAST	93	6,18	splP32569IMED17_YEAST	68	splP32569IMED17_YEAST	71	9,15
splP19263IMED14_YEAST	591	splP19263IMED14_YEAST	674	5,83	splP25648ISRB8_YEAST	888	splP25648ISRB8_YEAST	823	6,43
splP38931ISSN2_YEAST	1398	splP38931ISSN2_YEAST	1002	5,38	splP25648ISRB8_YEAST	665	splP25648ISRB8_YEAST	553	4,20
splP19263IMED14_YEAST	549	splP19263IMED14_YEAST	610	8,27	splP39073ISSN3_YEAST	116	splP39073ISSN3_YEAST	189	6,32
splP25648ISRB8_YEAST	888	splP25648ISRB8_YEAST	823	6,58	splP47822IMED21_YEAST	100	splP47822IMED21_YEAST	93	13,78
splP47822IMED21_YEAST	100	splP47822IMED21_YEAST	93	12,66	splP47822IMED21_YEAST	100	splP47822IMED21_YEAST	93	7,50
splP19263IMED14_YEAST	697	splP19263IMED14_YEAST	663	7,27	splP47822IMED21_YEAST	100	splP47822IMED21_YEAST	93	6,29
splP19263IMED14_YEAST	549	splP19263IMED14_YEAST	610	8,16	splP32569IMED17_YEAST	608	splP32569IMED17_YEAST	601	4,47
splP38304IMED8_YEAST	191	splP32570IMED22_YEAST	2	8,04	splP19263IMED14_YEAST	360	splQ12343IMED4_YEAST	2	5,61
splP19263IMED14_YEAST	360	splQ12343IMED4_YEAST	2	6,19	splQ99278IMED11_YEAST	53	splQ99278IMED11_YEAST	61	10,49
splP19263IMED14_YEAST	360	splQ12343IMED4_YEAST	2	7,90	splP25648ISRB8_YEAST	888	splP25648ISRB8_YEAST	823	7,88
splP47822IMED21_YEAST	100	splP47822IMED21_YEAST	93	8,51	splP47822IMED21_YEAST	100	splP47822IMED21_YEAST	93	10,32
splP47822IMED21_YEAST	100	splP47822IMED21_YEAST	93	7,26	splP25648ISRB8_YEAST	888	splP25648ISRB8_YEAST	823	5,03
splP47822IMED21_YEAST	100	splP47822IMED21_YEAST	93	8,17	splP39073ISSN3_YEAST	39	splP39073ISSN3_YEAST	43	15,12
splP32569IMED17_YEAST	333	splP32570IMED22_YEAST	2	6,53	splP32570IMED22_YEAST	2	splP32569IMED17_YEAST	324	7,91
splP47822IMED21_YEAST	100	splP47822IMED21_YEAST	93	13,70	splP38931ISSN2_YEAST	607	splP47822IMED21_YEAST	93	7,61
splP47822IMED21_YEAST	100	splP47822IMED21_YEAST	93	12,89	splP19263IMED14_YEAST	674	splP19263IMED14_YEAST	594	6,57
splP39073ISSN3_YEAST	550	splP39073ISSN3_YEAST	580	8,38	splP19263IMED14_YEAST	549	splP19263IMED14_YEAST	610	6,60
splP47822IMED21_YEAST	100	splP47822IMED21_YEAST	93	13,48	splP32569IMED17_YEAST	333	splP32570IMED22_YEAST	2	15,10
splP47822IMED21_YEAST	100	splP47822IMED21_YEAST	93	13,61	splP32570IMED22_YEAST	2	splP32569IMED17_YEAST	324	9,14
splP19263IMED14_YEAST	697	splP19263IMED14_YEAST	663	8,07	splP47822IMED21_YEAST	100	splP47822IMED21_YEAST	93	7,62

P1	R1	P2	R2	Score	P1	R1	P2	R2	Score
splP47822IMED21_YEAST	100	splP47822IMED21_YEAST	93	13,09	splP39073ISSN3_YEAST	804	splP39073ISSN3_YEAST	823	3,82
splP32569IMED17_YEAST	333	splP32570IMED22_YEAST	2	6,03	splP47822IMED21_YEAST	100	splP47822IMED21_YEAST	93	9,09
splP25648ISRB8_YEAST	888	splP25648ISRB8_YEAST	823	9,71	splP39073ISSN3_YEAST	39	splP39073ISSN3_YEAST	43	13,29
splP19263IMED14_YEAST	360	splQ12343IMED4_YEAST	2	6,03	splP19263IMED14_YEAST	549	splP19263IMED14_YEAST	591	11,66
splP33308IMED9_YEAST	78	splQ12343IMED4_YEAST	2	5,75	splP32569IMED17_YEAST	68	splP32569IMED17_YEAST	71	12,21
splP19263IMED14_YEAST	451	splP19263IMED14_YEAST	418	7,27	splP19263IMED14_YEAST	417	splQ12343IMED4_YEAST	2	12,97
splP47822IMED21_YEAST	100	splP47822IMED21_YEAST	93	9,35	splP47822IMED21_YEAST	100	splP47822IMED21_YEAST	93	7,34
splP39073ISSN3_YEAST	574	splP39073ISSN3_YEAST	580	8,60	splP47822IMED21_YEAST	75	splP47822IMED21_YEAST	93	5,40
splP47822IMED21_YEAST	100	splP47822IMED21_YEAST	93	8,88	splP47822IMED21_YEAST	100	splP47822IMED21_YEAST	93	9,34
splP38304IMED8_YEAST	191	splP32570IMED22_YEAST	2	7,08	splP38931ISSN2_YEAST	796	splP38931ISSN2_YEAST	204	8,63
splP47822IMED21_YEAST	100	splP47822IMED21_YEAST	93	14,15	splQ99278IMED11_YEAST	68	splQ99278IMED11_YEAST	61	7,45
splP47822IMED21_YEAST	100	splP47822IMED21_YEAST	93	7,42	splP19263IMED14_YEAST	697	splP19263IMED14_YEAST	663	8,94
splP47822IMED21_YEAST	100	splP47822IMED21_YEAST	93	13,47	splQ12343IMED4_YEAST	55	splQ12343IMED4_YEAST	64	7,55
splP39073ISSN3_YEAST	820	splP39073ISSN3_YEAST	782	11,51	splP19263IMED14_YEAST	609	splP19263IMED14_YEAST	591	10,34
splQ12321IMED1_YEAST	389	splQ12343IMED4_YEAST	2	7,36	splP19263IMED14_YEAST	282	splP19263IMED14_YEAST	257	13,00
splP19263IMED14_YEAST	417	splQ12343IMED4_YEAST	2	13,50	splP38304IMED8_YEAST	191	splP32570IMED22_YEAST	2	5,80
splP47822IMED21_YEAST	100	splP47822IMED21_YEAST	93	9,17	splP32585IMED18_YEAST	68	splP32569IMED17_YEAST	589	10,32
splP47822IMED21_YEAST	100	splP47822IMED21_YEAST	93	11,30	splP19263IMED14_YEAST	591	splP19263IMED14_YEAST	610	6,36
splQ99278IMED11_YEAST	68	splQ99278IMED11_YEAST	61	11,68	splQ99278IMED11_YEAST	53	splQ99278IMED11_YEAST	61	8,25
splP38931ISSN2_YEAST	607	splP47822IMED21_YEAST	93	8,32	splP19263IMED14_YEAST	609	splP19263IMED14_YEAST	591	10,22
splP19263IMED14_YEAST	697	splP19263IMED14_YEAST	663	9,63	splP19263IMED14_YEAST	591	splP19263IMED14_YEAST	610	5,64
splP47822IMED21_YEAST	100	splP47822IMED21_YEAST	93	6,93	splP19263IMED14_YEAST	360	splQ12343IMED4_YEAST	2	5,03
splP25648ISRB8_YEAST	88	splP47821ISSN8_YEAST	262	9,83	splP32570IMED22_YEAST	9	splP32569IMED17_YEAST	333	6,13
splP47822IMED21_YEAST	100	splP47822IMED21_YEAST	93	8,53	splP32569IMED17_YEAST	608	splP32569IMED17_YEAST	555	8,41
splP32569IMED17_YEAST	608	splP32569IMED17_YEAST	555	8,75	splP38931ISSN2_YEAST	796	splP38931ISSN2_YEAST	204	9,52
splP47822IMED21_YEAST	100	splP47822IMED21_YEAST	93	5,14	splP47822IMED21_YEAST	100	splP47822IMED21_YEAST	93	9,47

P1	R1	P2	R2	Score	P1	R1	P2	R2	Score
splP25648lSRB8_YEAST	899	splP25648lSRB8_YEAST	901	11,05	splP47822lMED21_YEAST	100	splP47822lMED21_YEAST	93	9,51
splP39073lSSN3_YEAST	530	splP39073lSSN3_YEAST	550	9,39	splP25648lSRB8_YEAST	616	splP25046lMED19_YEAST	65	8,76
splP39073lSSN3_YEAST	887	splP39073lSSN3_YEAST	580	8,83	splP19263lMED14_YEAST	667	splP19263lMED14_YEAST	674	6,05
splP25648lSRB8_YEAST	899	splP25648lSRB8_YEAST	901	10,86	splP39073lSSN3_YEAST	97	splP39073lSSN3_YEAST	319	8,08
splQ99278lMED11_YEAST	88	splP32570lMED22_YEAST	2	7,14	splP32570lMED22_YEAST	82	splP32570lMED22_YEAST	2	7,68
splP32569lMED17_YEAST	608	splP32569lMED17_YEAST	555	8,20	splP25648lSRB8_YEAST	888	splP25648lSRB8_YEAST	823	8,94
splP47822lMED21_YEAST	100	splP47822lMED21_YEAST	93	12,54	splP32570lMED22_YEAST	2	splP32569lMED17_YEAST	324	9,01
splP19263lMED14_YEAST	451	splP19263lMED14_YEAST	418	7,65	splP32569lMED17_YEAST	333	splP32570lMED22_YEAST	2	6,35
splP47822lMED21_YEAST	100	splP47822lMED21_YEAST	93	8,41	splP19263lMED14_YEAST	360	splQ12343lMED4_YEAST	2	7,75
splP19263lMED14_YEAST	417	splQ12343lMED4_YEAST	2	5,77	splP19263lMED14_YEAST	591	splP19263lMED14_YEAST	674	8,46
splP47822lMED21_YEAST	100	splP47822lMED21_YEAST	93	9,58	splP47822lMED21_YEAST	100	splP47822lMED21_YEAST	93	8,98
splQ12343lMED4_YEAST	64	splQ12343lMED4_YEAST	2	4,86	splP47822lMED21_YEAST	100	splP47822lMED21_YEAST	93	7,90
splP19263lMED14_YEAST	417	splQ12343lMED4_YEAST	2	9,91	splP47822lMED21_YEAST	100	splP47822lMED21_YEAST	93	7,33
splP19263lMED14_YEAST	436	splP19263lMED14_YEAST	418	6,21	splP19263lMED14_YEAST	697	splP19263lMED14_YEAST	663	9,98
splP32570lMED22_YEAST	9	splP32569lMED17_YEAST	333	7,88	splP38931lSSN2_YEAST	607	splP47822lMED21_YEAST	93	9,08
splP47822lMED21_YEAST	100	splP47822lMED21_YEAST	93	8,27	splP19263lMED14_YEAST	674	splP19263lMED14_YEAST	594	6,14
splP47822lMED21_YEAST	100	splP47822lMED21_YEAST	93	10,34	splP19263lMED14_YEAST	697	splP19263lMED14_YEAST	663	8,18
splP47822lMED21_YEAST	100	splP47822lMED21_YEAST	93	10,35	splP38931lSSN2_YEAST	457	splP38931lSSN2_YEAST	440	11,65
splP19263lMED14_YEAST	549	splP19263lMED14_YEAST	591	7,47	splP38931lSSN2_YEAST	1208	splP47821lSSN8_YEAST	23	7,45
splP47822lMED21_YEAST	100	splP47822lMED21_YEAST	93	13,86	splQ12343lMED4_YEAST	36	splQ12343lMED4_YEAST	2	12,31
splP38304lMED8_YEAST	191	splP32570lMED22_YEAST	2	8,70	splP19263lMED14_YEAST	549	splP19263lMED14_YEAST	610	9,59
splP47822lMED21_YEAST	100	splP47822lMED21_YEAST	93	10,71	splP39073lSSN3_YEAST	97	splP39073lSSN3_YEAST	319	6,93
splQ12343lMED4_YEAST	138	splQ12343lMED4_YEAST	147	10,57	splP32570lMED22_YEAST	2	splP32569lMED17_YEAST	324	9,31
splQ12343lMED4_YEAST	64	splQ12343lMED4_YEAST	2	4,82	splP33308lMED9_YEAST	78	splQ12343lMED4_YEAST	2	5,23
splP32570lMED22_YEAST	82	splP32570lMED22_YEAST	2	7,42	splP47822lMED21_YEAST	100	splP47822lMED21_YEAST	93	7,24
splQ12343lMED4_YEAST	55	splQ12343lMED4_YEAST	64	7,84	splP32569lMED17_YEAST	333	splP32570lMED22_YEAST	2	10,30

P1	R1	P2	R2	Score	P1	R1	P2	R2	Score
splQ12343IMED4_YEAST	36	splP33308IMED9_YEAST	117	12,16	splP39073ISSN3_YEAST	550	splP38931ISSN2_YEAST	919	8,31
splP25648ISRB8_YEAST	899	splP25648ISRB8_YEAST	901	13,36	splP32569IMED17_YEAST	333	splP32570IMED22_YEAST	2	14,12
splP32569IMED17_YEAST	333	splP32569IMED17_YEAST	324	8,79	splP19263IMED14_YEAST	609	splP19263IMED14_YEAST	591	11,14
splP19263IMED14_YEAST	417	splQ12343IMED4_YEAST	2	7,67	splP25648ISRB8_YEAST	88	splP47821ISSN8_YEAST	262	10,22
splP38782IMED6_YEAST	282	splP19263IMED14_YEAST	417	8,81	splP47822IMED21_YEAST	100	splP47822IMED21_YEAST	93	10,03
splQ12321IMED1_YEAST	389	splQ12343IMED4_YEAST	2	8,09	splP38931ISSN2_YEAST	233	splP38931ISSN2_YEAST	174	7,75
splP47822IMED21_YEAST	100	splP47822IMED21_YEAST	93	10,71	splP32570IMED22_YEAST	82	splP32570IMED22_YEAST	2	6,39
splP32569IMED17_YEAST	427	splP32569IMED17_YEAST	434	7,19	splP19263IMED14_YEAST	436	splP19263IMED14_YEAST	418	5,73
splP19263IMED14_YEAST	436	splQ12343IMED4_YEAST	2	5,82	splP39073ISSN3_YEAST	97	splP39073ISSN3_YEAST	319	6,71
splP47822IMED21_YEAST	100	splP47822IMED21_YEAST	93	12,51	splP25648ISRB8_YEAST	899	splP25648ISRB8_YEAST	901	9,78
splP19263IMED14_YEAST	594	splP19263IMED14_YEAST	610	5,68	splP38782IMED6_YEAST	282	splP19263IMED14_YEAST	417	10,59
splP38304IMED8_YEAST	191	splP32570IMED22_YEAST	2	9,79	splQ12343IMED4_YEAST	102	splQ12343IMED4_YEAST	2	7,86
splP47822IMED21_YEAST	100	splP47822IMED21_YEAST	93	8,65	splQ12343IMED4_YEAST	147	splQ12343IMED4_YEAST	162	2,57
splP38931ISSN2_YEAST	607	splP47822IMED21_YEAST	93	9,20	splP32570IMED22_YEAST	2	splP32569IMED17_YEAST	324	3,57
splP38931ISSN2_YEAST	796	splP38931ISSN2_YEAST	204	11,42	splP47822IMED21_YEAST	100	splP47822IMED21_YEAST	93	9,13
splP19263IMED14_YEAST	417	splQ12343IMED4_YEAST	2	8,30	splP38304IMED8_YEAST	191	splP32570IMED22_YEAST	2	9,11
splP32569IMED17_YEAST	333	splP32569IMED17_YEAST	324	12,52	splQ12343IMED4_YEAST	64	splQ12343IMED4_YEAST	2	4,88
splP39073ISSN3_YEAST	39	splP39073ISSN3_YEAST	43	12,04	splP47822IMED21_YEAST	100	splP47822IMED21_YEAST	93	9,82
splP25648ISRB8_YEAST	899	splP25648ISRB8_YEAST	901	14,01	splP32569IMED17_YEAST	333	splP32570IMED22_YEAST	2	8,02
splP39073ISSN3_YEAST	820	splP39073ISSN3_YEAST	782	13,85	splP47822IMED21_YEAST	100	splP47822IMED21_YEAST	93	11,11
splP47822IMED21_YEAST	100	splP47822IMED21_YEAST	93	9,72	splP39073ISSN3_YEAST	116	splP39073ISSN3_YEAST	189	5,04
splP32569IMED17_YEAST	319	splP32569IMED17_YEAST	427	7,52	splP47822IMED21_YEAST	100	splP47822IMED21_YEAST	93	11,67
splP39073ISSN3_YEAST	574	splP39073ISSN3_YEAST	580	11,20	splP19263IMED14_YEAST	549	splP19263IMED14_YEAST	610	4,32
splP19263IMED14_YEAST	678	splP19263IMED14_YEAST	667	5,66	splP25648ISRB8_YEAST	906	splP25648ISRB8_YEAST	954	8,65
splP38782IMED6_YEAST	282	splP19263IMED14_YEAST	417	7,83	splP47821ISSN8_YEAST	70	splP47821ISSN8_YEAST	23	9,06
splP25648ISRB8_YEAST	888	splP25648ISRB8_YEAST	823	7,60	splP47821ISSN8_YEAST	70	splP47821ISSN8_YEAST	23	9,29

P1	R1	P2	R2	Score	P1	R1	P2	R2	Score
sp|P32585|MED18_YEAST	68	sp|P32569|MED17_YEAST	589	9,19	sp|P19263|MED14_YEAST	678	sp|P19263|MED14_YEAST	667	6,88
sp|P39073|SSN3_YEAST	97	sp|P39073|SSN3_YEAST	319	6,81	sp|P47822|MED21_YEAST	100	sp|P47822|MED21_YEAST	93	6,49
sp|P32570|MED22_YEAST	9	sp|P32569|MED17_YEAST	333	7,96	sp|P39073|SSN3_YEAST	97	sp|P39073|SSN3_YEAST	319	7,25
sp|P19263|MED14_YEAST	697	sp|P19263|MED14_YEAST	663	7,46	sp|P25648|SRB8_YEAST	888	sp|P25648|SRB8_YEAST	823	10,38
sp|P25648|SRB8_YEAST	813	sp|P25648|SRB8_YEAST	820	10,56	sp|P32569|MED17_YEAST	333	sp|P32570|MED22_YEAST	2	7,41
sp|P19263|MED14_YEAST	549	sp|P19263|MED14_YEAST	591	10,24	sp|P19263|MED14_YEAST	549	sp|P19263|MED14_YEAST	591	7,48
sp|P19263|MED14_YEAST	549	sp|P19263|MED14_YEAST	610	9,37	sp|P47822|MED21_YEAST	100	sp|P47822|MED21_YEAST	93	11,25
sp|P47822|MED21_YEAST	75	sp|P38931|SSN2_YEAST	607	16,86	sp|P39073|SSN3_YEAST	550	sp|P47821|SSN8_YEAST	23	5,60
sp|P25648|SRB8_YEAST	888	sp|P25648|SRB8_YEAST	823	8,80	sp|P25648|SRB8_YEAST	888	sp|P25648|SRB8_YEAST	823	10,76
sp|P38782|MED6_YEAST	282	sp|P19263|MED14_YEAST	417	9,18	sp|P25648|SRB8_YEAST	888	sp|P25648|SRB8_YEAST	823	5,76
sp|P39073|SSN3_YEAST	820	sp|P39073|SSN3_YEAST	782	7,42	sp|P32569|MED17_YEAST	608	sp|P32569|MED17_YEAST	555	7,53
sp|P39073|SSN3_YEAST	820	sp|P39073|SSN3_YEAST	782	10,23	sp|P19263|MED14_YEAST	436	sp|Q12343|MED4_YEAST	2	4,90
sp|P39073|SSN3_YEAST	729	sp|P39073|SSN3_YEAST	782	10,89	sp|P19263|MED14_YEAST	360	sp|Q12343|MED4_YEAST	2	7,82
sp|P47822|MED21_YEAST	100	sp|P47822|MED21_YEAST	93	11,52	sp|P19263|MED14_YEAST	667	sp|P19263|MED14_YEAST	674	5,26
sp|Q99278|MED11_YEAST	68	sp|Q99278|MED11_YEAST	61	11,34	sp|P38304|MED8_YEAST	191	sp|P32570|MED22_YEAST	2	7,00
sp|P47822|MED21_YEAST	100	sp|P47822|MED21_YEAST	93	11,32	sp|P47822|MED21_YEAST	100	sp|P47822|MED21_YEAST	93	3,43
sp|P32569|MED17_YEAST	333	sp|P32569|MED17_YEAST	324	9,34	sp|P38782|MED6_YEAST	282	sp|P19263|MED14_YEAST	417	7,40
sp|P47822|MED21_YEAST	75	sp|P38931|SSN2_YEAST	607	18,30	sp|P47822|MED21_YEAST	100	sp|P47822|MED21_YEAST	93	10,10
sp|P19263|MED14_YEAST	697	sp|P19263|MED14_YEAST	663	4,33	sp|P19263|MED14_YEAST	418	sp|Q12343|MED4_YEAST	2	5,26
sp|P19263|MED14_YEAST	549	sp|P19263|MED14_YEAST	610	5,42	sp|P19263|MED14_YEAST	418	sp|Q12343|MED4_YEAST	2	6,93
sp|P38931|SSN2_YEAST	607	sp|P47822|MED21_YEAST	93	7,00	sp|P19263|MED14_YEAST	417	sp|Q12343|MED4_YEAST	2	11,60
sp|P39073|SSN3_YEAST	782	sp|P39073|SSN3_YEAST	777	5,83	sp|P25648|SRB8_YEAST	888	sp|P25648|SRB8_YEAST	823	4,68
sp|P38931|SSN2_YEAST	607	sp|P47822|MED21_YEAST	100	10,13	sp|P32569|MED17_YEAST	423	sp|P32569|MED17_YEAST	427	10,69
sp|Q99278|MED11_YEAST	68	sp|Q99278|MED11_YEAST	61	2,97	sp|P25648|SRB8_YEAST	899	sp|P25648|SRB8_YEAST	901	10,10
sp|P39073|SSN3_YEAST	820	sp|P39073|SSN3_YEAST	782	8,59	sp|P32585|MED18_YEAST	280	sp|P32569|MED17_YEAST	333	6,13
sp|P39073|SSN3_YEAST	820	sp|P39073|SSN3_YEAST	782	12,75	sp|P39073|SSN3_YEAST	574	sp|P39073|SSN3_YEAST	580	8,47

P1	R1	P2	R2	Score	P1	R1	P2	R2	Score
splP19263IMED14_YEAST	594	splP19263IMED14_YEAST	610	6,76	splP25648ISRB8_YEAST	88	splP47821ISSN8_YEAST	262	10,18
splP32569IMED17_YEAST	608	splP32569IMED17_YEAST	555	6,19	splP32569IMED17_YEAST	333	splP32569IMED17_YEAST	324	11,17
splP47821ISSN8_YEAST	262	splP25648ISRB8_YEAST	88	10,82	splP47822IMED21_YEAST	100	splP47822IMED21_YEAST	93	4,74
splP38304IMED8_YEAST	191	splP32570IMED22_YEAST	2	6,66	splP19263IMED14_YEAST	549	splP19263IMED14_YEAST	591	8,68
splP47822IMED21_YEAST	100	splP47822IMED21_YEAST	93	6,13	splP25648ISRB8_YEAST	899	splP25648ISRB8_YEAST	901	12,04
splP25648ISRB8_YEAST	888	splP25648ISRB8_YEAST	823	7,50	splP19263IMED14_YEAST	591	splP19263IMED14_YEAST	610	5,14
splQ99278IMED11_YEAST	53	splQ99278IMED11_YEAST	61	7,34	splP39073ISSN3_YEAST	574	splP39073ISSN3_YEAST	580	7,81
splP25648ISRB8_YEAST	899	splP25648ISRB8_YEAST	901	11,26	splP19263IMED14_YEAST	451	splP19263IMED14_YEAST	436	6,93
splP39073ISSN3_YEAST	574	splP39073ISSN3_YEAST	580	8,84	splQ12343IMED4_YEAST	36	splP33308IMED9_YEAST	117	9,83
splP38931ISSN2_YEAST	607	splP47822IMED21_YEAST	93	6,62	splP19263IMED14_YEAST	436	splP19263IMED14_YEAST	418	3,19
splP39073ISSN3_YEAST	574	splP39073ISSN3_YEAST	580	5,63	splP19263IMED14_YEAST	667	splP19263IMED14_YEAST	674	6,32
splP38782IMED6_YEAST	282	splP19263IMED14_YEAST	417	11,29	splP25648ISRB8_YEAST	888	splP25648ISRB8_YEAST	823	6,73
splP47822IMED21_YEAST	100	splP47822IMED21_YEAST	93	5,04	splP47822IMED21_YEAST	100	splP47822IMED21_YEAST	93	9,05
splP39073ISSN3_YEAST	39	splP39073ISSN3_YEAST	43	12,06	splP47822IMED21_YEAST	100	splP47822IMED21_YEAST	93	11,12
splP25648ISRB8_YEAST	888	splP25648ISRB8_YEAST	823	4,83	splP47822IMED21_YEAST	100	splP47822IMED21_YEAST	93	5,89
splP32569IMED17_YEAST	333	splP32570IMED22_YEAST	2	6,87	splP32569IMED17_YEAST	423	splP32569IMED17_YEAST	427	10,11
splQ12343IMED4_YEAST	36	splP33308IMED9_YEAST	117	8,91	splP19263IMED14_YEAST	436	splP19263IMED14_YEAST	418	6,42
splP47822IMED21_YEAST	100	splP47822IMED21_YEAST	93	10,09	splP38782IMED6_YEAST	282	splP19263IMED14_YEAST	417	13,62
splP38931ISSN2_YEAST	607	splP47822IMED21_YEAST	93	7,57	splP47822IMED21_YEAST	100	splP47822IMED21_YEAST	93	7,33
splP32569IMED17_YEAST	333	splP32570IMED22_YEAST	2	7,77	splP25648ISRB8_YEAST	899	splP25648ISRB8_YEAST	901	11,95
splP25648ISRB8_YEAST	665	splP25648ISRB8_YEAST	553	4,69	splP38304IMED8_YEAST	191	splP32570IMED22_YEAST	2	8,16
splP19263IMED14_YEAST	360	splQ12343IMED4_YEAST	2	6,18	splP32569IMED17_YEAST	247	splQ12343IMED4_YEAST	2	4,97
splP38304IMED8_YEAST	191	splP32570IMED22_YEAST	2	11,94	splP39073ISSN3_YEAST	574	splP39073ISSN3_YEAST	580	13,00
splP38931ISSN2_YEAST	555	splP38931ISSN2_YEAST	537	10,54	splP39073ISSN3_YEAST	804	splP39073ISSN3_YEAST	823	3,96
splP32569IMED17_YEAST	333	splP32569IMED17_YEAST	324	7,51	splP38931ISSN2_YEAST	233	splP38931ISSN2_YEAST	174	7,81
splP25648ISRB8_YEAST	88	splP47821ISSN8_YEAST	262	9,73	splP38931ISSN2_YEAST	1398	splP38931ISSN2_YEAST	1002	4,85

P1	R1	P2	R2	Score	P1	R1	P2	R2	Score
splP25648ISRB8_YEAST	88	splP47821ISSN8_YEAST	262	7,06	splQ12343IMED4_YEAST	102	splQ12343IMED4_YEAST	2	3,70
splP32570IMED22_YEAST	2	splP32569IMED17_YEAST	324	8,33	splQ12321IMED1_YEAST	389	splQ12343IMED4_YEAST	2	6,92
splP25648ISRB8_YEAST	888	splP25648ISRB8_YEAST	823	5,53	splP38304IMED8_YEAST	191	splP32570IMED22_YEAST	2	5,91
splP39073ISSN3_YEAST	782	splP39073ISSN3_YEAST	777	7,36	splP25648ISRB8_YEAST	899	splP25648ISRB8_YEAST	901	12,73
splP32569IMED17_YEAST	608	splP32569IMED17_YEAST	555	7,82	splQ12343IMED4_YEAST	228	splQ12343IMED4_YEAST	234	9,09
splP47822IMED21_YEAST	100	splP47822IMED21_YEAST	93	9,16	splP32569IMED17_YEAST	608	splP32569IMED17_YEAST	555	7,13
splQ12343IMED4_YEAST	102	splQ12343IMED4_YEAST	2	7,46	splP32569IMED17_YEAST	68	splP32569IMED17_YEAST	71	16,29
splP47822IMED21_YEAST	75	splP38931ISSN2_YEAST	607	14,50	splP19263IMED14_YEAST	697	splP19263IMED14_YEAST	663	12,35
splP47822IMED21_YEAST	100	splP47822IMED21_YEAST	93	7,17	splP38931ISSN2_YEAST	457	splP38931ISSN2_YEAST	440	11,91
splP25648ISRB8_YEAST	899	splP25648ISRB8_YEAST	901	17,16	splP32569IMED17_YEAST	333	splP32569IMED17_YEAST	324	5,77
splP32569IMED17_YEAST	333	splP32570IMED22_YEAST	2	5,33	splP47822IMED21_YEAST	100	splP47822IMED21_YEAST	93	7,82
splP32570IMED22_YEAST	9	splP32569IMED17_YEAST	333	4,78	splP25648ISRB8_YEAST	888	splP25648ISRB8_YEAST	823	6,86
splP25648ISRB8_YEAST	899	splP25648ISRB8_YEAST	901	11,84	splP38931ISSN2_YEAST	1024	splP39073ISSN3_YEAST	550	10,19
splP25648ISRB8_YEAST	899	splP25648ISRB8_YEAST	901	8,62	splP39073ISSN3_YEAST	116	splP39073ISSN3_YEAST	189	4,81
splQ12343IMED4_YEAST	55	splQ12343IMED4_YEAST	64	10,77	splP32569IMED17_YEAST	608	splP32569IMED17_YEAST	555	6,56
splP38782IMED6_YEAST	282	splP19263IMED14_YEAST	417	8,50	splP32585IMED18_YEAST	68	splP32569IMED17_YEAST	589	12,34
splP38931ISSN2_YEAST	607	splP47822IMED21_YEAST	93	6,75	splP19263IMED14_YEAST	417	splQ12343IMED4_YEAST	2	9,87
splQ12343IMED4_YEAST	55	splQ12343IMED4_YEAST	64	9,77	splP32569IMED17_YEAST	324	splP32570IMED22_YEAST	2	6,28
splP19263IMED14_YEAST	549	splP19263IMED14_YEAST	591	7,42	splP39073ISSN3_YEAST	116	splP39073ISSN3_YEAST	189	4,31
splP32569IMED17_YEAST	333	splP32569IMED17_YEAST	324	9,65	splP32585IMED18_YEAST	68	splP32569IMED17_YEAST	589	7,32
splP32585IMED18_YEAST	68	splP32569IMED17_YEAST	589	12,42	splP19263IMED14_YEAST	591	splP19263IMED14_YEAST	674	6,48
splP39073ISSN3_YEAST	887	splP39073ISSN3_YEAST	580	6,30	splQ12321IMED1_YEAST	389	splQ12343IMED4_YEAST	2	8,85
splQ99278IMED11_YEAST	68	splQ99278IMED11_YEAST	61	6,15	splP19263IMED14_YEAST	609	splP19263IMED14_YEAST	594	9,63
splP39073ISSN3_YEAST	574	splP39073ISSN3_YEAST	580	9,32	splP38931ISSN2_YEAST	537	splP38931ISSN2_YEAST	566	7,56
splQ99278IMED11_YEAST	53	splQ99278IMED11_YEAST	61	8,33	splP32569IMED17_YEAST	333	splP32570IMED22_YEAST	2	10,55
splP47822IMED21_YEAST	75	splP38931ISSN2_YEAST	607	16,87	splP38304IMED8_YEAST	191	splP32570IMED22_YEAST	2	9,29

P1	R1	P2	R2	Score	P1	R1	P2	R2	Score
splP19263IMED14_YEAST	549	splP19263IMED14_YEAST	591	11,91	splP25648ISRB8_YEAST	899	splP25648ISRB8_YEAST	901	11,56
splP19263IMED14_YEAST	436	splP19263IMED14_YEAST	418	5,23	splP32569IMED17_YEAST	333	splP32570IMED22_YEAST	2	11,64
splP25648ISRB8_YEAST	899	splP25648ISRB8_YEAST	901	11,60	splP25648ISRB8_YEAST	899	splP25648ISRB8_YEAST	901	12,45
splP38931ISSN2_YEAST	233	splP38931ISSN2_YEAST	174	4,49	splQ12343IMED4_YEAST	228	splQ12343IMED4_YEAST	234	8,23
splP47822IMED21_YEAST	75	splP38931ISSN2_YEAST	607	17,80	splP32570IMED22_YEAST	9	splP32569IMED17_YEAST	333	6,27
splP19263IMED14_YEAST	549	splP19263IMED14_YEAST	591	5,69	splQ12343IMED4_YEAST	55	splQ12343IMED4_YEAST	64	7,36
splP25648ISRB8_YEAST	888	splP25648ISRB8_YEAST	823	4,24	splQ99278IMED11_YEAST	68	splQ99278IMED11_YEAST	61	10,17
splP38931ISSN2_YEAST	457	splP38931ISSN2_YEAST	440	9,79	splP39073ISSN3_YEAST	804	splP39073ISSN3_YEAST	823	3,76
splP19263IMED14_YEAST	591	splP19263IMED14_YEAST	674	7,67	splP19263IMED14_YEAST	678	splP19263IMED14_YEAST	667	7,57
splP47821ISSN8_YEAST	262	splP25648ISRB8_YEAST	88	9,54	splP25648ISRB8_YEAST	899	splP25648ISRB8_YEAST	901	12,75
splP38931ISSN2_YEAST	233	splP38931ISSN2_YEAST	174	9,36	splP38782IMED6_YEAST	282	splP19263IMED14_YEAST	417	9,92
splP33308IMED9_YEAST	78	splQ12343IMED4_YEAST	2	5,35	splP25648ISRB8_YEAST	899	splP25648ISRB8_YEAST	901	7,56
splP25648ISRB8_YEAST	899	splP25648ISRB8_YEAST	901	17,44	splP38931ISSN2_YEAST	457	splP38931ISSN2_YEAST	440	10,86
splP32569IMED17_YEAST	589	splP32569IMED17_YEAST	601	5,47	splP32585IMED18_YEAST	280	splP32569IMED17_YEAST	333	5,25
splP39073ISSN3_YEAST	804	splP39073ISSN3_YEAST	823	1,72	splP32585IMED18_YEAST	280	splP32570IMED22_YEAST	2	7,86
splP32569IMED17_YEAST	333	splP32569IMED17_YEAST	324	10,27	splP32569IMED17_YEAST	608	splP32569IMED17_YEAST	555	9,07
splP25648ISRB8_YEAST	888	splP25648ISRB8_YEAST	823	7,35	splP38931ISSN2_YEAST	796	splP38931ISSN2_YEAST	204	8,82
splP32569IMED17_YEAST	68	splP32569IMED17_YEAST	71	9,33	splP19263IMED14_YEAST	549	splP19263IMED14_YEAST	591	10,25
splP39073ISSN3_YEAST	116	splP39073ISSN3_YEAST	189	6,06	splP32569IMED17_YEAST	333	splP32570IMED22_YEAST	2	15,32
splP19263IMED14_YEAST	697	splP19263IMED14_YEAST	663	5,15	splP39073ISSN3_YEAST	574	splP39073ISSN3_YEAST	580	8,27
splP25648ISRB8_YEAST	899	splP25648ISRB8_YEAST	901	12,00	splP19263IMED14_YEAST	549	splP19263IMED14_YEAST	591	9,14
splP25648ISRB8_YEAST	88	splP47821ISSN8_YEAST	262	10,10	splP39073ISSN3_YEAST	39	splP39073ISSN3_YEAST	43	7,13
splP47822IMED21_YEAST	100	splP47822IMED21_YEAST	93	10,14	splP32570IMED22_YEAST	95	splP32569IMED17_YEAST	319	9,75
splP25648ISRB8_YEAST	906	splP25648ISRB8_YEAST	954	3,44	splP32570IMED22_YEAST	82	splP32570IMED22_YEAST	2	7,78
splP25648ISRB8_YEAST	665	splP25648ISRB8_YEAST	553	4,63	splP25648ISRB8_YEAST	888	splP25648ISRB8_YEAST	823	6,84
splP19263IMED14_YEAST	678	splP19263IMED14_YEAST	667	6,72	splP32570IMED22_YEAST	2	splP32569IMED17_YEAST	324	7,91

P1	R1	P2	R2	Score	P1	R1	P2	R2	Score
splP32569IMED17_YEAST	333	splP32569IMED17_YEAST	324	12,60	splP39073ISSN3_YEAST	550	splP39073ISSN3_YEAST	580	7,84
splP39073ISSN3_YEAST	216	splP39073ISSN3_YEAST	151	6,30	splP39073ISSN3_YEAST	39	splP39073ISSN3_YEAST	43	16,36
splP25648ISRB8_YEAST	888	splP25648ISRB8_YEAST	823	6,24	splP32569IMED17_YEAST	333	splP32570IMED22_YEAST	2	8,66
splP32569IMED17_YEAST	608	splP32569IMED17_YEAST	555	7,62	splP19263IMED14_YEAST	549	splP19263IMED14_YEAST	567	8,16
splP47822IMED21_YEAST	100	splP47822IMED21_YEAST	93	6,50	splP47822IMED21_YEAST	100	splP47822IMED21_YEAST	93	8,34
splP47822IMED21_YEAST	100	splP47822IMED21_YEAST	93	8,16	splP38931ISSN2_YEAST	1398	splP38931ISSN2_YEAST	1002	2,57
splP47822IMED21_YEAST	100	splP47822IMED21_YEAST	93	8,29	splP39073ISSN3_YEAST	782	splP39073ISSN3_YEAST	777	7,23
splP32569IMED17_YEAST	608	splP32569IMED17_YEAST	555	6,46	splP32570IMED22_YEAST	82	splP32570IMED22_YEAST	2	7,60
splP38304IMED8_YEAST	191	splP32585IMED18_YEAST	279	8,03	splP32570IMED22_YEAST	82	splP32570IMED22_YEAST	2	7,45
splP32569IMED17_YEAST	589	splP32569IMED17_YEAST	601	6,57	splP32570IMED22_YEAST	2	splP32569IMED17_YEAST	324	12,37
splP25648ISRB8_YEAST	145	splP25648ISRB8_YEAST	168	3,30	splP47822IMED21_YEAST	45	splP25046IMED19_YEAST	56	3,58
splQ99278IMED11_YEAST	113	splP32569IMED17_YEAST	499	3,91	splP32570IMED22_YEAST	82	splP32570IMED22_YEAST	2	7,50
splP32570IMED22_YEAST	82	splP32570IMED22_YEAST	2	5,03	splP38304IMED8_YEAST	191	splP32570IMED22_YEAST	2	10,73
splP39073ISSN3_YEAST	574	splP39073ISSN3_YEAST	580	4,91	splP19263IMED14_YEAST	549	splP19263IMED14_YEAST	594	5,04
splP38931ISSN2_YEAST	1398	splP38931ISSN2_YEAST	1002	1,98	splP47822IMED21_YEAST	100	splP47822IMED21_YEAST	93	10,53
splP39073ISSN3_YEAST	550	splP47821ISSN8_YEAST	23	5,60	splP34162IMED20_YEAST	21	splP19263IMED14_YEAST	591	7,05
splP25648ISRB8_YEAST	665	splP19263IMED14_YEAST	35	3,12	splP39073ISSN3_YEAST	39	splP39073ISSN3_YEAST	43	10,27
splP47821ISSN8_YEAST	262	splP25648ISRB8_YEAST	88	11,72	splP32570IMED22_YEAST	9	splP32569IMED17_YEAST	333	9,29
splQ12343IMED4_YEAST	228	splQ12343IMED4_YEAST	234	6,11	splP25648ISRB8_YEAST	665	splP19263IMED14_YEAST	35	4,90
splP38931ISSN2_YEAST	1024	splP39073ISSN3_YEAST	550	10,79	splP32569IMED17_YEAST	333	splP32569IMED17_YEAST	324	9,92
splP32569IMED17_YEAST	589	splP32569IMED17_YEAST	601	3,08	splP32569IMED17_YEAST	333	splP32570IMED22_YEAST	2	4,75
splP32569IMED17_YEAST	608	splP32569IMED17_YEAST	555	6,26	splP47822IMED21_YEAST	100	splP47822IMED21_YEAST	93	6,62
splP32569IMED17_YEAST	333	splP32570IMED22_YEAST	2	3,92	splP32585IMED18_YEAST	280	splP32569IMED17_YEAST	333	7,06
splP19263IMED14_YEAST	50	splP19263IMED14_YEAST	35	9,08	splP47822IMED21_YEAST	100	splP47822IMED21_YEAST	93	3,62
splQ12343IMED4_YEAST	64	splQ12343IMED4_YEAST	2	2,96	splP32569IMED17_YEAST	333	splP32570IMED22_YEAST	2	9,94
splP32569IMED17_YEAST	427	splP32569IMED17_YEAST	434	2,96	splP32569IMED17_YEAST	608	splP32569IMED17_YEAST	555	6,85

P1	R1	P2	R2	Score	P1	R1	P2	R2	Score
splP39073ISSN3_YEAST	550	splP38931ISSN2_YEAST	919	4,36	splP38931ISSN2_YEAST	573	splP38931ISSN2_YEAST	566	3,07
splP32569IMED17_YEAST	122	splP19263IMED14_YEAST	282	8,53	splP25648ISRB8_YEAST	899	splP25648ISRB8_YEAST	901	14,57
splP19263IMED14_YEAST	697	splP19263IMED14_YEAST	663	2,79	splP25648ISRB8_YEAST	951	splP25648ISRB8_YEAST	959	7,81
splP19263IMED14_YEAST	549	splP19263IMED14_YEAST	567	2,22	splP32569IMED17_YEAST	608	splP32569IMED17_YEAST	555	10,11
splP32570IMED22_YEAST	95	splP32569IMED17_YEAST	601	4,80	splP32569IMED17_YEAST	324	splP32570IMED22_YEAST	2	11,56
splP25046IMED19_YEAST	74	splP25648ISRB8_YEAST	616	9,16	splP19263IMED14_YEAST	678	splP19263IMED14_YEAST	667	5,89
splP19263IMED14_YEAST	594	splP19263IMED14_YEAST	610	4,33	splP25648ISRB8_YEAST	888	splP25648ISRB8_YEAST	899	5,15
splP39073ISSN3_YEAST	530	splP39073ISSN3_YEAST	550	9,62	splP39073ISSN3_YEAST	97	splP39073ISSN3_YEAST	319	8,51
splP47822IMED21_YEAST	100	splP47822IMED21_YEAST	93	5,00	splP32585IMED18_YEAST	280	splP32570IMED22_YEAST	2	7,12
splP39073ISSN3_YEAST	216	splP39073ISSN3_YEAST	151	3,62	splP38931ISSN2_YEAST	555	splP38931ISSN2_YEAST	537	9,80
splP32569IMED17_YEAST	122	splP19263IMED14_YEAST	282	7,91	splP39073ISSN3_YEAST	574	splP39073ISSN3_YEAST	550	9,29
splP32569IMED17_YEAST	75	splP32569IMED17_YEAST	81	2,72	splP39073ISSN3_YEAST	216	splP39073ISSN3_YEAST	151	5,83
splP32569IMED17_YEAST	333	splP32570IMED22_YEAST	2	6,11	splP39073ISSN3_YEAST	820	splP39073ISSN3_YEAST	782	6,88
splP32569IMED17_YEAST	78	splP32569IMED17_YEAST	71	1,66	splP25648ISRB8_YEAST	888	splP25648ISRB8_YEAST	823	10,95
splP39073ISSN3_YEAST	574	splP39073ISSN3_YEAST	580	3,12	splP39073ISSN3_YEAST	574	splP39073ISSN3_YEAST	550	7,67
splP32569IMED17_YEAST	324	splP32569IMED17_YEAST	333	3,82	splP39073ISSN3_YEAST	574	splP39073ISSN3_YEAST	580	5,05
splQ08278IMED7_YEAST	30	splQ08278IMED7_YEAST	37	3,87	splP38931ISSN2_YEAST	607	splP47822IMED21_YEAST	93	7,39
splQ08278IMED7_YEAST	30	splQ08278IMED7_YEAST	37	4,53	splP25648ISRB8_YEAST	888	splP25648ISRB8_YEAST	823	6,65
splQ08278IMED7_YEAST	30	splQ08278IMED7_YEAST	37	4,06	splP19263IMED14_YEAST	549	splP19263IMED14_YEAST	591	7,90
splP25648ISRB8_YEAST	1324	splP25648ISRB8_YEAST	1220	4,34	splP19263IMED14_YEAST	609	splP19263IMED14_YEAST	594	9,71
splP32569IMED17_YEAST	589	splP32569IMED17_YEAST	601	3,61	splP39073ISSN3_YEAST	782	splP39073ISSN3_YEAST	777	6,28
splP47822IMED21_YEAST	100	splP47822IMED21_YEAST	93	5,82	splP38304IMED8_YEAST	191	splP32570IMED22_YEAST	2	9,24
splP25648ISRB8_YEAST	145	splP25648ISRB8_YEAST	168	2,68	splP47822IMED21_YEAST	100	splP47822IMED21_YEAST	93	12,04
splP38304IMED8_YEAST	210	splP32585IMED18_YEAST	97	15,62	splP25648ISRB8_YEAST	88	splP47821ISSN8_YEAST	262	12,19
splP25648ISRB8_YEAST	899	splP25648ISRB8_YEAST	901	11,37	splP19263IMED14_YEAST	591	splP19263IMED14_YEAST	674	3,62
splQ08278IMED7_YEAST	30	splQ08278IMED7_YEAST	37	5,86	splP39073ISSN3_YEAST	39	splP39073ISSN3_YEAST	43	10,07

P1	R1	P2	R2	Score	P1	R1	P2	R2	Score
splP32570IMED22_YEAST	82	splP32570IMED22_YEAST	2	3,03	splP32570IMED22_YEAST	82	splP32569IMED17_YEAST	333	6,00
splP38304IMED8_YEAST	191	splP32570IMED22_YEAST	2	4,37	splP25648ISRB8_YEAST	899	splP25648ISRB8_YEAST	901	9,49
splP38304IMED8_YEAST	191	splP32570IMED22_YEAST	2	4,40	splQ99278IMED11_YEAST	68	splQ99278IMED11_YEAST	61	8,07
splP19263IMED14_YEAST	549	splP19263IMED14_YEAST	591	6,48	splP32569IMED17_YEAST	333	splP32570IMED22_YEAST	2	7,24
splQ08278IMED7_YEAST	202	splQ12343IMED4_YEAST	110	1,85	splP38304IMED8_YEAST	191	splP32570IMED22_YEAST	2	7,75
splP32569IMED17_YEAST	78	splP32569IMED17_YEAST	71	3,63	splQ12343IMED4_YEAST	55	splQ12343IMED4_YEAST	64	8,91
splP19263IMED14_YEAST	678	splP19263IMED14_YEAST	667	5,90	splP32569IMED17_YEAST	423	splP32569IMED17_YEAST	427	11,62
splP32569IMED17_YEAST	333	splP32570IMED22_YEAST	2	2,45	splP32585IMED18_YEAST	280	splP32569IMED17_YEAST	333	6,10
splP47822IMED21_YEAST	100	splP47822IMED21_YEAST	93	3,07	splP47822IMED21_YEAST	75	splP47822IMED21_YEAST	93	5,43
splP19263IMED14_YEAST	549	splP19263IMED14_YEAST	567	2,37	splP38931ISSN2_YEAST	1208	splP47821ISSN8_YEAST	23	7,31
splP47822IMED21_YEAST	100	splP47822IMED21_YEAST	93	5,85	splP19263IMED14_YEAST	549	splP19263IMED14_YEAST	610	3,35
splP47822IMED21_YEAST	100	splP47822IMED21_YEAST	93	3,41	splP19263IMED14_YEAST	674	splP19263IMED14_YEAST	594	4,94
splP38304IMED8_YEAST	191	splP32585IMED18_YEAST	279	3,50	splP39073ISSN3_YEAST	39	splP39073ISSN3_YEAST	43	15,65
splP25046IMED19_YEAST	74	splP25648ISRB8_YEAST	616	7,12	splP38304IMED8_YEAST	191	splP32570IMED22_YEAST	2	5,07
splP47822IMED21_YEAST	100	splP47822IMED21_YEAST	93	4,42	splP39073ISSN3_YEAST	782	splP39073ISSN3_YEAST	777	6,62
splP32569IMED17_YEAST	349	splP32585IMED18_YEAST	225	8,08	splQ12343IMED4_YEAST	159	splQ12343IMED4_YEAST	165	8,11
splP38304IMED8_YEAST	210	splP38304IMED8_YEAST	194	2,69	splQ12343IMED4_YEAST	36	splP33308IMED9_YEAST	117	10,50
splQ08278IMED7_YEAST	30	splQ08278IMED7_YEAST	37	5,66	splP32570IMED22_YEAST	82	splP32569IMED17_YEAST	333	5,61
splP32569IMED17_YEAST	122	splP19263IMED14_YEAST	282	7,39	splP39073ISSN3_YEAST	39	splP39073ISSN3_YEAST	43	8,44
splP39073ISSN3_YEAST	550	splP47821ISSN8_YEAST	23	6,04	splP25648ISRB8_YEAST	899	splP25648ISRB8_YEAST	901	10,20
splP38304IMED8_YEAST	210	splP38304IMED8_YEAST	194	1,97	splP25648ISRB8_YEAST	888	splP25648ISRB8_YEAST	823	6,93
splQ08278IMED7_YEAST	30	splQ08278IMED7_YEAST	37	4,08	splP32569IMED17_YEAST	78	splP32569IMED17_YEAST	71	3,65
splP47822IMED21_YEAST	100	splP47822IMED21_YEAST	93	2,56	splP25648ISRB8_YEAST	665	splP25648ISRB8_YEAST	553	3,02
splP32569IMED17_YEAST	608	splP32569IMED17_YEAST	555	3,14	splP32569IMED17_YEAST	333	splP32570IMED22_YEAST	2	6,89
splP38931ISSN2_YEAST	1398	splP38931ISSN2_YEAST	1002	3,46	splP47822IMED21_YEAST	100	splP47822IMED21_YEAST	93	7,76
splP47821ISSN8_YEAST	70	splP47821ISSN8_YEAST	23	2,08	splQ08278IMED7_YEAST	30	splQ08278IMED7_YEAST	37	6,15

P1	R1	P2	R2	Score	P1	R1	P2	R2	Score
splP19263IMED14_YEAST	417	splQ12343IMED4_YEAST	2	4,70	splP38931ISSN2_YEAST	1208	splP47821ISSN8_YEAST	23	6,42
splQ08278IMED7_YEAST	30	splQ08278IMED7_YEAST	37	4,08	splP47821ISSN8_YEAST	70	splP47821ISSN8_YEAST	23	10,40
splP38931ISSN2_YEAST	573	splP38931ISSN2_YEAST	566	2,35	splP19263IMED14_YEAST	591	splP19263IMED14_YEAST	674	5,31
splQ08278IMED7_YEAST	30	splQ08278IMED7_YEAST	37	5,43	splP25648ISRB8_YEAST	888	splP25648ISRB8_YEAST	823	2,83
splP19263IMED14_YEAST	549	splP19263IMED14_YEAST	591	4,11	splP19263IMED14_YEAST	609	splP19263IMED14_YEAST	594	10,34
splQ08278IMED7_YEAST	30	splQ08278IMED7_YEAST	37	4,91	splP19263IMED14_YEAST	594	splP19263IMED14_YEAST	610	6,98
splP38931ISSN2_YEAST	573	splP38931ISSN2_YEAST	566	2,19	splP19263IMED14_YEAST	549	splP19263IMED14_YEAST	591	11,27
splP47821ISSN8_YEAST	23	splP34162IMED20_YEAST	180	6,30	splP25648ISRB8_YEAST	888	splP25648ISRB8_YEAST	823	5,15
splQ08278IMED7_YEAST	30	splQ08278IMED7_YEAST	37	3,70	splQ12343IMED4_YEAST	55	splQ12343IMED4_YEAST	64	6,89
splP25046IMED19_YEAST	74	splP25648ISRB8_YEAST	616	8,54	splP19263IMED14_YEAST	417	splQ12343IMED4_YEAST	2	8,33
splP25648ISRB8_YEAST	899	splP25648ISRB8_YEAST	901	9,56	splP25046IMED19_YEAST	74	splP25648ISRB8_YEAST	616	6,62
splP39073ISSN3_YEAST	782	splP39073ISSN3_YEAST	777	1,69	splP32569IMED17_YEAST	333	splP32570IMED22_YEAST	2	4,86
splP32569IMED17_YEAST	333	splP32570IMED22_YEAST	2	2,92	splP32585IMED18_YEAST	83	splP32585IMED18_YEAST	91	13,25
splP19263IMED14_YEAST	609	splP19263IMED14_YEAST	594	9,14	splP19263IMED14_YEAST	549	splP19263IMED14_YEAST	567	7,15
splQ08278IMED7_YEAST	202	splP39073ISSN3_YEAST	580	1,58	splP32570IMED22_YEAST	9	splP32569IMED17_YEAST	333	4,84
splQ08278IMED7_YEAST	30	splQ08278IMED7_YEAST	37	6,13	splP47822IMED21_YEAST	100	splP47822IMED21_YEAST	93	2,60
splP47822IMED21_YEAST	100	splP47822IMED21_YEAST	93	4,81	splP33308IMED9_YEAST	78	splQ12343IMED4_YEAST	64	7,92
splP19263IMED14_YEAST	609	splP19263IMED14_YEAST	594	6,99	splP19263IMED14_YEAST	678	splP19263IMED14_YEAST	594	2,82
splP47821ISSN8_YEAST	70	splP47821ISSN8_YEAST	23	2,73	splQ12343IMED4_YEAST	36	splP33308IMED9_YEAST	117	5,84
splP19263IMED14_YEAST	549	splP19263IMED14_YEAST	591	2,14	splP32570IMED22_YEAST	9	splP32569IMED17_YEAST	333	7,71
splP38304IMED8_YEAST	210	splP38304IMED8_YEAST	194	2,86	splP25648ISRB8_YEAST	888	splP25648ISRB8_YEAST	823	7,59
splQ12321IMED1_YEAST	389	splQ12343IMED4_YEAST	2	5,06	splP47822IMED21_YEAST	100	splP47822IMED21_YEAST	93	7,88
splP19263IMED14_YEAST	609	splP19263IMED14_YEAST	594	5,83	splP25648ISRB8_YEAST	888	splP25648ISRB8_YEAST	823	6,96
splP32570IMED22_YEAST	82	splP32569IMED17_YEAST	333	5,94	splP33308IMED9_YEAST	78	splQ12343IMED4_YEAST	2	5,38
splP25648ISRB8_YEAST	899	splP25648ISRB8_YEAST	901	5,90	splP39073ISSN3_YEAST	804	splP39073ISSN3_YEAST	823	3,63
splP32569IMED17_YEAST	349	splP32585IMED18_YEAST	225	5,07	splP19263IMED14_YEAST	678	splP19263IMED14_YEAST	667	6,53

P1	R1	P2	R2	Score	P1	R1	P2	R2	Score
splP19263IMED14_YEAST	609	splP19263IMED14_YEAST	594	6,14	splP39073ISSN3_YEAST	574	splP39073ISSN3_YEAST	550	11,66
splP32569IMED17_YEAST	78	splP32569IMED17_YEAST	71	2,21	splP32570IMED22_YEAST	95	splP32569IMED17_YEAST	601	4,86
splP39073ISSN3_YEAST	550	splP47821ISSN8_YEAST	23	2,71	splP39073ISSN3_YEAST	97	splP39073ISSN3_YEAST	319	8,18
splP19263IMED14_YEAST	549	splP19263IMED14_YEAST	609	3,89	splP39073ISSN3_YEAST	39	splP39073ISSN3_YEAST	43	15,78
splQ12343IMED4_YEAST	228	splQ12343IMED4_YEAST	234	5,00	splP25648ISRB8_YEAST	888	splP25648ISRB8_YEAST	823	6,30
splP32569IMED17_YEAST	608	splP32569IMED17_YEAST	555	5,17	splP32569IMED17_YEAST	589	splP32569IMED17_YEAST	601	4,67
splP38931ISSN2_YEAST	1024	splP39073ISSN3_YEAST	574	3,13	splP32569IMED17_YEAST	608	splP32569IMED17_YEAST	555	6,71
splP39073ISSN3_YEAST	216	splP39073ISSN3_YEAST	151	1,97	splP38931ISSN2_YEAST	573	splP38931ISSN2_YEAST	555	9,04
splP32570IMED22_YEAST	82	splP32569IMED17_YEAST	324	3,15	splQ12343IMED4_YEAST	36	splQ12343IMED4_YEAST	2	8,80
splQ08278IMED7_YEAST	30	splQ08278IMED7_YEAST	37	5,53	splP32570IMED22_YEAST	82	splP32569IMED17_YEAST	333	4,15
splP19263IMED14_YEAST	609	splP19263IMED14_YEAST	591	3,02	splP32570IMED22_YEAST	2	splP32569IMED17_YEAST	324	12,30
splP19263IMED14_YEAST	609	splP19263IMED14_YEAST	594	6,16	splP47822IMED21_YEAST	100	splP47822IMED21_YEAST	93	8,65
splP38931ISSN2_YEAST	1398	splP38931ISSN2_YEAST	1002	2,03	splP32569IMED17_YEAST	608	splP32569IMED17_YEAST	555	8,56
splP39073ISSN3_YEAST	550	splP47821ISSN8_YEAST	23	2,55	splP39073ISSN3_YEAST	574	splP39073ISSN3_YEAST	580	6,95
splP38931ISSN2_YEAST	573	splP38931ISSN2_YEAST	566	3,90	splQ12343IMED4_YEAST	147	splQ12343IMED4_YEAST	162	2,78
splP32569IMED17_YEAST	349	splP32585IMED18_YEAST	225	6,75	splP39073ISSN3_YEAST	550	splP47821ISSN8_YEAST	23	7,93
splQ12343IMED4_YEAST	228	splQ12343IMED4_YEAST	234	6,58	splP47822IMED21_YEAST	100	splP47822IMED21_YEAST	93	6,41
splP39073ISSN3_YEAST	782	splP38304IMED8_YEAST	191	1,31	splP19263IMED14_YEAST	591	splP19263IMED14_YEAST	674	8,13
splP38931ISSN2_YEAST	1398	splP38931ISSN2_YEAST	1002	2,47	splP38931ISSN2_YEAST	607	splP47822IMED21_YEAST	93	7,81
splP39073ISSN3_YEAST	804	splP39073ISSN3_YEAST	823	1,70	splP38782IMED6_YEAST	282	splP19263IMED14_YEAST	417	8,04
splP32570IMED22_YEAST	82	splP32569IMED17_YEAST	333	4,76	splP32569IMED17_YEAST	608	splP32569IMED17_YEAST	555	6,84
splP38931ISSN2_YEAST	573	splP38931ISSN2_YEAST	566	2,43	splP39073ISSN3_YEAST	550	splP38931ISSN2_YEAST	919	4,70
splP38931ISSN2_YEAST	1398	splP38931ISSN2_YEAST	1002	3,09	splP32569IMED17_YEAST	333	splP32570IMED22_YEAST	2	12,05
splP19263IMED14_YEAST	609	splP19263IMED14_YEAST	594	6,61	splP32569IMED17_YEAST	608	splP32569IMED17_YEAST	555	10,98
splQ08278IMED7_YEAST	30	splQ08278IMED7_YEAST	37	6,39	splP19263IMED14_YEAST	609	splP19263IMED14_YEAST	591	7,52
splP32585IMED18_YEAST	83	splP32585IMED18_YEAST	91	3,58	splP32570IMED22_YEAST	82	splP32569IMED17_YEAST	324	3,93

P1	R1	P2	R2	Score	P1	R1	P2	R2	Score
splQ08278IMED7_YEAST	30	splQ08278IMED7_YEAST	37	4,90	splP39073ISSN3_YEAST	550	splP47821ISSN8_YEAST	23	7,49
splQ08278IMED7_YEAST	30	splQ08278IMED7_YEAST	37	2,60	splP19263IMED14_YEAST	609	splP19263IMED14_YEAST	594	11,05
splP39073ISSN3_YEAST	550	splP47821ISSN8_YEAST	23	3,28	splQ08278IMED7_YEAST	30	splQ08278IMED7_YEAST	37	5,68
splP38304IMED8_YEAST	191	splP32570IMED22_YEAST	2	5,04	splQ12343IMED4_YEAST	159	splQ12343IMED4_YEAST	165	11,32
splP47821ISSN8_YEAST	23	splP34162IMED20_YEAST	180	6,84	splP25648ISRB8_YEAST	888	splP25648ISRB8_YEAST	823	7,93
splP39073ISSN3_YEAST	216	splP39073ISSN3_YEAST	151	4,46	splP19263IMED14_YEAST	591	splP19263IMED14_YEAST	674	7,80
splQ08278IMED7_YEAST	30	splQ08278IMED7_YEAST	37	6,67	splP32570IMED22_YEAST	9	splP32569IMED17_YEAST	333	7,32
splP38931ISSN2_YEAST	1069	splP38931ISSN2_YEAST	920	3,55	splP19263IMED14_YEAST	591	splP19263IMED14_YEAST	674	6,51
splP32570IMED22_YEAST	9	splP32569IMED17_YEAST	333	3,19	splP25648ISRB8_YEAST	888	splP25648ISRB8_YEAST	823	10,02
splP19263IMED14_YEAST	609	splP19263IMED14_YEAST	594	9,30	splP39073ISSN3_YEAST	530	splP39073ISSN3_YEAST	550	8,30
splP38931ISSN2_YEAST	555	splP38931ISSN2_YEAST	537	3,31	splP47822IMED21_YEAST	100	splP47822IMED21_YEAST	93	11,18
splP38931ISSN2_YEAST	573	splP38931ISSN2_YEAST	566	1,67	splP39073ISSN3_YEAST	804	splP39073ISSN3_YEAST	823	3,44
splP25648ISRB8_YEAST	1324	splP25648ISRB8_YEAST	1220	3,91	splP32569IMED17_YEAST	122	splP19263IMED14_YEAST	282	8,11
splP19263IMED14_YEAST	549	splP19263IMED14_YEAST	591	7,64	splP32569IMED17_YEAST	333	splP32570IMED22_YEAST	2	4,13
splQ12343IMED4_YEAST	228	splQ12343IMED4_YEAST	234	8,21	splP39073ISSN3_YEAST	39	splP39073ISSN3_YEAST	43	10,32
splP47822IMED21_YEAST	100	splP47822IMED21_YEAST	93	6,73	splP25648ISRB8_YEAST	888	splP25648ISRB8_YEAST	823	7,66
splP32569IMED17_YEAST	349	splP32585IMED18_YEAST	225	6,14	splP39073ISSN3_YEAST	39	splP39073ISSN3_YEAST	43	11,98
splP39073ISSN3_YEAST	804	splP39073ISSN3_YEAST	823	1,40	splP19263IMED14_YEAST	678	splP19263IMED14_YEAST	667	4,53
splP32569IMED17_YEAST	608	splP32569IMED17_YEAST	555	5,31	splP19263IMED14_YEAST	549	splP19263IMED14_YEAST	591	8,04
splP39073ISSN3_YEAST	782	splP38304IMED8_YEAST	191	2,63	splP32569IMED17_YEAST	608	splP32569IMED17_YEAST	555	6,78
splP47821ISSN8_YEAST	23	splP34162IMED20_YEAST	180	4,93	splP19263IMED14_YEAST	697	splP19263IMED14_YEAST	663	5,50
splP32570IMED22_YEAST	82	splP32569IMED17_YEAST	333	4,85	splP47822IMED21_YEAST	100	splP47822IMED21_YEAST	93	8,84
splP47821ISSN8_YEAST	70	splP47821ISSN8_YEAST	23	2,18	splP38931ISSN2_YEAST	1208	splP47821ISSN8_YEAST	23	8,17
splP32569IMED17_YEAST	333	splP32570IMED22_YEAST	2	4,73	splP25648ISRB8_YEAST	145	splP25648ISRB8_YEAST	168	3,62
splP19263IMED14_YEAST	609	splP19263IMED14_YEAST	591	4,37	splQ08278IMED7_YEAST	30	splQ08278IMED7_YEAST	37	6,03
splP38304IMED8_YEAST	210	splP38304IMED8_YEAST	194	2,23	splQ12343IMED4_YEAST	64	splQ12343IMED4_YEAST	2	4,91

P1	R1	P2	R2	Score	P1	R1	P2	R2	Score
splP39073ISSN3_YEAST	39	splP39073ISSN3_YEAST	43	3,84	splP47822IMED21_YEAST	75	splP38931ISSN2_YEAST	607	17,27
splP32569IMED17_YEAST	333	splP32569IMED17_YEAST	324	6,02	splP32585IMED18_YEAST	68	splP32569IMED17_YEAST	589	9,07
splP32570IMED22_YEAST	95	splP32569IMED17_YEAST	319	3,98	splP47822IMED21_YEAST	100	splP47822IMED21_YEAST	93	11,46
splP39073ISSN3_YEAST	550	splP47821ISSN8_YEAST	23	2,14	splQ99278IMED11_YEAST	53	splQ99278IMED11_YEAST	61	7,29
splP32570IMED22_YEAST	82	splP32569IMED17_YEAST	333	3,94	splP38931ISSN2_YEAST	607	splP47822IMED21_YEAST	93	10,36
splP38931ISSN2_YEAST	1398	splP38931ISSN2_YEAST	1002	1,57	splP32569IMED17_YEAST	427	splP32569IMED17_YEAST	434	4,44
splP47822IMED21_YEAST	45	splP25046IMED19_YEAST	56	3,81	splQ99278IMED11_YEAST	68	splQ99278IMED11_YEAST	61	8,90
splQ08278IMED7_YEAST	30	splQ08278IMED7_YEAST	37	4,21	splP39073ISSN3_YEAST	39	splP39073ISSN3_YEAST	43	8,94
splP38304IMED8_YEAST	191	splP32585IMED18_YEAST	279	3,73	splP19263IMED14_YEAST	451	splP19263IMED14_YEAST	436	6,69
splP38931ISSN2_YEAST	573	splP38931ISSN2_YEAST	566	1,15	splP19263IMED14_YEAST	609	splP19263IMED14_YEAST	594	10,29
splP39073ISSN3_YEAST	550	splP47821ISSN8_YEAST	23	1,23	splQ12343IMED4_YEAST	36	splP33308IMED9_YEAST	117	7,39
splP32570IMED22_YEAST	95	splP32569IMED17_YEAST	319	5,97	splP38931ISSN2_YEAST	233	splP38931ISSN2_YEAST	174	6,62
splP32570IMED22_YEAST	95	splP32569IMED17_YEAST	601	5,07	splP38931ISSN2_YEAST	607	splP47822IMED21_YEAST	93	6,92
splP25648ISRB8_YEAST	906	splP25648ISRB8_YEAST	954	4,46	splP39073ISSN3_YEAST	574	splP39073ISSN3_YEAST	580	6,40
splQ08278IMED7_YEAST	30	splQ08278IMED7_YEAST	37	4,12	splP19263IMED14_YEAST	451	splP19263IMED14_YEAST	436	6,55
splP47822IMED21_YEAST	45	splP25046IMED19_YEAST	56	3,71	splP39073ISSN3_YEAST	97	splP39073ISSN3_YEAST	319	8,98
splP19263IMED14_YEAST	674	splP19263IMED14_YEAST	594	3,46	splP32569IMED17_YEAST	608	splP32569IMED17_YEAST	555	8,37
splP32569IMED17_YEAST	333	splP32569IMED17_YEAST	324	7,37	splP39073ISSN3_YEAST	265	splP39073ISSN3_YEAST	203	17,27
splP38304IMED8_YEAST	191	splP32585IMED18_YEAST	279	2,82	splP25648ISRB8_YEAST	899	splP25648ISRB8_YEAST	901	7,58
splQ08278IMED7_YEAST	30	splQ08278IMED7_YEAST	37	4,95	splP19263IMED14_YEAST	609	splP19263IMED14_YEAST	594	11,51
splP32569IMED17_YEAST	349	splP32585IMED18_YEAST	225	8,32	splP19263IMED14_YEAST	609	splP19263IMED14_YEAST	594	10,41
splP38931ISSN2_YEAST	1398	splP38931ISSN2_YEAST	1002	1,96	splP19263IMED14_YEAST	609	splP19263IMED14_YEAST	594	9,87
splP47822IMED21_YEAST	45	splP25046IMED19_YEAST	56	2,87	splP39073ISSN3_YEAST	97	splP39073ISSN3_YEAST	319	8,34
splP19263IMED14_YEAST	609	splP19263IMED14_YEAST	594	4,15	splP34162IMED20_YEAST	21	splP19263IMED14_YEAST	591	11,17
splP38931ISSN2_YEAST	573	splP38931ISSN2_YEAST	566	2,09	splP32569IMED17_YEAST	589	splP32569IMED17_YEAST	601	5,04
splQ12343IMED4_YEAST	228	splQ12343IMED4_YEAST	234	2,92	splP47822IMED21_YEAST	113	splP47822IMED21_YEAST	117	10,95

P1	R1	P2	R2	Score	P1	R1	P2	R2	Score
splP38304IMED8_YEAST	210	splP38304IMED8_YEAST	194	2,74	splP32569IMED17_YEAST	333	splP32570IMED22_YEAST	2	4,91
splP38304IMED8_YEAST	210	splP38304IMED8_YEAST	194	2,60	splP19263IMED14_YEAST	678	splP19263IMED14_YEAST	667	6,25
splP38931ISSN2_YEAST	537	splP38931ISSN2_YEAST	566	2,36	splP32569IMED17_YEAST	349	splQ99278IMED11_YEAST	89	17,56
splP32570IMED22_YEAST	95	splP32569IMED17_YEAST	319	3,59	splP19263IMED14_YEAST	678	splP19263IMED14_YEAST	667	9,06
splP25046IMED19_YEAST	74	splP25648ISRB8_YEAST	616	7,22	splP38931ISSN2_YEAST	555	splP38931ISSN2_YEAST	537	6,60
splQ12343IMED4_YEAST	64	splQ12343IMED4_YEAST	2	2,65	splP32569IMED17_YEAST	324	splP32570IMED22_YEAST	2	12,38
splP39073ISSN3_YEAST	782	splP39073ISSN3_YEAST	777	2,85	splP32570IMED22_YEAST	82	splP32569IMED17_YEAST	333	5,28
splP33308IMED9_YEAST	31	splP33308IMED9_YEAST	43	12,91	splP19263IMED14_YEAST	697	splP19263IMED14_YEAST	663	4,22
splP38931ISSN2_YEAST	537	splP38931ISSN2_YEAST	566	4,83	splP32569IMED17_YEAST	333	splP32570IMED22_YEAST	2	5,87
splP39073ISSN3_YEAST	550	splP38931ISSN2_YEAST	919	4,44	splP32570IMED22_YEAST	2	splP32569IMED17_YEAST	324	3,75
splP32569IMED17_YEAST	115	splP19263IMED14_YEAST	360	5,55	splP19263IMED14_YEAST	678	splP19263IMED14_YEAST	667	5,54
splP19263IMED14_YEAST	549	splP19263IMED14_YEAST	594	2,81	splP38304IMED8_YEAST	191	splP32570IMED22_YEAST	2	8,69
splQ08278IMED7_YEAST	30	splQ08278IMED7_YEAST	37	2,70	splP32569IMED17_YEAST	333	splP32570IMED22_YEAST	2	5,59
splP38304IMED8_YEAST	191	splP32585IMED18_YEAST	279	4,78	splP32569IMED17_YEAST	608	splP32569IMED17_YEAST	555	9,30
splQ08278IMED7_YEAST	30	splQ08278IMED7_YEAST	37	5,95	splQ08278IMED7_YEAST	202	splQ12343IMED4_YEAST	110	6,21
splP25648ISRB8_YEAST	88	splP38931ISSN2_YEAST	1114	4,70	splP32569IMED17_YEAST	608	splP32569IMED17_YEAST	555	6,35
splP32569IMED17_YEAST	333	splP32570IMED22_YEAST	2	3,63	splP33308IMED9_YEAST	78	splQ12343IMED4_YEAST	71	5,72
splP47821ISSN8_YEAST	70	splP47821ISSN8_YEAST	23	1,43	splP39073ISSN3_YEAST	39	splP39073ISSN3_YEAST	43	13,71
splP32569IMED17_YEAST	75	splP32569IMED17_YEAST	81	3,47	splP19263IMED14_YEAST	674	splP19263IMED14_YEAST	594	5,13
splP47821ISSN8_YEAST	23	splP34162IMED20_YEAST	180	9,42	splP38931ISSN2_YEAST	1398	splP38931ISSN2_YEAST	1002	2,53
splP19263IMED14_YEAST	609	splP19263IMED14_YEAST	594	6,27	splP39073ISSN3_YEAST	574	splP39073ISSN3_YEAST	550	4,51
splP38931ISSN2_YEAST	1024	splP39073ISSN3_YEAST	530	6,38	splP25648ISRB8_YEAST	888	splP25648ISRB8_YEAST	899	3,35
splP25648ISRB8_YEAST	899	splP25648ISRB8_YEAST	901	6,80	splP47822IMED21_YEAST	100	splP47822IMED21_YEAST	93	9,27
splP19263IMED14_YEAST	678	splP19263IMED14_YEAST	667	3,65	splP33308IMED9_YEAST	78	splQ12343IMED4_YEAST	64	7,56
splP19263IMED14_YEAST	282	splP19263IMED14_YEAST	257	5,20	splP25648ISRB8_YEAST	899	splP25648ISRB8_YEAST	901	6,98
splQ08278IMED7_YEAST	30	splQ08278IMED7_YEAST	37	4,31	splP32569IMED17_YEAST	608	splP32569IMED17_YEAST	555	8,06

P1	R1	P2	R2	Score	P1	R1	P2	R2	Score
splP25648ISRB8_YEAST	899	splP25648ISRB8_YEAST	901	3,91	splQ12343IMED4_YEAST	36	splQ12343IMED4_YEAST	2	0,80
splP25648ISRB8_YEAST	899	splP25648ISRB8_YEAST	901	9,61	splP38931ISSN2_YEAST	573	splP38931ISSN2_YEAST	566	4,35
splP19263IMED14_YEAST	360	splQ12343IMED4_YEAST	2	2,68	splP39073ISSN3_YEAST	116	splP39073ISSN3_YEAST	189	2,66
splQ08278IMED7_YEAST	30	splQ08278IMED7_YEAST	37	4,44	splP19263IMED14_YEAST	614	splP19263IMED14_YEAST	594	2,96
splQ12343IMED4_YEAST	228	splQ12343IMED4_YEAST	234	7,20	splP25648ISRB8_YEAST	813	splP25648ISRB8_YEAST	789	4,80
splP32570IMED22_YEAST	2	splP32569IMED17_YEAST	324	3,37	splP39073ISSN3_YEAST	550	splP47821ISSN8_YEAST	23	5,22
splP19263IMED14_YEAST	609	splP19263IMED14_YEAST	594	4,00	splP32569IMED17_YEAST	333	splP32570IMED22_YEAST	2	6,23
splP39073ISSN3_YEAST	782	splP38304IMED8_YEAST	191	2,59	splP32570IMED22_YEAST	2	splP32569IMED17_YEAST	324	11,91
splQ08278IMED7_YEAST	30	splQ08278IMED7_YEAST	37	5,07	splP25648ISRB8_YEAST	813	splP25648ISRB8_YEAST	789	5,35
splP38304IMED8_YEAST	191	splP32585IMED18_YEAST	279	3,97	splP32570IMED22_YEAST	82	splP32570IMED22_YEAST	2	5,31
splP32569IMED17_YEAST	333	splP32569IMED17_YEAST	324	4,67	splP32569IMED17_YEAST	333	splP32570IMED22_YEAST	2	6,70
splP19263IMED14_YEAST	609	splP19263IMED14_YEAST	594	6,00	splP25648ISRB8_YEAST	665	splP25648ISRB8_YEAST	553	3,52
splP19263IMED14_YEAST	591	splP19263IMED14_YEAST	610	3,06	splP38782IMED6_YEAST	282	splP19263IMED14_YEAST	417	6,34
splP47822IMED21_YEAST	100	splP47822IMED21_YEAST	93	3,10	splP32569IMED17_YEAST	608	splP32569IMED17_YEAST	555	3,53
splQ08278IMED7_YEAST	30	splQ08278IMED7_YEAST	37	4,79	splP32569IMED17_YEAST	608	splP32569IMED17_YEAST	555	6,89
splP39073ISSN3_YEAST	804	splP39073ISSN3_YEAST	823	1,52	splP25648ISRB8_YEAST	951	splP25648ISRB8_YEAST	959	5,90
splP32569IMED17_YEAST	386	splP32569IMED17_YEAST	427	2,14	splP32570IMED22_YEAST	95	splP32569IMED17_YEAST	319	4,04
splP32569IMED17_YEAST	333	splP32570IMED22_YEAST	2	6,18	splQ08278IMED7_YEAST	202	splQ12343IMED4_YEAST	110	3,14
splP39073ISSN3_YEAST	550	splP25648ISRB8_YEAST	168	2,35	splP38931ISSN2_YEAST	1398	splP38931ISSN2_YEAST	1002	3,75
splQ12321IMED1_YEAST	81	splP25648ISRB8_YEAST	354	1,86	splP32570IMED22_YEAST	82	splP32569IMED17_YEAST	333	4,87
splP32569IMED17_YEAST	333	splP32570IMED22_YEAST	2	5,25	splP39073ISSN3_YEAST	804	splP39073ISSN3_YEAST	823	2,76
splP32585IMED18_YEAST	280	splP32569IMED17_YEAST	333	5,05	splP38931ISSN2_YEAST	573	splP38931ISSN2_YEAST	566	3,46
splP32569IMED17_YEAST	115	splQ12343IMED4_YEAST	2	2,13	splP32585IMED18_YEAST	280	splP32569IMED17_YEAST	333	6,97
splP32570IMED22_YEAST	95	splP32569IMED17_YEAST	319	4,74	splP32569IMED17_YEAST	333	splP32570IMED22_YEAST	2	10,48
splP32569IMED17_YEAST	333	splP32570IMED22_YEAST	2	5,61	splP39073ISSN3_YEAST	530	splP47821ISSN8_YEAST	23	4,15
splP32570IMED22_YEAST	82	splP32569IMED17_YEAST	333	4,02	splP38931ISSN2_YEAST	573	splP38931ISSN2_YEAST	566	2,48

P1	R1	P2	R2	Score	P1	R1	P2	R2	Score
splP34162IMED20_YEAST	21	splP19263IMED14_YEAST	591	5,58	splP39073ISSN3_YEAST	39	splP39073ISSN3_YEAST	43	14,41
splP38304IMED8_YEAST	191	splP32585IMED18_YEAST	279	4,68	splP32570IMED22_YEAST	95	splP32569IMED17_YEAST	319	5,61
splQ99278IMED11_YEAST	113	splP32569IMED17_YEAST	499	6,56	splQ08278IMED7_YEAST	103	splQ12343IMED4_YEAST	162	3,42
splP32585IMED18_YEAST	68	splP32569IMED17_YEAST	589	9,93	splP32569IMED17_YEAST	608	splP32569IMED17_YEAST	555	7,97
splP19263IMED14_YEAST	360	splQ12343IMED4_YEAST	2	3,64	splP39073ISSN3_YEAST	39	splP39073ISSN3_YEAST	43	13,21
splP32569IMED17_YEAST	333	splP32570IMED22_YEAST	2	3,81	splP39073ISSN3_YEAST	116	splP39073ISSN3_YEAST	189	3,89
splQ08278IMED7_YEAST	103	splQ12343IMED4_YEAST	162	5,17	splP32569IMED17_YEAST	122	splP19263IMED14_YEAST	257	4,22
splP25046IMED19_YEAST	74	splP25648ISRB8_YEAST	616	8,08	splQ12343IMED4_YEAST	36	splP33308IMED9_YEAST	117	4,45
splP33308IMED9_YEAST	24	splQ12343IMED4_YEAST	2	1,89	splP25648ISRB8_YEAST	145	splP25648ISRB8_YEAST	168	0,90
splP25046IMED19_YEAST	74	splP25648ISRB8_YEAST	616	3,87	splQ99278IMED11_YEAST	68	splQ99278IMED11_YEAST	61	8,30
splP25046IMED19_YEAST	65	splQ12343IMED4_YEAST	71	4,03	splP32570IMED22_YEAST	2	splP32569IMED17_YEAST	324	8,34
splP32569IMED17_YEAST	333	splP32570IMED22_YEAST	2	4,54	splP32569IMED17_YEAST	115	splP19263IMED14_YEAST	360	10,65
splP19263IMED14_YEAST	360	splQ12343IMED4_YEAST	2	2,03	splP47822IMED21_YEAST	100	splP38931ISSN2_YEAST	1270	1,56
splP32569IMED17_YEAST	333	splP32570IMED22_YEAST	2	5,37	splP39073ISSN3_YEAST	116	splP39073ISSN3_YEAST	189	5,39
splP38782IMED6_YEAST	1	splP32569IMED17_YEAST	499	1,94	splP32569IMED17_YEAST	608	splP32569IMED17_YEAST	555	7,25
splP32570IMED22_YEAST	82	splP32569IMED17_YEAST	333	5,13	splP19263IMED14_YEAST	678	splP19263IMED14_YEAST	667	7,67
splP39073ISSN3_YEAST	782	splP38304IMED8_YEAST	191	1,78	splP39073ISSN3_YEAST	550	splP38931ISSN2_YEAST	919	5,85
splP39073ISSN3_YEAST	550	splP47821ISSN8_YEAST	23	1,52	splP39073ISSN3_YEAST	550	splP38931ISSN2_YEAST	919	2,68
splP32569IMED17_YEAST	1	splP38931ISSN2_YEAST	534	1,35	splQ99278IMED11_YEAST	53	splQ99278IMED11_YEAST	61	6,17
splP38304IMED8_YEAST	191	splP32585IMED18_YEAST	279	2,32	splP47821ISSN8_YEAST	262	splP38931ISSN2_YEAST	1114	6,38
splP39073ISSN3_YEAST	782	splP38304IMED8_YEAST	191	2,06	splP19263IMED14_YEAST	549	splP19263IMED14_YEAST	610	6,84
splP38304IMED8_YEAST	2	splP32569IMED17_YEAST	247	7,78	splP32569IMED17_YEAST	333	splP32569IMED17_YEAST	324	5,23
splP38304IMED8_YEAST	191	splP32585IMED18_YEAST	279	2,94	splP32569IMED17_YEAST	608	splP32569IMED17_YEAST	555	6,77
splP47822IMED21_YEAST	45	splP25046IMED19_YEAST	56	2,08	splP25648ISRB8_YEAST	665	splP25648ISRB8_YEAST	553	4,03
splQ99278IMED11_YEAST	113	splP32569IMED17_YEAST	499	4,48	splP25648ISRB8_YEAST	906	splP25648ISRB8_YEAST	954	4,22
splP39073ISSN3_YEAST	550	splP47821ISSN8_YEAST	23	0,96	splP19263IMED14_YEAST	591	splP19263IMED14_YEAST	674	5,07

P1	R1	P2	R2	Score	P1	R1	P2	R2	Score
splP38304IMED8_YEAST	191	splP32585IMED18_YEAST	279	3,64	splP39073ISSN3_YEAST	97	splP39073ISSN3_YEAST	319	6,70
splP39073ISSN3_YEAST	550	splP38931ISSN2_YEAST	919	2,79	splP32570IMED22_YEAST	82	splP32569IMED17_YEAST	333	4,78
splQ06213IMED10_YEAST	76	splP47821ISSN8_YEAST	23	1,58	splP19263IMED14_YEAST	609	splP19263IMED14_YEAST	594	7,97
splP33308IMED9_YEAST	24	splQ12343IMED4_YEAST	2	2,18	splP38782IMED6_YEAST	282	splP19263IMED14_YEAST	417	9,49
splP32585IMED18_YEAST	280	splP32569IMED17_YEAST	333	3,88	splQ12343IMED4_YEAST	147	splQ12343IMED4_YEAST	162	2,45
splP38304IMED8_YEAST	2	splP32569IMED17_YEAST	247	12,60	splP38931ISSN2_YEAST	1398	splP38931ISSN2_YEAST	1002	2,77
splP39073ISSN3_YEAST	550	splP38931ISSN2_YEAST	919	3,88	splP25648ISRB8_YEAST	899	splP25648ISRB8_YEAST	901	4,70
splP32569IMED17_YEAST	333	splP32570IMED22_YEAST	2	4,20	splP19263IMED14_YEAST	591	splP19263IMED14_YEAST	674	4,23
splQ99278IMED11_YEAST	113	splP32569IMED17_YEAST	499	4,15	splQ12343IMED4_YEAST	228	splQ12343IMED4_YEAST	234	6,75
splQ99278IMED11_YEAST	113	splP32569IMED17_YEAST	499	3,45	splP19263IMED14_YEAST	614	splP19263IMED14_YEAST	594	3,14
splP19263IMED14_YEAST	360	splQ12343IMED4_YEAST	2	2,75	splQ12343IMED4_YEAST	159	splQ12343IMED4_YEAST	165	5,38
splQ06213IMED10_YEAST	145	splP38931ISSN2_YEAST	1322	2,76	splP32585IMED18_YEAST	83	splP32585IMED18_YEAST	97	9,17
splQ99278IMED11_YEAST	113	splP32569IMED17_YEAST	499	5,09	splQ99278IMED11_YEAST	68	splQ99278IMED11_YEAST	61	5,99
splP47821ISSN8_YEAST	23	splP34162IMED20_YEAST	180	3,81	splP32569IMED17_YEAST	608	splP32569IMED17_YEAST	555	8,93
splP38931ISSN2_YEAST	1398	splP38931ISSN2_YEAST	1002	2,12	splP32585IMED18_YEAST	280	splP32569IMED17_YEAST	333	5,92
splP32569IMED17_YEAST	333	splP32569IMED17_YEAST	324	4,08	splP32569IMED17_YEAST	589	splP32569IMED17_YEAST	601	2,90
splP32569IMED17_YEAST	608	splP32569IMED17_YEAST	555	5,24	splP38304IMED8_YEAST	191	splP32570IMED22_YEAST	2	5,32
splP25648ISRB8_YEAST	145	splP25648ISRB8_YEAST	168	1,89	splP32570IMED22_YEAST	9	splP32569IMED17_YEAST	333	3,01
splQ08278IMED7_YEAST	30	splQ08278IMED7_YEAST	37	5,94	splP25648ISRB8_YEAST	899	splP25648ISRB8_YEAST	901	10,97
splP38931ISSN2_YEAST	1398	splP38931ISSN2_YEAST	1002	0,65	splP25648ISRB8_YEAST	665	splP25648ISRB8_YEAST	553	4,54
splP25648ISRB8_YEAST	1324	splP25648ISRB8_YEAST	1220	3,52	splP38931ISSN2_YEAST	1208	splP47821ISSN8_YEAST	23	10,23
splQ12343IMED4_YEAST	228	splQ12343IMED4_YEAST	234	6,34	splP32570IMED22_YEAST	82	splP32569IMED17_YEAST	333	5,78
splQ08278IMED7_YEAST	30	splQ08278IMED7_YEAST	37	5,55	splP32570IMED22_YEAST	82	splP32569IMED17_YEAST	333	6,34
splQ08278IMED7_YEAST	30	splQ08278IMED7_YEAST	37	3,92	splP19263IMED14_YEAST	609	splP19263IMED14_YEAST	594	8,65
splP32569IMED17_YEAST	386	splP32569IMED17_YEAST	427	3,22	splP19263IMED14_YEAST	594	splP19263IMED14_YEAST	610	4,72
splQ08278IMED7_YEAST	30	splQ08278IMED7_YEAST	37	4,14	splP38931ISSN2_YEAST	555	splP38931ISSN2_YEAST	537	3,66

P1	R1	P2	R2	Score	P1	R1	P2	R2	Score
splQ08278IMED7_YEAST	30	splQ08278IMED7_YEAST	37	4,21	splQ08278IMED7_YEAST	103	splQ12343IMED4_YEAST	162	2,98
splP25648ISRB8_YEAST	145	splP25648ISRB8_YEAST	168	1,63	splP32569IMED17_YEAST	333	splP32569IMED17_YEAST	324	6,45
splQ08278IMED7_YEAST	30	splQ08278IMED7_YEAST	37	3,82	splP32569IMED17_YEAST	608	splP32569IMED17_YEAST	601	2,84
splP47821ISSN8_YEAST	70	splP47821ISSN8_YEAST	23	1,27	splP47822IMED21_YEAST	75	splP38931ISSN2_YEAST	607	18,72
splQ08278IMED7_YEAST	30	splQ08278IMED7_YEAST	37	3,46	splP32569IMED17_YEAST	427	splP32569IMED17_YEAST	434	6,96
splQ12343IMED4_YEAST	228	splQ12343IMED4_YEAST	234	6,03	splP39073ISSN3_YEAST	574	splP39073ISSN3_YEAST	580	4,07
splP25648ISRB8_YEAST	145	splP25648ISRB8_YEAST	168	1,54	splP25648ISRB8_YEAST	899	splP25648ISRB8_YEAST	901	4,80
splQ08278IMED7_YEAST	30	splQ08278IMED7_YEAST	37	6,15	splP39073ISSN3_YEAST	550	splP47821ISSN8_YEAST	23	3,34
splP38931ISSN2_YEAST	537	splP38931ISSN2_YEAST	566	2,15	splP32569IMED17_YEAST	333	splP32570IMED22_YEAST	2	7,62
splP38931ISSN2_YEAST	555	splP38931ISSN2_YEAST	537	4,96	splP39073ISSN3_YEAST	782	splP39073ISSN3_YEAST	777	4,84
splP39073ISSN3_YEAST	782	splP39073ISSN3_YEAST	777	1,54	splP32569IMED17_YEAST	78	splP32569IMED17_YEAST	71	3,44
splP19263IMED14_YEAST	50	splP19263IMED14_YEAST	35	6,62	splP39073ISSN3_YEAST	804	splP39073ISSN3_YEAST	823	2,85
splP25648ISRB8_YEAST	145	splP25648ISRB8_YEAST	168	0,59	splP39073ISSN3_YEAST	804	splP39073ISSN3_YEAST	823	3,45
splQ08278IMED7_YEAST	30	splQ08278IMED7_YEAST	37	1,99	splP32570IMED22_YEAST	2	splP32569IMED17_YEAST	324	6,71
splQ08278IMED7_YEAST	30	splQ08278IMED7_YEAST	37	3,75	splP19263IMED14_YEAST	697	splP19263IMED14_YEAST	663	4,13
splP32569IMED17_YEAST	68	splP32569IMED17_YEAST	71	3,12	splP39073ISSN3_YEAST	574	splP39073ISSN3_YEAST	580	4,39
splQ08278IMED7_YEAST	30	splQ08278IMED7_YEAST	37	6,09	splP19263IMED14_YEAST	678	splP19263IMED14_YEAST	667	6,59
splP25648ISRB8_YEAST	899	splP25648ISRB8_YEAST	901	4,26	splP38931ISSN2_YEAST	607	splP47822IMED21_YEAST	93	6,93
splP32569IMED17_YEAST	555	splP32569IMED17_YEAST	548	2,79	splP19263IMED14_YEAST	549	splP19263IMED14_YEAST	591	10,80
splQ08278IMED7_YEAST	30	splQ08278IMED7_YEAST	37	5,26	splP25648ISRB8_YEAST	888	splP25648ISRB8_YEAST	823	4,75
splP19263IMED14_YEAST	50	splP19263IMED14_YEAST	35	7,30	splP25648ISRB8_YEAST	145	splP25648ISRB8_YEAST	168	1,11
splP38931ISSN2_YEAST	573	splP38931ISSN2_YEAST	566	1,87	splP38931ISSN2_YEAST	607	splP47822IMED21_YEAST	93	8,06
splP25648ISRB8_YEAST	1324	splP25648ISRB8_YEAST	1220	2,89	splP32569IMED17_YEAST	319	splP32569IMED17_YEAST	427	7,41
splP19263IMED14_YEAST	697	splP19263IMED14_YEAST	663	1,09	splQ12343IMED4_YEAST	228	splQ12343IMED4_YEAST	234	7,25
splP47821ISSN8_YEAST	70	splP47821ISSN8_YEAST	23	0,41	splP38931ISSN2_YEAST	1398	splP38931ISSN2_YEAST	1002	2,02
splP25648ISRB8_YEAST	899	splP25648ISRB8_YEAST	901	7,76	splP32570IMED22_YEAST	9	splP32569IMED17_YEAST	333	6,87

P1	R1	P2	R2	Score	P1	R1	P2	R2	Score
splP25648lSRB8_YEAST	145	splP25648lSRB8_YEAST	168	1,13	splP19263lMED14_YEAST	667	splP19263lMED14_YEAST	674	6,68
splP39073lSSN3_YEAST	39	splP39073lSSN3_YEAST	43	9,84	splP38931lSSN2_YEAST	573	splP38931lSSN2_YEAST	566	3,18
splQ08278lMED7_YEAST	30	splQ08278lMED7_YEAST	37	5,22	splP32569lMED17_YEAST	247	splQ12343lMED4_YEAST	2	4,89
splQ08278lMED7_YEAST	30	splQ08278lMED7_YEAST	37	3,85	splP19263lMED14_YEAST	549	splP19263lMED14_YEAST	591	9,55
splP47822lMED21_YEAST	100	splP47822lMED21_YEAST	93	3,68	splQ12343lMED4_YEAST	71	splQ12321lMED1_YEAST	118	7,87
splP25648lSRB8_YEAST	145	splP25648lSRB8_YEAST	168	0,99	splP38782lMED6_YEAST	282	splP19263lMED14_YEAST	417	10,91
splP47822lMED21_YEAST	100	splP47822lMED21_YEAST	93	3,93	splP32570lMED22_YEAST	2	splP32569lMED17_YEAST	324	3,72
splP38304lMED8_YEAST	210	splP38304lMED8_YEAST	194	1,89	splP25648lSRB8_YEAST	813	splP25648lSRB8_YEAST	789	7,37
splP38931lSSN2_YEAST	573	splP38931lSSN2_YEAST	566	1,68	splQ12343lMED4_YEAST	228	splQ12343lMED4_YEAST	234	9,30
splP38931lSSN2_YEAST	573	splP38931lSSN2_YEAST	950	2,24	splP47822lMED21_YEAST	45	splP25046lMED19_YEAST	56	3,90
splP25648lSRB8_YEAST	899	splP25648lSRB8_YEAST	901	5,85	splP33308lMED9_YEAST	78	splQ12343lMED4_YEAST	71	5,35
splP19263lMED14_YEAST	697	splP19263lMED14_YEAST	663	2,56	splP32569lMED17_YEAST	78	splP32569lMED17_YEAST	71	3,82
splP19263lMED14_YEAST	594	splP19263lMED14_YEAST	610	3,97	splP32569lMED17_YEAST	333	splP32570lMED22_YEAST	2	5,74
splP38931lSSN2_YEAST	573	splP38931lSSN2_YEAST	950	1,87	splP19263lMED14_YEAST	549	splP19263lMED14_YEAST	567	8,61
splP38304lMED8_YEAST	210	splP38304lMED8_YEAST	194	3,43	splP19263lMED14_YEAST	436	splP19263lMED14_YEAST	418	4,51
splP19263lMED14_YEAST	451	splP19263lMED14_YEAST	418	4,51	splP32569lMED17_YEAST	75	splP32569lMED17_YEAST	81	2,74
splP25648lSRB8_YEAST	145	splP25648lSRB8_YEAST	168	1,56	splP32569lMED17_YEAST	608	splP32569lMED17_YEAST	555	7,49
splP19263lMED14_YEAST	436	splP19263lMED14_YEAST	418	0,79	splP32569lMED17_YEAST	115	splP19263lMED14_YEAST	360	6,22
splQ08278lMED7_YEAST	30	splQ08278lMED7_YEAST	37	5,07	splQ08278lMED7_YEAST	202	splQ12343lMED4_YEAST	110	7,38
splP38931lSSN2_YEAST	1398	splP38931lSSN2_YEAST	1002	0,98	splP39073lSSN3_YEAST	804	splP39073lSSN3_YEAST	823	2,43
splP25648lSRB8_YEAST	145	splP25648lSRB8_YEAST	168	1,64	splP32569lMED17_YEAST	68	splP32569lMED17_YEAST	71	9,26
splP25648lSRB8_YEAST	145	splP25648lSRB8_YEAST	168	2,58	splQ12343lMED4_YEAST	228	splQ12343lMED4_YEAST	234	10,03
splQ08278lMED7_YEAST	115	splQ08278lMED7_YEAST	102	5,57	splP39073lSSN3_YEAST	550	splP47821lSSN8_YEAST	23	1,69
splP19263lMED14_YEAST	609	splP19263lMED14_YEAST	594	5,79	splP39073lSSN3_YEAST	39	splP39073lSSN3_YEAST	43	11,04
splP25648lSRB8_YEAST	145	splP25648lSRB8_YEAST	168	2,54	splP32585lMED18_YEAST	83	splP32585lMED18_YEAST	97	11,06
splQ12343lMED4_YEAST	159	splQ12343lMED4_YEAST	165	6,27	splP32569lMED17_YEAST	115	splP19263lMED14_YEAST	360	6,20

P1	R1	P2	R2	Score	P1	R1	P2	R2	Score
splP39073ISSN3_YEAST	39	splP39073ISSN3_YEAST	43	5,48	splP39073ISSN3_YEAST	60	splP25648ISRB8_YEAST	901	3,05
splP19263IMED14_YEAST	282	splP19263IMED14_YEAST	257	2,75	splP39073ISSN3_YEAST	550	splP25648ISRB8_YEAST	168	2,79
splP25648ISRB8_YEAST	888	splP25648ISRB8_YEAST	820	3,42	splP25648ISRB8_YEAST	785	splP25648ISRB8_YEAST	813	6,49
splQ08278IMED7_YEAST	30	splQ08278IMED7_YEAST	37	5,57	splP25648ISRB8_YEAST	888	splP25648ISRB8_YEAST	823	4,62
splP32569IMED17_YEAST	68	splP32569IMED17_YEAST	71	2,91	splP38782IMED6_YEAST	282	splP19263IMED14_YEAST	417	5,55
splP19263IMED14_YEAST	609	splP19263IMED14_YEAST	594	7,53	splP33308IMED9_YEAST	117	splQ12343IMED4_YEAST	36	10,71
splP25648ISRB8_YEAST	145	splP25648ISRB8_YEAST	168	0,97	splP19263IMED14_YEAST	549	splP19263IMED14_YEAST	610	3,73
splP25648ISRB8_YEAST	888	splP25648ISRB8_YEAST	823	1,39	splP32569IMED17_YEAST	333	splP32570IMED22_YEAST	2	6,14
splP32569IMED17_YEAST	68	splP32569IMED17_YEAST	75	5,24	splP39073ISSN3_YEAST	309	splP39073ISSN3_YEAST	327	6,04
splP39073ISSN3_YEAST	804	splP39073ISSN3_YEAST	823	2,16	splP32569IMED17_YEAST	608	splP32569IMED17_YEAST	555	3,56
splP25648ISRB8_YEAST	899	splP25648ISRB8_YEAST	901	3,18	splP19263IMED14_YEAST	591	splP19263IMED14_YEAST	674	3,90
splQ12343IMED4_YEAST	228	splQ12343IMED4_YEAST	234	4,43	splP25648ISRB8_YEAST	899	splP25648ISRB8_YEAST	901	11,82
splP25648ISRB8_YEAST	145	splP25648ISRB8_YEAST	168	1,67	splP34162IMED20_YEAST	21	splP19263IMED14_YEAST	591	9,49
splP25648ISRB8_YEAST	145	splP25648ISRB8_YEAST	168	1,17	splP38931ISSN2_YEAST	573	splP38931ISSN2_YEAST	566	3,19
splP38931ISSN2_YEAST	537	splP38931ISSN2_YEAST	566	2,03	splP38931ISSN2_YEAST	573	splP38931ISSN2_YEAST	566	3,04
splQ08278IMED7_YEAST	30	splQ08278IMED7_YEAST	37	2,99	splP38931ISSN2_YEAST	573	splP38931ISSN2_YEAST	566	0,79
splP39073ISSN3_YEAST	804	splP39073ISSN3_YEAST	823	1,61	splP19263IMED14_YEAST	678	splP19263IMED14_YEAST	667	4,86
splP38931ISSN2_YEAST	555	splP38931ISSN2_YEAST	537	3,41	splP32569IMED17_YEAST	427	splP32569IMED17_YEAST	434	5,44
splQ08278IMED7_YEAST	30	splQ08278IMED7_YEAST	37	4,74	splP32570IMED22_YEAST	82	splP32569IMED17_YEAST	333	5,69
splP38931ISSN2_YEAST	1398	splP38931ISSN2_YEAST	1002	2,38	splP38931ISSN2_YEAST	537	splP38931ISSN2_YEAST	566	4,40
splP25648ISRB8_YEAST	145	splP25648ISRB8_YEAST	168	1,24	splP38931ISSN2_YEAST	1398	splP38931ISSN2_YEAST	1002	2,60
splQ12343IMED4_YEAST	228	splQ12343IMED4_YEAST	234	5,73	splP19263IMED14_YEAST	609	splP19263IMED14_YEAST	594	10,13
splP38931ISSN2_YEAST	573	splP38931ISSN2_YEAST	566	1,51	splP38931ISSN2_YEAST	1398	splP38931ISSN2_YEAST	1002	4,39
splP47822IMED21_YEAST	100	splP47822IMED21_YEAST	93	1,92	splQ12343IMED4_YEAST	55	splQ12343IMED4_YEAST	64	4,54
splP38931ISSN2_YEAST	796	splP38931ISSN2_YEAST	1398	0,00	splP39073ISSN3_YEAST	39	splP39073ISSN3_YEAST	43	7,92
splP19263IMED14_YEAST	697	splP19263IMED14_YEAST	663	1,78	splP39073ISSN3_YEAST	116	splP39073ISSN3_YEAST	189	4,89

P1	R1	P2	R2	Score	P1	R1	P2	R2	Score
splP38931ISSN2_YEAST	545	splP38931ISSN2_YEAST	534	2,73	splP38931ISSN2_YEAST	1398	splP38931ISSN2_YEAST	1002	2,20
splQ99278IMED11_YEAST	53	splQ99278IMED11_YEAST	61	4,56	splQ12343IMED4_YEAST	228	splQ12343IMED4_YEAST	234	6,73
splP32570IMED22_YEAST	82	splP32569IMED17_YEAST	333	4,34	splQ12343IMED4_YEAST	71	splQ12321IMED1_YEAST	118	8,76
splP32569IMED17_YEAST	333	splP32569IMED17_YEAST	324	3,14	splP32569IMED17_YEAST	333	splP32570IMED22_YEAST	2	2,59
splQ08278IMED7_YEAST	30	splQ08278IMED7_YEAST	37	4,78	splQ08278IMED7_YEAST	30	splQ08278IMED7_YEAST	37	4,98
splP25648ISRB8_YEAST	828	splP25648ISRB8_YEAST	163	3,72	splP32585IMED18_YEAST	280	splP32569IMED17_YEAST	333	4,43
splQ08278IMED7_YEAST	30	splQ08278IMED7_YEAST	37	5,49	splP32569IMED17_YEAST	333	splP32569IMED17_YEAST	324	2,80
splQ08278IMED7_YEAST	30	splQ08278IMED7_YEAST	37	3,56	splQ08278IMED7_YEAST	1	splP38633IMED31_YEAST	2	16,17
splQ99278IMED11_YEAST	53	splQ99278IMED11_YEAST	61	5,62	splP19263IMED14_YEAST	674	splP19263IMED14_YEAST	667	3,87
splP38304IMED8_YEAST	210	splP38304IMED8_YEAST	194	3,24	splP39073ISSN3_YEAST	116	splP39073ISSN3_YEAST	189	3,55
splP38304IMED8_YEAST	210	splP38304IMED8_YEAST	194	2,09	splP38304IMED8_YEAST	191	splP32570IMED22_YEAST	2	6,54
splQ08278IMED7_YEAST	30	splQ08278IMED7_YEAST	37	4,05	splP47822IMED21_YEAST	100	splP47822IMED21_YEAST	93	5,18
splQ12321IMED1_YEAST	389	splQ12321IMED1_YEAST	421	2,31	splP25648ISRB8_YEAST	813	splP25648ISRB8_YEAST	820	3,07
splP38931ISSN2_YEAST	573	splP38931ISSN2_YEAST	950	1,82	splQ99278IMED11_YEAST	113	splP32569IMED17_YEAST	499	4,61
splP19263IMED14_YEAST	697	splP19263IMED14_YEAST	663	1,56	splQ12343IMED4_YEAST	55	splQ12343IMED4_YEAST	64	8,03
splQ08278IMED7_YEAST	30	splQ08278IMED7_YEAST	37	4,99	splP39073ISSN3_YEAST	574	splP39073ISSN3_YEAST	580	3,53
splP19263IMED14_YEAST	697	splP19263IMED14_YEAST	663	1,55	splP47821ISSN8_YEAST	70	splP47821ISSN8_YEAST	23	3,22
splP25648ISRB8_YEAST	888	splP25648ISRB8_YEAST	823	3,78	splQ08278IMED7_YEAST	30	splQ08278IMED7_YEAST	37	7,00
splQ08278IMED7_YEAST	30	splQ08278IMED7_YEAST	37	5,72	splP38931ISSN2_YEAST	457	splP38931ISSN2_YEAST	440	11,57
splP19263IMED14_YEAST	549	splP19263IMED14_YEAST	591	3,57	splP19263IMED14_YEAST	360	splQ12343IMED4_YEAST	2	2,54
splP19263IMED14_YEAST	609	splP19263IMED14_YEAST	594	3,56	splP32569IMED17_YEAST	115	splP19263IMED14_YEAST	360	6,50
splP25648ISRB8_YEAST	813	splP25648ISRB8_YEAST	789	3,00	splP38931ISSN2_YEAST	573	splP38931ISSN2_YEAST	566	4,60
splP25648ISRB8_YEAST	145	splP25648ISRB8_YEAST	168	1,36	splP39073ISSN3_YEAST	782	splP39073ISSN3_YEAST	777	5,31
splQ08278IMED7_YEAST	30	splQ08278IMED7_YEAST	37	4,07	splP47822IMED21_YEAST	100	splP47822IMED21_YEAST	93	2,34
splQ99278IMED11_YEAST	113	splP32569IMED17_YEAST	499	4,75	splP39073ISSN3_YEAST	782	splP39073ISSN3_YEAST	777	5,69
splQ06213IMED10_YEAST	145	splP25648ISRB8_YEAST	901	5,12	splP25648ISRB8_YEAST	888	splP25648ISRB8_YEAST	823	4,33

P1	R1	P2	R2	Score	P1	R1	P2	R2	Score
splQ99278IMED11_YEAST	113	splP32569IMED17_YEAST	499	4,72	splP32569IMED17_YEAST	81	splP32569IMED17_YEAST	71	2,96
splP39073ISSN3_YEAST	579	splQ06213IMED10_YEAST	114	0,62	splP38304IMED8_YEAST	191	splP32585IMED18_YEAST	279	6,29
splQ08278IMED7_YEAST	30	splQ08278IMED7_YEAST	37	4,55	splP19263IMED14_YEAST	609	splP19263IMED14_YEAST	594	9,69
splP19263IMED14_YEAST	609	splP19263IMED14_YEAST	594	5,73	splQ12343IMED4_YEAST	147	splQ12343IMED4_YEAST	162	2,85
splP39073ISSN3_YEAST	116	splP39073ISSN3_YEAST	189	3,80	splP32569IMED17_YEAST	1	splP38931ISSN2_YEAST	534	1,66
splP39073ISSN3_YEAST	804	splP39073ISSN3_YEAST	823	1,01	splP25648ISRB8_YEAST	899	splP25648ISRB8_YEAST	901	12,67
splP25648ISRB8_YEAST	145	splP25648ISRB8_YEAST	168	1,19	splP32569IMED17_YEAST	247	splQ12343IMED4_YEAST	2	5,23
splP19263IMED14_YEAST	549	splP19263IMED14_YEAST	609	3,15	splP33308IMED9_YEAST	78	splQ12343IMED4_YEAST	64	9,23
splP38931ISSN2_YEAST	555	splP38931ISSN2_YEAST	537	1,97	splP19263IMED14_YEAST	678	splP19263IMED14_YEAST	667	5,84
splP47822IMED21_YEAST	100	splP47822IMED21_YEAST	93	2,26	splP39073ISSN3_YEAST	97	splP39073ISSN3_YEAST	319	3,83
splP19263IMED14_YEAST	614	splP19263IMED14_YEAST	418	0,93	splQ12343IMED4_YEAST	228	splQ12343IMED4_YEAST	234	8,75
splQ08278IMED7_YEAST	115	splQ08278IMED7_YEAST	102	4,97	splP39073ISSN3_YEAST	804	splP39073ISSN3_YEAST	823	3,10
splQ12343IMED4_YEAST	113	splQ12343IMED4_YEAST	110	1,32	splP25648ISRB8_YEAST	951	splP25648ISRB8_YEAST	959	4,26
splP19263IMED14_YEAST	609	splP19263IMED14_YEAST	594	5,72	splP47822IMED21_YEAST	100	splP47822IMED21_YEAST	93	6,17
splQ08278IMED7_YEAST	30	splQ08278IMED7_YEAST	37	3,80	splP38931ISSN2_YEAST	1398	splP38931ISSN2_YEAST	1002	2,42
splQ08278IMED7_YEAST	30	splQ08278IMED7_YEAST	37	3,91	splP25648ISRB8_YEAST	899	splP25648ISRB8_YEAST	901	11,59
splP39073ISSN3_YEAST	156	splP38304IMED8_YEAST	203	0,89	splP38931ISSN2_YEAST	457	splP38931ISSN2_YEAST	440	9,40
splP38931ISSN2_YEAST	1398	splP38931ISSN2_YEAST	1002	1,51	splP32569IMED17_YEAST	333	splP32569IMED17_YEAST	324	6,71
splP32569IMED17_YEAST	250	splP32569IMED17_YEAST	266	0,00	splP32569IMED17_YEAST	333	splP32569IMED17_YEAST	324	5,87
splP25648ISRB8_YEAST	785	splP25648ISRB8_YEAST	813	4,62	splP25648ISRB8_YEAST	88	splP47821ISSN8_YEAST	262	13,57
splP19263IMED14_YEAST	549	splP19263IMED14_YEAST	591	5,79	splP25648ISRB8_YEAST	665	splP25648ISRB8_YEAST	553	3,28
splP25648ISRB8_YEAST	813	splP25648ISRB8_YEAST	789	4,00	splP19263IMED14_YEAST	407	splP19263IMED14_YEAST	434	1,50
splP39073ISSN3_YEAST	804	splP39073ISSN3_YEAST	823	1,38	splP38931ISSN2_YEAST	1398	splP38931ISSN2_YEAST	1002	3,09
splQ12343IMED4_YEAST	147	splQ12343IMED4_YEAST	162	2,53	splP39073ISSN3_YEAST	782	splP39073ISSN3_YEAST	777	6,34
splP19263IMED14_YEAST	678	splP19263IMED14_YEAST	667	6,29	splP19263IMED14_YEAST	282	splP19263IMED14_YEAST	257	3,75
splP32570IMED22_YEAST	95	splP32569IMED17_YEAST	319	6,18	splP38304IMED8_YEAST	191	splP32570IMED22_YEAST	2	7,74

P1	R1	P2	R2	Score	P1	R1	P2	R2	Score
splP32569IMED17_YEAST	608	splP32569IMED17_YEAST	555	7,20	splP47822IMED21_YEAST	100	splP47822IMED21_YEAST	93	4,99
splP39073ISSN3_YEAST	216	splP39073ISSN3_YEAST	151	4,80	splP19263IMED14_YEAST	549	splP19263IMED14_YEAST	591	7,19
splP32569IMED17_YEAST	349	splQ99278IMED11_YEAST	89	6,59	splP25648ISRB8_YEAST	906	splP25648ISRB8_YEAST	954	5,67
splP38304IMED8_YEAST	191	splP32585IMED18_YEAST	279	2,56	splP19263IMED14_YEAST	678	splP19263IMED14_YEAST	667	6,42
splP19263IMED14_YEAST	417	splQ12343IMED4_YEAST	2	5,05	splP25648ISRB8_YEAST	899	splP25648ISRB8_YEAST	901	9,59
splQ08278IMED7_YEAST	30	splQ08278IMED7_YEAST	37	5,45	splQ08278IMED7_YEAST	30	splQ08278IMED7_YEAST	37	6,04
splP38931ISSN2_YEAST	573	splP38931ISSN2_YEAST	566	1,81	splQ08278IMED7_YEAST	30	splQ08278IMED7_YEAST	37	5,74
splP32570IMED22_YEAST	95	splP32569IMED17_YEAST	319	5,61	splP19263IMED14_YEAST	50	splP19263IMED14_YEAST	35	9,09
splP25648ISRB8_YEAST	888	splP25648ISRB8_YEAST	899	4,97	splP25648ISRB8_YEAST	145	splP25648ISRB8_YEAST	168	3,39
splP32569IMED17_YEAST	122	splP19263IMED14_YEAST	282	7,29	splP39073ISSN3_YEAST	530	splP47821ISSN8_YEAST	23	4,44
splP32585IMED18_YEAST	280	splP32569IMED17_YEAST	333	5,40	splP39073ISSN3_YEAST	550	splP47821ISSN8_YEAST	23	2,78
splP39073ISSN3_YEAST	530	splP47821ISSN8_YEAST	23	4,37	splP32570IMED22_YEAST	2	splP32569IMED17_YEAST	324	5,75
splP34162IMED20_YEAST	21	splP19263IMED14_YEAST	591	6,40	splP39073ISSN3_YEAST	216	splP39073ISSN3_YEAST	151	7,52
splP38304IMED8_YEAST	191	splP32570IMED22_YEAST	2	4,18	splP32569IMED17_YEAST	589	splP32569IMED17_YEAST	601	2,60
splP33308IMED9_YEAST	78	splQ12343IMED4_YEAST	64	7,22	splP19263IMED14_YEAST	678	splP19263IMED14_YEAST	667	6,67
splP47822IMED21_YEAST	100	splP47822IMED21_YEAST	93	6,54	splP39073ISSN3_YEAST	804	splP39073ISSN3_YEAST	823	2,68
splP39073ISSN3_YEAST	97	splP39073ISSN3_YEAST	319	4,15	splP38931ISSN2_YEAST	632	splP38931ISSN2_YEAST	566	0,73
splP38931ISSN2_YEAST	1398	splP38931ISSN2_YEAST	1002	2,47	splP38931ISSN2_YEAST	555	splP38931ISSN2_YEAST	534	3,40
splP19263IMED14_YEAST	591	splP19263IMED14_YEAST	674	5,05	splP32569IMED17_YEAST	122	splP19263IMED14_YEAST	282	6,88
splQ12343IMED4_YEAST	36	splQ12343IMED4_YEAST	2	0,77	splP32569IMED17_YEAST	608	splP32569IMED17_YEAST	555	2,97
splQ12343IMED4_YEAST	36	splQ12343IMED4_YEAST	2	0,55	splP19263IMED14_YEAST	609	splP19263IMED14_YEAST	591	9,65
splP32570IMED22_YEAST	82	splP32569IMED17_YEAST	333	4,35	splP38931ISSN2_YEAST	1398	splP38931ISSN2_YEAST	1002	1,97
splQ12343IMED4_YEAST	228	splQ12343IMED4_YEAST	234	7,02	splP25648ISRB8_YEAST	88	splP38931ISSN2_YEAST	1114	6,87
splP19263IMED14_YEAST	674	splP19263IMED14_YEAST	594	2,96	splP32570IMED22_YEAST	95	splP32569IMED17_YEAST	319	8,12
splP19263IMED14_YEAST	726	splP19263IMED14_YEAST	594	3,20	splP25648ISRB8_YEAST	899	splP25648ISRB8_YEAST	901	9,85
splP19263IMED14_YEAST	591	splP19263IMED14_YEAST	674	5,92	splP19263IMED14_YEAST	50	splP19263IMED14_YEAST	35	8,92

P1	R1	P2	R2	Score	P1	R1	P2	R2	Score
splP38931ISSN2_YEAST	1398	splP38931ISSN2_YEAST	1002	3,45	splP34162IMED20_YEAST	21	splP19263IMED14_YEAST	591	5,33
splQ12343IMED4_YEAST	228	splQ12343IMED4_YEAST	234	7,04	splP39073ISSN3_YEAST	97	splP39073ISSN3_YEAST	319	7,74
splP39073ISSN3_YEAST	97	splP39073ISSN3_YEAST	319	7,62	splP38782IMED6_YEAST	282	splP19263IMED14_YEAST	417	7,66
splP47821ISSN8_YEAST	262	splP25648ISRB8_YEAST	88	8,75	splP32569IMED17_YEAST	349	splP32585IMED18_YEAST	225	6,28
splQ12343IMED4_YEAST	228	splQ12343IMED4_YEAST	234	7,10	splP32569IMED17_YEAST	122	splP19263IMED14_YEAST	257	6,69
splP19263IMED14_YEAST	609	splP19263IMED14_YEAST	594	8,40	splP32570IMED22_YEAST	82	splP32569IMED17_YEAST	324	4,76
splP25648ISRB8_YEAST	665	splP25648ISRB8_YEAST	553	1,94	splP38782IMED6_YEAST	282	splP19263IMED14_YEAST	417	7,91
splP32570IMED22_YEAST	82	splP32570IMED22_YEAST	2	5,80	splP32570IMED22_YEAST	95	splP32569IMED17_YEAST	601	4,36
splQ08278IMED7_YEAST	30	splQ08278IMED7_YEAST	37	5,00	splP32570IMED22_YEAST	95	splP32569IMED17_YEAST	319	9,23
splP47822IMED21_YEAST	45	splP25046IMED19_YEAST	56	2,46	splP34162IMED20_YEAST	21	splP19263IMED14_YEAST	591	5,23
splP25648ISRB8_YEAST	1251	splP25648ISRB8_YEAST	1309	1,19	splP39073ISSN3_YEAST	97	splP39073ISSN3_YEAST	319	6,35
splP34162IMED20_YEAST	21	splP19263IMED14_YEAST	591	4,51	splQ08278IMED7_YEAST	30	splQ08278IMED7_YEAST	37	3,45
splP32570IMED22_YEAST	95	splP32569IMED17_YEAST	319	9,68	splP32569IMED17_YEAST	608	splP32569IMED17_YEAST	555	7,06
splQ08278IMED7_YEAST	30	splQ08278IMED7_YEAST	37	6,94	splQ12343IMED4_YEAST	147	splQ12343IMED4_YEAST	162	2,71
splP19263IMED14_YEAST	674	splP19263IMED14_YEAST	594	2,48	splP39073ISSN3_YEAST	804	splP39073ISSN3_YEAST	823	3,08
splP38931ISSN2_YEAST	573	splP38931ISSN2_YEAST	566	3,44	splP38931ISSN2_YEAST	1398	splP38931ISSN2_YEAST	1002	3,02
splP32569IMED17_YEAST	589	splP32569IMED17_YEAST	601	2,74	splP32569IMED17_YEAST	333	splP32570IMED22_YEAST	2	6,13
splP47822IMED21_YEAST	75	splP38931ISSN2_YEAST	566	1,96	splP32569IMED17_YEAST	68	splP32569IMED17_YEAST	75	9,02
splP38304IMED8_YEAST	191	splP32585IMED18_YEAST	279	5,34	splP38304IMED8_YEAST	210	splP38304IMED8_YEAST	194	2,59
splP19263IMED14_YEAST	726	splP19263IMED14_YEAST	667	4,84	splP32569IMED17_YEAST	333	splP32569IMED17_YEAST	324	5,69
splP19263IMED14_YEAST	594	splP19263IMED14_YEAST	610	3,43	splP32569IMED17_YEAST	608	splP32569IMED17_YEAST	601	2,51
splP32570IMED22_YEAST	95	splP32569IMED17_YEAST	319	6,83	splP19263IMED14_YEAST	549	splP19263IMED14_YEAST	610	4,16
splP25648ISRB8_YEAST	665	splP25648ISRB8_YEAST	553	3,07	splP33308IMED9_YEAST	78	splQ12343IMED4_YEAST	71	4,05
splQ08278IMED7_YEAST	30	splQ08278IMED7_YEAST	37	7,39	splQ99278IMED11_YEAST	68	splQ99278IMED11_YEAST	61	5,42
splP32569IMED17_YEAST	608	splP32569IMED17_YEAST	555	5,06	splP19263IMED14_YEAST	549	splP19263IMED14_YEAST	594	4,61
splP19263IMED14_YEAST	678	splP19263IMED14_YEAST	667	6,57	splP38304IMED8_YEAST	191	splP32585IMED18_YEAST	279	6,63

P1	R1	P2	R2	Score	P1	R1	P2	R2	Score
splP25648ISRB8_YEAST	951	splP25648ISRB8_YEAST	959	7,00	splP38931ISSN2_YEAST	573	splP38931ISSN2_YEAST	537	5,09
splP38931ISSN2_YEAST	1398	splP38931ISSN2_YEAST	1002	3,63	splP25648ISRB8_YEAST	951	splP25648ISRB8_YEAST	959	5,10
splP19263IMED14_YEAST	697	splP19263IMED14_YEAST	663	3,20	splQ12343IMED4_YEAST	172	splQ12343IMED4_YEAST	162	2,84
splQ08278IMED7_YEAST	30	splQ08278IMED7_YEAST	37	4,79	splP19263IMED14_YEAST	609	splP19263IMED14_YEAST	594	7,15
splP39073ISSN3_YEAST	550	splP47821ISSN8_YEAST	23	1,30	splP32569IMED17_YEAST	333	splP32569IMED17_YEAST	324	2,35
splP32569IMED17_YEAST	333	splP32569IMED17_YEAST	324	7,20	splP39073ISSN3_YEAST	550	splP47821ISSN8_YEAST	23	2,14
splP39073ISSN3_YEAST	804	splP39073ISSN3_YEAST	823	1,94	splP39073ISSN3_YEAST	39	splP39073ISSN3_YEAST	43	12,64
splQ08278IMED7_YEAST	30	splQ08278IMED7_YEAST	37	3,30	splQ12343IMED4_YEAST	159	splQ12343IMED4_YEAST	165	9,74
splP39073ISSN3_YEAST	804	splP39073ISSN3_YEAST	823	2,95	splP34162IMED20_YEAST	21	splP19263IMED14_YEAST	674	6,37
splP19263IMED14_YEAST	360	splQ12343IMED4_YEAST	2	1,98	splP32569IMED17_YEAST	333	splP32569IMED17_YEAST	324	7,46
splP25648ISRB8_YEAST	1251	splP25648ISRB8_YEAST	1309	1,33	splP38931ISSN2_YEAST	573	splP38931ISSN2_YEAST	566	2,94
splP32569IMED17_YEAST	68	splP32569IMED17_YEAST	71	9,86	splP32570IMED22_YEAST	95	splP32569IMED17_YEAST	319	4,93
splP19263IMED14_YEAST	609	splP19263IMED14_YEAST	594	10,41	splP39073ISSN3_YEAST	550	splP38931ISSN2_YEAST	919	5,99
splP33308IMED9_YEAST	24	splQ12343IMED4_YEAST	2	1,81	splP19263IMED14_YEAST	609	splP19263IMED14_YEAST	594	7,63
splP32569IMED17_YEAST	122	splP19263IMED14_YEAST	282	7,77	splP39073ISSN3_YEAST	782	splP39073ISSN3_YEAST	777	6,50
splQ12343IMED4_YEAST	55	splQ12343IMED4_YEAST	64	9,41	splP32570IMED22_YEAST	2	splP32569IMED17_YEAST	324	7,76
splQ99278IMED11_YEAST	68	splQ99278IMED11_YEAST	61	7,82	splQ08278IMED7_YEAST	30	splQ08278IMED7_YEAST	37	4,18
splP19263IMED14_YEAST	591	splP19263IMED14_YEAST	674	5,36	splP32569IMED17_YEAST	333	splP32570IMED22_YEAST	2	6,39
splP38931ISSN2_YEAST	607	splP47822IMED21_YEAST	93	8,60	splP32569IMED17_YEAST	589	splP32569IMED17_YEAST	601	3,21
splP38931ISSN2_YEAST	607	splP47822IMED21_YEAST	93	8,58	splP32569IMED17_YEAST	608	splP32569IMED17_YEAST	555	7,61
splP19263IMED14_YEAST	674	splP19263IMED14_YEAST	594	5,64	splQ08278IMED7_YEAST	103	splQ12343IMED4_YEAST	162	5,85
splP39073ISSN3_YEAST	820	splP39073ISSN3_YEAST	782	12,07	splP25648ISRB8_YEAST	888	splP25648ISRB8_YEAST	899	4,94
splQ99278IMED11_YEAST	68	splQ99278IMED11_YEAST	61	7,97	splP32569IMED17_YEAST	324	splP32569IMED17_YEAST	333	3,25
splP32585IMED18_YEAST	280	splP32570IMED22_YEAST	2	8,48	splQ08278IMED7_YEAST	30	splQ08278IMED7_YEAST	37	5,95
splP25648ISRB8_YEAST	888	splP25648ISRB8_YEAST	823	5,66	splP47822IMED21_YEAST	100	splP47822IMED21_YEAST	93	5,17
splP47822IMED21_YEAST	100	splP47822IMED21_YEAST	93	12,06	splP39073ISSN3_YEAST	550	splP38931ISSN2_YEAST	919	6,23

P1	R1	P2	R2	Score	P1	R1	P2	R2	Score
splP47822IMED21_YEAST	100	splP47822IMED21_YEAST	93	5,18	splP39073ISSN3_YEAST	216	splP39073ISSN3_YEAST	151	7,28
splP39073ISSN3_YEAST	574	splP39073ISSN3_YEAST	580	9,64	splP32570IMED22_YEAST	82	splP32570IMED22_YEAST	2	4,41
splQ12343IMED4_YEAST	147	splQ12343IMED4_YEAST	162	2,63	splP32585IMED18_YEAST	68	splP32569IMED17_YEAST	589	11,97
splP32569IMED17_YEAST	608	splP32569IMED17_YEAST	555	6,95	splQ12343IMED4_YEAST	228	splQ12343IMED4_YEAST	234	6,18
splP39073ISSN3_YEAST	97	splP39073ISSN3_YEAST	319	6,72	splQ08278IMED7_YEAST	30	splQ08278IMED7_YEAST	37	4,82
splP32570IMED22_YEAST	9	splP32569IMED17_YEAST	333	7,55	splP32569IMED17_YEAST	427	splP32569IMED17_YEAST	434	7,19
splP19263IMED14_YEAST	549	splP19263IMED14_YEAST	591	4,63	splP32570IMED22_YEAST	82	splP32569IMED17_YEAST	324	2,62
splQ08278IMED7_YEAST	103	splQ12343IMED4_YEAST	162	5,04	splP19263IMED14_YEAST	360	splQ12343IMED4_YEAST	2	4,09
splP38931ISSN2_YEAST	607	splP47822IMED21_YEAST	93	8,27	splP25648ISRB8_YEAST	88	splP47821ISSN8_YEAST	262	10,11
splP32585IMED18_YEAST	280	splP32569IMED17_YEAST	333	3,53	splP39073ISSN3_YEAST	97	splP39073ISSN3_YEAST	319	9,32
splP47822IMED21_YEAST	100	splP47822IMED21_YEAST	93	11,57	splP39073ISSN3_YEAST	39	splP39073ISSN3_YEAST	43	12,54
splP38304IMED8_YEAST	191	splP32570IMED22_YEAST	2	6,73	splQ12343IMED4_YEAST	55	splQ12343IMED4_YEAST	64	6,26
splQ99278IMED11_YEAST	68	splQ99278IMED11_YEAST	61	8,59	splP25648ISRB8_YEAST	888	splP25648ISRB8_YEAST	823	6,58
splP32585IMED18_YEAST	280	splP32569IMED17_YEAST	333	6,21	splP19263IMED14_YEAST	614	splP19263IMED14_YEAST	609	8,35
splP19263IMED14_YEAST	418	splQ12343IMED4_YEAST	2	6,54	splP25648ISRB8_YEAST	899	splP25648ISRB8_YEAST	901	16,34
splP38782IMED6_YEAST	282	splP19263IMED14_YEAST	417	7,75	splP32569IMED17_YEAST	608	splP32569IMED17_YEAST	555	7,30
splP39073ISSN3_YEAST	39	splP39073ISSN3_YEAST	43	11,19	splP39073ISSN3_YEAST	820	splP39073ISSN3_YEAST	782	12,42
splP19263IMED14_YEAST	360	splQ12343IMED4_YEAST	2	8,68	splP19263IMED14_YEAST	591	splP19263IMED14_YEAST	674	6,33
splP47822IMED21_YEAST	100	splP47822IMED21_YEAST	93	7,71	splP47822IMED21_YEAST	100	splP47822IMED21_YEAST	93	8,64
splP39073ISSN3_YEAST	820	splP39073ISSN3_YEAST	782	8,02	splP39073ISSN3_YEAST	550	splP47821ISSN8_YEAST	23	6,73
splP19263IMED14_YEAST	360	splQ12343IMED4_YEAST	2	7,52	splP34162IMED20_YEAST	21	splP19263IMED14_YEAST	591	5,06
splP47822IMED21_YEAST	100	splP47822IMED21_YEAST	93	12,85	splP32569IMED17_YEAST	608	splP32569IMED17_YEAST	555	7,04
splP19263IMED14_YEAST	697	splP19263IMED14_YEAST	663	4,04	splP38931ISSN2_YEAST	428	splP38931ISSN2_YEAST	440	9,22
splP39073ISSN3_YEAST	550	splP39073ISSN3_YEAST	580	8,97	splP38304IMED8_YEAST	191	splP32570IMED22_YEAST	2	12,10
splP47822IMED21_YEAST	100	splP47822IMED21_YEAST	93	11,50	splQ12343IMED4_YEAST	64	splQ12343IMED4_YEAST	2	3,32
splP25648ISRB8_YEAST	888	splP25648ISRB8_YEAST	823	11,03	splP32569IMED17_YEAST	333	splP32570IMED22_YEAST	2	8,21

P1	R1	P2	R2	Score	P1	R1	P2	R2	Score
splP47822lMED21_YEAST	100	splP47822lMED21_YEAST	93	9,99	splP32585lMED18_YEAST	68	splP32569lMED17_YEAST	589	10,87
splP19263lMED14_YEAST	549	splP19263lMED14_YEAST	610	10,39	splP32569lMED17_YEAST	608	splP32569lMED17_YEAST	555	7,78
splP47822lMED21_YEAST	75	splP38931lSSN2_YEAST	607	15,80	splP19263lMED14_YEAST	360	splQ12343lMED4_YEAST	2	7,17
splP19263lMED14_YEAST	697	splP19263lMED14_YEAST	663	9,69	splP47821lSSN8_YEAST	262	splP25648lSRB8_YEAST	88	10,96
splP39073lSSN3_YEAST	550	splP47821lSSN8_YEAST	23	4,32	splP32569lMED17_YEAST	319	splP32569lMED17_YEAST	427	8,45
splP19263lMED14_YEAST	667	splP19263lMED14_YEAST	674	6,00	splP39073lSSN3_YEAST	804	splP39073lSSN3_YEAST	823	2,19
splP19263lMED14_YEAST	436	splQ12343lMED4_YEAST	2	6,05	splP25648lSRB8_YEAST	888	splP25648lSRB8_YEAST	823	5,21
splP25648lSRB8_YEAST	899	splP25648lSRB8_YEAST	901	15,72	splP19263lMED14_YEAST	549	splP19263lMED14_YEAST	591	12,44
splP38931lSSN2_YEAST	1208	splP47821lSSN8_YEAST	23	9,00	splP39073lSSN3_YEAST	116	splP39073lSSN3_YEAST	189	4,59
splP32585lMED18_YEAST	68	splP32569lMED17_YEAST	589	11,99	splP32570lMED22_YEAST	9	splP32569lMED17_YEAST	333	7,65
splQ99278lMED11_YEAST	68	splQ99278lMED11_YEAST	61	6,97	splP32569lMED17_YEAST	555	splP32569lMED17_YEAST	608	4,62
splP19263lMED14_YEAST	591	splP19263lMED14_YEAST	610	6,80	splQ12343lMED4_YEAST	55	splQ12343lMED4_YEAST	64	6,81
splP32569lMED17_YEAST	333	splP32570lMED22_YEAST	2	8,86	splP32569lMED17_YEAST	608	splP32569lMED17_YEAST	555	8,14
splP25648lSRB8_YEAST	888	splP25648lSRB8_YEAST	823	6,20	splP47822lMED21_YEAST	100	splP47822lMED21_YEAST	93	12,11
splP32569lMED17_YEAST	78	splP32569lMED17_YEAST	71	5,53	splP34162lMED20_YEAST	21	splP19263lMED14_YEAST	591	7,83
splP19263lMED14_YEAST	697	splP19263lMED14_YEAST	663	8,28	splP47822lMED21_YEAST	100	splP47822lMED21_YEAST	93	8,87
splP47822lMED21_YEAST	100	splP47822lMED21_YEAST	93	7,32	splQ12343lMED4_YEAST	36	splP33308lMED9_YEAST	117	5,33
splP39073lSSN3_YEAST	804	splP39073lSSN3_YEAST	823	2,73	splP39073lSSN3_YEAST	97	splP39073lSSN3_YEAST	319	5,98
splP32569lMED17_YEAST	333	splP32569lMED17_YEAST	324	12,84	splQ12343lMED4_YEAST	55	splQ12343lMED4_YEAST	64	11,65
splP19263lMED14_YEAST	674	splP19263lMED14_YEAST	594	8,01	splP39073lSSN3_YEAST	804	splP39073lSSN3_YEAST	823	3,21
splP39073lSSN3_YEAST	550	splP39073lSSN3_YEAST	580	10,90	splP25648lSRB8_YEAST	888	splP25648lSRB8_YEAST	823	7,20
splP32569lMED17_YEAST	333	splP32569lMED17_YEAST	324	11,18	splP19263lMED14_YEAST	282	splP19263lMED14_YEAST	257	5,81
splP19263lMED14_YEAST	697	splP19263lMED14_YEAST	663	4,75	splP38931lSSN2_YEAST	796	splP38931lSSN2_YEAST	204	11,53
splP19263lMED14_YEAST	451	splP19263lMED14_YEAST	418	5,12	splP25648lSRB8_YEAST	899	splP25648lSRB8_YEAST	901	17,07
splP19263lMED14_YEAST	697	splP19263lMED14_YEAST	663	5,42	splP39073lSSN3_YEAST	782	splP39073lSSN3_YEAST	777	7,85
splP47822lMED21_YEAST	100	splP47822lMED21_YEAST	93	11,48	splP39073lSSN3_YEAST	550	splP39073lSSN3_YEAST	580	9,64

P1	R1	P2	R2	Score	P1	R1	P2	R2	Score
splP32569IMED17_YEAST	78	splP32569IMED17_YEAST	71	4,43	splQ12343IMED4_YEAST	55	splQ12343IMED4_YEAST	64	8,13
splP32569IMED17_YEAST	115	splP19263IMED14_YEAST	360	7,85	splP32570IMED22_YEAST	9	splP32569IMED17_YEAST	333	7,39
splP32569IMED17_YEAST	608	splP32569IMED17_YEAST	555	6,56	splQ12343IMED4_YEAST	64	splQ12343IMED4_YEAST	2	5,74
splP38931ISSN2_YEAST	1024	splP39073ISSN3_YEAST	550	13,71	splQ99278IMED11_YEAST	68	splQ99278IMED11_YEAST	61	5,52
splP25648ISRB8_YEAST	888	splP25648ISRB8_YEAST	823	4,83	splP39073ISSN3_YEAST	39	splP39073ISSN3_YEAST	43	12,89
splP19263IMED14_YEAST	697	splP19263IMED14_YEAST	663	9,36	splQ12321IMED1_YEAST	198	splQ12321IMED1_YEAST	217	5,89
splP32569IMED17_YEAST	319	splP32569IMED17_YEAST	427	8,64	splQ99278IMED11_YEAST	68	splQ99278IMED11_YEAST	61	7,90
splP19263IMED14_YEAST	417	splQ12343IMED4_YEAST	2	11,32	splP32570IMED22_YEAST	2	splP32569IMED17_YEAST	324	10,72
splP38304IMED8_YEAST	191	splP32570IMED22_YEAST	2	5,91	splP47822IMED21_YEAST	100	splP47822IMED21_YEAST	93	8,52
splP25648ISRB8_YEAST	888	splP25648ISRB8_YEAST	823	5,39	splP39073ISSN3_YEAST	216	splP39073ISSN3_YEAST	151	7,49
splP25648ISRB8_YEAST	899	splP25648ISRB8_YEAST	901	10,15	splP38782IMED6_YEAST	282	splP19263IMED14_YEAST	417	8,81
splP38931ISSN2_YEAST	1398	splP38931ISSN2_YEAST	1002	2,44	splP19263IMED14_YEAST	418	splQ12343IMED4_YEAST	2	7,17
splP38304IMED8_YEAST	191	splP32570IMED22_YEAST	2	10,00	splP32569IMED17_YEAST	333	splP32569IMED17_YEAST	324	10,57
splP39073ISSN3_YEAST	216	splP39073ISSN3_YEAST	151	7,09	splP32569IMED17_YEAST	608	splP32569IMED17_YEAST	555	8,99
splP25648ISRB8_YEAST	665	splP25648ISRB8_YEAST	553	4,11	splQ99278IMED11_YEAST	68	splQ99278IMED11_YEAST	61	7,27
splP32569IMED17_YEAST	333	splP32570IMED22_YEAST	2	5,48	splP47822IMED21_YEAST	100	splP47822IMED21_YEAST	93	10,23
splP25648ISRB8_YEAST	88	splP38931ISSN2_YEAST	1114	8,08	splP33308IMED9_YEAST	78	splQ12343IMED4_YEAST	71	7,02
splP25648ISRB8_YEAST	899	splP25648ISRB8_YEAST	901	2,97	splP32569IMED17_YEAST	427	splP32569IMED17_YEAST	434	5,24
splP19263IMED14_YEAST	674	splP19263IMED14_YEAST	594	5,66	splP25648ISRB8_YEAST	899	splP25648ISRB8_YEAST	901	12,07
splP39073ISSN3_YEAST	804	splP39073ISSN3_YEAST	823	3,32	splP25648ISRB8_YEAST	888	splP25648ISRB8_YEAST	823	7,56
splP19263IMED14_YEAST	549	splP19263IMED14_YEAST	594	5,68	splP38782IMED6_YEAST	282	splP19263IMED14_YEAST	417	12,49
splP19263IMED14_YEAST	609	splP19263IMED14_YEAST	591	9,54	splP47822IMED21_YEAST	100	splP47822IMED21_YEAST	93	7,48
splP39073ISSN3_YEAST	116	splP39073ISSN3_YEAST	189	6,14	splP25648ISRB8_YEAST	888	splP25648ISRB8_YEAST	823	6,66
splQ08278IMED7_YEAST	30	splQ08278IMED7_YEAST	37	4,35	splP32569IMED17_YEAST	608	splP32569IMED17_YEAST	555	9,49
splP38304IMED8_YEAST	191	splP32570IMED22_YEAST	2	6,76	splP39073ISSN3_YEAST	782	splP39073ISSN3_YEAST	777	5,45
splP32570IMED22_YEAST	2	splP32569IMED17_YEAST	324	9,02	splP39073ISSN3_YEAST	550	splP47821ISSN8_YEAST	23	7,91

P1	R1	P2	R2	Score	P1	R1	P2	R2	Score
splP39073ISSN3_YEAST	216	splP39073ISSN3_YEAST	151	8,94	splP32569IMED17_YEAST	324	splP32569IMED17_YEAST	333	8,46
splP25648ISRB8_YEAST	899	splP25648ISRB8_YEAST	901	16,69	splP38931ISSN2_YEAST	233	splP38931ISSN2_YEAST	174	8,80
splP39073ISSN3_YEAST	97	splP39073ISSN3_YEAST	319	9,12	splP38931ISSN2_YEAST	573	splP38931ISSN2_YEAST	566	3,75
splP25648ISRB8_YEAST	145	splP25648ISRB8_YEAST	168	3,39	splP47822IMED21_YEAST	100	splP47822IMED21_YEAST	93	9,37
splP25648ISRB8_YEAST	899	splP25648ISRB8_YEAST	901	11,75	splQ99278IMED11_YEAST	53	splQ99278IMED11_YEAST	61	5,64
splP47821ISSN8_YEAST	262	splP25648ISRB8_YEAST	88	13,31	splP19263IMED14_YEAST	451	splP19263IMED14_YEAST	418	6,83
splP38931ISSN2_YEAST	428	splP38931ISSN2_YEAST	440	7,40	splP38782IMED6_YEAST	282	splP19263IMED14_YEAST	417	9,10
splP19263IMED14_YEAST	678	splP19263IMED14_YEAST	667	5,95	splP47822IMED21_YEAST	100	splP47822IMED21_YEAST	93	8,15
splP19263IMED14_YEAST	609	splP19263IMED14_YEAST	594	14,72	splQ12343IMED4_YEAST	55	splQ12343IMED4_YEAST	64	11,32
splQ99278IMED11_YEAST	68	splQ99278IMED11_YEAST	61	8,25	splP39073ISSN3_YEAST	782	splP39073ISSN3_YEAST	777	6,12
splP39073ISSN3_YEAST	550	splP47821ISSN8_YEAST	23	4,18	splP39073ISSN3_YEAST	820	splP39073ISSN3_YEAST	782	9,74
splP38931ISSN2_YEAST	555	splP38931ISSN2_YEAST	537	7,85	splP32569IMED17_YEAST	427	splP32569IMED17_YEAST	434	7,89
splP39073ISSN3_YEAST	550	splP47821ISSN8_YEAST	23	6,58	splP32585IMED18_YEAST	68	splP32569IMED17_YEAST	589	9,96
splP47822IMED21_YEAST	100	splP47822IMED21_YEAST	93	5,41	splP19263IMED14_YEAST	360	splQ12343IMED4_YEAST	2	5,79
splP38931ISSN2_YEAST	573	splP38931ISSN2_YEAST	566	4,92	splP47822IMED21_YEAST	100	splP47822IMED21_YEAST	93	7,44
splP19263IMED14_YEAST	549	splP19263IMED14_YEAST	591	7,37	splQ99278IMED11_YEAST	68	splQ99278IMED11_YEAST	61	6,81
splP19263IMED14_YEAST	417	splQ12343IMED4_YEAST	2	10,96	splP38931ISSN2_YEAST	573	splP38931ISSN2_YEAST	566	4,39
splP38931ISSN2_YEAST	537	splP38931ISSN2_YEAST	566	4,76	splP32570IMED22_YEAST	2	splP32569IMED17_YEAST	324	10,22
splP25648ISRB8_YEAST	665	splP25648ISRB8_YEAST	553	4,83	splP38304IMED8_YEAST	191	splP32570IMED22_YEAST	2	10,43
splP33308IMED9_YEAST	78	splQ12343IMED4_YEAST	2	5,42	splP19263IMED14_YEAST	451	splP19263IMED14_YEAST	418	5,82
splP34162IMED20_YEAST	21	splP19263IMED14_YEAST	591	6,99	splP32569IMED17_YEAST	333	splP32570IMED22_YEAST	2	6,28
splQ99278IMED11_YEAST	68	splQ99278IMED11_YEAST	61	8,64	splP19263IMED14_YEAST	591	splP19263IMED14_YEAST	674	6,07
splP38931ISSN2_YEAST	573	splP38931ISSN2_YEAST	566	3,51	splP19263IMED14_YEAST	418	splQ12343IMED4_YEAST	2	7,72
splP39073ISSN3_YEAST	97	splP39073ISSN3_YEAST	319	8,84	splP25648ISRB8_YEAST	899	splP25648ISRB8_YEAST	901	7,30
splP38931ISSN2_YEAST	573	splP38931ISSN2_YEAST	555	9,84	splP19263IMED14_YEAST	678	splP19263IMED14_YEAST	667	6,08
splP19263IMED14_YEAST	549	splP19263IMED14_YEAST	591	8,85	splP32569IMED17_YEAST	608	splP32569IMED17_YEAST	555	8,20

P1	R1	P2	R2	Score	P1	R1	P2	R2	Score
splP39073ISSN3_YEAST	39	splP39073ISSN3_YEAST	43	13,60	splP32569IMED17_YEAST	333	splP32570IMED22_YEAST	2	7,57
splP25648ISRB8_YEAST	665	splP25648ISRB8_YEAST	553	4,14	splP47822IMED21_YEAST	100	splP47822IMED21_YEAST	93	12,66
splP47822IMED21_YEAST	100	splP47822IMED21_YEAST	93	10,37	splP19263IMED14_YEAST	591	splP19263IMED14_YEAST	674	8,82
splP19263IMED14_YEAST	678	splP19263IMED14_YEAST	667	7,56	splP32569IMED17_YEAST	423	splP32569IMED17_YEAST	427	9,56
splP32585IMED18_YEAST	280	splP32569IMED17_YEAST	333	6,89	splP25648ISRB8_YEAST	813	splP25648ISRB8_YEAST	789	7,83
splP19263IMED14_YEAST	678	splP19263IMED14_YEAST	594	5,33	splP25648ISRB8_YEAST	899	splP25648ISRB8_YEAST	901	12,66
splP25648ISRB8_YEAST	899	splP25648ISRB8_YEAST	901	13,08	splQ99278IMED11_YEAST	68	splQ99278IMED11_YEAST	61	7,52
splP19263IMED14_YEAST	417	splQ12343IMED4_YEAST	2	3,62	splQ99278IMED11_YEAST	68	splQ99278IMED11_YEAST	61	5,92
splP32570IMED22_YEAST	82	splP32569IMED17_YEAST	333	4,36	splP38304IMED8_YEAST	191	splP32570IMED22_YEAST	2	9,03
splP19263IMED14_YEAST	436	splP19263IMED14_YEAST	418	5,67	splQ99278IMED11_YEAST	68	splQ99278IMED11_YEAST	61	8,51
splP32569IMED17_YEAST	333	splP32570IMED22_YEAST	2	10,63	splP39073ISSN3_YEAST	216	splP39073ISSN3_YEAST	151	7,96
splP47821ISSN8_YEAST	262	splP25648ISRB8_YEAST	88	10,71	splP32569IMED17_YEAST	319	splP32569IMED17_YEAST	427	9,73
splP38931ISSN2_YEAST	1398	splP38931ISSN2_YEAST	1002	2,43	splP19263IMED14_YEAST	360	splQ12343IMED4_YEAST	2	7,55
splP32585IMED18_YEAST	280	splP32569IMED17_YEAST	333	5,15	splP25648ISRB8_YEAST	888	splP25648ISRB8_YEAST	823	6,13
splP19263IMED14_YEAST	436	splQ12343IMED4_YEAST	2	4,49	splP39073ISSN3_YEAST	574	splP39073ISSN3_YEAST	550	8,14
splP38931ISSN2_YEAST	573	splP38931ISSN2_YEAST	566	2,64	splP25648ISRB8_YEAST	899	splP25648ISRB8_YEAST	901	6,56
splP25648ISRB8_YEAST	632	splP25648ISRB8_YEAST	665	8,45	splP19263IMED14_YEAST	549	splP19263IMED14_YEAST	591	10,85
splP47822IMED21_YEAST	100	splP47822IMED21_YEAST	93	4,45	splP25648ISRB8_YEAST	888	splP25648ISRB8_YEAST	820	4,19
splP32569IMED17_YEAST	608	splP32569IMED17_YEAST	555	6,40	splP32585IMED18_YEAST	68	splP32569IMED17_YEAST	589	11,36
splP32569IMED17_YEAST	427	splP32569IMED17_YEAST	434	4,87	splP19263IMED14_YEAST	594	splP19263IMED14_YEAST	610	6,94
splP39073ISSN3_YEAST	804	splP39073ISSN3_YEAST	823	4,46	splP47822IMED21_YEAST	100	splP47822IMED21_YEAST	93	10,76
splP47821ISSN8_YEAST	70	splP47821ISSN8_YEAST	23	3,64	splP32569IMED17_YEAST	68	splP32569IMED17_YEAST	71	10,59
splP38931ISSN2_YEAST	1398	splP38931ISSN2_YEAST	1002	1,97	splP32569IMED17_YEAST	333	splP32570IMED22_YEAST	2	13,69
splP19263IMED14_YEAST	591	splP19263IMED14_YEAST	674	6,01	splP34162IMED20_YEAST	21	splP19263IMED14_YEAST	591	5,48
splP38931ISSN2_YEAST	1398	splP38931ISSN2_YEAST	1002	3,44	splP25648ISRB8_YEAST	899	splP25648ISRB8_YEAST	901	8,55
splP39073ISSN3_YEAST	39	splP39073ISSN3_YEAST	43	12,13	splP32585IMED18_YEAST	280	splP32570IMED22_YEAST	2	6,38

P1	R1	P2	R2	Score	P1	R1	P2	R2	Score
splP32569IMED17_YEAST	608	splP32569IMED17_YEAST	555	6,89	splP38931ISSN2_YEAST	457	splP38931ISSN2_YEAST	440	9,34
splP38304IMED8_YEAST	191	splP32585IMED18_YEAST	279	3,88	splP19263IMED14_YEAST	549	splP19263IMED14_YEAST	567	8,95
splP47822IMED21_YEAST	100	splP47822IMED21_YEAST	93	4,91	splP19263IMED14_YEAST	418	splQ12343IMED4_YEAST	2	5,55
splP19263IMED14_YEAST	549	splP19263IMED14_YEAST	610	5,76	splP19263IMED14_YEAST	591	splP19263IMED14_YEAST	674	8,40
splP25648ISRB8_YEAST	899	splP25648ISRB8_YEAST	901	15,09	splP19263IMED14_YEAST	697	splP19263IMED14_YEAST	663	2,68
splP19263IMED14_YEAST	282	splP19263IMED14_YEAST	257	5,91	splP19263IMED14_YEAST	591	splP19263IMED14_YEAST	674	6,79
splP47822IMED21_YEAST	100	splP47822IMED21_YEAST	93	7,09	splP25648ISRB8_YEAST	888	splP25648ISRB8_YEAST	823	5,08
splP38304IMED8_YEAST	191	splP32570IMED22_YEAST	2	7,67	splP39073ISSN3_YEAST	804	splP39073ISSN3_YEAST	823	3,14
splQ99278IMED11_YEAST	68	splQ99278IMED11_YEAST	61	5,21	splP32569IMED17_YEAST	608	splP32569IMED17_YEAST	555	7,45
splP39073ISSN3_YEAST	216	splP39073ISSN3_YEAST	151	5,42	splQ08278IMED7_YEAST	30	splQ08278IMED7_YEAST	37	6,44
splP39073ISSN3_YEAST	97	splP39073ISSN3_YEAST	319	7,89	splP32585IMED18_YEAST	280	splP32569IMED17_YEAST	333	4,98
splP38931ISSN2_YEAST	573	splP38931ISSN2_YEAST	566	3,30	splP32585IMED18_YEAST	280	splP32570IMED22_YEAST	2	5,44
splP25648ISRB8_YEAST	888	splP25648ISRB8_YEAST	823	4,88	splP47822IMED21_YEAST	45	splP25046IMED19_YEAST	56	2,67
splP19263IMED14_YEAST	614	splP19263IMED14_YEAST	594	3,59	splP19263IMED14_YEAST	282	splP19263IMED14_YEAST	257	10,33
splP39073ISSN3_YEAST	39	splP39073ISSN3_YEAST	43	10,91	splP38931ISSN2_YEAST	607	splP47822IMED21_YEAST	93	6,84
splP19263IMED14_YEAST	697	splP19263IMED14_YEAST	663	5,77	splP19263IMED14_YEAST	591	splP19263IMED14_YEAST	674	5,45
splP39073ISSN3_YEAST	782	splP38304IMED8_YEAST	191	2,67	splP38782IMED6_YEAST	282	splP19263IMED14_YEAST	417	7,60
splP19263IMED14_YEAST	697	splP19263IMED14_YEAST	663	4,55	splP38931ISSN2_YEAST	1024	splP39073ISSN3_YEAST	574	9,44
splP38931ISSN2_YEAST	573	splP38931ISSN2_YEAST	555	10,95	splP47822IMED21_YEAST	75	splP38931ISSN2_YEAST	607	13,19
splP39073ISSN3_YEAST	804	splP39073ISSN3_YEAST	823	3,51	splP19263IMED14_YEAST	549	splP19263IMED14_YEAST	610	7,70
splP39073ISSN3_YEAST	574	splP39073ISSN3_YEAST	580	5,43	splP25648ISRB8_YEAST	899	splP25648ISRB8_YEAST	901	13,22
splP39073ISSN3_YEAST	804	splP39073ISSN3_YEAST	823	3,47	splP25648ISRB8_YEAST	888	splP25648ISRB8_YEAST	823	3,42
splP32570IMED22_YEAST	9	splP32569IMED17_YEAST	333	7,55	splP47822IMED21_YEAST	100	splP47822IMED21_YEAST	93	4,38
splP38931ISSN2_YEAST	457	splP38931ISSN2_YEAST	440	10,30	splP25648ISRB8_YEAST	665	splP25648ISRB8_YEAST	553	6,42
splP34162IMED20_YEAST	21	splP19263IMED14_YEAST	591	6,19	splP19263IMED14_YEAST	678	splP19263IMED14_YEAST	667	5,45
splP32569IMED17_YEAST	333	splP32570IMED22_YEAST	2	5,34	splP32585IMED18_YEAST	280	splP32569IMED17_YEAST	333	6,71

P1	R1	P2	R2	Score	P1	R1	P2	R2	Score
splP32570IMED22_YEAST	95	splP32569IMED17_YEAST	319	8,69	splP19263IMED14_YEAST	609	splP19263IMED14_YEAST	594	13,47
splP38304IMED8_YEAST	191	splP32570IMED22_YEAST	2	6,57	splQ99278IMED11_YEAST	68	splQ99278IMED11_YEAST	61	8,68
splP25648ISRB8_YEAST	899	splP25648ISRB8_YEAST	901	12,20	splP25648ISRB8_YEAST	813	splP25648ISRB8_YEAST	820	11,77
splP19263IMED14_YEAST	609	splP19263IMED14_YEAST	594	11,82	splP47822IMED21_YEAST	100	splP47822IMED21_YEAST	93	7,09
splP19263IMED14_YEAST	674	splP19263IMED14_YEAST	594	3,43	splP19263IMED14_YEAST	549	splP19263IMED14_YEAST	567	5,27
splP25648ISRB8_YEAST	888	splP25648ISRB8_YEAST	823	7,02	splP47822IMED21_YEAST	100	splP47822IMED21_YEAST	93	3,29
splP38931ISSN2_YEAST	457	splP38931ISSN2_YEAST	440	10,12	splP32585IMED18_YEAST	68	splP32569IMED17_YEAST	589	11,16
splQ12321IMED1_YEAST	389	splQ12321IMED1_YEAST	421	4,06	splP19263IMED14_YEAST	678	splP19263IMED14_YEAST	667	5,28
splP25648ISRB8_YEAST	145	splP25648ISRB8_YEAST	168	1,45	splP39073ISSN3_YEAST	97	splP39073ISSN3_YEAST	319	8,51
splQ06213IMED10_YEAST	119	splP38931ISSN2_YEAST	566	6,06	splP47822IMED21_YEAST	100	splP47822IMED21_YEAST	93	8,33
splP32570IMED22_YEAST	9	splP32569IMED17_YEAST	333	6,25	splP39073ISSN3_YEAST	574	splP39073ISSN3_YEAST	580	4,45
splP38931ISSN2_YEAST	573	splP38931ISSN2_YEAST	566	4,26	splP19263IMED14_YEAST	549	splP19263IMED14_YEAST	610	5,03
splP25648ISRB8_YEAST	888	splP25648ISRB8_YEAST	823	5,20	splP38931ISSN2_YEAST	573	splP38931ISSN2_YEAST	555	8,21
splQ12343IMED4_YEAST	55	splQ12343IMED4_YEAST	64	8,23	splP19263IMED14_YEAST	549	splQ12343IMED4_YEAST	2	8,17
splQ08278IMED7_YEAST	30	splQ08278IMED7_YEAST	37	5,56	splP47821ISSN8_YEAST	70	splP38931ISSN2_YEAST	1212	6,73
splP32569IMED17_YEAST	333	splP32569IMED17_YEAST	324	10,10	splP25648ISRB8_YEAST	888	splP25648ISRB8_YEAST	823	4,34
splP32570IMED22_YEAST	82	splP32569IMED17_YEAST	333	5,67	splQ08278IMED7_YEAST	30	splQ08278IMED7_YEAST	37	5,32
splP47822IMED21_YEAST	100	splP47822IMED21_YEAST	93	2,48	splP39073ISSN3_YEAST	574	splP39073ISSN3_YEAST	580	4,80
splP32570IMED22_YEAST	2	splP32569IMED17_YEAST	324	10,02	splP39073ISSN3_YEAST	530	splP47821ISSN8_YEAST	23	4,82
splP19263IMED14_YEAST	678	splP19263IMED14_YEAST	594	3,02	splP25648ISRB8_YEAST	888	splP25648ISRB8_YEAST	823	5,55
splP19263IMED14_YEAST	549	splP19263IMED14_YEAST	591	6,62	splP39073ISSN3_YEAST	782	splP39073ISSN3_YEAST	777	6,48
splP19263IMED14_YEAST	549	splP19263IMED14_YEAST	610	3,35	splQ08278IMED7_YEAST	30	splQ08278IMED7_YEAST	37	5,02
splP25648ISRB8_YEAST	899	splP25648ISRB8_YEAST	901	5,79	splP25648ISRB8_YEAST	899	splP25648ISRB8_YEAST	901	9,32
splP19263IMED14_YEAST	360	splQ12343IMED4_YEAST	2	5,94	splP38304IMED8_YEAST	191	splP32570IMED22_YEAST	2	5,06
splP39073ISSN3_YEAST	116	splP39073ISSN3_YEAST	189	3,94	splP32570IMED22_YEAST	82	splP32569IMED17_YEAST	333	5,20
splP25648ISRB8_YEAST	665	splP25648ISRB8_YEAST	553	4,84	splP32570IMED22_YEAST	2	splP32569IMED17_YEAST	324	5,92

P1	R1	P2	R2	Score	P1	R1	P2	R2	Score
splQ99278IMED11_YEAST	68	splQ99278IMED11_YEAST	61	6,79	splQ08278IMED7_YEAST	1	splP38633IMED31_YEAST	2	19,19
splQ12343IMED4_YEAST	64	splQ12343IMED4_YEAST	2	3,21	splP32569IMED17_YEAST	122	splP19263IMED14_YEAST	282	8,62
splP32569IMED17_YEAST	333	splP32570IMED22_YEAST	2	7,24	splP38931ISSN2_YEAST	1398	splP38931ISSN2_YEAST	1002	5,39
splP39073ISSN3_YEAST	574	splP39073ISSN3_YEAST	580	5,55	splP19263IMED14_YEAST	417	splQ12343IMED4_YEAST	2	8,75
splP32570IMED22_YEAST	82	splP32569IMED17_YEAST	333	6,70	splP39073ISSN3_YEAST	804	splP39073ISSN3_YEAST	823	4,00
splP32569IMED17_YEAST	333	splP32570IMED22_YEAST	2	5,57	splP32570IMED22_YEAST	82	splP32569IMED17_YEAST	333	4,54
splP38931ISSN2_YEAST	607	splP47822IMED21_YEAST	93	8,15	splP25648ISRB8_YEAST	899	splP25648ISRB8_YEAST	901	10,64
splP39073ISSN3_YEAST	39	splP39073ISSN3_YEAST	43	12,13	splP38931ISSN2_YEAST	545	splP38931ISSN2_YEAST	534	2,36
splP39073ISSN3_YEAST	530	splP39073ISSN3_YEAST	550	10,02	splQ12343IMED4_YEAST	55	splQ12343IMED4_YEAST	64	5,14
splP39073ISSN3_YEAST	804	splP39073ISSN3_YEAST	823	3,62	splP32570IMED22_YEAST	2	splP32569IMED17_YEAST	324	9,93
splP32570IMED22_YEAST	9	splP32569IMED17_YEAST	333	3,61	splP32570IMED22_YEAST	2	splP32569IMED17_YEAST	324	7,43
splP34162IMED20_YEAST	21	splP19263IMED14_YEAST	591	6,24	splP32585IMED18_YEAST	280	splP32569IMED17_YEAST	333	8,01
splP47822IMED21_YEAST	100	splP47822IMED21_YEAST	93	6,47	splP32569IMED17_YEAST	589	splP32569IMED17_YEAST	601	6,09
splP19263IMED14_YEAST	697	splP19263IMED14_YEAST	663	7,11	splP39073ISSN3_YEAST	39	splP39073ISSN3_YEAST	43	11,17
splP25648ISRB8_YEAST	899	splP25648ISRB8_YEAST	901	14,10	splP25648ISRB8_YEAST	899	splP25648ISRB8_YEAST	901	11,14
splP38931ISSN2_YEAST	1398	splP38931ISSN2_YEAST	1002	2,58	splP32585IMED18_YEAST	280	splP32569IMED17_YEAST	333	10,30
splP25648ISRB8_YEAST	888	splP25648ISRB8_YEAST	823	3,70	splP19263IMED14_YEAST	678	splP19263IMED14_YEAST	667	5,75
splP19263IMED14_YEAST	678	splP19263IMED14_YEAST	667	7,98	splP32585IMED18_YEAST	83	splP32585IMED18_YEAST	97	9,38
splP33308IMED9_YEAST	78	splQ12343IMED4_YEAST	2	5,33	splP32569IMED17_YEAST	608	splP32569IMED17_YEAST	555	7,46
splP38782IMED6_YEAST	282	splP19263IMED14_YEAST	417	7,64	splP19263IMED14_YEAST	549	splP19263IMED14_YEAST	610	7,60
splQ99278IMED11_YEAST	53	splQ99278IMED11_YEAST	61	7,84	splP32569IMED17_YEAST	608	splP32569IMED17_YEAST	555	7,64
splP32569IMED17_YEAST	333	splP32569IMED17_YEAST	324	5,06	splP38304IMED8_YEAST	191	splP32570IMED22_YEAST	2	7,35
splQ12343IMED4_YEAST	138	splQ12343IMED4_YEAST	147	8,71	splP19263IMED14_YEAST	417	splQ12343IMED4_YEAST	2	10,17
splP32570IMED22_YEAST	2	splP32569IMED17_YEAST	324	11,12	splP32569IMED17_YEAST	333	splP32570IMED22_YEAST	2	9,04
splP25648ISRB8_YEAST	888	splP25648ISRB8_YEAST	823	6,91	splP39073ISSN3_YEAST	804	splP39073ISSN3_YEAST	823	3,01
splP19263IMED14_YEAST	697	splP19263IMED14_YEAST	663	4,97	splP32569IMED17_YEAST	333	splP32570IMED22_YEAST	2	9,53

P1	R1	P2	R2	Score	P1	R1	P2	R2	Score
splP32569IMED17_YEAST	75	splP32569IMED17_YEAST	81	4,03	splP19263IMED14_YEAST	674	splP19263IMED14_YEAST	594	5,39
splP39073ISSN3_YEAST	804	splP39073ISSN3_YEAST	823	2,36	splP32569IMED17_YEAST	333	splP32569IMED17_YEAST	324	5,67
splP39073ISSN3_YEAST	550	splP47821ISSN8_YEAST	23	2,95	splP32569IMED17_YEAST	333	splP32570IMED22_YEAST	2	10,32
splP38931ISSN2_YEAST	1398	splP38931ISSN2_YEAST	1002	3,71	splP39073ISSN3_YEAST	550	splP47821ISSN8_YEAST	23	8,19
splP32570IMED22_YEAST	82	splP32570IMED22_YEAST	2	5,82	splQ12343IMED4_YEAST	55	splQ12343IMED4_YEAST	64	7,41
splP19263IMED14_YEAST	674	splP19263IMED14_YEAST	594	6,11	splP19263IMED14_YEAST	609	splP19263IMED14_YEAST	594	15,25
splP32570IMED22_YEAST	9	splP32569IMED17_YEAST	333	5,43	splP32570IMED22_YEAST	2	splP32569IMED17_YEAST	324	8,05
splP39073ISSN3_YEAST	804	splP39073ISSN3_YEAST	823	2,47	splP39073ISSN3_YEAST	782	splP39073ISSN3_YEAST	777	5,47
splP32570IMED22_YEAST	82	splP32569IMED17_YEAST	333	4,68	splP32570IMED22_YEAST	9	splP32569IMED17_YEAST	333	7,16
splP39073ISSN3_YEAST	804	splP39073ISSN3_YEAST	823	1,47	splP19263IMED14_YEAST	591	splP19263IMED14_YEAST	674	5,82
splP39073ISSN3_YEAST	550	splP38931ISSN2_YEAST	919	7,00	splP39073ISSN3_YEAST	804	splP39073ISSN3_YEAST	823	3,57
splP19263IMED14_YEAST	282	splP19263IMED14_YEAST	257	7,03	splP19263IMED14_YEAST	549	splP19263IMED14_YEAST	591	6,10
splQ12343IMED4_YEAST	71	splQ12321IMED1_YEAST	118	8,24	splP38931ISSN2_YEAST	537	splP38931ISSN2_YEAST	566	4,68
splP47822IMED21_YEAST	100	splP47822IMED21_YEAST	93	4,64	splP39073ISSN3_YEAST	550	splP38931ISSN2_YEAST	919	7,06
splP19263IMED14_YEAST	417	splQ12343IMED4_YEAST	2	3,33	splP32570IMED22_YEAST	2	splP32569IMED17_YEAST	324	4,95
splP32569IMED17_YEAST	333	splP32569IMED17_YEAST	324	4,37	splP19263IMED14_YEAST	360	splQ12343IMED4_YEAST	2	5,80
splQ12343IMED4_YEAST	147	splQ12343IMED4_YEAST	162	2,72	splP25648ISRB8_YEAST	888	splP25648ISRB8_YEAST	823	7,03
splP19263IMED14_YEAST	591	splP19263IMED14_YEAST	674	4,47	splP25648ISRB8_YEAST	899	splP25648ISRB8_YEAST	901	11,37
splP39073ISSN3_YEAST	39	splP39073ISSN3_YEAST	43	10,72	splP39073ISSN3_YEAST	782	splP39073ISSN3_YEAST	777	6,91
splP32569IMED17_YEAST	333	splP32569IMED17_YEAST	324	6,87	splP19263IMED14_YEAST	360	splQ12343IMED4_YEAST	2	3,21
splP32570IMED22_YEAST	2	splP32569IMED17_YEAST	324	7,77	splP32569IMED17_YEAST	386	splP32569IMED17_YEAST	427	7,06
splP32569IMED17_YEAST	333	splP32569IMED17_YEAST	324	8,87	splP39073ISSN3_YEAST	804	splP39073ISSN3_YEAST	823	2,92
splP19263IMED14_YEAST	674	splP19263IMED14_YEAST	594	5,90	splP32569IMED17_YEAST	608	splP32569IMED17_YEAST	555	7,69
splP39073ISSN3_YEAST	97	splP39073ISSN3_YEAST	319	8,00	splP39073ISSN3_YEAST	804	splP39073ISSN3_YEAST	823	3,60
splP47822IMED21_YEAST	100	splP47822IMED21_YEAST	93	8,30	splP19263IMED14_YEAST	436	splQ12343IMED4_YEAST	2	5,64
splP32570IMED22_YEAST	82	splP32570IMED22_YEAST	2	6,64	splP25648ISRB8_YEAST	899	splP25648ISRB8_YEAST	901	12,38

P1	R1	P2	R2	Score	P1	R1	P2	R2	Score
splP39073ISSN3_YEAST	97	splP39073ISSN3_YEAST	319	7,74	splP32569IMED17_YEAST	608	splP32569IMED17_YEAST	555	5,71
splQ12343IMED4_YEAST	55	splQ12343IMED4_YEAST	64	6,95	splP32570IMED22_YEAST	82	splP32569IMED17_YEAST	333	5,71
splP32569IMED17_YEAST	333	splP32569IMED17_YEAST	324	7,45	splP47822IMED21_YEAST	100	splP47822IMED21_YEAST	93	7,96
splP32585IMED18_YEAST	280	splP32569IMED17_YEAST	333	5,60	splQ12321IMED1_YEAST	389	splQ12321IMED1_YEAST	421	4,72
splP32569IMED17_YEAST	427	splP32569IMED17_YEAST	434	4,73	splP39073ISSN3_YEAST	820	splP39073ISSN3_YEAST	782	13,69
splP19263IMED14_YEAST	697	splP19263IMED14_YEAST	663	4,59	splP25648ISRB8_YEAST	88	splP47821ISSN8_YEAST	262	11,57
splP32569IMED17_YEAST	122	splP19263IMED14_YEAST	257	6,45	splP39073ISSN3_YEAST	39	splP39073ISSN3_YEAST	43	9,43
splP39073ISSN3_YEAST	804	splP39073ISSN3_YEAST	823	3,11	splP19263IMED14_YEAST	50	splP19263IMED14_YEAST	35	9,25
splP39073ISSN3_YEAST	804	splP39073ISSN3_YEAST	823	2,59	splP39073ISSN3_YEAST	550	splP38931ISSN2_YEAST	919	9,12
splQ99278IMED11_YEAST	53	splQ99278IMED11_YEAST	61	5,70	splP39073ISSN3_YEAST	820	splP39073ISSN3_YEAST	782	8,86
splP34162IMED20_YEAST	21	splP19263IMED14_YEAST	591	5,67	splP25648ISRB8_YEAST	888	splP25648ISRB8_YEAST	823	4,78
splQ12343IMED4_YEAST	55	splQ12343IMED4_YEAST	64	8,67	splP19263IMED14_YEAST	697	splP19263IMED14_YEAST	663	4,52
splP39073ISSN3_YEAST	804	splP39073ISSN3_YEAST	823	2,46	splQ12343IMED4_YEAST	71	splQ12321IMED1_YEAST	118	6,74
splP25648ISRB8_YEAST	899	splP25648ISRB8_YEAST	901	9,62	splQ12321IMED1_YEAST	198	splQ12321IMED1_YEAST	329	4,88
splP39073ISSN3_YEAST	804	splP39073ISSN3_YEAST	823	2,97	splP19263IMED14_YEAST	674	splP19263IMED14_YEAST	594	6,44
splP25648ISRB8_YEAST	899	splP25648ISRB8_YEAST	901	10,84	splP32569IMED17_YEAST	78	splP32569IMED17_YEAST	71	2,05
splP25648ISRB8_YEAST	899	splP25648ISRB8_YEAST	901	12,56	splP38782IMED6_YEAST	282	splP19263IMED14_YEAST	417	9,30
splP19263IMED14_YEAST	614	splP19263IMED14_YEAST	609	7,92	splP19263IMED14_YEAST	697	splP19263IMED14_YEAST	663	8,11
splP19263IMED14_YEAST	697	splP19263IMED14_YEAST	663	5,29	splP32569IMED17_YEAST	78	splP32569IMED17_YEAST	71	2,60
splP19263IMED14_YEAST	282	splP32569IMED17_YEAST	122	5,86	splP32585IMED18_YEAST	83	splP32585IMED18_YEAST	97	12,61
splP25648ISRB8_YEAST	899	splP25648ISRB8_YEAST	901	17,03	splP39073ISSN3_YEAST	574	splP39073ISSN3_YEAST	580	9,48
splP19263IMED14_YEAST	594	splP19263IMED14_YEAST	610	4,96	splQ99278IMED11_YEAST	68	splQ99278IMED11_YEAST	61	8,69
splP32569IMED17_YEAST	333	splQ99278IMED11_YEAST	88	3,96	splP32569IMED17_YEAST	589	splP32569IMED17_YEAST	601	6,48
splQ08278IMED7_YEAST	30	splQ08278IMED7_YEAST	37	5,54	splP32570IMED22_YEAST	9	splP32569IMED17_YEAST	333	5,27
splP32570IMED22_YEAST	82	splP32569IMED17_YEAST	333	4,88	splP32585IMED18_YEAST	280	splP32569IMED17_YEAST	333	4,98
splP32569IMED17_YEAST	608	splP32569IMED17_YEAST	555	5,03	splQ99278IMED11_YEAST	68	splQ99278IMED11_YEAST	61	8,44

P1	R1	P2	R2	Score	P1	R1	P2	R2	Score
splP47822IMED21_YEAST	100	splP47822IMED21_YEAST	93	8,63	splP32569IMED17_YEAST	78	splP32569IMED17_YEAST	71	4,51
splP38931ISSN2_YEAST	1398	splP38931ISSN2_YEAST	1002	2,80	splP25648ISRB8_YEAST	88	splP38931ISSN2_YEAST	1114	6,26
splP19263IMED14_YEAST	697	splP19263IMED14_YEAST	663	6,34	splP32569IMED17_YEAST	589	splP32569IMED17_YEAST	601	5,21
splP32570IMED22_YEAST	82	splP32569IMED17_YEAST	333	4,64	splP25648ISRB8_YEAST	888	splP25648ISRB8_YEAST	823	4,60
splP25648ISRB8_YEAST	899	splP25648ISRB8_YEAST	901	10,83	splP47821ISSN8_YEAST	70	splP47821ISSN8_YEAST	23	10,24
splP25648ISRB8_YEAST	888	splP25648ISRB8_YEAST	823	4,38	splP39073ISSN3_YEAST	804	splP39073ISSN3_YEAST	823	2,43
splP19263IMED14_YEAST	678	splP19263IMED14_YEAST	667	4,42	splP38931ISSN2_YEAST	1260	splP38931ISSN2_YEAST	1270	3,78
splQ12343IMED4_YEAST	55	splQ12343IMED4_YEAST	64	8,13	splP38304IMED8_YEAST	191	splP32570IMED22_YEAST	2	6,14
splP33308IMED9_YEAST	24	splQ12343IMED4_YEAST	2	1,95	splP39073ISSN3_YEAST	39	splP39073ISSN3_YEAST	43	14,33
splP38931ISSN2_YEAST	1024	splP39073ISSN3_YEAST	550	16,30	splP32569IMED17_YEAST	333	splP32570IMED22_YEAST	2	6,96
splQ12343IMED4_YEAST	138	splQ12343IMED4_YEAST	147	5,81	splQ12343IMED4_YEAST	64	splQ12343IMED4_YEAST	2	3,98
splP39073ISSN3_YEAST	97	splP39073ISSN3_YEAST	319	3,87	splP32569IMED17_YEAST	608	splP32569IMED17_YEAST	555	6,92
splP32570IMED22_YEAST	9	splP32569IMED17_YEAST	333	5,65	splP39073ISSN3_YEAST	97	splP39073ISSN3_YEAST	319	7,64
splP19263IMED14_YEAST	609	splP19263IMED14_YEAST	594	10,25	splP39073ISSN3_YEAST	804	splP39073ISSN3_YEAST	823	2,87
splP32569IMED17_YEAST	608	splP32569IMED17_YEAST	555	7,90	splQ99278IMED11_YEAST	68	splQ99278IMED11_YEAST	61	5,22
splP39073ISSN3_YEAST	39	splP39073ISSN3_YEAST	43	9,85	splP33308IMED9_YEAST	78	splQ12343IMED4_YEAST	64	9,27
splP25648ISRB8_YEAST	899	splP25648ISRB8_YEAST	901	10,67	splP32569IMED17_YEAST	608	splP32569IMED17_YEAST	555	7,31
splP32569IMED17_YEAST	78	splP32569IMED17_YEAST	71	2,97	splP38931ISSN2_YEAST	573	splP38931ISSN2_YEAST	566	3,39
splP19263IMED14_YEAST	549	splP19263IMED14_YEAST	591	7,01	splP25648ISRB8_YEAST	888	splP25648ISRB8_YEAST	823	4,58
splQ12343IMED4_YEAST	172	splP38931ISSN2_YEAST	628	4,06	splP19263IMED14_YEAST	674	splP19263IMED14_YEAST	594	3,98
splP38931ISSN2_YEAST	1398	splP38931ISSN2_YEAST	1002	4,29	splP34162IMED20_YEAST	21	splP19263IMED14_YEAST	591	5,51
splP32569IMED17_YEAST	319	splP32569IMED17_YEAST	427	8,11	splP32585IMED18_YEAST	280	splP32569IMED17_YEAST	333	7,43
splP39073ISSN3_YEAST	216	splP39073ISSN3_YEAST	151	5,75	splP19263IMED14_YEAST	549	splP19263IMED14_YEAST	610	10,65
splQ08278IMED7_YEAST	202	splQ12343IMED4_YEAST	110	5,78	splP19263IMED14_YEAST	594	splP19263IMED14_YEAST	610	4,81
splP39073ISSN3_YEAST	550	splP47821ISSN8_YEAST	23	2,55	splP25648ISRB8_YEAST	899	splP25648ISRB8_YEAST	901	10,64
splP25648ISRB8_YEAST	899	splP25648ISRB8_YEAST	901	12,66	splP38931ISSN2_YEAST	607	splP47822IMED21_YEAST	100	9,25

P1	R1	P2	R2	Score	P1	R1	P2	R2	Score
splP38931ISSN2_YEAST	573	splP38931ISSN2_YEAST	566	3,19	splQ99278IMED11_YEAST	88	splP32570IMED22_YEAST	2	6,08
splP39073ISSN3_YEAST	804	splP39073ISSN3_YEAST	823	3,02	splP25648ISRB8_YEAST	888	splP25648ISRB8_YEAST	823	5,21
splP25648ISRB8_YEAST	951	splP25648ISRB8_YEAST	959	6,63	splP25648ISRB8_YEAST	813	splP25648ISRB8_YEAST	820	6,18
splP32570IMED22_YEAST	95	splP32569IMED17_YEAST	319	6,62	splP25648ISRB8_YEAST	888	splP25648ISRB8_YEAST	823	5,35
splP25648ISRB8_YEAST	888	splP25648ISRB8_YEAST	823	6,83	splP19263IMED14_YEAST	549	splP19263IMED14_YEAST	567	7,42
splP25648ISRB8_YEAST	888	splP25648ISRB8_YEAST	820	4,82	splP32569IMED17_YEAST	608	splP32569IMED17_YEAST	555	7,06
splP39073ISSN3_YEAST	804	splP39073ISSN3_YEAST	823	2,47	splP32569IMED17_YEAST	333	splP32570IMED22_YEAST	2	7,85
splP47822IMED21_YEAST	100	splP47822IMED21_YEAST	93	5,23	splP47822IMED21_YEAST	75	splP38931ISSN2_YEAST	607	14,09
splP19263IMED14_YEAST	614	splP19263IMED14_YEAST	594	3,30	splP19263IMED14_YEAST	282	splP19263IMED14_YEAST	257	7,42
splP39073ISSN3_YEAST	116	splP39073ISSN3_YEAST	189	5,93	splP19263IMED14_YEAST	451	splP19263IMED14_YEAST	418	4,55
splP25648ISRB8_YEAST	899	splP25648ISRB8_YEAST	901	10,38	splP19263IMED14_YEAST	678	splP19263IMED14_YEAST	667	5,76
splP32569IMED17_YEAST	608	splP32569IMED17_YEAST	555	7,69	splP32570IMED22_YEAST	82	splP32569IMED17_YEAST	333	4,88
splP39073ISSN3_YEAST	116	splP39073ISSN3_YEAST	189	7,74	splP38931ISSN2_YEAST	457	splP38931ISSN2_YEAST	440	11,91
splP39073ISSN3_YEAST	804	splP39073ISSN3_YEAST	823	2,27	splP39073ISSN3_YEAST	804	splP39073ISSN3_YEAST	823	2,73
splP32569IMED17_YEAST	333	splP32570IMED22_YEAST	2	14,79	splP32569IMED17_YEAST	324	splP32569IMED17_YEAST	333	5,80
splP25648ISRB8_YEAST	906	splP25648ISRB8_YEAST	954	4,10	splP32569IMED17_YEAST	608	splP32569IMED17_YEAST	555	6,18
splP32569IMED17_YEAST	608	splP32569IMED17_YEAST	555	7,07	splP39073ISSN3_YEAST	804	splP39073ISSN3_YEAST	823	1,55
splP19263IMED14_YEAST	407	splP19263IMED14_YEAST	434	2,03	splP38931ISSN2_YEAST	457	splP38931ISSN2_YEAST	440	6,29
splQ12343IMED4_YEAST	113	splQ12343IMED4_YEAST	110	4,52	splP32569IMED17_YEAST	333	splP32570IMED22_YEAST	2	7,34
splP39073ISSN3_YEAST	574	splP39073ISSN3_YEAST	580	5,79	splP38931ISSN2_YEAST	1024	splP39073ISSN3_YEAST	574	7,97
splQ12343IMED4_YEAST	36	splQ12343IMED4_YEAST	2	0,51	splP47821ISSN8_YEAST	23	splP34162IMED20_YEAST	180	4,56
splP19263IMED14_YEAST	697	splP19263IMED14_YEAST	663	5,67	splP32569IMED17_YEAST	608	splP32569IMED17_YEAST	555	5,04
splP32570IMED22_YEAST	82	splP32569IMED17_YEAST	333	6,39	splP39073ISSN3_YEAST	804	splP39073ISSN3_YEAST	823	3,80
splP38931ISSN2_YEAST	607	splP47822IMED21_YEAST	93	8,93	splP39073ISSN3_YEAST	39	splP39073ISSN3_YEAST	43	14,73
splQ99278IMED11_YEAST	53	splQ99278IMED11_YEAST	61	11,39	splP38304IMED8_YEAST	191	splP32570IMED22_YEAST	2	7,85
splP25648ISRB8_YEAST	888	splP25648ISRB8_YEAST	823	4,24	splP47822IMED21_YEAST	100	splP47822IMED21_YEAST	93	3,36

P1	R1	P2	R2	Score	P1	R1	P2	R2	Score
splP19263IMED14_YEAST	549	splP19263IMED14_YEAST	567	7,52	splP39073ISSN3_YEAST	804	splP39073ISSN3_YEAST	823	3,08
splP39073ISSN3_YEAST	550	splP38931ISSN2_YEAST	919	6,75	splP25648ISRB8_YEAST	888	splP25648ISRB8_YEAST	823	5,11
splP38931ISSN2_YEAST	555	splP38931ISSN2_YEAST	537	7,60	splQ12343IMED4_YEAST	228	splQ12343IMED4_YEAST	234	7,47
splP32569IMED17_YEAST	115	splP19263IMED14_YEAST	360	3,58	splP32570IMED22_YEAST	2	splP32569IMED17_YEAST	324	10,62
splP39073ISSN3_YEAST	216	splP39073ISSN3_YEAST	151	7,36	splQ99278IMED11_YEAST	68	splQ99278IMED11_YEAST	61	8,40
splP19263IMED14_YEAST	697	splP19263IMED14_YEAST	663	7,62	splP32569IMED17_YEAST	333	splP32570IMED22_YEAST	2	5,71
splP39073ISSN3_YEAST	804	splP39073ISSN3_YEAST	823	3,00	splP19263IMED14_YEAST	282	splP19263IMED14_YEAST	257	6,50
splP47821ISSN8_YEAST	23	splP34162IMED20_YEAST	180	10,60	splP39073ISSN3_YEAST	216	splP39073ISSN3_YEAST	151	8,43
splP39073ISSN3_YEAST	97	splP39073ISSN3_YEAST	319	8,85	splP39073ISSN3_YEAST	97	splP39073ISSN3_YEAST	319	7,39
splP47821ISSN8_YEAST	262	splP25648ISRB8_YEAST	88	13,35	splP19263IMED14_YEAST	591	splP19263IMED14_YEAST	674	7,41
splP34162IMED20_YEAST	21	splP19263IMED14_YEAST	591	8,56	splP25648ISRB8_YEAST	899	splP25648ISRB8_YEAST	901	4,58
splQ12343IMED4_YEAST	55	splQ12343IMED4_YEAST	64	10,10	splP25648ISRB8_YEAST	899	splP25648ISRB8_YEAST	901	17,25
splP39073ISSN3_YEAST	216	splP39073ISSN3_YEAST	151	5,59	splP19263IMED14_YEAST	674	splP19263IMED14_YEAST	594	4,17
splP19263IMED14_YEAST	436	splP19263IMED14_YEAST	418	5,11	splP32569IMED17_YEAST	324	splP32569IMED17_YEAST	333	10,65
splQ12321IMED1_YEAST	198	splQ12321IMED1_YEAST	329	2,55	splP32569IMED17_YEAST	333	splP32570IMED22_YEAST	2	9,33
splP25648ISRB8_YEAST	899	splP25648ISRB8_YEAST	901	16,71	splP32569IMED17_YEAST	333	splP32570IMED22_YEAST	2	5,97
splP32569IMED17_YEAST	333	splP32570IMED22_YEAST	2	4,18	splP38931ISSN2_YEAST	573	splP38931ISSN2_YEAST	566	2,38
splP25648ISRB8_YEAST	813	splP25648ISRB8_YEAST	820	4,09	splP34162IMED20_YEAST	21	splP19263IMED14_YEAST	591	8,37
splQ12321IMED1_YEAST	389	splQ12321IMED1_YEAST	421	4,99	splP38931ISSN2_YEAST	573	splP38931ISSN2_YEAST	566	4,14
splP25648ISRB8_YEAST	88	splP47821ISSN8_YEAST	262	10,34	splP39073ISSN3_YEAST	804	splP39073ISSN3_YEAST	823	3,43
splP25648ISRB8_YEAST	813	splP25648ISRB8_YEAST	789	6,21	splP38931ISSN2_YEAST	1398	splP38931ISSN2_YEAST	1002	2,50
splP32569IMED17_YEAST	68	splP32569IMED17_YEAST	71	6,39	splP19263IMED14_YEAST	549	splP19263IMED14_YEAST	610	3,53
splP32570IMED22_YEAST	82	splP32569IMED17_YEAST	333	6,69	splP25648ISRB8_YEAST	665	splP25648ISRB8_YEAST	553	3,56
splQ99278IMED11_YEAST	53	splQ99278IMED11_YEAST	61	7,09	splQ08278IMED7_YEAST	202	splQ12343IMED4_YEAST	110	3,85
splP39073ISSN3_YEAST	216	splP39073ISSN3_YEAST	151	6,56	splQ08278IMED7_YEAST	202	splQ12343IMED4_YEAST	110	3,35
splP19263IMED14_YEAST	678	splP19263IMED14_YEAST	667	4,80	splP38931ISSN2_YEAST	632	splP38931ISSN2_YEAST	566	2,41

P1	R1	P2	R2	Score	P1	R1	P2	R2	Score
splP38931lSSN2_YEAST	607	splP38931lSSN2_YEAST	1270	1,20	splP19263lMED14_YEAST	417	splQ12343lMED4_YEAST	2	7,41
splQ12343lMED4_YEAST	55	splQ12343lMED4_YEAST	64	8,83	splP25046lMED19_YEAST	74	splP25648lSRB8_YEAST	616	8,10
splP47822lMED21_YEAST	75	splP38931lSSN2_YEAST	607	12,52	splP32570lMED22_YEAST	82	splP32569lMED17_YEAST	333	4,92
splP39073lSSN3_YEAST	804	splP39073lSSN3_YEAST	823	3,73	splQ08278lMED7_YEAST	103	splQ12343lMED4_YEAST	162	4,09
splP25648lSRB8_YEAST	632	splP25648lSRB8_YEAST	665	11,16	splP25046lMED19_YEAST	74	splP25648lSRB8_YEAST	616	8,11
splP38931lSSN2_YEAST	1398	splP38931lSSN2_YEAST	1002	2,68	splP32569lMED17_YEAST	589	splP32569lMED17_YEAST	601	3,99
splP38931lSSN2_YEAST	607	splP47822lMED21_YEAST	93	8,17	splP32569lMED17_YEAST	608	splP32569lMED17_YEAST	555	7,57